AD-A129 554 COORDINATED RESEARCH PROGRAM IN PULSED POWER PHYSICS (U) TEXAS TECH UNIV LUBBOCK DEPT OF ELECTRICAL ENGINEERING M KRISTIANSEN ET AL. 01 DEC 82 1/3

UNCLASSIFIED AFOSR-TR-83-0503 F49620-79-C-0191 F/G 20/3 NL

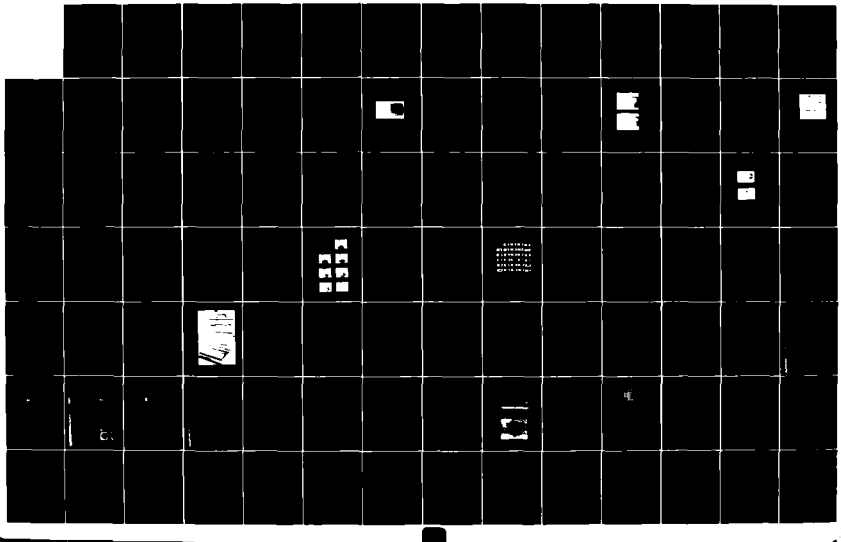

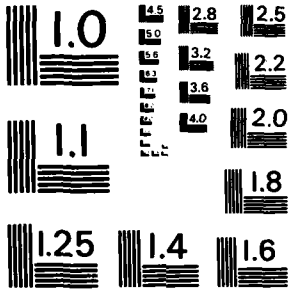

THIRD ANNUAL REPORT

on

COORDINATED RESEARCH PROGRAM
in
PULSED POWER PHYSICS

December 1, 1982

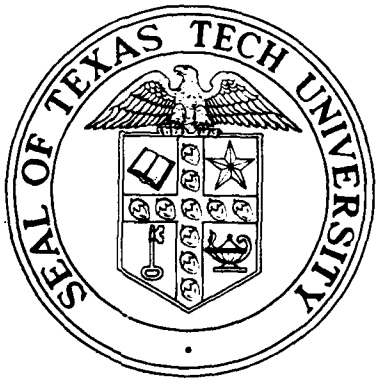

Air Force Office of Scientific Research
Contract No. F49620-79-C-0191

PLASMA AND SWITCHING LABORATORY
LASER LABORATORY

Department of Electrical Engineering
TEXAS TECH UNIVERSITY

Lubbock, Texas 79409

UNCLASSIFIED

SECURITY CLASSIFICATION OF THIS PAGE (When Data Entered)

REPORT DOCUMENTATION PAGE		READ INSTRUCTIONS BEFORE COMPLETING FORM
1. REPORT NUMBER AFOSR-TR- 83-0503	2. GOVT ACCESSION NO. AD-A129 554	3. RECIPIENT'S CATALOG NUMBER
4. TITLE (and Subtitle) Coordinated Research Program in Pulsed Power Physics		5. TYPE OF REPORT & PERIOD COVERED 10/1/81 - 9/30/82 Annual 6. PERFORMING ORG. REPORT NUMBER
7. AUTHOR(s) M. Kristiansen, L. Hatfield M. Hagler, G. Schaefer J. Craig, K. Schoenbach F. Williams		8. CONTRACT OR GRANT NUMBER(s) F49620-79-C-0191
9. PERFORMING ORGANIZATION NAME AND ADDRESS Department of Electrical Engineering Texas Tech University Lubbock, Texas 79409		10. PROGRAM ELEMENT, PROJECT, TASK AREA & WORK UNIT NUMBERS 61102F 2301A7
11. CONTROLLING OFFICE NAME AND ADDRESS Air Force Office of Scientific Research BLdg. 410, Bolling AFB, Washington, D.C. 20332		12. REPORT DATE December 1, 1982 13. NUMBER OF PAGES 278
14. MONITORING AGENCY NAME & ADDRESS(if different from Controlling Office)		15. SECURITY CLASS. (of this report) Unclassified 15a. DECLASSIFICATION DOWNGRADING SCHEDULE
16. DISTRIBUTION STATEMENT (of this Report) Distribution Unlimited Approved for public release; distribution unlimited.		
17. DISTRIBUTION STATEMENT (of the abstract entered in Block 20, if different from Report)		
18. SUPPLEMENTARY NOTES		
19. KEY WORDS (Continue on reverse side if necessary and identify by block number) Pulsed Power, Switching, Electromechanical Pulse Device, Laser Triggering, Electron Beam Triggering, Surface Physics, Electrode Erosion, Spark Gap, Discharge, Spectroscopy, Opening Switches		

20. ABSTRACT (Continue on reverse side if necessary and identify by block number)
Eight program elements related to pulsed power research are described. These program elements form a multi-disciplinary, coordinated program whose main emphasis is to gain improved understanding of high power, repetitive closing and opening switches. The main emphasis is concerned with triggering of discharges in gas filled spark gaps and the associated electrode erosion and insulator damage. Considerable efforts are also being made to understand the limitations and fundamental discharge phenomena in fast opening switches for inductive energy storage. A novel electromechanical pulse generator which promises to

Continued on back

DD FORM 1 JAN 73 1473 EDITION OF 1 NOV 65 IS OBSOLETE

Unclassified

SECURITY CLASSIFICATION OF THIS PAGE (When Data Entered)

20. deliver fast, repetitive pulses to a load is also being investigated.

Third Annual Report on

COORDINATED RESEARCH PROGRAM IN PULSED POWER PHYSICS

AFOSR Contract #F49620-79-C-0191

December 1, 1982

Program Director:	M. Kristiansen
Associate Program Director:	M. Hagler
Principal Investigators:	J. Craig M. Hagler L. Hatfield M. Kristiansen G. Schaefer K. Schoenbach F. Williams
Post Doctoral Fellow:	D. Pease
Associate Investigators:	H. Carper H. Krompoltz J. Marx R. Pederson
Technician III:	K. Zinsmeyer
Secretary III:	M. Byrd J. Davis
Secretary II:	B. Cornitius
Graduate Students:	R. Biesele S. Dahli R. Cooper R. Curry A. Donaldson R. Dougal H. Dunlap J. Gahl L. Gordon H. Harjes G. Hutcheson G. Jackson D. Johnson G. Leiker B. Maas R. Ness K. Pinegar L. Thurmond C. Yeh*

* Paid by Republic of China (Taiwan)

TABLE OF CONTENTS

SUMMARY OF RESEARCH OBJECTIVES FOR 1981-82

Project No. 1: No work was planned for this year.

Project No. 2: The main goal was to gain an experimental and theoretical understanding of laser triggered spark gap phenomena.

Project No. 3: The main effort was directed at developing and experimentally verifying a theoretical model which can be used to predict pre-breakdown and restrike phenomena in spark gaps. Other efforts were directed at an understanding of electrode erosion processes.

Project No. 4: This work had two main objectives:

a) to gain an understanding of the flashover occurence along UV irradiated insulator samples, and

b) to make insulator and electrode surfaces studies which aid in the model development in Project No. 3.

Project No. 5: The emphasis here is on developing laser induced fluorescence techniques to be used in Project No. 2 and to develop multiphoton ionization techniques to be used in studies of charge transport during the breakdown process.

Project No. 6: Several smaller investigations are carried out in this project element. The main goal of these investigations being to verify if certain ideas merit more extensive

studies. The present Project No. 3 as well as AFOSR Grant #82-0327 to our M.E. Department are examples of projects which were originally funded by this program element.

Project No. 7: This project is concerned with the theoretical development and experimental verification of a new electromechanical pulser concept with relatively short pulse widths (as electromechanical pulsers go).

Project No. 8: The studies under this project are concerned with the theoretical development and experimental verification of various concepts for optical modulation of discharge impedances. The ultimate goal is to demonstrate the feasibility of using these techniques in a fast opening switch for inductive energy storage.

Project No. 9: This project works in close cooperation with Project No. 8 but emphasizes electron beam control of the discharge impedance. The basic goals and theoretical considerations are similar to those in Project No. 8. The main experimental effort has been on designing and constructing a suitable facility for verifying some of the theoretical predictions.

SUMMARY

The Coordinated Research Program in Pulsed Power Physics is a multi-investigator program which involves seven Principal Investigators, four Associate Investigators, one Postdoctoral Fellow and 19 Graduate Students from the departments of Electrical Engineering, Physics and Chemistry at Texas Tech University. It is mainly concerned with the physics of high power switching and has 8 active program elements. The research is supported by AFOSR and ARO.

The study of spark gap closing switches has four active program elements. The first one which was concerned with electron-beam initiated (triggered) discharges, has been completed and the results accepted for publication. Some future, additional work is contemplated in connection with Project No. 9.

Under the second program element we have conducted extensive, fast photographic and spectroscopic studies of the optical emission from laser triggered spark gaps. A simple model for the laser triggered breakdown process has been developed and several trigger geometries have been investigated. A novel laser-induced-fluorescence imaging technique has been used to monitor the motion of electrode material ejected as a result of the laser-triggered breakdown event.

In the third project we have studied the electrode erosion process for various electrode materials. Histograms of the voltage breakdown of a spark gap have been recorded with a data acquisition system. These histograms have been used to check a model which has been developed for the breakdown process and its statistics. Surface analysis techniques

are also used both in connection with the electrode erosion investigation and the statistical breakdown studies.

Project No. 4 is carried out in close cooperation with No. 3 and is concerned with the damage that occurs to insulators in high power switches and in surface discharge spark gaps. The studies of insulator material deposition on the electrodes is also of importance to the statistics of the breakdown process. In addition there are efforts to develop a model for dielectric surface flashover phenomena in vacuum and gases. Irradiation of certain insulator surfaces with UV has indicated increased flashover strength which may result from thin surface coatings from the UV source.

In Project No. 5 we study multiphoton ionization phenomena in order to improve (better determine) the initial conditions in laser induced spark gap breakdown. We have also developed a computer code to calculate the charge motion under space-charge-limited conditions. Studies of inverse bremsstrahlung heating in laser induced breakdown and of photodetachment of negative ions as an optical control of diffuse discharge conditions have also been initiated.

In order to evaluate new ideas that inevitably occur during the various other investigations we study, under program element No. 6, some exploratory switch concepts. Among these are optical studies of density gradients in gas blown spark gaps; investigations of multichanneling, erosion, and triggering phenomena in surface discharge switches; determination of resistive losses is spark gaps; evaluation of several novel opening switch concepts; and others.

Project No. 7 is quite different in nature from the others since it deals with a novel electromechanical pulser concept. The advantage of this pulser is that it has a very short rise time ($\lesssim$ 10 μs) compared to other electromechanical pulse devices and that it lends itself to a modest rep-rate of more than 1000 pps. A proof-of-concept model of the pulser was built and verified the basic concept. The report included here constitutes the final report for this project. Conditions under which the pulser may have the best performance are outlined.

Project No. 8 and 9 are closely related. Both are primarily concerned with diffuse discharge opening switches for inductive energy storage. In one case, Project No. 8, the emphasis is on optical (laser) control mechanisms and in the other case, Project No. 9, the emphasis is on electron-beam sustained discharges. Both mechanisms may be used together to enhance the switch performance and much of the theory pertains to both concepts. Several novel approaches have been developed and two experimental facilities have been constructed.

The interactions with numerous national, university, and industrial laboratories have been strengthened and expanded. It is felt that these interactions,which include numerous visits between the participating parties, have been extremely beneficial for everyone involved.

Project No. 1

Electron Beam Initiated Breakdown

(T. Tzeng, E. Kunhardt, and M. Kristiansen)

This work has been completed. A summary of the results will appear in the December, 1982 issue of the IEEE Transactions on Plasma Science.

Some future, additional work is contemplated in connection with Project No. 9.

Project No. 2

Transient Process in Laser-Triggered Breakdown

(R.A. Dougal, R.A. Biesele, D. Pease, and P.F. Williams)

A. SUMMARY

Accomplishments during the contract period include: 1) Acquisition and implementation of a high power, pulsed Nd:YAG laser system along with a very fast optical diagnostic system for studies of laser-triggered switching in the fast-triggering regime, 2) conduction of extensive, fast photographic and spectroscopic studies of the optical emission from laser-triggered spark gaps, 3) Development of a simple model which describes the laser-triggered breakdown process, 4) Studies of laser-triggering of spark gaps using several geometries for introducing the laser into the gap, 5) Monitoring the motion of electrode material ejected as a result of a laser-triggered breakdown event using a novel laser-induced-fluorescence imaging technique, 6) The acquisition of beautiful shadowgraphs of the shock wave propagation into the gap following a laser-triggered breakdown event.

B. ACCOMPLISHMENTS

As a result of this work and of that reported under Project No. 5, we now have a solidly based qualitative understanding of the laser-triggered breakdown process and work is continuing to provide enhanced

quantitative understanding. Reliable information at both levels is required for proper design of laser-triggered spark gap switches. Additionally, this work is expected to provide significant advances in the understanding of conventional, over-volted breakdown and of other triggering methods for both under- and over-volted gaps.

Modifications to the experimental setup, described in Section 1, below, have allowed us to study breakdown in the very fast triggering regime. This change is very important since most devices of practical interest operate in this regime. Making use of this capability, we inititated fast, streak, photographic and spectroscopic studies of laser triggered breakdown, both in the conventional triggering configuration in which the laser is longitudinally incident into the gap and strikes an electrode, as well as in other configurations. This work, described in Sections 2 and 4, has provided us with a great deal of insight into the physical operation of laser-triggered devices and has led to the model of laser-triggered breakdown described in Section 3. In a separate effort, we investigated the practicality of using laser-induced-fluorescence to monitor the ejection and subsequent migration of electrode vapor into the gap, following a breakdown event. As discussed in Section 5, this work was quite successfule, and clear pictures of the electrode vapor cloud migration were obtained. Finally, as an unexpected side benefit of the imaging work, we obtained beautiful shadowgraphs of the propagation of shock waves and other turbulent phenomena in the spark gap following a laser-triggered breakdown event.

These results are presented in Section 6.

1. Experimental Setup

Early in the current contract period we acquired a high power Nd:YAG laser system for use in spark gap triggering and in a wide range of diagnostic and other uses. The system consists of a Quanta-Ray, Model DCR-1A, Nd:YAG laser oscillatior-amplifier, a PDL-1 YAG-pumped dye laser, and WEX-1 frequency mixer. The system provides up to 700 mJ at 1064 nm, 225 mJ at 532 nm or 125 mJ at 335 nm. The dye laser and frequency mixer provide continuously tunable output throughout the visible and near ultraviolet spectral regions.

Acquisition of this system has allowed us to carry out expriments which we were previously unable to do. Primary among these are experiments in the fast triggering regime. The YAG laser provides ample power for reliably triggering our spark gap with delays under 10 ns and negligible jitter. The capability for operation in this fast-triggering regime is important because practical laser triggered switches are generally operated here. Experiments carried out under conditions for which slower triggering is observed are important for clarifying the roles of various mechanisms in the laser-triggering process, but the ability to carry out fast-triggering experiments is a necessary one.

The experimental setup in current use is shown in Fig. 1. A portion of the 1.06 μm output of the YAG laser is directed down the axis of the spark gap cell, described in a previous report [1]. In normal operation,

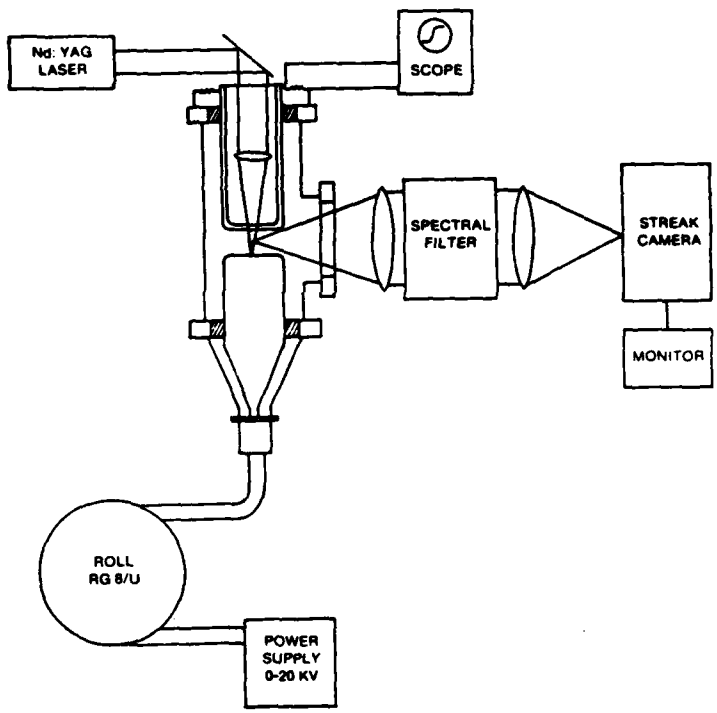

Fig. 1 Schematic diagram of experimental setup for laser-triggered breakdown studies.

the beam is focused onto the surface of the lower electrode where it makes a small plasma fireball. Voltage is supplied to the gap from a coaxial cable system, charged by a regulated power supply. As discussed previously [1], high vacuum technology is used in the cell in order to provide an exceptionally clean and reproducible environment. The cable is discharged through the gap into a matched load resistor, and the gap current is monitored by measuring the voltage at a tap on this resistor. Although several electrode materials have been tried, we commonly use stainless steel electrodes because they seem to provide the most consistent and reproducible results. With this system we find that laser energies of 1-10 mJ will reliably trigger our gap, charged to 80-90% of static breakdown, with under 10 ns delay, and very low jitter.

The principal optical diagnostic probes are a Hamamatsu C979 Temporal Disperser streak camera and an optical-multichannel-analyzer-based spectroscopic system. The streak camera provides time resolution of down to $\sim$ 10 ps with very good sensitivity. The problems discussed in the last report [1], regarding inadequate rejection of intense emission occuring after the sweep, have been reduced thorough the addition of a gating modification to the streak camera, but problems of this type remain, and the rejection capability of the system for strong, unwanted emission often determines the effective sensitivity of the system in our experiments. The spectroscopic detection systems we use have been described in previous reports. Briefly, they allow us to

acquire spectra in a single shot with near-single-photon sensitivity. Time resolution to 5 ns is provided, and the data are acquired with a computer-controlled system.

2. Fast Photographic and Spectroscopic Studies

Following the acquisition of the high power Nd:YAG laser and the partial correction of problems in the streak camera associated with excessive feedthrough of intense, but out-of-time-frame optical signals (extinction ratio), a program of extensive, sweep photographic investigations of laser-triggered breakdown was initiated. As shown in Fig. 2, the laser trigger may be introduced into the gap in three geometries. Of these, both the second and third geometry can provide excellent switching characteristics, but the third geometry, in which the laser trigger strikes an electrode, requires lower laser energy and beam quality than does the second. All results in this section will be for triggering in the third geometry. Triggering with the other geomteries is discussed in a later section. All experiments were carried out in a pure N_2 atmosphere at a pressure of 800 Torr.

Figure 3 shows a typical streak photograph of a laser-triggered breakdown event in the fast-triggered regime. The slit of the streak camera is parallel to the axis of the gap and positioned so that it intercepts the image of the laser fireball and the arc channel. The first visible event is the appearance of intense emission from the laser-produced plasma fireball on the surface of the struck electrode. With

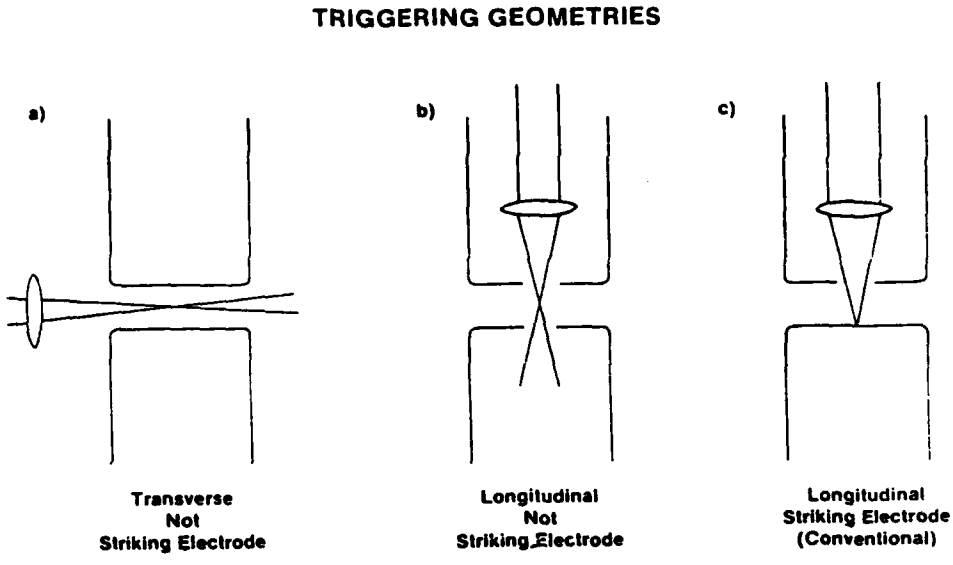

Fig. 2 Schematic diagram of triggering geometries commonly employed in laser-triggered switching.

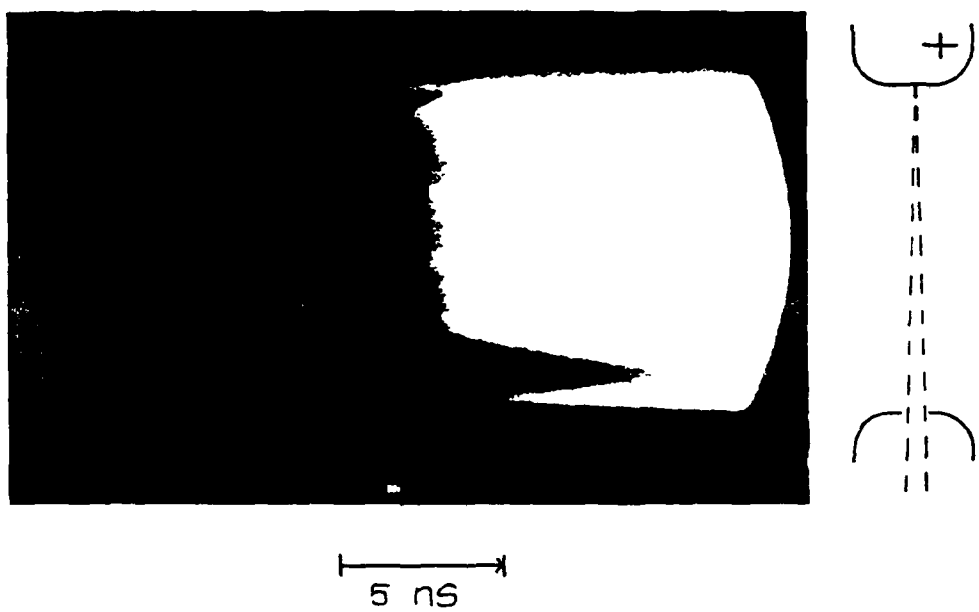

Fig. 3 Typical streak photograph of laser-triggered breakdown in N_2 at 800 Torr. The laser fireball was masked and is barely visible in the top of the photo.

this sensitivity, there is no evidence of other activity in the gap until the appearance of a diffuse glow in the region of the opposite electrode. Immediately following the appearance of this glow, an intense front of luminosity starts from the struck electrode and propagates towards the opposite electrode. The appearance of these luminous fronts coincides with the closure of the gap and the collapse of gap voltage.

If the gap breaks down while the laser is still on, luminous striations associated with the interaction between the laser and the spark channel are seen. These features generally appear only after the formation of the luminous spark channel and seem to be associated with "hot spots" in the focused laser. We believe these striations to be manifestations of inverse bremsstrahlung heating of the spark channel plasma.

By placing a 1/4 meter spectrometer in front of the streak camera, we have obtained spectral information about these events. We find that the emission from the laser-produced plasma fireball is mostly a continuum, indicating a high degree of ionization of the plasma. Other emission observed before gap closure, including emission from the diffuse glow, which appears in front of the electrode not struck by the laser, is strongly molecular in nature. Following gap closure the molecular component disappears and is replaced by strong continuum emission superimposed on an atomic and ionic line emission spectrum.

These spectroscopic results may be explained by assuming that the electronic and vibronic modes of the N_2 molecule are heated by the

ohmic heating of the free electrons. This observation led us to develop the model of laser-triggered breakdown discussed in the next section of this report. The model assumes that the laser triggers the gap by creating a weakly conducting channel bridging the gap. Breakdown then occurs as a result of cycles of ohmic heating of the channel followed by increased channel conductivity.

In the model the mechanism for producing the initial conducting channel is not specified. Several such mechanisms are possible, including fast streamer propagation across the gap, photoionization of the gas due to intense, enegetic U.V. emission from the laser-produced plasma fireball, direct interaction of the laser beam with the fill gas, perhaps through inverse bremsstrahlung heating, and heating due to drift across the gap of electrons emitted from the plasma fireball.

In order to clarify the role of each of these mechanisms in the laser-triggering process, high sensitivity streak photographs were obtained. The principal limitation on sensitivity resulted from the presence of very intense emission from the laser-produced plasma fireball and, at later times, from the spark. The emission from the fireball was substantially reduced by blocking this emission with a mask on the input slit of the streak camera, and emission from the spark was reduced by using a very short charging cable to reduce the time-integrated intensity of the spark.

For observation of events (using the streak camera) occurring early in the breakdown process, the spark emission can be discriminated against by choosing the sweep speed so that the spark occurs off-screen. Only limited discrimination could be obtained in this manner, however, because of scattering of some electrons from the intense off-frame image back into the frame. Further discrimination was provided by noting that the emission we wish to observe is expected to be of molecular character, whereas the spark emission is continuous with some atomic and ionic line emission. Thus, by pre-filtering the input light with a monochrometer tuned to a strong molecular emission line, the intensity of the early-times emission can be enhanced relative to the spark emission.

Figure 4 shows a streak photograph of the breakdown obtained in this manner. A luminous front propagating across the gap is barely discernable in this photograph. The feature is observed in several photographs. The front starts at the leading edge of the laser-produced plasma fireball and propagates across the gap at a speed of $\sim 10^8$ cm/sec. We believe this front to be the result of a streamer, initiated by the self-shielding action of the plasma fireball. The streamer produces the weakly conducting channel which is the starting point for the model of laser-triggered breakdown discussed in the next section.

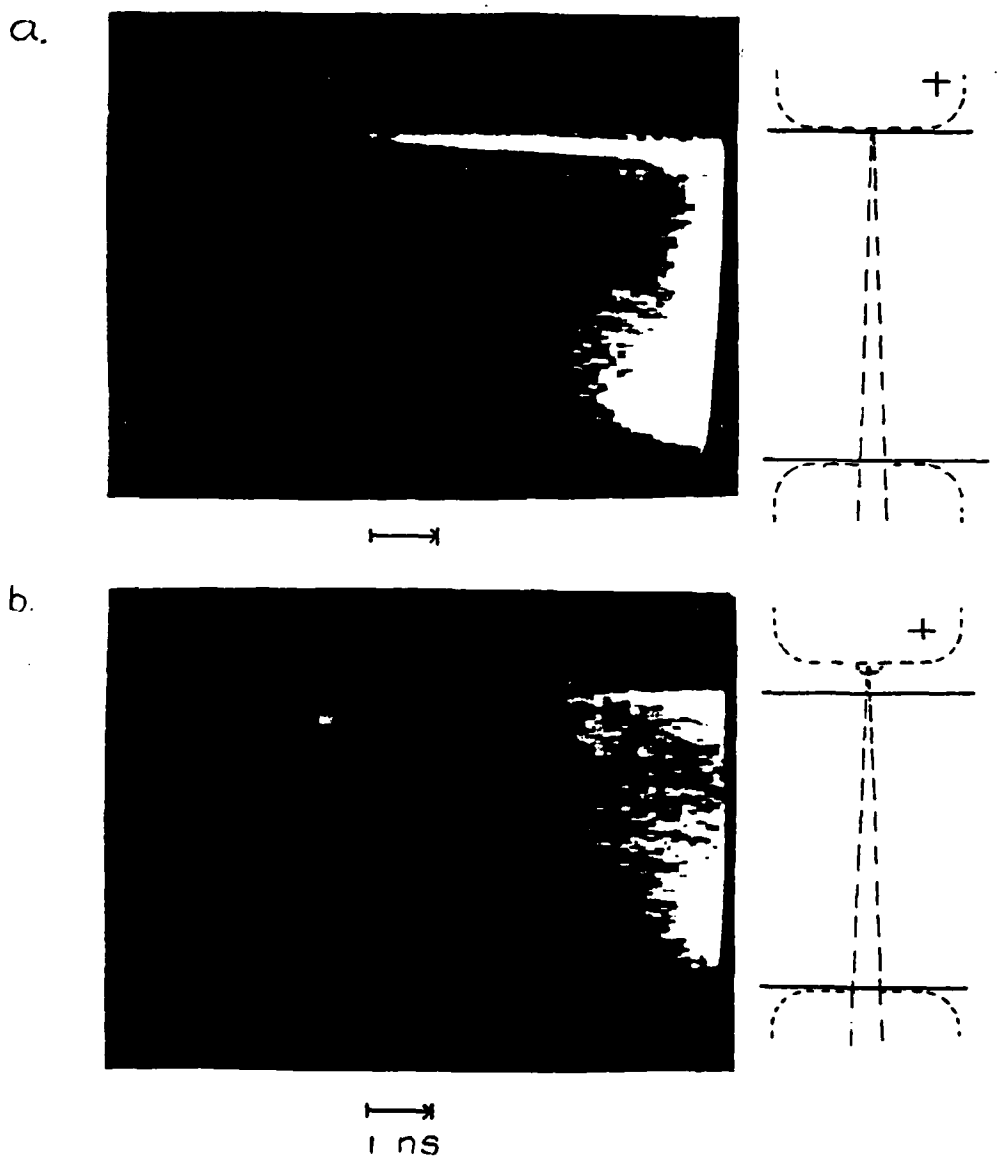

Fig. 4 High sensitivity streak photographs of a laser-triggered breakdown event in 800 Torr N_2. The conditions in the two photos were the same except that in b) the laser fireball was masked, whereas in a) it was not. The photo was taken from the vidicon monitor of the streak camera system, and the pixel size for the digitization is clearly visible.

3. A Simple Model of Laser-Triggered Breakdown

In spite of the impressive capabilities of laser-triggered spark gap switches, the principles of operation, particularly the basic physical mechanisms important to the laser-triggered breakdown process, are poorly understood. We have developed a model of the initial stages of breakdown which lead to arc channel formation and switch closure. The model describes well the major qualitative features of laser-triggered breakdown and can serve as the basis for an engineering model of the closing phase of laser-triggered switches.

Although many variations have been described, laser-triggered, gas-filled spark gaps normally conform to one of three geometries, as shown in Fig. 2. In the earliest work, the laser was introduced into the gap transverse to the gap axis [2]. Although this geometry is convenient for laser access, it requires high laser power, and exhibits comparatively poor switching characteristics. Most devices introduce the beam into the gap in a longitudinal geometry as shown in Figures 2b and 2c. This geometry generally provides much improved triggering characteristics over the transverse geometry. In the geometery of Figure 2b, the laser does not strike an electrode and triggering results from the ionization it produces in the gap. Excellent switching characteristics have been reported in devices with this geometry, but a high laser intensity is required [3].

The geometry shown in Figure 2c, where the laser strikes one

electrode, also provides excellent switching characteristics, and requires more moderate intensities than that of Figure 2b. In this case, the laser is focused approximately on the electrode surface, where it produces a small plasma fireball due to interaction with the electrode surface. The production of the fireball seems to be necessary for the triggering process, but "good" triggering requires considerably more laser power than the threshold power for fireball production. Here, we will be primarily concerned with gaps employing the third, or "conventional" geometry.

The development of a qualitative model describing the laser-triggered breakdown process is badly needed for switch engineering applications. In constructing such a model, there are several puzzling experimental observations which must be accounted for [4,5]. One of these is the question of how even a laser pulse of moderate energy ($\tilde{<}$ 0.1 mJ) can induce a strongly under-volted (~ 70% of static breakdown voltage) gap to break down. Another is the observation that with relatively high laser energy ($\tilde{<}$ 1 mJ) similar results are obtained, for either gap polarity (i.e. the polarity of the struck electrode), whereas with much lower laser energy a negative target electrode produces faster, more reliable switching than does a positive struck electrode. Finally, it is observed, using sensitive electrical and optical diagnostics, that during the time period roughly between the arrival of the triggering laser pulse and the closure of the gap there is little external evidence of activity in the gap region. Figure 5 shows a current oscillogram for gap closure which illustrates this behavior. The quiet period, which may have a duration ranging from several ns to several μs, depending upon

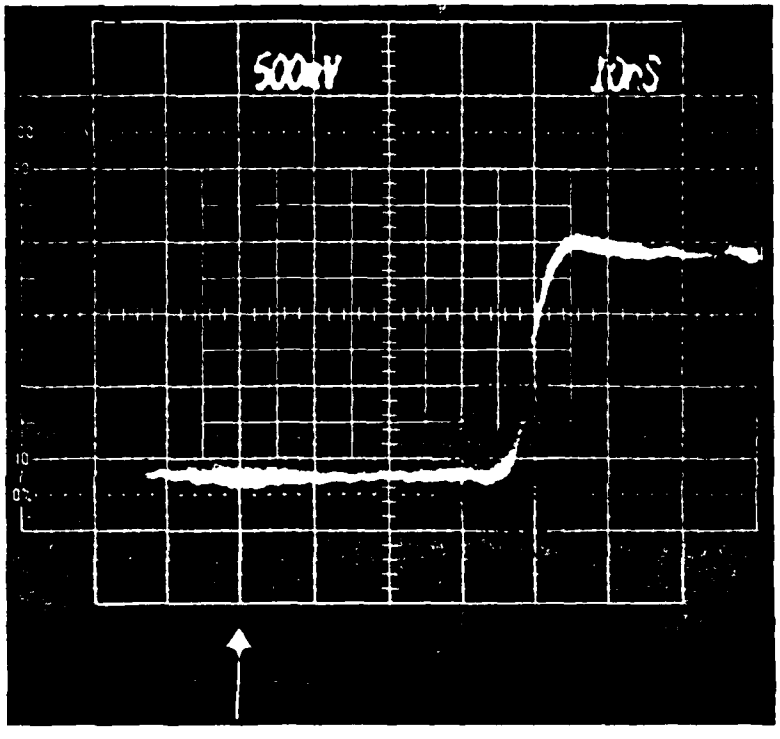

Fig. 5 Current oscillogram for a laser-triggered switch in 800 Torr N_2. Laser trigger pulse arrived at the switch at the time indicated by the arrow. Vertical scale is 50 Amps/div, and horizontal is 10 ns/div.

spark gap operating conditions (laser power, gap voltage, gas composition, etc.), is followed by a very abrupt current rise which corresponds to gap closure. A simple breakdown process, involving multiple avalanches, would predict a smoother, more continuous current rise. The model we describe here qualitiatively explains these features and predicts current waveforms and luminescence intensities very similar to those which are observed experimentally.

Briefly, our model is similar to that proposed first by Drabkina [6], and later extended by others [7-9], to explain the later stages of conventional over-volted breakdown. We postulate that at t = 0 the laser deposits a quantity of energy in the spark gap through one of several mechanisms discussed in the previous section. This energy results in the production of weak ionization which produces a finite resistivity and allows some current to flow. This current deposits additional energy in the gas due to ohmic heating, producing more ionization and heating. If the energy gain exceeds the losses, the process will continue until an arc forms.

Accurate calculations of the current, voltage, temperature, etc. in the incipient arc channel are difficult. Determining the gas resitivity from the energy input is especially troublesome because the situation under study is dynamic and is not in thermodynamic equilibrium. The free electron gas may be in thermodynamic equilibrium with itself, but probably not with the bound electrons, and certainly not with the nuclei (vibrational, rotational, and translational states) on the time scales of interest. In order to explore qualitatively the

consequences of our model, we have made calculations of current, temperatures, etc. for several sets of approximations. Two extreme sets were chosen to bracket the actual behavior of the system. In both cases, energy losses to the outside world were ignored since they should not be important for the short time scales of interest here. In the first case, we assumed that the free electrons were completely decoupled from the bound electrons and the nuclear motions and that all energy input into the system went into ionizing the atoms. Then the number density of free electrons, n, in a volume, following the deposition of an energy density, E, into this volume, is given by $n = E/E_{ionization}$ where $E_{ionization}$ is the ionization energy for the gas. The conductivity was approximated from a simple mobility equation,

$$\sigma = n\, q\, \mu, \tag{1}$$

where q is the electronic charge and μ the electron mobility (assumed constant) for the fill gas. This approximation represents an extreme, in that the energy is channeled into producing conductivity in the most efficient manner possible, and thus should predict breakdown occuring in shorter times, with lower initial energies than are actually observed.

In the absence of information about the initial energy deposition process, we will assume the energy to be deposited uniformly along the gap axis. We do not expect that the results of calculations using reasonable, non-uniform distributions to differ greatly from these since preferential ohmic heating of highly resistive regions will tend to

smooth out initial non-uniformities. With this assumption, the conductivity can easily be found analytically for this case,

$$\sigma = \sigma_0 \exp\left\{\frac{q}{E_i \ell^2} \int_0^t V^2(\tau)\, d\tau\right\}, \qquad (2)$$

where q is the electronic charge, E_i the ionization energy of the gas molecules, ℓ the length of the gap, and V(t) the gap voltage. If the initial resistance of the gap is $R_o = \left[\frac{1}{\ell} \int \sigma_0\, dA\right]^{-1}$ and the voltage source resistance is R_g, then the voltage across the gap at time t is determined by

$$V(t) = V_0 \left[1 + \frac{R_g}{R_0} \exp\left(\frac{q}{E_i \ell^2} \int_0^t V^2(\tau)\, d\tau\right)\right]^{-1} \qquad (3)$$

where $V_0 = V(0)$. This integral equation is easily solved numerically, Results are discussed below and an example is shown in Figure 6.

In a second case, we assumed the opposite extreme, with complete thermodynamic equilibrium between the free electrons and the rest of the system. In order to avoid difficulties associated with solving the hydrodynamic equations for the gas pressure and temperature, we assumed constant pressure and used published tables of specific heat vs temprature for N_2 to determine the temperature [10]. The validity of the constant pressure assumption depends on the actual degree of thermalization of the free electrons with the translational motions of the gas. Qualitatively, the results should not be strongly dependent on this assumption. Since we do not expect the free electron gas to reach thermodynamic equilibrium with the rest of the system on the

time scales of interest, this second case represents an opposite extreme to the first, and the actual behavior of the system should be bracketed by these two cases.

Another computer program was written to simulate the operation of the model under the second set of assumptions. Very large plane-parallel electrodes were assumed and the gap was viewed as a set of thin circular rings stacked on top of each other and then assembled concentrically. Each ring was taken to have a resistance determined by the resistivity of the gas inside it and by the ring dimensions. The gap then appears as a simple square lattice resistor network, and capactitive effects between adjacent rings are ignored. The resistivity of the gas in a ring was determined by the total energy deposited into it, either initially by the laser, or by ohmic heating. Since the time scales of interest are short, we have ignored diffusion effects.

The computer program operates by calculating voltages, currents, power dissipations, and resistances for each ring at each of a uniformly-spaced set of times, $\{t_i\}$. The initial resistance of each ring is determined from the energy deposited by the laser into the ring. Thereafter, the change in resistance at t_i is determined by the energy deposited, through ohmic heating, into the ring for times between t_{i-1} and t_i. In light of the short time scales involved, energy loss terms are not included. The energy in a ring at t_i, E_i, is determined from

$$E_i = E_{i-1} + P_{i-1} (t_i - t_{i-1}) \qquad (4)$$

where P_i is the power being deposited in the ring at t_i. The resistivity of the ring is determined from the energy through use of tables of resistivity vs temperature and of specific heat vs temperature for the gap fill gas [10]. The voltage at each point in the resistor network is determined using Kirchoff's current law.

The results of the calculations for the two cases are shown in Figs. 6 and 7. Gap parameters are shown in the figure captions. In absence of better information, the laser energy was assumed to be deposited uniformly along the length of the incipient spark channel for both cases. Under these assumptions, the behavior of the system in the first case depends only on the initial resistance of the incipient channel. In the second case, the laser energy was assumed to be deposited with a Gaussian radial profile in the channel. The plasma fireball was simulated by an additional, hemispherically - symmetric Gaussian profile energy distribution centered on one electrode. The total energy and the radii of the distributions were input parameters for the program and are given in the figure captions.

Figure 6 shows the results for the first case where all energy is assumed to go into ionizing the gas, and Fig. 7 shows results for the second case where complete thermodynamic equilibrium of the electrons is assumed. In the first case, as seen in Fig. 7, very rapid breakdown occurs even with very small amounts of energy deposited initially into the channel. As the current rises the ohmic heating decreases due to the finite generator impedance. Since the conductivity of the gas is assumed to vary linearly with energy

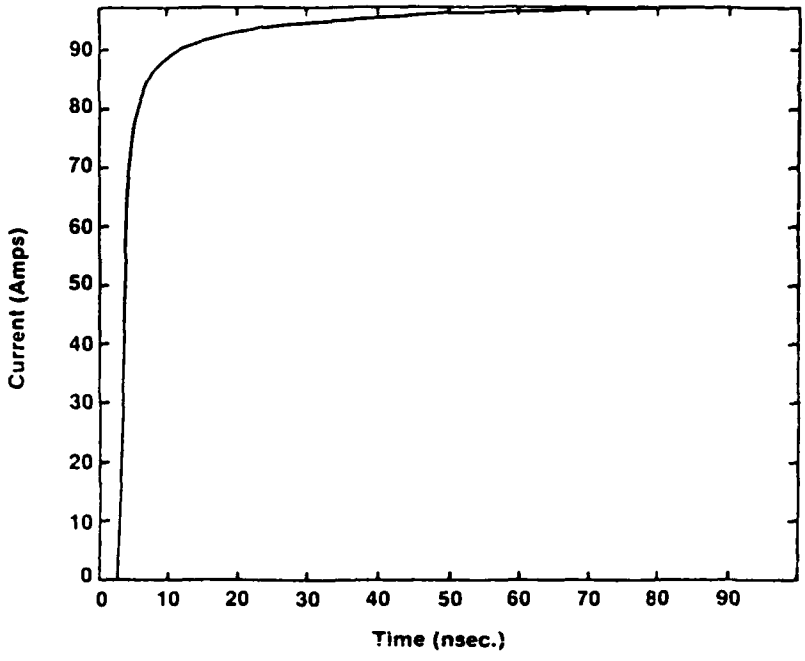

Fig. 6 Calculated current vs. time for the completely-decoupled electron approximation. Assumed conditions were: initial energy deposition of 10^{-13} J in 2 mm, cylindrical channel; charging voltage 10 kV across a 1 cm gap; 50 Ω load with 50 Ω generator; N_2 fill gas at 1 atmosphere.

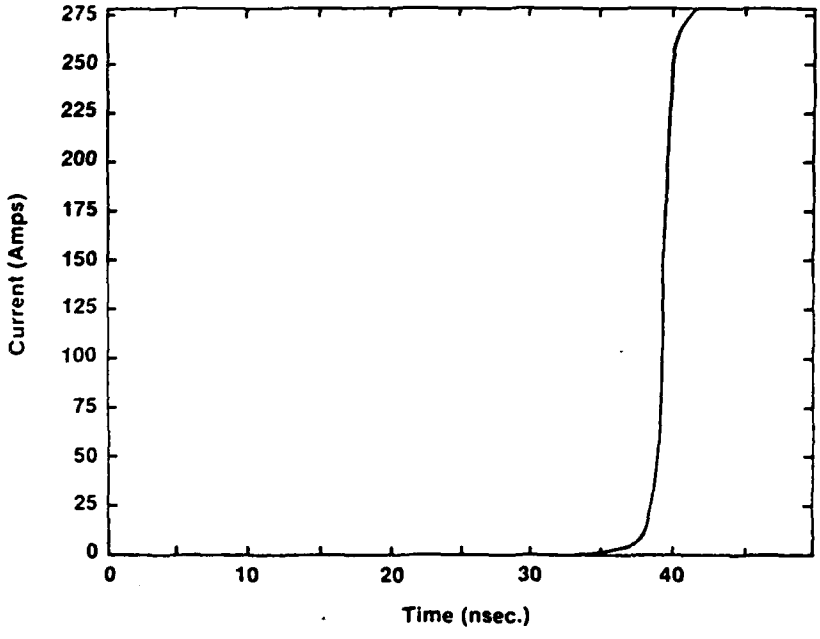

Fig. 7 Calculated current vs. time for the comple thermodynamic equilibrium approximation. Assumed conditions were: initial energy depositon of 150 mJ into a 2 mm dia, cylindrical channel and 10 mJ into a 2 mm dia , spherical fireball; charging voltage 30 kV across 1 cm gap; 50 Ω load with 50 Ω generator; N_2 fill gas at 1 atomosphere.

deposition, the rate of current rise decreases at higher currents, resulting in a slow approach to complete closure. Due to the exponential dependence of the conductivity with time, the delay in gap closure is a very weak function of the initial energy deposited into the incipient spark channel.

Figure 7 shows a typical calculated current waveform for the second case, where complete thermodynamic equilibrium is assumed. Here only very small currents are predicted up to about 40 ns. whereupon an abrupt current rise occurs with a rise time of ~ 1 ns. This characteristic is qualitatively very similar to that observed with laser-triggered gaps, as shown in Figure 5. The very rapid rise to complete closure, following the long silent period, is primarily a result of the form of the conductivity vs temperature curve for the fill gas. In nitrogren, as in other gases, the conductivity is a nearly expontential function of temeperature up to about 10,000 K. The strongly increasing conductivity offsets the decreasing power being put into the gap due to the collapse of the gap voltage and contributes to the rapid completion of gap closure. As expected, a much larger quantity of energy must be initially deposited in the arc channel in this case in order to produce breakdown in a time comparable to that found in the first case.

In summary, we find that our model reproduces well the qualitative features of laser-triggered breakdown over a wide range of assumptions about the degree of thermalization of the free electrons with the rest of the system. Quantitative predictions must await more accurate

calculations which include the effects of non-equilibrium electron distributions. Particularly, in the slow triggering regime (>1 μs) gas heating and thermal conductivity effects may also have to be considered. The development of a quantitatively-reliable numerical model of laser-triggered breakdown would be an important advance for the engineering design of laser-triggered spark gaps.

4. Other Triggering Geometries

As shown in Figure 2, several configurations for introducing the laser trigger beam into the gap are possible. Because of the engineering importance of the third configuration most of our work has involved studies of triggering in this geometry. The characteristics of the breakdown produced by triggering with the other two geometries shown in the figure are notably different from those observed with the third, and comparison of these with the characteristics of the conventional triggering provided useful insight into the processes of importance in laser-triggered breakdown.

In all three geometries we found that the production of a small plasma fireball, directly with the laser, was necessary for reliable gap triggering. In the third geometery, the laser strikes the lower electrode and the firebal results from the interaction of the laser radiation with the electrode surface, whereas in the other two geometries, the laser must itself break down the fill gas. Thus

several orders of magnitude more laser power is required in configurations a and b than in c.

The characteristics of the breakdown observed with the geometries of Figure 2a and b are distinctly different from those observed with configuration c. In both a and b, sizable current flows immediately upon breakdown of the gas by the laser, whereas there is very little external evidence of activity from the gap in configuration c until shortly before the final closure occurs. A typical current trace for the transverse triggering configuration is shown in Figure 8. Here we see that, coincident with the first appearance of light from the laser spark, the current rises to an intermediate value corresponding to about 50% of the final, closed switch, value. Subsequently, after a nearly constant period, the current again rises, but more slowly, to complete closure. Similar behavior is observed with the longitudinal, but not striking an electrode, configuration of Figure 2b.

We first were inclined to interpret the initial current as being due to a diplacement current component resulting from the separation of charge in the laser-induced plasma firebabll in the middle of the gap. As the electrons liberated from the plasma by the shielding process drift across the gap in the applied field, they would further ionize the gas, producing their own giant avalanche. The free charge thus generated would then "short" out the field between the anode and the mid-gap plasma fireball, significantly over-volting the remaining gap to the cathode, and resulting in rapid breakdown.

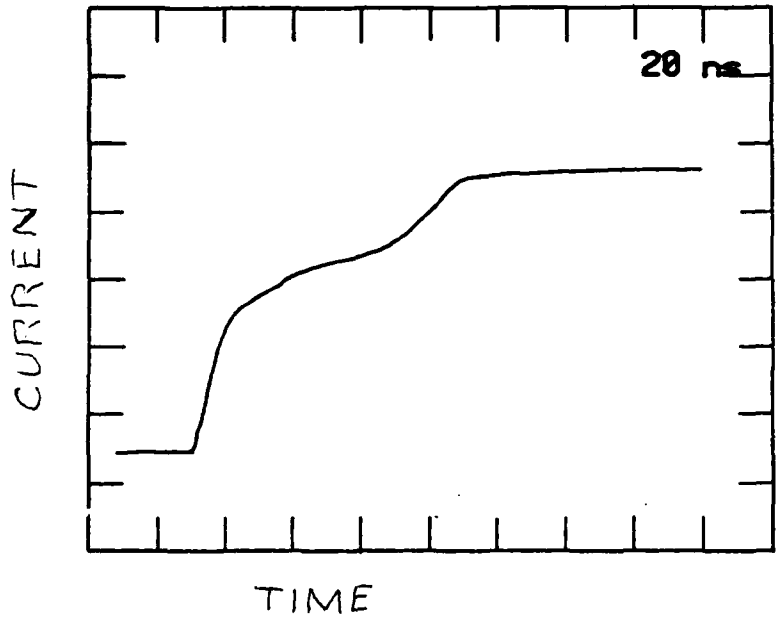

Fig. 8 Typical current trace for transverse triggereing in 800 Torr N_2. Horizontal scale is 20 ns/div and vertical is about 40 amp/div.

A streak photograph of breakdown in this configuration is shown in Figure 9. The dark band in the center of the photo is the shadow of a mask placed over the entrance slit of the streak camera to block the intense emission from the laser plasma fireball. This photograph does not support our hypothesized breakdown mechanism in that there is a uniform, vertical band of emission corresponding to the time that the laser was on, followed by a more or less uniform, but weaker, emission throughout the gap, finally followed by intense luminous wave fronts propagating into the gap from both electrodes. The appearance of these intense fronts corresponds to the final current rise to complete closure. There is no evidence of the gaint avalanche moving across the gap before the appearance of these fronts. Further, the transient glow observed during the laser pulse has no explanation in terms of this model.

We now believe that the early current we observed in these experiments is due to photoionization. The hot fireball undoubtedly emits intense ultra-violet radiation under the strong heating of the intense laser. This radiation propagates into the gap, providing the transient glow we observe and also providing free electrons through photoionizaion. At atmospheric pressure, the penetration depth of a photon, energetic enough to ionize the nitrogen fill gas, would be < 1 mm. Thus if a relatively uniform density of electrons throughout the gap is to be produced by this process, the photoionization must proceed either through a relatively weak, multi-photon process, or, more likely, through direct photoionization of some impurity gas with lower ionization

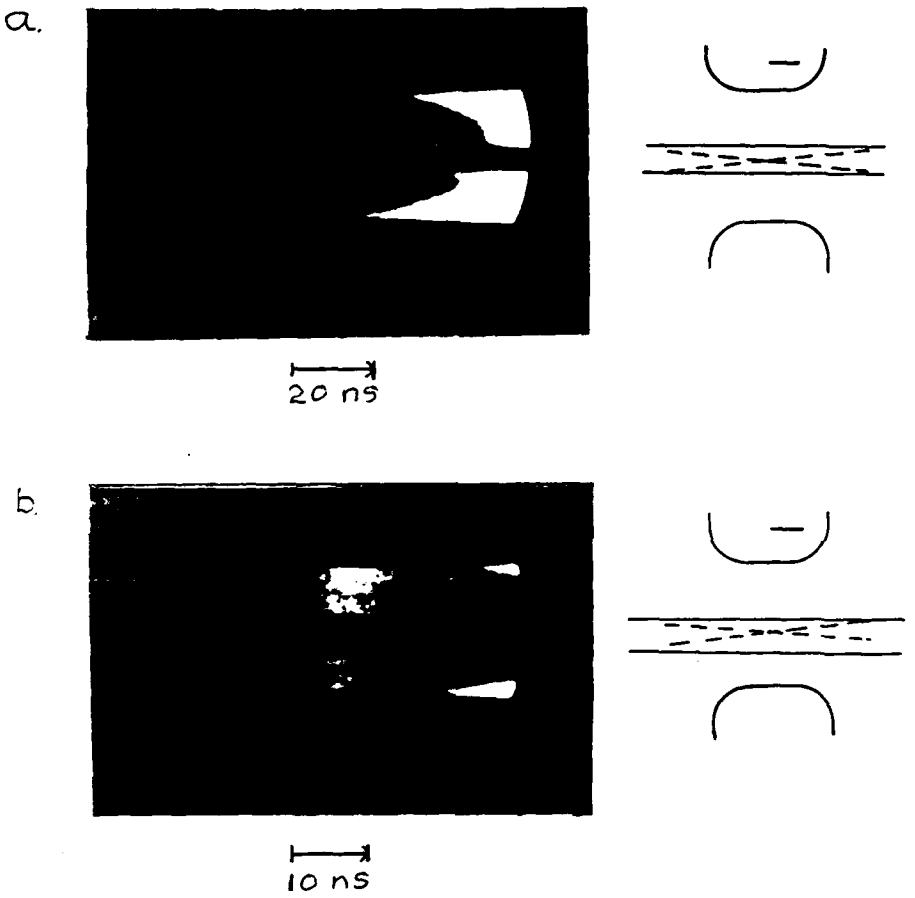

Fig. 9 Streak photographs of breakdown with transverse laser triggering in 800 Torr N_2. The dark space in the center of each photo is the shadow of a mask used to block the intense emission from the laser fireball. The sensivitivity in photo b) is 10 times that in a) and the time scales are as indicated.

energy than the host nitrogen. The initial current we observe then would result from the displacement current of these photoionized electrons drifting in the field. There likely are streamers propagating in both directions outward from the fireball toward the electrodes. Their propagation may be enhanced by the tenuous free electron gas they pass through, and in the case of configuration b, perhaps by interaction with the laser beam. After both streamers have reached an electrode, the gap is bridged, and a larger, much more constricted. current flows. This very high current density ohmically heats the incipient spark channel, producing the intense luminous fronts seen in Figure 9.

This model can also explain the differences we observe between triggering in configurations where the laser does not strike an electrode, and those where it does. In configuration c, much lower laser power is required to trigger the gap, and the experiments we report here were carried out with an energy of roughly 1-10% that used in configurations a and b. In streak photographs, we do not see a a transient uniform glow from the gap region, and there is very little initial current. We would expect much less ultra-violet emission from laser heating of the plasma fireball because of the lower laser power, consistent with the absence of a uniform glow and an initial current. Using much higher laser powers in the triggering experiments with configuration c, we observe breakdown in very short times, and are unable to determine if there are two distinct regions in the breakdown, as observed in the other configurations.

5. Ejection of Electrode Material

In an effort to study the behavior of metal vapor evaporated from spark gap electrodes a new technique for directly and selectively observing the metal vapor cloud has been devised. This technique relies on laser-induced fluorescence (LIF) to make the vapor visible and an SIT (Silicon Intensified Target) vidicon to record the image. The technique provides excellent time resolution, determined by the width of the laser pulse and the lifetime of the excited state involved, and is generally applicable for observation of any species with energy levels accessible to tunable laser systems. In contrast to conventional fluorescence techniques, the LIF technique is well suited to the detection of ground state species.

Using this technique, we have obtained, for the first time, two-dimensional, time-resolved images of the migration of ground state electrode vapor into the gap, following a laser-triggered breakdown event. The Laser-Induced-Fluorescence-Imaging (LIFI) technique which we have developed is based on Laser-Induced Fluorescence (LIF). LIF is a convenient technique for causing species in the ground or a metastable state to emit light [11,12]. The process is generally used as a spectroscopic tool, and it can be very effectively used for imaging applications. The LIF process is illustrated in Figure 10. E_1, E_2, and E_3 are three energy levels of the species under consideration. The level E_1 need not be the ground state, but the strength of the emission will be proportional to the population of E_1. If the $E_1 \rightarrow E_2$

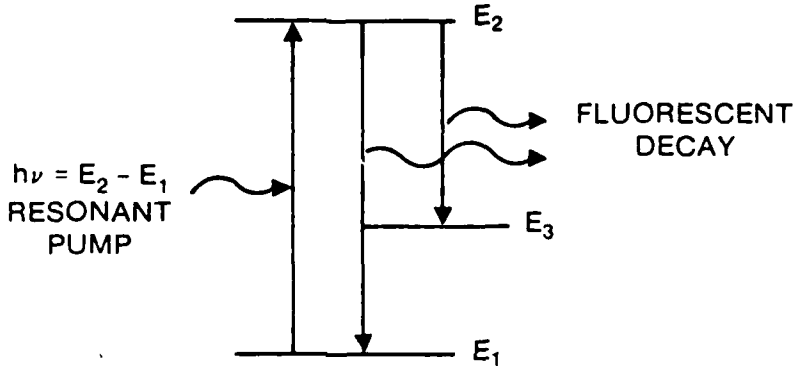

Fig. 10 Energy level diagram of a laser-induced fluorescence process.

transition is optically allowed then a photon of energy $h\nu = E_2 - E_1$ can resonantly pump the system from state E_1 to E_2. Decay to a lower-lying state will follow and the presence of species in E_2 can be detected by observing the emission resulting from radiative transitions. If, in the absence of laser excitation, the population of E_2 is low, then for a given laser pump intensity, the intensity of the re-emission will be proportional to the population of E_1 during the laser pulse. Temporal resolution is provided, therefore, by the excitation laser, and the detector need not be gated unless it is necessary to reduce interference from background emission.

We have used this technique to study the migration of aluminum metal vapor expelled from the electrodes of a laser-triggered spark gap. Time-resolved images of the ground state Al vapor cloud obtained with the apparatus clearly show the evolution of the cloud for several hundred μs after the spark. The laser was tuned to resonance with the 394.4 nm transition between the ground, $3^2P^0_{1/2}$, state and the $4^2S_{1/2}$ excited state of Al. Re-emission from transitions back to the ground state at 394.4 nm and to the $3^2P^0_{3/2}$ state at 396.1 nm was monitored to provide the image.

A schematic diagram of the experimental set up is shown in Figure 11. The spark gap switches a DC charged 20 kV, 50 Ω transmission line into a matched 50 Ω load. The gap is undervolted and is triggered to break down by about 50 mJ of focused 1.06 μm radiation from the Nd:YAG laser in a 15 ns pulse. The matched transmission line system produces clean, square-wave pulses of 1 μs duration and peak current of 200A. Both the 1.06 μm laser pulse and the spark current are capable of eroding

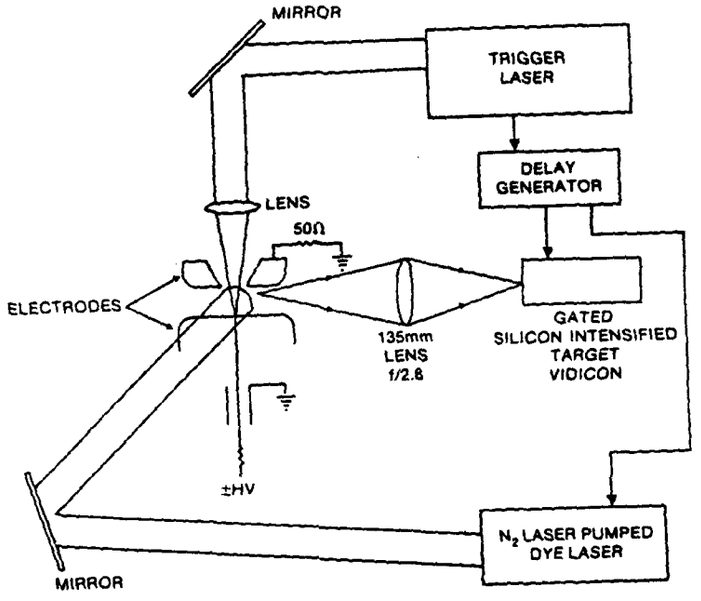

Fig. 11 Schematic diagram of the experimental apparatus for laser-induced fluorescence. The pump laser beam passes through the gap perpendicularly to the imaging axis.

electrode material, and we have obtained photographs of electrode vapor clouds produced by each of these processes.

The basic LIFI system consists of a Molectron DL-II dye laser pumped by a Molectron UV400 N_2 laser, and a PAR 1254 Gated SIT vidicon. The dye laser produces pulses with energy between 10 and 500 μJ, depending on the spectral region, and duration of 8 ns. The active region of the spark gap is imaged onto the face of the vidicon with a 135 mm focal length photographic lens. In order to reduce the interference from the intense emission from the spark the SIT detector was gated off, except during a 50 ns window which contained the pump laser pulse. Further rejection of the unwanted background was provided by placing an interference bandpass filter (400 nm ± 5 nm) between the lens and the vidicon. The pump laser and the vidicon gate generator are triggered by a mulitichannel delay generator which is in turn triggered by the laser used to initiate the spark gap. Varying the delay of the multi-channel delay generator provided a convenient means of changing the the observation time.

A sequence of LIFI photos obtained in this manner is shown in Fig. 12. For the pump transition we chose, the pump laser was strongly absorbed by the Al vapor. As a result, the beam intensity was depleted in crossing the vapor cloud and LIF was observed only from the surface of the vapor cloud first struck by the beam. Some improvement was obtained by reflecting the pump beam back through the cell, thereby illuminating the cloud from both sides (the beam diameter was much larger than that of the vapor cloud), but an asymmetry is still evident in the pictures we obtained.

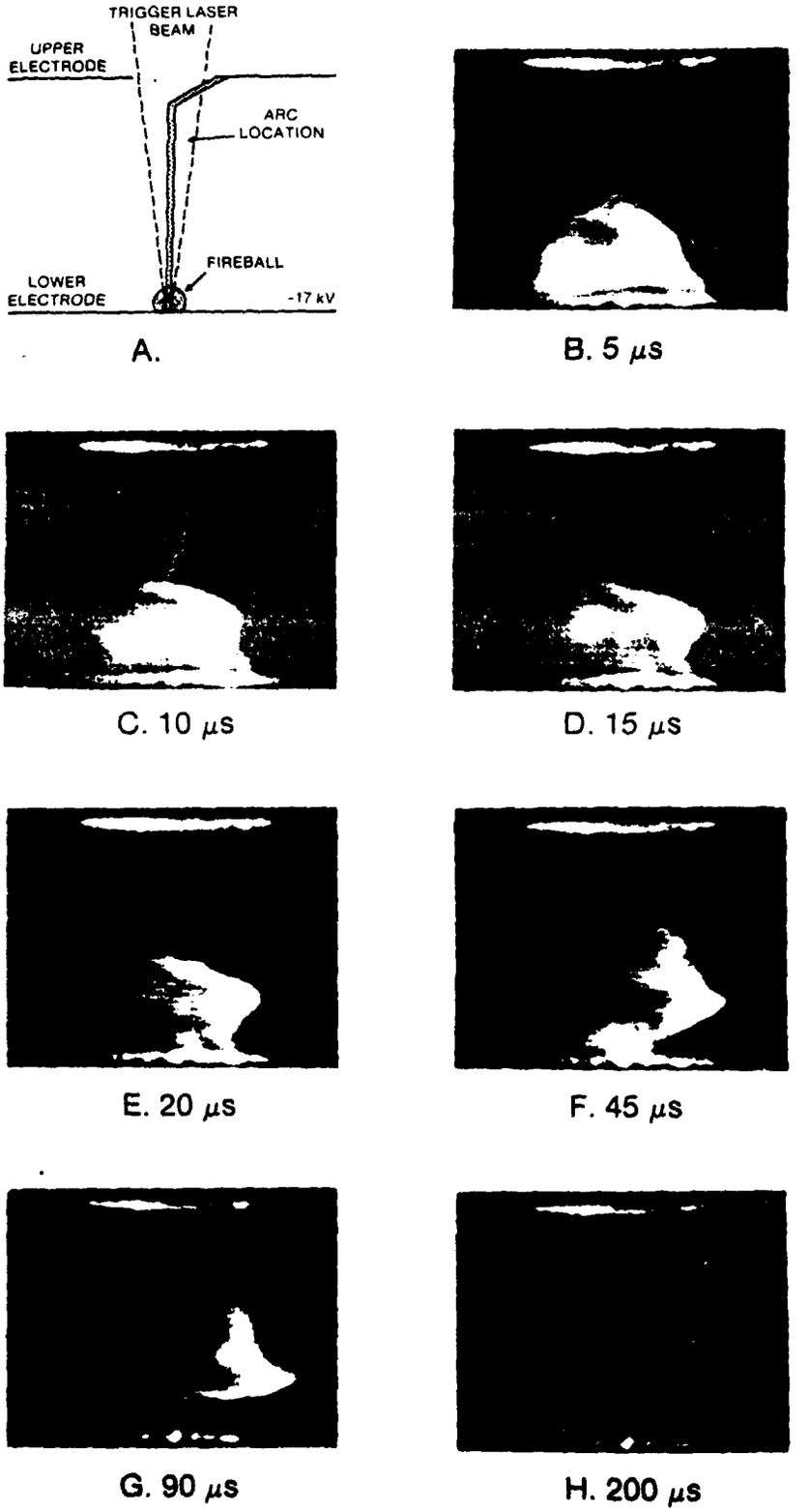

Fig. 12 Time-sequenced photographs showing the migration of aluminum vapor eroded from the spark gap electrodes by the triggering laser and the arc. a) shows the location of electrodes in pictures, b) - h) shows images of aluminum vapor at times as indicated after the arc.

Material is ejected from the electrode during the event because of the effects on the struck electrode of the triggering laser pulse and because of the effects on both electrodes of the spark. In our experiments, we are able to clearly separate material ejected as a result of both effects. Material ejected from the plasma fireball resulting from the laser trigger expands rapidly at first, until it occupies a roughly hemispherical volume a few mm in diameter, whereupon expansion slows drastically. These results indicate that the material is carried into the gap by the intially explosive expansion of the gas surrounding the fireball. This expansion front rapidly decays into turbulence, however, leaving the ejected material adrift in the gap.

Ejected material resulting from the spark is also clearly seen in these experiments. This material appears to move much more slowly than does the material ejected from the fireball, requiring tens of μs to traverse the 0.5 cm gap. For relatively low spark currents there is a clear channeling effect observed in the migration of this material, however, in that the ejected material follows a path coincident with the old spark channel. At higher currents, the material is ejected in the form of electrode jets emanating from both electrodes. These jets are similar to those observed by other in studies of conventional overvolted breakdown.

6. Shock Wave Propagation

As a side effect of the LIFI studies described in the previous section, we have recorded some beautiful shadowgrams of shock waves resulting from the laser-triggered breakdown process in our spark gap.

In these experiments the collimated output beam of the dye laser passes through the gap, illuminating its entire length. Shock waves or other turbulent phenomena in the path of the laser diffract the collimated light and result in a dark shadow appearing in the beam photograph after traversing the gap. By allowing the beam to fall on a white screen after exiting the gap and then photographing the resulting shadowgram, a record of the passage of these fronts is obtained. The time resolution of these "snapshots" of the gap is determined by the pulse width of the laser, which in this case is about 10 ns. For studying hydrodynamic phenomena such as shock waves, this is excellent temporal resolution.

Figure 13 shows a sequence of shadowgrams of laser-triggered breakdown obtained in this manner. A cylindrical shock wave from the explosive expansion of the spark channel is clearly evident in these photos. In other experiments in which no voltage was applied to the gas we clearly saw the hemispherical shock wave from the laser fireball.

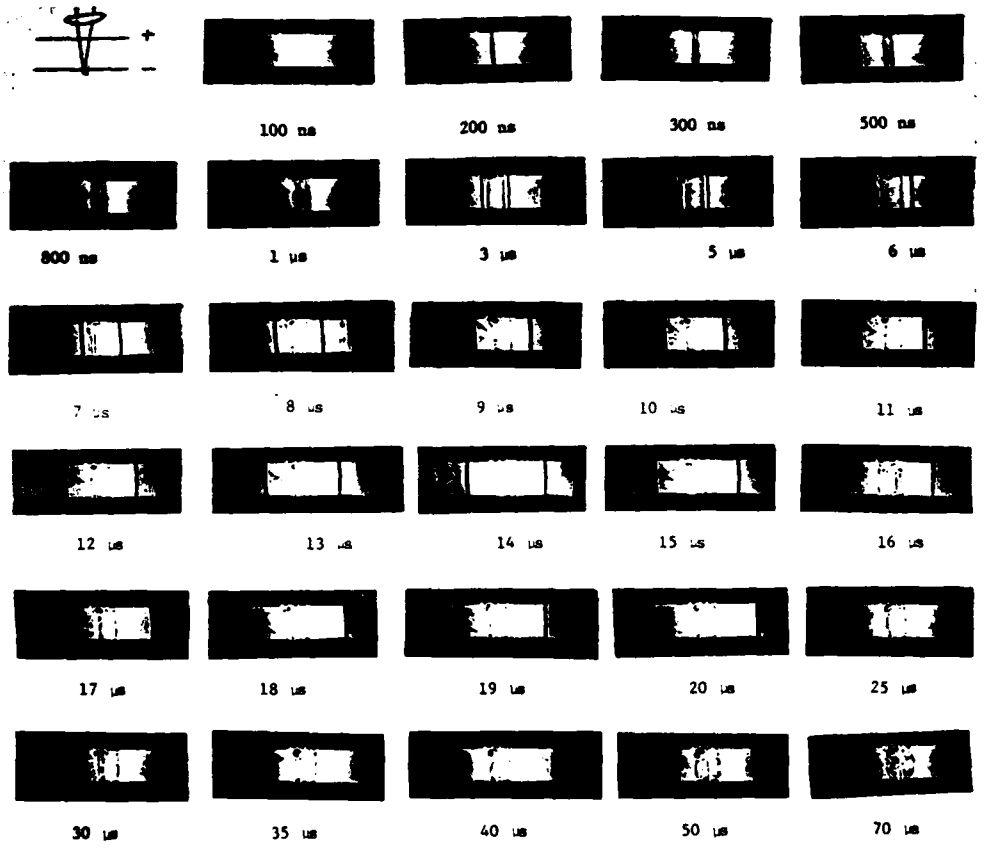

Fig. 13 Time sequence of shadowgrams showing the propagation of shock waves and other turbulent phenomena during and after a laser-triggered event. The arc lasted for 1 µs. The times shown are measured from the time of the laser trigger and are a accurate to about 100 ns due to a timing jitter problem.

C. REFERENCES

[1] P.F. Williams, et. al, "Transient Processes in Laser-Triggered Spark Gaps", pp. 35-37, Second Annual Report on Coordinated Research Program in Pulsed Power Physics, AFOSR Contract No. F49620-79-C-0191 (1981).

[2] W.K. Pendleton and A.H. Guenther, "Investigation of a Laser-Triggered Spark Gap," Rev. Sci. Instr. 36, pp. 1546-1550, (1965).

[3] J.R. Woodworth, C.A. Frost, T.A. Green, "U.V.-Laser-Triggered Switches," 3rd IEEE International Pulsed Power Conference Digest, ed. by T.H. Martin and A.H. Guenther, pp. 154-156, (1981); J.R. Woodworth, C.A. Frost, and T.A. Green, "U.V.-Laser-Triggering of High-Voltage Gas Switches," J. Appl. Phys. 53, pp. 4736-4739, (1982).

[4] For a comprehensive review of laser-triggered switching see A.H. Guenther and J.R. Bettis, "The Laser Triggering of High-Voltage Switches," J. Phys. D. 11, pp. 1577-1613, (1978); and references therein.

[5] A.H. Guenther and J.R. Bettis, "Laser-Triggered Megavolt Switching," IEEE J. Quant. Elect. QE-3, pp. 581-588, (1967).

[6] S.I. Drabkina, "The Theory of the Development of the Channel in Spark Gap Discharge," Zh. Eksp. Teor. Fiz., Pisma pp. 473-493, (1951).

[7] S.I. Braginskii, "Theory of the Development of a Spark Channel," Sov. Phys. JETP 34, pp. 1068-1074, (1958).

[8] M. Ketez, M.R. Barrault, and J.D. Craggs, "Spark Channel Formation," J. Phys. D.: Appl. Phys. 3, pp. 1886-1896 , (1970).

[9] E. Morode, F. Bastien, and M. Bakker, "A Model of the Streamer-Induced Spark Formation Based on Neutral Dynamics," J. Appl. Phys. 50, pp. 140-146, (1979).

[10] T.H. Lee, Physics and Engineering of High Power Switching Devices, Cambridge: Mit Press, pp. 110-112, 135, (1975).

[11] Lasers in Chemical Analysis , ed. by G.M. Hieftje, J.C. Travis, and F.E. Lytle, Humana Press (1981).

[12] V.E. Bondybey and J.H. English, J. Chem. Phys. 74, pp. 6975-6959, (1981).

Project No. 3

Spark Gap Discharge and Erosion Phenomena

(A. Donaldson, C. Yeh, R. Ness
M. Hagler, L. Hatfield, and M. Kristiansen)

A. SUMMARY

The chemical interactions and physical processes occurring in a high energy spark gap with different combinations of gases, electrodes, and insulators have been investigated. The self-breakdown voltage histograms differ significantly for different combinations of materials and change with time. Changes with time of the histograms correlate mainly with changes in the electrode surfaces. The usual statistical-delay-in-the-appearance-of-an-electron model has therefore been reformulated to include the effects of the cathode surface microstructure. The microstructure is assumed to affect the self-breakdown voltage histograms through the effect on impact ionization processes in the filler gas by the enhanced electric field near the cahtode surface microstructures. Experiments to verify the model are in progress.

Erosion rates for hemispherical electrodes made of graphite, copper-graphite, copper-tungsten, brass and stainless steel have been measured in a spark gap filled with air or nitrogren. The electrode erosion rates and mechanisms are highly polarity dependent, so that results for oscillatory and unipolar discharges can be considerably different.

The voltage recovery process in spark gaps seems to be dominated by density variations in the hot gas or possibly the presence of metastables. As a consequence, the basic breakdown model mentioned above seems applicable to the recovery process as well. Voltage recovery measurements are in progress with a test circuit that provides two identical pulses with the same energy and dv/dt so the self-breakdown voltage histograms can be easily compared using the model.

B. SPARK GAP CHEMICAL STUDIES WITH THE MARK I GENERATOR

The chemical interactions and physical processes occurring in a high energy spark gap with different combinations of gases, electrodes, and insulators have been investigated this past year with the Mark I generator (single capacitor, critically damped, RLC discharge; 20-50 kV, 30-50 kA, 45 mC/shot charge transfer). The electrodes studied were rass, graphite, and a tungsten-copper composite (K-33); the insulators were Lexan and Blue Nylon; and the gases were N_2, SF_6, and air. Gas composition was monitored with an on-line mass spectrometer. Optical spectroscopy was used to detect certain elements in the discharge. In cooperation with Project No. 4, the electrode surfaces were studied with scanning electron microscopy, electron spectroscopy for chemical analysis, Auger electron spectroscopy, and x-ray fluorescence. The self-breakdown voltage histograms were examined for different material combinations. A journal article describing much of this work has been accepted for publication [1].

Apart from details, these studies showed measurement of the self-breakdown voltage histogram (probability density function) [2] to be one of the most useful on-line diagnostic techniques. Not only do the histograms display directly an important measure of spark gap performance, they show conclusively that scatter in self-breakdown voltage is significantly different for different combinations of materials and that the scatter for a given combination of materials changes with time. Figure 1 for example, shows the different character of the histograms for four different combinations of materials. An important experimental result was that changes with time of the histograms correlate mainly with changes in the electrode surfaces rather than, for example, changes in the filler gas composition. The results strongly suggest that the filler gas and the insulator material affect the self-breakdown voltage scatter primarily by through chemical reactions with, or deposition of a coating on, the electrodes. Thus, it became apparent that a model was needed which would correctly incorporate the physical processes occuring at the cathode of the spark gap.

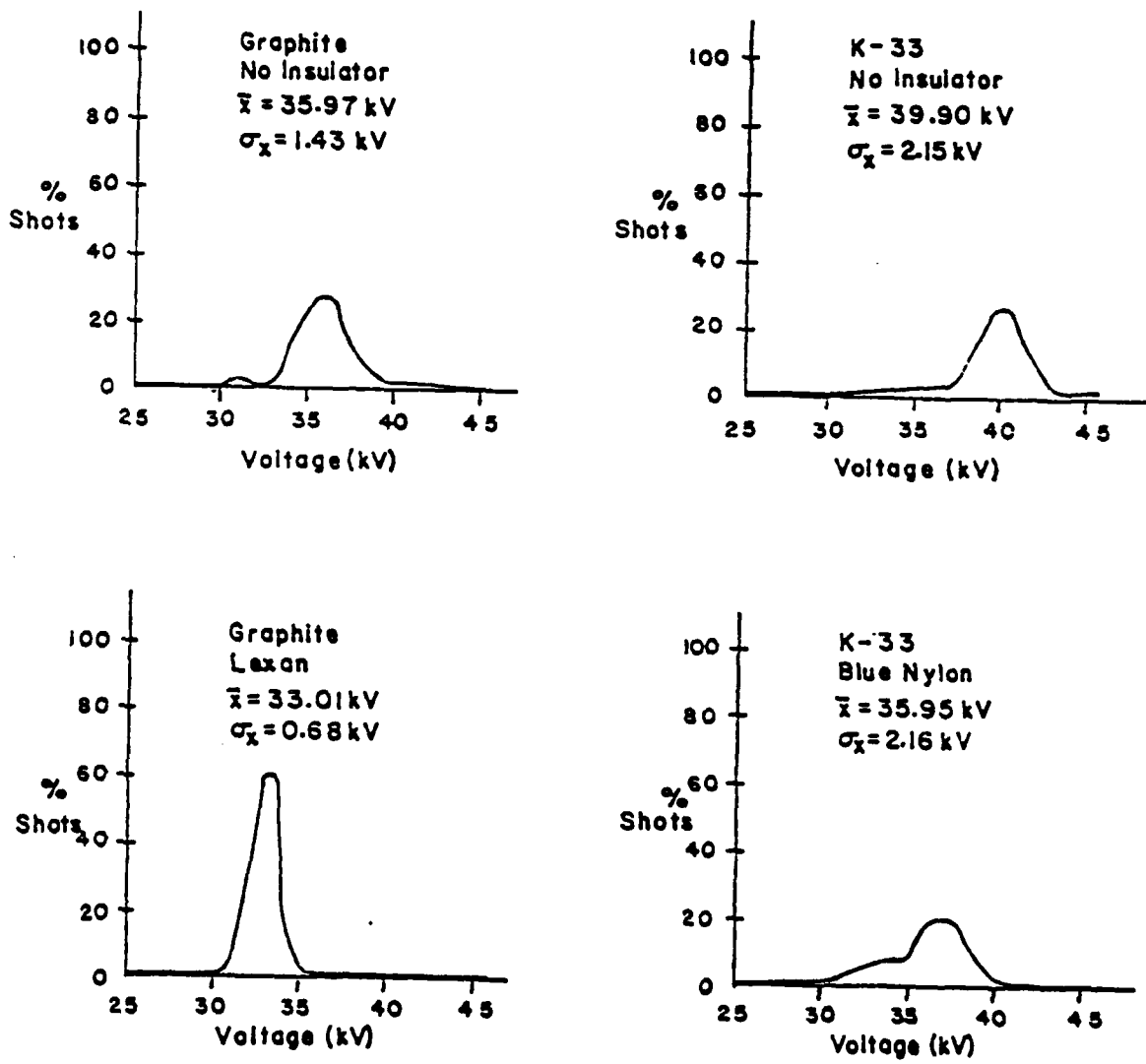

Fig. 1 Mark I Self-Breakdown Voltage Distributions After 10,000 Shots

C. A SPARK GAP PERFORMANCE MODEL

1. Background Theory

The effect of the electrode surface structure on the self-breakdown voltage of gas discharges [3], even in spark gaps [4], is well documented. However, much of the previous work considers the effect of the electrode surface micro-structures that result from machining and/or polishing the electrodes during their preparation for use rather than the micro-structure that evolves from chemical and physical processes that occur during use. Furthermore, the analyses are mainly qualitative. An exception is the work of Avrutskii et al. [5,6] who 1) introduced a simple model that permits calculation of a probability density function for the self breakdown voltage in terms of parameters characteristic of the electrode surface microstructure, and 2) compared calculations from the model with experimental data for stainless steel and copper electrodes in air-filled spark gaps.

The model is based upon Townsend breakdown theory [7], which should be valid for ordinary self breakdown operation of the gap. (Townsend theory fails only when pulses are applied to the gap sufficiently fast to overvoltage it by more than about 20% [7].) The mechanism through which the electrode surface microstructure is assumed to affect the voltage self-breakdown probability density function is the effect on impact ionization processes in the filler gas by the enhanced electric field near the electrode surface

irregularities. In the specific model development given by Avrutskii et al., a surface irregularity is modeled as a tall, slender, prolate semiellipsoid of revolution that produces a local enhancement of the electric field. The Townsend condition, modified to include field enhancement, for a self maintained discharge is then used to calculate the breakdown voltage, V, as a function of the height, h, of the prolate semiellipsoid microprojections: V = V(h). By assuming that an actual electrode surface can be modeled as a large number of separate microprojections with a distribution of heights and by assuming that breakdown is initiated by the random appearance of an electron at the site of a microprojection of some particlular height, then V(h) is used to convert the probability distribution function for the microprojection heights into a probability distribution function for the self-breakdown voltage, V.

2. Model Development and Verification

The model described above has undergone significant theoretical developement and experimental verification during the last year. summary of the more important results is given below:

a. The model for breakdown was reformulated in terms of the field enhancement factor rather than the actual dimensions of the surface microstructure. Several different approximations of the field enhancement factor were used, as well as one "exact" representation which is valid for prolate

ellipsoidal surface protrusions.

b. Equation (1), below, was derived, which enables one to calculate the field enhancement probability distribution ($F_M(m_t(v))$ directly from the experimentally measured voltage probability density ($p_V(v)$), its distribution function ($F_V(v)$), and the charging rate V_o', which are all easily measureable quantities.

$$F_M(m_t(v)) = 1 - \frac{ev_o' p_V(v)}{i_e F_V(v)} \qquad (1)$$

$m_t(v) \equiv$ the field enhancement factor required to satisfy the Townsend breakdown criteria at a given voltage v

$e \equiv$ electron charge

$i_e \equiv$ primary electron current from the cathode.

This implies that, with very little data processing of the self-breakdown voltages, an estimate of typical field enhancement factors and thus a typical surface structure, can be obtained.

The data acquisition system shown in Figure 2 was installed and the computer software needed to acquire, store, and process the self-breakdown voltage distribution data has been developed and tested on an experimental run using the Mark I generator. Included in the software are programs

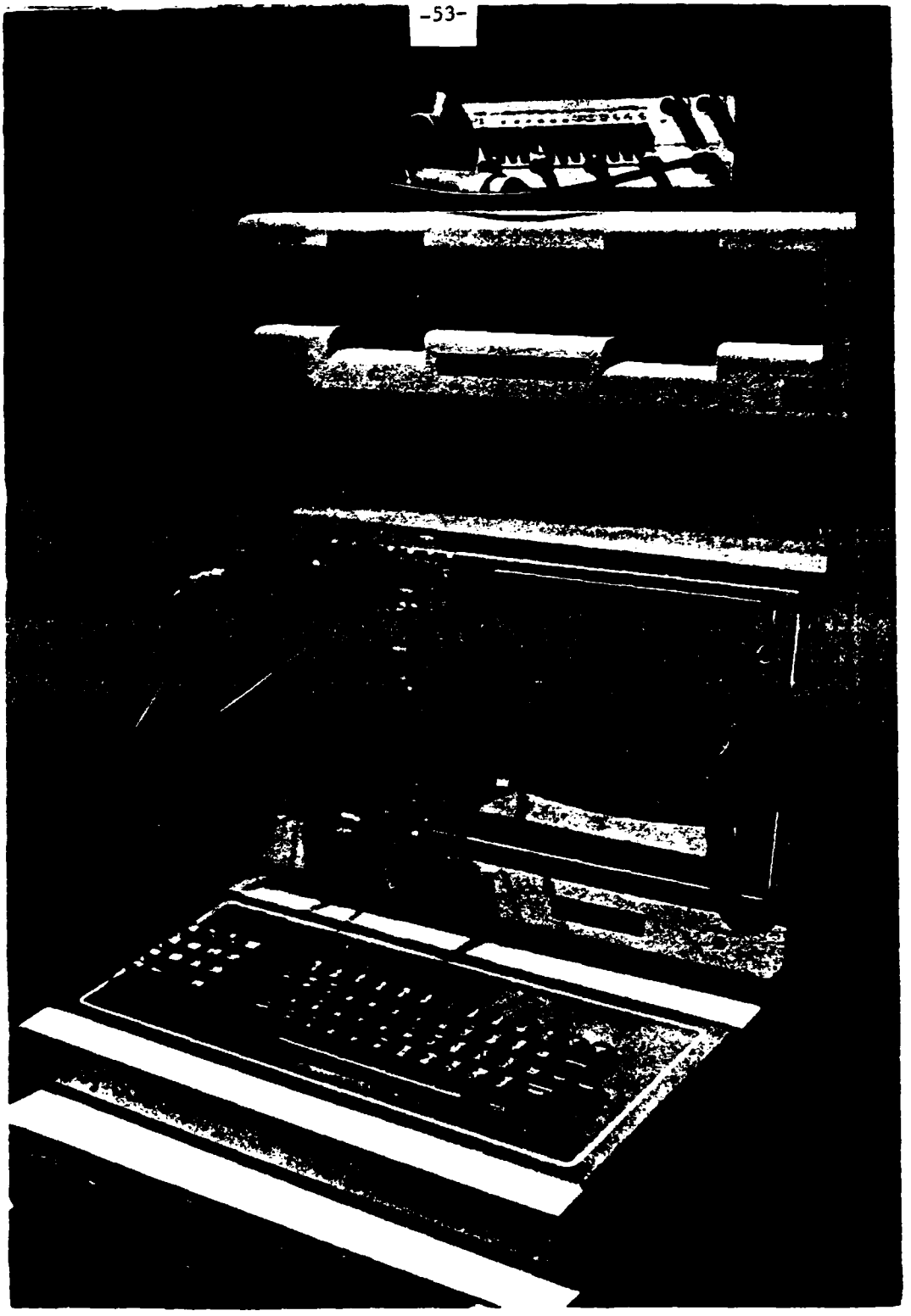

Fig. 2 On-Line Data Acquisition and Processing Hardware for Mark I-IV

to calculate the various moments of the voltage distribution function as well as subroutines to plot the distributions and their density functions. Another program is currently being tested which will calculate the field enhancement density distributions of Equation (1).

d. The main physical mechanism assumed by the model to account for the spread in the self-breakdown voltage distribution function, namely the "waiting" for the appearance of an electron at the cathode has been verified experimentally. This was accomplished by running the Mark I generator with and without the presence of a UV source, focused, on the cathode. With a UV source, one effectively guarantees the appearance on numerous electrons at the cathode. Thus, if the physics of the model is valid, the voltage distribution function should become quite narrow and shift to the lower end of the original distribution, produced without UV illumination. The results from this experiment, shown in Figure 3, indicate that this quite dramatic process did indeed occur. In addition, an isolated "bump" in the distribution occurred at voltages as low as 40% of the mean, which indicates that a second and most likely separate breakdown mechanism is also occurring.

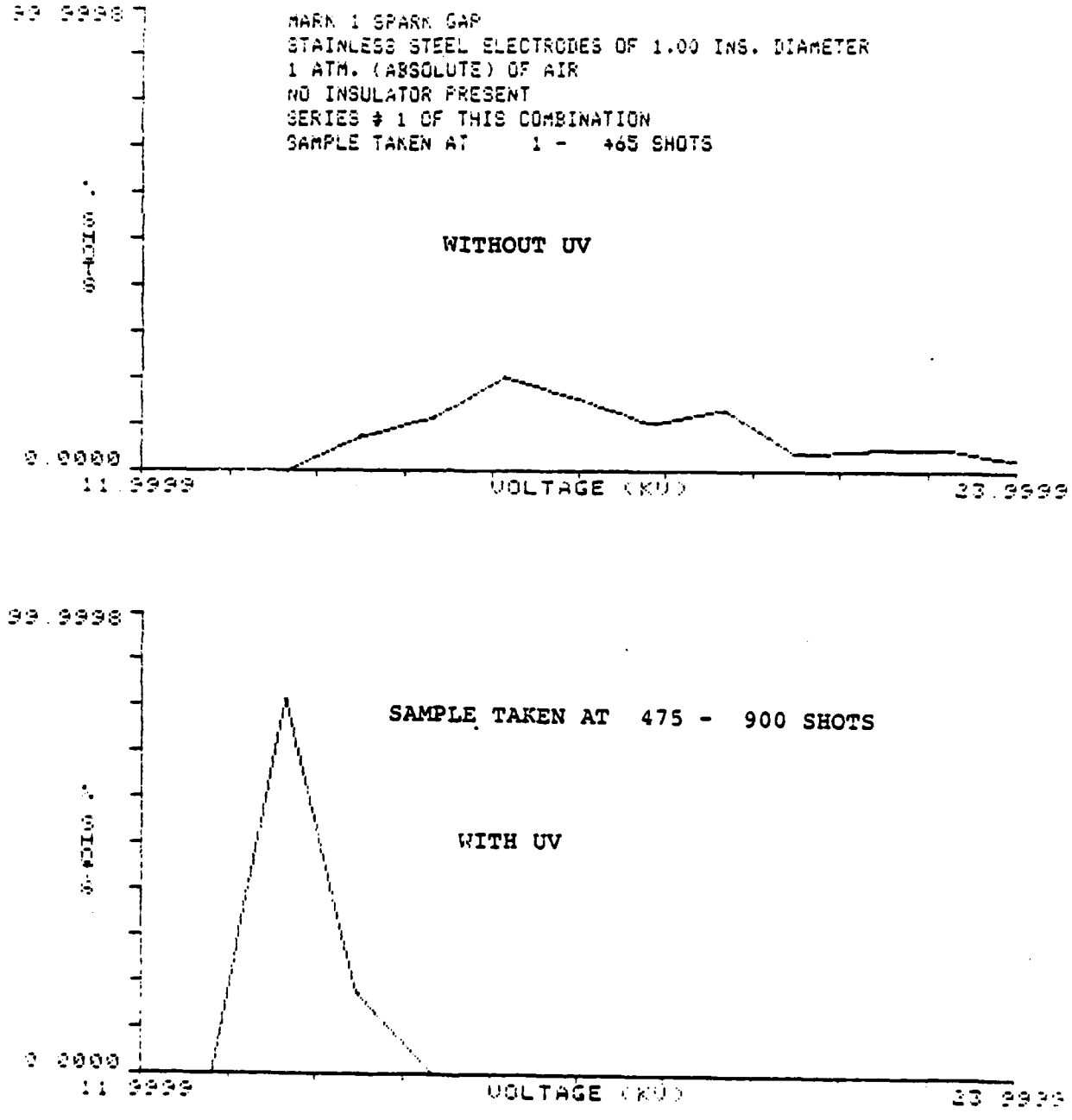

Fig. 3. **Self Breakdown Voltage Distribution of Stainless Steel Electrodes in Nitrogen With and Without UV Illumination**

3. Model Implications

Implications of the model include increasing width of the self-breakdown voltage probability density function with increasing pressure and changes in the width of the probability density function as the secondary emission characteristics of the cathode are modified by, for example, oxide and nitride coatings and/or deposits from the insulator. The model indicates that a narrow self-breakdown voltage histogram requires selection of materials combinations that ensure sufficiently sharp and sufficiently numerous field enhancement sites, operation at lower pressure, and relatively slow application of voltage to the gap. In addition, and perhaps most importantly, the model provides an extremely useful, and physically reasonable, framework from which the properties of spark gaps under a wide variety of experimental conditions may be evaluated. This is accomplished by isolating the most fundamental parameters which affect spark gap performance, namely the ionization and attachment coefficient of the gas and the secondary emission properties of the electrode surface. An example of the relationship of these fundamental parameters to the myriad of possible parameters affecting spark gap performance is shown in Figure 4.

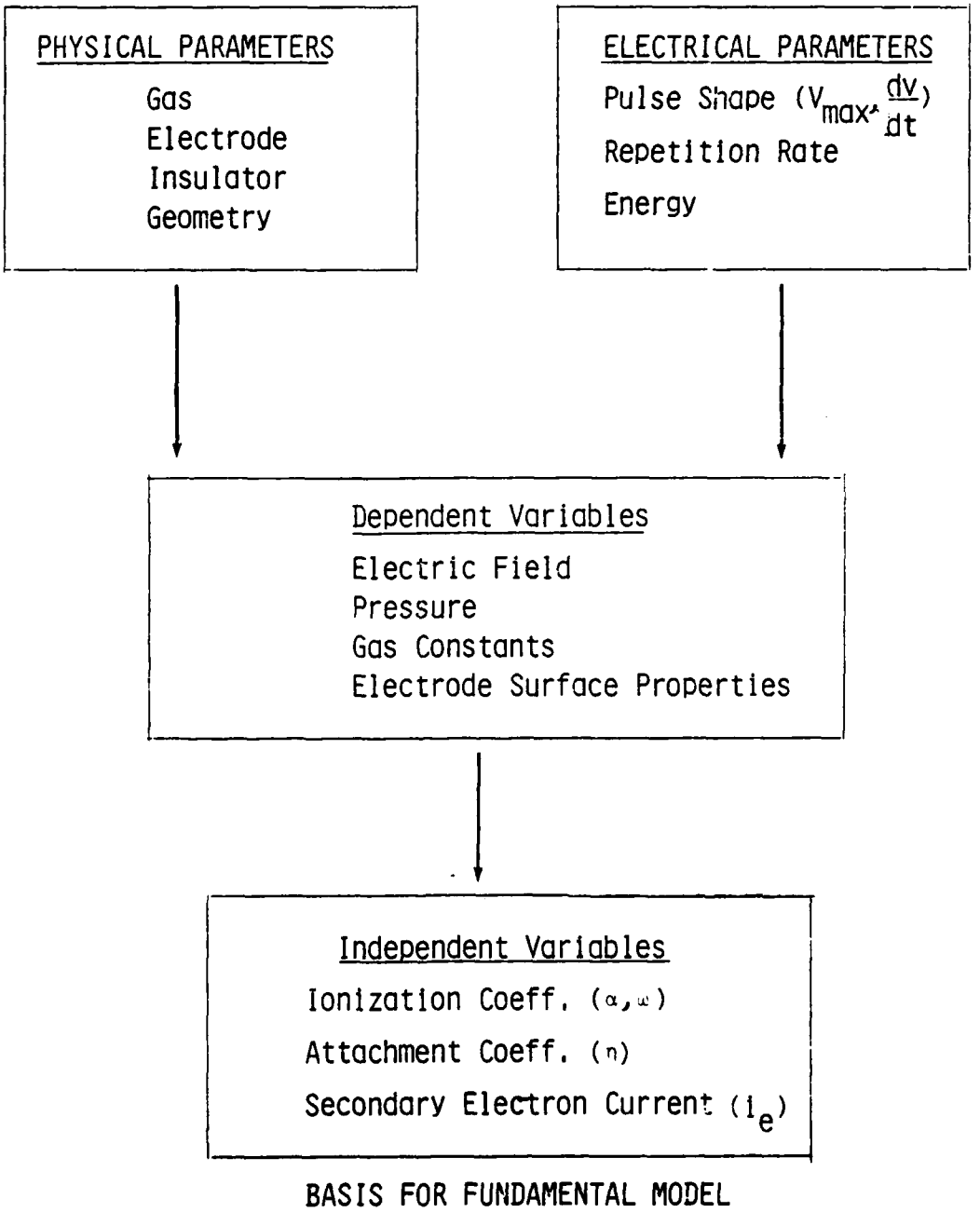

Fig. 4 Relation of Various Sparkgap Parameters

D. EROSION RESULTS

Electrode erosion measurements have continued on the Mark II generator. A paper entitled "Electrode Erosion in a High Power Spark Gap" was presented at the 15th Power Modulator Symposium in June 1982 [8] and a M.S.E.E. thesis on the same subject was completed in August [9]. A summary of the important results are given in the attached paper.

At the request of Maxwell Laboratories, another tungsten composite (Elkonite) was tested in order to provide a comparison with the more expensive K-33, previously tested. Preliminary results indicate that, contrary to popular opinion, Elkonite gives erosion rates similar to K-33 in the parameter range tested.

E. VOLTAGE RECOVERY

Several papers indicate that the voltage recovery process in spark gaps could be dominated by the density variation in the hot gas or [10-22] or the presence of metastables [22]. Although some have held that the recovery process is dominated by the presence of space charge, rather straightforward calculations of the recombination and diffusion times seem to indicate that this is not the case. As a consequence, the basic breakdown model discussed above seems applicable to the recovery process as well. Data about properties of N_2 relevant to recovery has been exchanged with personnel on Projects Nos. 8 and 9 with Dr. Kunhardt's group in our department. The Mark I generator described

in the Second Annual Report pp. 70,71 (ref. [23]) modified to operate at a higher rep-rate (1 pulse per 7 sec.) so that sufficient data to determine the recovery voltage statistics can be collected in a resonable time. The test circuit, shown in Figure 5, was designed and built to provide two identical pulses with the same energy and dv/dt so that the self-breakdown distribution could be easily compared using the model described earlier.

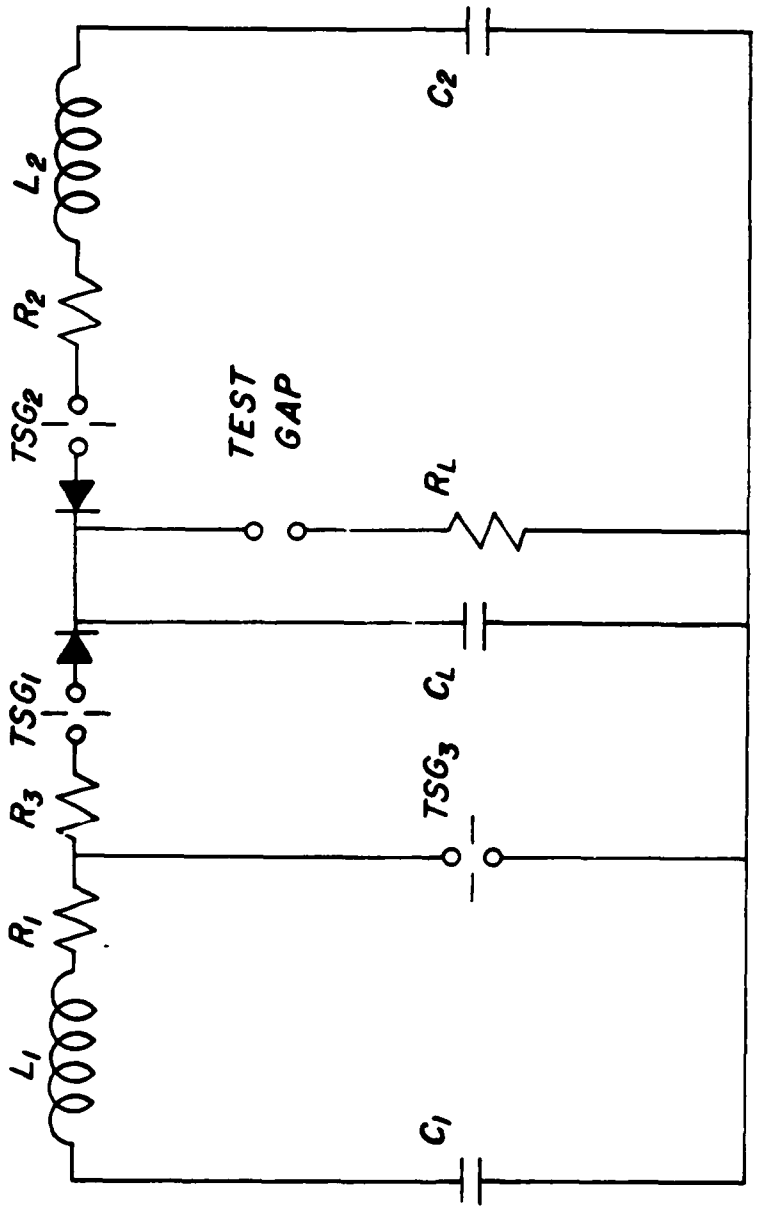

Fig. 5 Modified Test Circuit for Recovery Studies on Mark I

E. REFERENCES

[1] L.B. Gordon, M. Kristiansen, M.O. Hagler, H.C. Kirbie, J.N. Marx, R.M. Ness, and L.L. Hatfield, "Material Studies in a High Energy Spark Gap," accepted for publication in the IEEE Transactions on Plasma Science.

[2] M.T. Buttram, "Stability of a 100 kV Self-Firing Spark Gap," Report LSAND81-1552 on U.S. Department of Energy Contract DE-AC04-76-DP00789, Pulsed Power Applications Division-4253, Sandia National Laboratories, Albuquerque, NM 87185, 1981.

[3] See, for example, B.A. Goryunov, "Dielectric Strength of Compressed Sulfur Hexafluoride and the Electrode Material and Surface Structure," Sov. Phys. Tech. Phys. 20, 66 (1975).

[4] Juan J. Ramirez, "Effect of Electrode Surface Conditions on the Self-Breakdown Strength and Jitter of a High-Pressure Pulsed Gas Switch," J. Appl. Phys. 47, 1925 (1976).

[5] V.A. Avrutskii, G.M. Goncharenko and E.N. Prokhorov, "Effect of Electrode Roughness on the Electrical Strength of Compressed Gases," Sov. Phys. Tech. Phys. 18, 386 (1973).

[6] V.A. Avrutskii, "Effect of Electrode Roughness on Breakdown Voltage," Sov. Phys. Tech. Phys. 18, 389 (1973).

[7] E.E. Kunhardt, "Electrical Breakdown of Gases: The Pre-breakdown Stage," IEEE Trans. Plasma Sci. PS-8, 130 (1980).

[8] A.L. Donaldson, et. al., "Electrode Erosion in a High Power Spark Gap," Proceedings of the IEEE 15th Power Modulator Symposium, p. 84, June (1981).

[9] A.L. Donaldson, "Electrode Erosion Measurements in a High Energy Spark Gap," MS Thesis, Texas Tech University, August 1982.

[10] J.D. Cobine and G.A. Farrall, "Recovery Characteristics of Vacuum Arcs," AIEE Winter General Meeting, New York, NY January 28 - February 2, 1962.

[11] F.L. Curzon and M.S. Gautam, "The Influence of Electrode Heat Transport in Spark Recovery," Brit. J. Appl. Phys., 18, 79 (1967).

[12] E.P. Bel'kov, "Dielectric Strength of Spark Gaps Following Strong Current Pulses," Sov. Phys. Tech. Phys. 19, 1210 (1975).

[13] R.J. Churchill, A.B. Parker and J.D. Graggs, "Measurement of Reignition Voltage Characteristics for High Current Spark Gaps in Air," J. Electron. Contr. 11, 17 (1961).

[14] R.J. Churchill, "Reignition of Freely Recovering Spark Channels in Hydrogen," Canadian Journal of Physics 41, 610 (1963).

[15] E.P. Bel'kov, "Gas Cooling and Electric Strength Recovery After A Spark Discharge," Sov. Phys. Tech. Phys. 16, 1321 (1972).

[16] F.W. Crawford and H. Edels, "The Reignition Voltage Characteristics of Freely Recovering Arcs," IEE Paper No. 3185 S, 202 (1960).

[17] G.A. Farrall and J.D. Cobine, "Recovery Strength Measurements in Arcs From Atmospheric Pressure to Vacuum," IEEE Trans. Power Apparatus and Systems, PAS-86, 927 (1967).

[18] H. Edels and F.W. Crawford, "Arc Interruption - Part 2. Theory and Experiment on Gap Recovery," J.I.E.E., 88 (1957).

[19] E.P. Bel'kov, "Operation of Controlled Spark Gaps for a High Resolution Frequency of Powerful Current Pulses," Translated From Pribory i Tekhnika Eksperimenta, 1, 230 (1972).

[20] G.D. McCann and J.J. Clark, "Dielectric-Recovery Characterisitics of Large Air Gaps," Trans. Electrical Engineering, 62, 45 (1943).

[21] G.A. Farrall, "Recovery of Dielectric Strength After Current Interruption in Vacuum," IEEE Trans. on Plasma Sci. PS-6, 360 (1978).

[22] M.M. Pejovic and B. Dimitrijevic, "Electrical Breakdown Induced by Long-Lived Metastable States in Nitrogen," J. Phys. D: Appl. Phys. 15, L 87 (1982).

[23] Second Annual Report on Coordinated Research Program in Pulsed Power Physics, December 1, 1981, AFOSR Contract #F 49620-79-C-0191, Texas Tech University, Department of Electrical Engineering, Lubbock, TX.

APPENDIX 1

ELECTRODE EROSION IN HIGH POWER SPARK GAPS*

A.L. Donaldson, R. Ness, M.O. Hagler, and M. Kristiansen
Plasma and Switching Laboratory
Department of Electrical Engineering
P.O. Box 4439
Texas Tech University
Lubbock, Texas 79409

Summary

The erosion rate for hemispherical electrodes 2.5 cm in diameter made of graphite, copper-graphite, copper-tungsten, brass, and stainless steel has been examined in a spark gap filled with air or nitrogen at 1 atmosphere. The electrodes were subjected to 50,000 unipolar pulses (25 μs, 4-25 kA, 5-30 kV, .1-.6 coul/shot) at repetition rates ranging from 0.5 to 5 Hz. A conditioning process, indicated by a shifting and narrowing of the self-breakdown voltage distribution, and several spectacular surface patterns (craters, nipples and dendrites) up to .6 cm were observed. Anode erosion rates varied from a slight gain for several materials in nitrogen to 5μcm^3/coul for graphite in air. Cathode erosion rates of .4 μcm^3/coul for copper-tungsten in nitrogen to 25 μcm^3/coul for graphite in air were also measured.

Introduction

High energy spark gaps capable of lasting for 10^8 shots are seen as one of the critical components in pulsed power systems used for nuclear isotope separation, electromagnetic pulse simulation and thermonuclear fusion reactors. The performance of a pressurized spark gap as a high energy rep-rated switching device is characterized by the following parameters: hold-off voltage, recovery time, delay time, and jitter.[1] The switch lifetime is determined by the degradation of these parameters resulting from electrode erosion, gas decomposition and disassociation and insulator damage occurring as energy is dissipated in the switch.[2]

The purpose of this study was to measure the erosion rate of different electrode materials as a function of current in order to generate a data base from which theoretical models describing the complex erosion porcess could be developed and verified. In addition, the self-breakdown voltage distributions and the electrode and insulator surfaces were examined in an effort to further define the erosion characteristics and to reduce the material parameter space used in future studies.

Experimental Apparatus

Spark Gap

The spark gap shown in Fig. 1 was designed to facilitate frequent electrode and insulator replacement and to allow for accurate control over electrode alignment and gap spacing. The electrodes are composed of three parts: the brass support (which also serves as a channel for air flow), the brass adapter and the electrode tip. The hemispherically shaped electrode tips are 2.5 cm in diameter and are made from the various materials studied. The Lucite inserts provide protection for the main gap housing and also provide a surface which gives a permanent history of the discharge debris which is deposited on the walls.

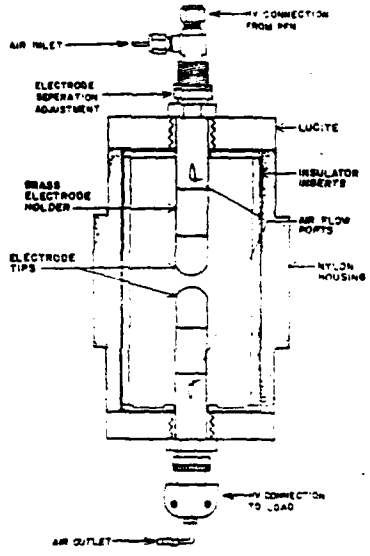

MARK I SPARK GAP

Fig. 1. Spark gap for erosion studies.

Test Circuit and Conditions

Numerous experiments have measured erosion rates for high current (10-800 kA) oscillatory discharges, and a few exist for high current (> 10 kA) unipolar discharges in brass and copper.[3-9] Because of the nature of many switching applications, a test circuit capable of delivering a unipolar pulse was chosen for this study. The circuit, shown in Fig. 2, consists of a six section type E pulse forming network (PFN) which is resistively charged to the self-breakdown voltage of the spark gap by a 30 kV, 1 Amp constant voltage power supply.[10] When the gap breaks down, the PFN is discharged into a matched 2 Ω high power load. The wave form of the discharge current is shown in Fig. 3. The test conditions are summarized below:

Voltage:	≤ 30 kV
Current:	≤ 25 kA
Total Capacitance:	21 μF
Charge/shot:	≤ .6 coul
Energy/shot:	≤ 9 kJ
Pulse width:	≈ 25 μs
Rep-rate:	.5-5 Hz
Gas:	Air or N_2
Pressure:	1 Atm (absolute)
Flow rate:	≈ 1 Gap volume every 5 sec.
Gap spacing:	≤ .8 cm

* This work was supported by the Air Force Office of Scientific Research

CH1785-5/82/0000-0084$00.75 © 1982 IEEE

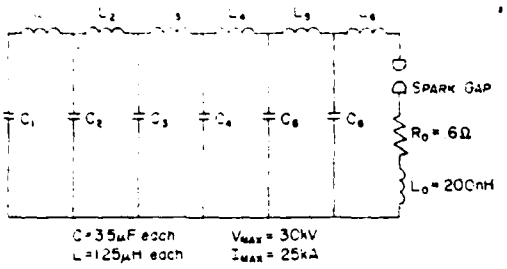

PFN Equivalent Circuit

Fig. 2. Test circuit for erosion studies.

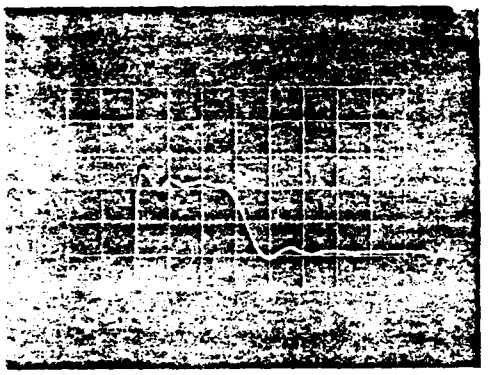

Fig. 3. Discharge current waveform (time base is 10μs/div).

Materials Tested

The electrode materials tested were: brass (SAE 660), stainless steel (304), copper-tungsten (K-33),[11] graphite (ACF-10Q), and copper-graphite (DFP-1C).[12] This combination allowed for: 1) a comparison with existing data given for brass and stainless steel,[13] 2) utilization of materials thought to give good spark gap performance,[14] and 3) the testing of one new material, namely copper-graphite. The major properties of the materials tested are given in Table I.

Table I. Properties of Electrode Materials Tested

Material	Composition	Tmp	ρ	λ	c
B	Cu 83%, Pb 7%, Sn 7%, Zn 3%	980	8.7	.29	.09
SS	Fe 69%, Cr 19%, Ni 9%, Mn 2%	1430	8.0	.04	.14
CT	W 67%, Cu 33%	W-3400 Cu-1080	13.5	NA	NA
G	C 100%	4200	1.83	.21	.20
CG	C 84%, Cu 16%	Cu-1080	2.97	.42	.21

Tmp: Melting temperature, °C (graphite sublimes); ρ: Density, g/cm³; λ: Thermal conductivity, cal/cm-sec-°C; c: Specific heat, cal/gm-°C; B: Brass, SS: Stainless-steel, CT: Copper-tungsten, G: Graphite, CG: Copper-graphite.

Experimental Results

Erosion Characteristics

The change in mass of the [illegible] after 30,000 shots was measured [illegible] balance with a precision of ± 5 mg. The [illegible] test conditions and resulting erosion rates are given in Table II. Although many authors report erosion rates in μgm/coul, the actual factor determining [illegible] lifetime is the volume eroded, hence the units [illegible] coul. The results for brass are discussed later because of the failure of the electrodes due to [illegible] material extraction.

Table II. Electrode Erosion Rates

Electrode	Gas	$\bar{V}$	Q	CE	AE
SS	Air	10.3	.21	1.8	1.2
SS	Air	10.6	.22	1.5	1.0
SS[1]	Air	18.0	.37	1.6	1.5
SS[2,3]	N_2	7.8	.16	0.7	+0.0
CT	Air	9.5	.20	1.2	0.4
CT	Air	11.5	.24	1.2	0.3
CT	Air	18.0	.37	1.2	0.5
CT[3]	N_2	14.8	.31	0.4	0.4
CG	Air	8.3	.17	8.5	0.4
CG	Air	16.2	.34	8.6	+0.0
CG[3]	Air	11.4	.24	7.2	0.0
CG[3]	N_2	14.8	.31	13.5	0.8
G	Air	9.2	.19	24.1	3.5
G	Air	10.6	.22	24.6	3.6
G	Air	16.0	.33	23.5	5.0
G[3]	N_2	12.9	.27	15.7	0.0

$\bar{V}$: Average Voltage, kV; Q: Charge/shot, coulombs; CE: Cathode erosion, 10^{-3}cm³/coul; AE: Anode erosion, 10^{-3}cm³/coul; 1: 32,000 shots, 2: 22,000 shots, 3: Experiment performed at approximately 85% of maximum power; + indicates a gain in mass was measured.

Material: A ranking of the erosion rate for each material from smallest to largest is:

Cathode: Copper-tungsten, stainless steel, copper-graphite, graphite
Anode: Copper-graphite, copper-tungsten, stainless steel, graphite

As expected, the copper-tungsten composite gave the lowest erosion rate. Somewhat suprising, however, was the excellent performance of the stainless steel and the poor performances of the graphite materials as cathodes. From the results given for stainless steel in a pulsed discharge it is seen that the high erosion rate reported by Grueber and Suess for an oscillatory discharge was primarily due to its poor performance as an anode material.[15] The studies for graphite were done at a much slower repetition rate (0.03 Hz) and thus, gave significantly lower erosion rates.[16]

Polarity: Unlike previous experiments where oscillatory current conditions masked any polarity effect, a distinct difference in the cathode and anode erosion rate and most likely the erosion mechanisms themselves was observed for a unipolar pulse. The ratio of cathode to anode erosion varied from 1.5 for stainless steel to 16 for copper-graphite. Carder reported ratios of 2.5 to 5 for brass under similar conditions.[17]

Cathode erosion rates are plotted in Fig. 4 and show a linear dependence upon the quantity $Q = \int i dt$ over the entire range of currents. This indicates that the main source of energy producing molten material and subsequent vaporization and droplet ejection is the arc and not localized i^2R losses in the electrode material.

Anode erosion rates are widely scattered with some anodes experiencing a gain in mass due to material transfer from the cathode to the anode. For graphite

and copper-tungsten, an anode erosion rate approximately proportional to $Q^{1.5}$ was observed.[18]

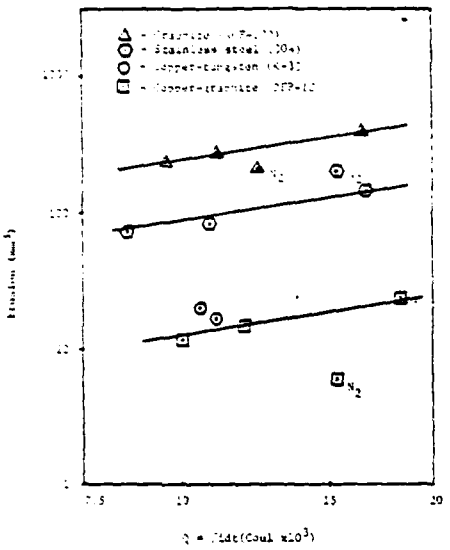

Fig. 4. Cathode erosion rates for different electrode materials.

Gas: The erosion rate for copper-graphite increased slightly in N_2, whereas the rates for all the other materials were smaller by a factor of 2-3. However, because of other factors effecting spark gap performance, namely the voltage distribution and the coating of the insulator surfaces, the use of pure N_2 is not recommended.

Surface Conditions

The surface of the electrode tips and the insulator inserts were examined after 50,000 shots. The analysis techniques utilized were Auger electron spectroscopy (AES), scanning electron spectroscopy (SEM), and optical photography and microscopy. Some of the more general results are presented here with a more thorough discussion to be given in another paper.

Brass: The surfaces of the brass electrodes are shown in Fig. 5. Large scale melting is evident with dendrites or metallic protusions up to .6 cm in height existing on the surface. The self-breakdown voltage for these electrodes dropped from 20 kV to 30 kV in approximately 2000 shots as a result of the macroscopic field enhancement. In addition, the voltage distribution was characterized by a series of "jumps" due to large particles being blown off the ends of the protusions. Originally it was thought that the material being "pulled out" of the bulk electrode was lead but AES analysis indicated the surface is composed primarily of copper and oxygen with a noteable absence of zinc. From these results and those found by Marchesi and Maschio it is quite obvious that brass is limited in its use at higher levels of charge transfer.[19]

Cathode: The cathodes for the remaining materials are shown in Fig. 6. Considerable erosion has taken place, especially on the graphite materials, and the stainless steel and copper-tungsten cathodes show evidence of severe melting. All the cathodes showed a distinct tendency to form a large scale crater whose diameter increases with increasing gap spacing and current. The idea of using a cathode cup in spark gaps is not new, but it is interesting that the electrode erosion results in this shape.[20,21]

Anode: The anodes corresponding to the cathodes shown in Fig. 6 are shown in Fig. 7. The copper-graphite anode erosion pattern consists of a ring band .8 cm wide located .3 cm from the center of the electrode. This pattern is consistent with the work of Johnson and Pfender which showed that an annular-shaped attachment region of high current density will exist at the anode.[22] The copper-tungsten and stainless steel anodes indicate that melting and vaporization has taken place over the entire surface. Like the cathode, the diameter of the anode erosion region increases with increasing current.

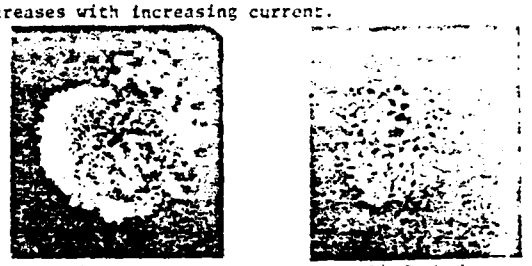

a) Anode b) Cathode

Fig. 5. Surface of brass electrodes after 50,000 shot

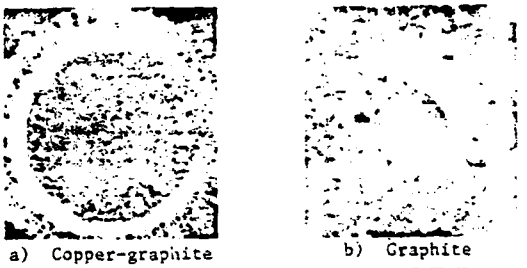

a) Copper-graphite b) Graphite

c) Copper-tungsten d) Stainless steel

Fig. 6. Surface of cathodes after 50,000 shots.

a) Copper-graphite b) Graphite

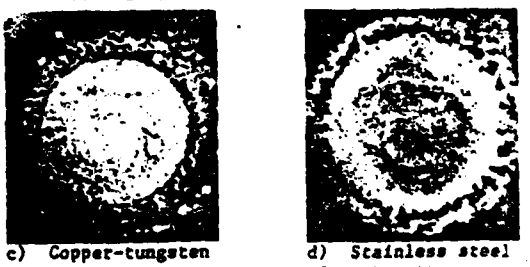

c) Copper-tungsten d) Stainless steel

Fig. 7 Surface of anodes after 50,000 shots.

Insulator: The insulator surfaces are covered by a coating of recondensed electrode material. The one noteable exception was for graphite electrodes in air in which no coating was found on the insulator surface. A dramatic difference is seen in Fig. 8 for the case of graphite run in nitrogen. The entire surface of the insulator is covered with a thick coating of fluffy black material which is thought to consist of monoatomic layers of amorphous carbon.[23]

Fig. 8 Lucite insulators inserts for graphite electrodes in air and nitrogen.

All the insulators were covered with solid particles 10-100 μm in size scattered within a 5 cm band centered on a plane passing through the center of the gap and parallel to the electrode surfaces. This indicates that a considerable portion of the solid or molten material is ejected parallel to the electrode surfaces. Although the mechanism for this ejection is not fully understood, similar results have been reported in vacuum arcs.[24] A typical particle which was found on the insulator surface is shown in Fig. 9.

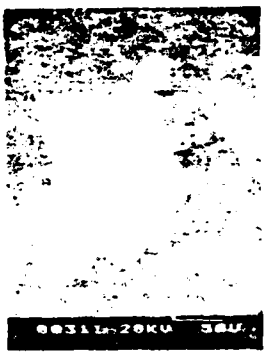

Fig. 9 A stainless steel particle 50μm in diameter on the surface of the lucite insulator insert.

Self-breakdown Voltage Distribution

The self-breakdown voltage of the spark gap was recorded continuously for the first 2000 shots and thereafter was sampled at intervals of 10,000 shots. A sample of approximately 400 shots was taken and used to calculate the mean ($\bar{V}$) and the standard deviation (σ_V) of the self-breakdown voltage.

Material: The standard deviations for different electrode materials are shown in Fig. 10 and 11. In an air atmosphere the graphite electrodes have the smallest σ_V, and therefore, the most narrow distribution of breakdown voltages. This combination is followed by copper-graphite, stainless steel, and copper-tungsten, respectively. Examination of the electrode surfaces with SEM indicated a direct relationship between the width of the distribution and the field enhancement due to the different microscopic surface conditions for each material.

Shot Number: In both air and nitrogen the mean decreases 5-20% during the first 15,000 shots and then increases at different rates, depending on the electrode material. This increase in $\bar{V}$ is a result of the electrode erosion producing an increase in the gap length. Also, in Fig. 10, it is seen that except for the case of stainless steel σ_V remains fairly constant after 20,000 shots. This suggests a conditioning process during the first 10-20,000 shots where the tip of the electrode is worn away and the electrode surface conditions required to initiate a discharge become more uniform. It is thought that the conditioning process for stainless steel occurs on a larger time scale, and thus, was not fully completed after 50,000 shots.

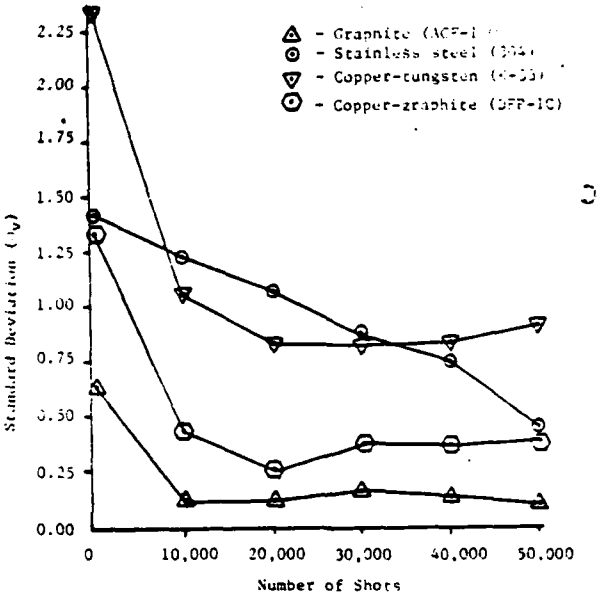

Fig. 10 The standard deviation of the self-breakdown voltage vs. shot number for different electrode materials in air.

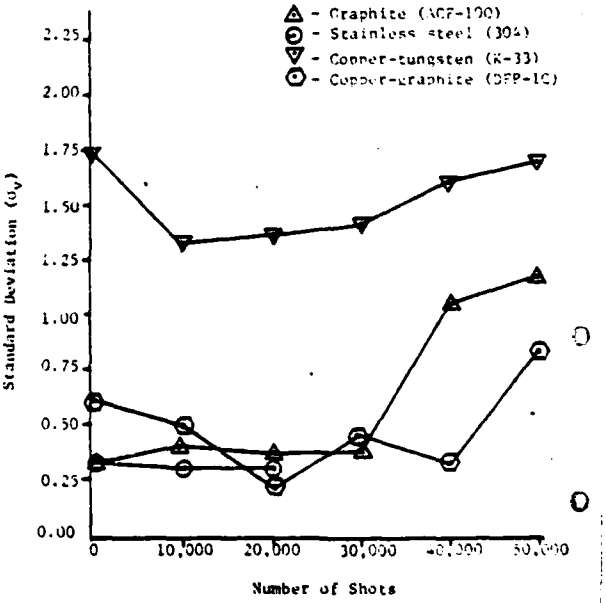

Fig. 11 The standard deviation of the self-breakdown voltage vs. shot number for different electrode materials in nitrogen.

Gas: Data from the same experiments in a nitrogen atmosphere, shown in Fig. 11, indicate that the best electrode materials for a narrow distribution are the graphite composites. The large changes in σ_v for both graphite and copper-graphite are due to low voltage dropouts where the breakdown was often as low as 50% of the mean. These dropouts occur primarily in nitrogen with increasing frequency after 20-30,000 shots. The graphite electrodes were examined after the experiment and a macroscopic growth was found on the anode which may have caused the dropouts. These results, as well as those obtained by Affinito et.al. indicate that the combination of graphite and nitrogen should be avoided.[25]

Conclusion

The erosion rates and self-breakdown voltage distributions were determined for several materials utilized in high energy spark gaps. The results from these preliminary studies have led to the following conclusions:

1) The electrode erosion rates and mechanisms are highly polarity dependent, and thus, results for oscillatory and unipolar discharges can be considerably different.

2) A large amount of the erosion occurs in the form of solid and molten material which is removed parallel to the electrode surface.

3) Cathode erosion rates are proportional to the total amount of charge transferred.

4) Stainless steel may be an economical replacement for copper-tungsten composites as a cathode material.

5) Graphite composites can give narrow self-breakdown voltage distributions but have very high cathode erosion rates.

6) The stability of the self-breakdown voltage is dependent upon electrode micro-surface structure which is a distinct property of the electrode material.

7) Certain electrode-gas combinations lead to "dropouts" or voltage breakdown as low as 50% of the mean. One of the worst of these combinations was graphite and pure nitrogen.

Acknowledgements

The authors wish to express their sincere appreciation to the following people for their various contributions to this work and its presentation: Dr. Allen Bowling, Sam Prine, Dr. Lynn Hatfield, George Jackson, Ken Rathbun, Brian Maas, Aamer Shauket, Bob Conover, Pat Darden, Don Johnson, Marie Byrd, Sharon Lipscomb, and the photography crew at Texas Tech University Engineering Services.

References

1) Lloyd B. Gordon, dissertation (Texas Tech Univ., 1982) (unpublished).
2) L.B. Gordon, M. Kristiansen, M.O. Hagler, H.C. Kirbie, R.M. Ness, and L.L. Hatfield, "Material Studies in a High Energy Spark Gap," submitted to the IEEE Transactions on Plasma Science.
3) J.E. Gruber and R. Suess, "Investigations of the Erosion Phenomenon in High Current, High Pressure Gas Discharges," Max Planck Inst. fur Plasmaphysik Garching, bei Munchen IPP 4/72 (Dec, 1969)
4) R.A. Burden and T.E James, "Statistical Performance Data for a High Current 60 kV Spark Gap Switch," Proc. 7th Symp. Fusion Technology, Grenoble, France (Oct, 1972) 24-27.
5) G.S. Belkin and V. Ya. Kiselev, "Electrode Erosion in Pulsed High-Current Discharges," Soviet Phys.-Tech. Phys. 11, (1966) 280.
6) G. Marchesi and A. Maschio, "Influence of Electrode Materials on Arc Voltage Waveforms in Pressurized Field Distortion Spark Gaps," 5th Int. Conf. on Gas Discharges, (Sept, 1978).
7) Y. Suzuki, Y. Kawakita, M. Kume, and M. Kawai, "A 150-kV, 100-kA Spark Gap Switch for Marx Generators," Proc. 3rd IEEE Int. Pulsed Power Conf., Albuquerque, New Mexico, USA (1981) 444.
8) B. Carder, "Gas Spark Gap Electrode Heating and Erosion," Physics International Report PIIR-13-74, (Dec, 1974).
9) R. Basharov, E.N. Gavrilovskaya, O.A. Malkin, and E.S. Trekhov, "Erosion of Cathode Material in a Pulsed Discharge between Parallel Electrodes," Soviet Phys.-Tech. Phys. 12, (1968) 1383.
10) G.N. Glasoe and J.V. Lebacqz, Pulse Generators, Dover Publishing Co., New York, (1965) 175.
11) Manufactured by Schwarzkopf Development Corp. Holliston, Ma.
12) Manufactured by Poco Graphite, Inc., Decatur, Tx.
13) J.E. Gruber and R. Suess
14) G. Marchesi and A. Maschio
15) J.E. Gruber and R. Suess
16) D. Affinito, E. Bar-Avraham, and A. Fisher, "Design and Structure of an Extended Life High Current Sparkgap," IEEE Trans. on Plasma Science, PS-7, (Sept, 1979) 162.
17) B. Carder
18) H.W. Turner, and C. Turner, "Choosing Contact Materials," Electronics and Power 14, (1968) 437.
19) G. Marchesi and A. Maschio
20) F.S. Goucher, J.R. Haynes, W.A. Depp, and E.J. Ryder, "Spark Switches for Radar," Bell Sys. Tech. Journal, 25, (1946) 563.
21) Rodney Petre, thesis (Texas Tech Univ., 1980) (unpublished).
22) D. Johnson and E. Pfender, "Modeling and Measurement of the Initial Anode Heat Fluxes in Pulsed High-Current Arcs," IEEE Trans. on Plasma Science PS-7, (1979) 44.
23) Lloyd B. Gordon, dissertation
24) J.E. Daalder, "Cathode Spots and Vacuum Arcs," Physica, 104C, (1981) 91.
25) D. Affinito, E. Bar-Avraham, and A. Fisher

Project No. 4

Pulsed Power Surface Physics and Applications

(G. Jackson, D. Johnson, L. Hatfield, and M. Kristiansen)

A. SUMMARY

Surface analysis techniques including ESCA, AES, SEM with EDS, FTIR, UV induced fluorescence, optical microscopy, and surface resistivity measurements, have been applied to investigate the processes occuring on the surfaces of electrodes and insulators used in pulsed power switches in cooperation with A. Bowling, Texas Inst. Inc., CRISS, at Bozeman, Montana, and SCR, Houston, Texas. In cooperation with Project No. 3, samples of electrodes and insulators used in several combinations of electrode material, filling gas, and insulator material have been analyzed to determine the erosion and damage processes. One combination, graphite electrode, Lucite insulator, and flowing air has been demonstrated superior to the others in the sense that no discernible damage occured to the insulator. Other combinations show heavy deposits of electrode material on the insulators. Evidence that the insulator material is transferred to the electrode surface implies that the insulator surface is eroded away, although, probably at a low rate. A new surface resistivity technique has made possible measurements on damaged insulator samples on which the standard techniques would not work. It has also been shown that surface analysis is important to the development of a model to describe the breakdown voltage distribution of the spark gaps used in Project No. 3.

The flashover experiment now yields reproducible values of the flashover potential for damaged and undamaged insulators in vacuum and in gases at 1 atm. pressure. An attempt is underway to modify an existing theory of flashover in vacuum with d.c. voltages so it applies to pulsed operation in vacuum and also in the presence of gases. Surface analysis on flashover samples has given qualitative agreement between experimental results and theoretical predictions made on the basis of surface characteristics.

Preliminary surface analysis on insulators used in the surface discharge switch (Project No. 6) do not yet give a clear picture of the processes occuring. It is clear, however, that Lucite erodes away much more rapidly than Delrin or G-10, and that all dielectrics (even Boron Nitride) used in the switch end up with heavy coatings of hydrocarbons.

B. INTRODUCTION

Several developments during the last year have improved our ability to obtain quantitative surface analysis. The Physics Department and the University purchased a used JEOL Model JSM-2 scanning electron microscope for use on this project. This SEM is now in excellent operating condition and has been in use for about six months. We have also initiated a collaboration with A. Bowling of Texas Instruments in Dallas, Texas. Through this collaboration we obtain the expertise of a surface scientist as well as data from ESCA, AES, and SEM with EDS on samples from our laboratories. Some of the following results were

obtained through SCR Laboratories in Houston, Texas, a commercial analysis firm. We have also made use of the facilities of CRISS (Center for Research in Surface Science and Submicron Analysis) an NSF regional instrumentation facility in Bozeman, Montana. The machines at CRISS are operated by the researcher himself, a definite advantage, and their ESCA machine has the high resolution necessary to study the surfaces of polymer insulators.

Also, the Chemistry Department at Texas Tech has purchased an FTIR (Fourier Transform Infrared Spectroscopy) which can be used in the ATR (Attenuated Total Reflection) mode. We have already initiated work with FTIR diagnostic through our consulting chemist (J. Marx).

C. RESULTS FROM THE MARK I AND II SPARK GAPS AND THE SURFACE DISCHARGE SWITCH

1. Results of Insulator Studies

As reported previously, the major effect on insulators used in the Mark I and Mark II spark gaps of Project No. 3 is the formation of electrode material coatings on the inside surface of the insulator. The combination of Lucite insulator, flowing N_2 gas, and graphite electrode, used for 50,000 shots in the Mark II gap, produced a heavy coating of carbon on the Lucite. Visual inspection shows the coating to be some tenths of a mm thick, with easily discernible cracks. This coating might eventually lead to gap failure through insulator flashover. In constrast, the combination of Lucite insulator, flowing air, and graphite electrode resulted in a visually undamaged and clean insulator.

This is one of the samples we have analyzed in some detail. ESCA shows the Lucite surface to be uncontaminated, in other words, identical to a virgin sample. SEM micrographs show a very low density of micro-particles on, and embedded in, the surface. A typical area, 1000 microns by 1000 microns, contained 39 particles, 4 of which measured to be 70 to 80 microns in diameter while the rest were about 10 microns in diameter. This is consistent with the ESCA data if the particles are assumed to be graphite. ESCA analyzes a large area (2 to 4 mm diameter) so the low density of graphite particles would not produce a significant increase in the carbon percentage detected (71% for virgin Lucite). Any other element, except O, would have been detected through ESCA. Figure 1a shows a typical SEM micrograph. Note that the large particles appear to be stuck on the surface while most of the smaller ones are embedded in the surface as if the Lucite melted on impact. The discontinuous size distribution must be related to the mechanism producing the micro-particles. This requires more investigation before any firm conclusions can be drawn.

A second example of electrode material coating arose from the combination graphite-Cu composite electrode, flowing air, and Lucite insulator. Figure 1b shows the granulated deposit formed on the Lucite. ESCA data from this surface showed carbon present, but no copper. Either there is no copper on the surface (doubtful) or the surface is masked by a hydrocarbon layer. This problem will be resolved by using SEM with EDS and/or etching the surface with an argon ion beam in the ESCA machine. The important point is to find out if there is a material selective process occurring in the erosion of the electrodes or the coating of the insulators.

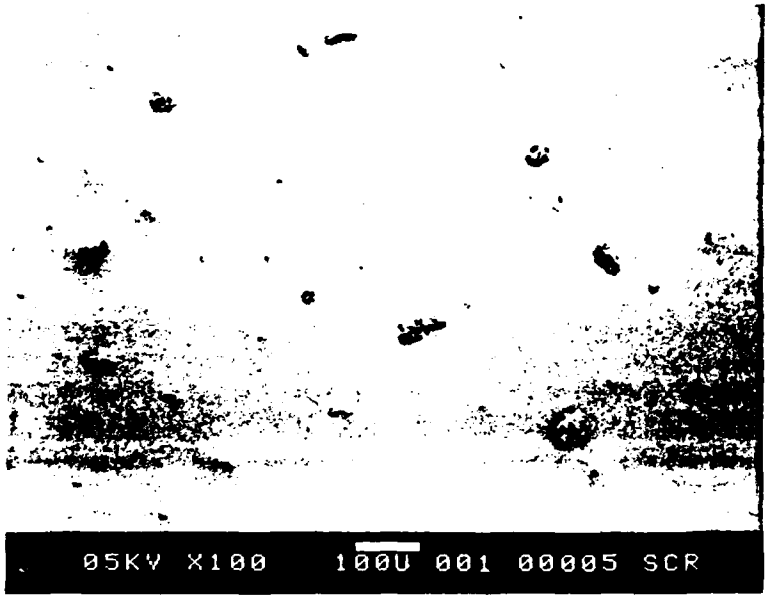

Fig. 1a Lucite insulator from Mark II with Graphite electrodes in flowing air

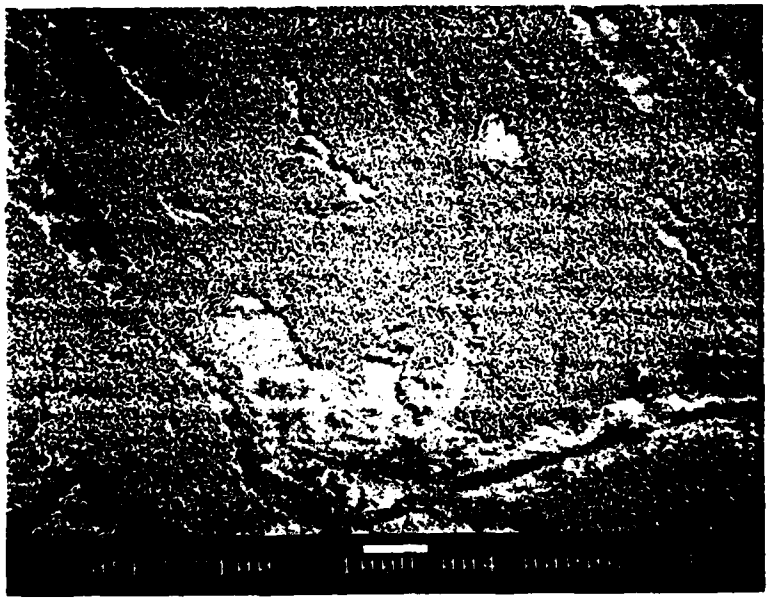

Fig. 1b Lucite insulator from Mark II with Copper Graphite electrodes in flowing air

We have previously reported measurements of the surface resistivity of insulators [1]. The standard instruments and techniques we were using could not be applied to the coated surfaces which were obtained from the Mark I and II gaps because they required pressing the electrodes against the surface [2]. This alters the surface, unless the coating is very thin and uniform. This problem was assigned to a student as a senior project and the results obtained are promising. The proposed solution is to place the damaged insulator in a vacuum evaporator in which an electrode pattern of copper is vacuum deposited on the surface through a mask. These electrodes are then used to measure the current across a known gap length and width for a known voltage. Figure 2 shows an enlarged view of the electrodes and the expression for the surface resistivity in terms of the gap width, g, and length, l. The results for a Blue Nylon virgin sample, and a Blue Nylon sample subjected to 50,000 shots in the Mark I device are shown in Table 1. The "no sample" entry gives the upper limit of the apparatus due to leakage currents. The chart recording of the output of the electrometer over a period of several minutes is also shown in Figure 2. In our application, the significant part of the recording is the constant value of the current after a sufficiently long time. The time required for the current to become constant depends on the particular dielectric being measured. Therefore, the starting time for the chart recording is unimportant and not well defined. It is necessary to make the

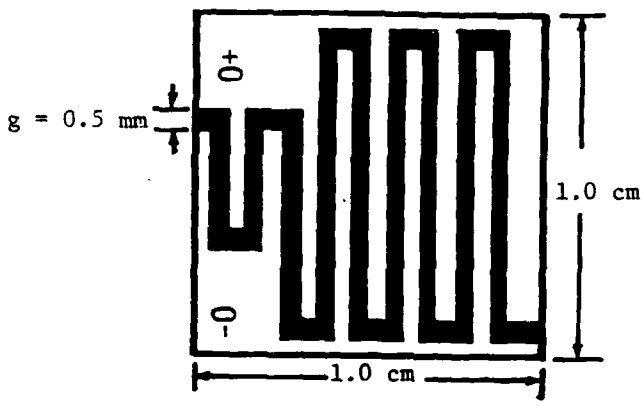

Surface Resistivity = $\sigma_s = V/I(\ell/g)$

ℓ = length of gap between the two electrods

The electrode deposition pattern for measuring the surface resistivity

TABLE 1. Resistivity Values of Blue Nylon

Sample	Voltage	Current	Resistivity
Damaged	400	4.55×10^{-9}	1.96×10^{13}
Undamaged	400	8.00×10^{-11}	1.12×10^{15}
No Sample	400	5.00×10^{-14}	1.78×10^{18}

Typical Current Versus Time

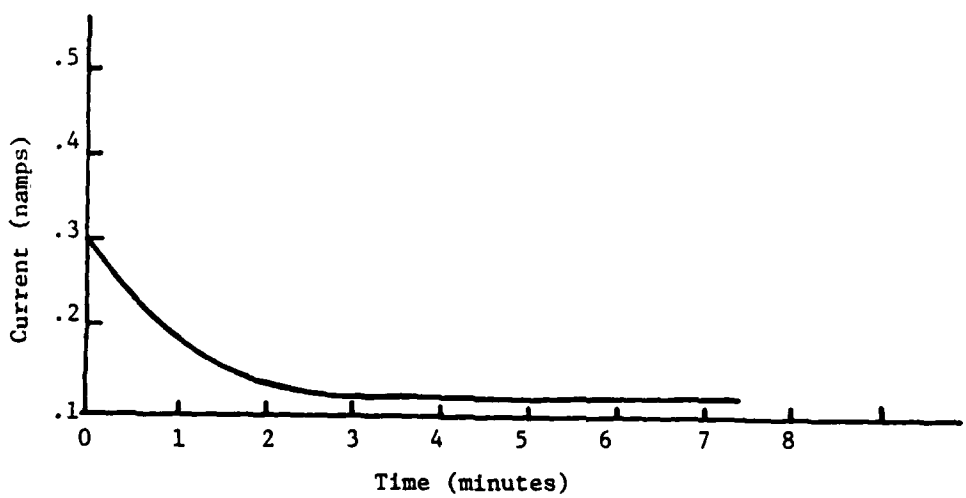

Fig. 2 Surface Resistivity Measurements

measurement in a dry atmosphere and the polymer samples must be dried for at least 24 hrs to remove absorbed water before the measurements are made. This technique will work on any sample that is at least 1 cm by 1 cm square in size. These measurements are important to the understanding of the role of insulator surface charging in a spark gap. For example the rate of deposition of surface coatings on the insulator may depend on the surface charge density, which in turn depends on the surface resistivity (leak down rate) and the rate of surface charge deposition.

A number of dielectric materials have been used as the switching surface in the surface discharge switch (Project No. 6). As explained in the Appendix to the Project No. 6 report, these materials have been exposed to 10,000 shots each in a multichannel mode and 1000 shots each in a single channel mode. Lucite, Delrin, Blue Nylon, and Kapton exhibit melting and erosion when examined with the naked eye. The G-10 material erodes such that the glass fibers are raised above the resin binder, but overall erosion seems to be less than for the polymer (i.e. Lucite). The G-10 material coated with Boron Nitride from an aerosol can did not give satisfactory performance. The Boron Nitride coating eroded away quickly and very non-uniformly, leaving arc trails that were essentially on the G-10 surface itself. The machinable ceramic Macor and the solid Boron Nitride exhibit less erosion than the other materials but do have visible dark deposits in the form of dark lines across the surface from one electrode to the other.

One would assume that the arcs occured preferentially along these lines.

The ESCA data on these materials is summarized in Table 2. The heading "Exposed" means after use in the switch. The virgin sample for each material was cut from the piece used in the switch but from a region lying under one of the electrodes, as far away from the exposed portion as possible. This presents a problem, however. Transformer oil was used to fill the voids between the sample and the Blue Nylon line dielectric. Although every precaution was taken to see that no oil got on the surface of the sample, the ESCA data indicates heavy hydrocarbon contamination.

The following conclusions can be drawn from the ESCA data. The surface composition of the so called "virgin" sample does not necessarily correspond to the bulk chemical composition. For Lucite, it does, but for Macor and Boron Nitride it does not. Although Macor consists of a mixture of oxides of potassium, silicon, magnesium, etc., only carbon and oxygen are seen. Large concentrations of carbon and oxygen are also seen on the Boron Nitride. The samples may have been contaminated with transformer oil which would explain the results in Table 2 for the virgin samples. However, this should have been eroded away when the materials were used in the switch. The results for the exposed samples also show large amounts of carbon and oxygen. It is possible that the surfaces are coated, during operation of the switch,

TABLE 2

SUMMARY OF ESCA DATA FOR

SAMPLES FROM SURFACE DISCHARGE SWITCH

Material	Multichannel	Single Channel
G-10 (C:O)*	(10,000 shots)	(1000 shots)
Virgin	74:26	
Exposed	60:40	
Lucite (C:O)*		
Virgin	70:30	71:29
Exposed	77:23	69:32
Delrin(1) (C:O)*		
Virgin	75:25	
Exposed	33:67	
Delrin(2) (C:O)*		
Virgin	86:14	86:14
Exposed	49:51	48:52
Blue Nylon (C:O:N)*		
Virgin		86:14:0
Exposed		70:30:0
Macor (C:O)*		
Virgin		67:33
Exposed		44:56
Boron Nitride (B:N:C:O)*		
Virgin		32:38:23:7
Exposed		22:30:31:19

* Ratios of elements detected, (1) and (2), see text

with the products of plasma chemistry occuring in the compressed air which is blown across the surface. Changing to pure nitrogen gas flow, as planned, will answer this question. The quite different results for Macor and Boron Nitride could be due to differences in surface temperature. Boron Nitride has a much higher thermal conductivity than Macor. Thus, the surface temperature of the Macor is probably much higher, leading to differences in the plasma chemistry.

The Delrin (1) results were obtained with the Physical Electronics ESCA machine at Texas Instruments. This machine is, however, not in good condition. The Delrin (2) results were obtained with the Leybold machine at CRISS. This machine is new and we believe it is properly calibrated. All single channel results in Table I were obtained using the Leybold machine at CRISS.

It is worth mentioning, that so far we have not seen any effects, such as chemical bonding changes, due to UV or X-ray on any insulator sample. The flux of such radiation may not be large enough in our present gaps to produce an observable effect. Or, the effects of radiation may not be important on insulators that are not highly stressed. We have also not had an insulator flashover in Mark I or II, even though some of them were heavily coated with electrode material. This is presumably due to the gap designs which place a very low electric stress on the insulators. These points deserve further attention.

2. Results of Electrode Studies

Electrode materials used in the Mark I and II gaps have been analyzed using AES (Auger Electron Spectroscopy), ESCA (Electron Spectroscopy for Chemical Analysis), and SEM (Scanning Electron Spectroscopy), with EDS (Energy Dispersive Analaysis). One surprising result is that on materials such as brass and stainless steel, large percentages of carbon are found after a large number of shots in the Mark II gap. The filling gas in the gap was air and the insulator was Lucite. One conclusion is that the insulator material is eroded and injected into the filling gas and some of it is then deposited on the electrode. The high temperature produced by the arcs would reduce such material to carbon. Inspection of electrodes made of a graphite-copper composite also reveals too high a percentage of carbon, compared to the known composition of the bulk material. On these electrodes small spheres of copper showing a thin layer of copper oxide appear to have been melted out of the composite. Auger data shows that even these spheres are coated with carbon. In the case of stainless steel a moderate amount of etching with an argon ion beam removes all the carbon from the surface. This is proof that the carbon is a surface layer, rather than part of the bulk material.

There is also other evidence for insulator material deposits on electrodes. During Auger analysis of a copper-graphite electrode the electron beam was placed on what appeared to be a metal particle on the surface. Before the analysis could be completed the particle disappeared. The underlying material could not be analyzed due to

charging, which means it was an insulator. Presumably, the metal particle charged up and was repelled from the also charged insulating surface. We have also observed UV excited fluorescence on the surface of graphite electrodes used in the Mark I device with a Lexan insulator and with both N_2 and SF_6 gas. No fluorescence was observed for electrodes run under otherwise identical circumstances when no insulator was present.

Other results regarding the decomposition products on the electrodes are available [2] but the above discussion is particularly important considering the breakdown voltage distribution model described in the Project No. 3 report. If insulator material deposits onto the surface of the electrode, surface dependent parameters which are important in the model, such as for instance, the secondary electron emission due to ion bombardment, are altered.

Another application of surface analysis, important to the modeling effort, is the determination of the size and spatial distribution of microprojections on the electrode surface. Stereoscopic SEM micrographs can be used for this purpose. We have already used our SEM to look at stainless steel and the copper-graphite composite but have not yet taken stereo pairs.

3. The Flashover Experiment

a. New Equipment and Procedures

Several new developments have improved the reproducibility of our flashover potential measurements. All samples (1 cm by 6.35 cm dia. cylinders) are polished with toothpaste and then with 1 micron Al_2O_3. The samples are place in vacuum (1×10^{-6} Torr) for 24 hours to remove absorbed water. Then the sample is conditioned with a 60 Hz breakdown voltage. During the flashover tests, fifteen minutes are allowed between voltage pulse applications to allow surface charges to decay or redistribute on the surface.

b. Flashover in Vacuum

Lucite, Lexan, Blue Nylon, and Delrin have been tested, in vacuum, before and after exposure to 80,000 shots by a spark gap. In general, the flashover potential changes after irradiation, increasing by 68% for Delrin, by 69% for Lucite, and by 65% for Lexan. Blue Nylon is the exception to the increase in flashover voltage, decreasing by 10% after irradiation. The flashover potential also generally increases for the first few shots, reaches a plateau for a few shots, and then successively decreases as the sample developes a track [4]. The decreasing voltage and the formation of the track are correlated with the occurance of the flashover at the track location, whereas, before the track forms the flashover location is random. More detailed results are given in the paper "Pulse Flashover of Solid Dielectrics in Vacuum," (see Appendix). This paper was presented at the 10th International Symposium on Discharge

and Insulation in Vacuum. Columbia, S.C., October 25, 1982.

c. Flashover in Gases

Lexan and Blue Nylon have been subjected to flashover measurments in which all steps are exactly as described for the vacuum case except that the chamber is filled with one atmosphere of gas before the voltage pulse is applied. In SF_6, no sample flashover occured at up to 126 kV (the limit of our apparatus at that time). For Lexan in N_2, the irradiated Lexan sample flashes over at about 70% of the value observed with the virgin sample. In the same gas mixture results for Blue Nylon are too scattered, so far, to make any quantitative statements but the flashover potential seems to be always lower for the irradiated sample in both N_2 and the 20% SF_6 and 80% N_2 mixture. Obviously, more measurements are necessary and the upper voltage limit of the apparatus has been raised in order to increase the measurement range.

d. Surface Analysis of Flashover Samples

Surface analysis with SEM and ESCA has been performed on Lexan and Blue Nylon samples that were irradiated, flashed over, and tracked in vacuum. In the SEM pictures of the tracked region the track appears brighter than the surrounding surface. This indicates a higher secondary electron production from the tracked area. ESCA data were taken both from the region of the track and from a region not showing a track. The analysis is very complicated but the conclusion is that the irradiated samples have a carbon coating more than 30 A thick. When the flashover forms a track, the carbon coating is removed. The carbon

coating must come from the igniter plug which is used as the spark source in the vacuum chamber. These conclusions can be used qualitatively in a simple model to explain the change in flashover potential after irradiation.

One attempt to determine the thickness of this carbon coating, using ellipsometry, gave an indeterminate answer (the coating may be too thin). Analysis of the surface with FTIR using an ATR attachment showed no change in the chemical structure of the surface of a Lucite sample after irradiation. This strengthens the carbon coating hypothesis since a thin carbon coating would not be seen with this technique.

e. Flashover Theory

A recent article by Pillai and Hackam [5] describes a theory based on the model of Anderson and Brainard [6] for insulator flashover. Although this theory is for d.c. and vacuum only, we have begun to modify it for pulsed operation and to include the effects of operation in a gas. This theory relates the flashover potential to surface dependent parameters such as the secondary electron coefficient, the surface resistivity, the length of the surface, the probability of desorbing gas from the surface by electron bombardment. Qualitatively, a surface with a higher secondary electron coefficient will have a lower flashover potential. This correlates with our data on irradiated samples and predicts that once a track forms, the flashover potential will be much lower in the region of the track. Assuming that the carbon coating on our irradiated samples lowers the surface resistivity, and therefore lowers the surface charge density, the flashover potential should be higher, which also agrees with our data. We can also correlate the

sample length and gas desorption probability with our data and get qualitative agreement. Thus, it seems promising to attempt to pursue this model for application to our pulsed system.

REFERENCES

[1] First Annual Report on *Coordinated Research Program in* Pulsed Power Physics, p. 93 Texas Tech University, December 1, 1980.

[2] ASTM D257-61, Standard Methods of Test for Electrical Resistance of Insulating Materials, 1961.

[3] L.B. Gordon, M. Kristiansen, M.O. Hagler, H.C. Kirbie, R.M. Ness and L.L. Hatfield. "Material Studies in a High Energy Spark Gap." accepted for publication in IEEE Transacations on Plasma Sciences.

[4] S. Grzybowski, E. Kuffel, "Electric Surface Strength of High Voltage Insulators in Vacuum," IEEE Trans. on Power Apparatus and Systems, PAS-99, 1788, (1980).

[5] A. Sivathanu Pillai and Reuben Hackam, "Surface Flashover of Solid Dielectric in Vacuum," J. Appl. Phys. 53, 2983 (1982).

[6] R.A. Anderson and J.B. Brainard, "Mechanism of Pulsed Surface Flashover Involving Electron-Stimulated Desorption," J. Appl. Phys. 51, 1414 (1980).

APPENDIX I

PULSE FLASHOVER OF SOLID DIELECTRICS IN VACUUM*

G.L. Jackson and L.L. Hatfield
Department of Physics

M. Kristiansen
Department of Electrical Engineering

J. Marx
Department of Chemistry
Texas Tech University
Lubbock, Texas 79409

and

A. Bowling
Texas Instruments, Inc.
P.O. Box 225936, MS 147
Dallas, Texas 75265

Abstract

A solid dielectric placed between two electrodes in a vacuum has a lower flashover potential than a system of two electrodes with the same gap separation in vacuum. Very little is known about the mechanisms which cause this phenomenon. The purpose of this work was to investigate the flashover potential of various organic insulators, both before and after they have been exposed to the byproducts of an arc from a surface discharge ignitor plug located approximately 8 cm away from the edge of the sample. The insulators were cylinders, 1 cm in height and 6.35 cm in diameter. They were placed between two Bruce profile, brass electrodes with an equipotential surface, 8.8 cm in diameter, in a vacuum of about 1 x 10^{-6} Torr. Lexan (polycarbonate), Lucite (methyl methacrylate), Delrin (acetal) and Blue Nylon were the four different materials investigated. The flashover pulse duration was approximately 5 μs with a maximum amplitude of 161 kV/cm. Each insulator was first polished to a fine finish using 1 micron size grit of alumina, then placed in the vacuum system and allowed to outgas for 24 hours. The samples were then conditioned with 60 Hz AC up to a maximum voltage of approximately 70% of the AC flashover potential, after which the pulsed flashover potentials of the samples were measured. Other, identically prepared samples, were irradiated while rotating at 2.67 RPM for 80,000 shots, with an energy of about 2 Joules per shot delivered to the ignitor plug, after which the pulsed flashover potentials were measured. The flashover potential on one Delrin sample increased by a minimum of 68% after it was irradiated, a Lucite sample increased by a minimum of 69%, a Lexan sample increased by 65% and finally a Blue Nylon sample decreased by 10% after they were irradiated. The results of these tests are presented in this paper. In addition, results from the use of ESCA (Electron Spectroscopy for Chemical Analysis) and SEM (Scanning Electron Microscopy) to analyze the surfaces of these insulators are presented in an effort to relate the flashover potential to changes in the surface structure and condition.

*This work was supported by the Air Force Office of Scientific Research

Introduction

In an effort to understand the mechanisms which lead to changes in the surface flashover potential of insulators used in high power spark gaps a systematic study of the flashover potential of various organic insulators was undertaken. The flashover potential of these insulators was measured both before and after they had been exposed to the byproducts of an arc from a surface discharge ignitor plug. These insulators were analyzed using Electron Spectroscopy for Chemical Analysis (ESCA)[1] to determine what, if any, structural changes occurred on the surface of the insulator as a result of the flashover events and/or irradiation. A Scanning Electron Microscope (SEM)[2] was also used to investigate the tracks formed on the insulators as the result of a surface flashover.

Experimental Setup

The insulator samples are solid cylinders with a diameter of 6.35 cm and a height of 1 cm. Each sample is polished to a fine finish with 1 μm size grit of alumina and then washed with cyclohexane before being placed between two polished, Bruce profile, brass electrodes. The sample is then placed in the vacuum chamber, shown schematically in Figure 1, and allowed to outgas for at least 24 hours at a pressure of 1 x 10^{-6} Torr before further treatment. After the sample is vacuum conditioned it is then AC conditioned, using a 60 Hz, 0-60 kV power supply.

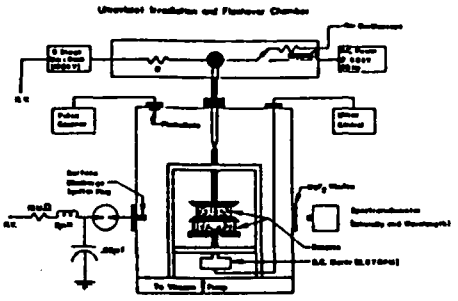

Figure 1. Ultraviolet Irradiation and Flashover Chamber

The AC conditioning is accomplished by raising the voltage of the power supply in 5 kV steps with a 5 minute interval between steps. This is continued until the voltage is approximately 70% of the AC flashover voltage, obtained from measurements on several trial samples. This voltage is subsequently maintained for 30 minutes.

The pulsed flashover potential of the sample is measured by erecting a seven stage 170 kV Marx bank into an RC load. The value of the load capacitance is about 70 pf due to a 1 meter length of RG 17 coaxial cable and the inherent capacitance of the parallel plate electrodes of the test cell. The value of the load resistor was then chosen so that the 1/e rise time of the pulse was approximately 3 μs. The voltage across the sample is measured by using a 45,000 to 1 resistive divider.

A series of pulsed flashover measurements on each sample is performed by applying the pulse to the sample, recording the voltage across the sample and then waiting 15 minutes before applying another pulse. It was assumed that by waiting 15 minutes between voltage pulses any surface charge which the sample may have accumulated from the previous flashover would become more uniformly distributed along the surface. When the flashover measurements were taken with a 3 minute wait or immediately after a previous shot the results were inconsistent, a 15 minute wait gave more consistent results.

Another identically prepared sample is then placed in the vacuum chamber and irradiated by the surface discharge ignitor plug for 80,000 shots, at a rate of 5 per second. The surface discharge ignitor plug is located about 8 cm from the edge of the sample and uniformly irradiates the sample, as it rotates at 2.67 RPM. The voltage at which this ignitor plug fires is determined by an external spark gap which is preset at 13 kV and discharges the .02 μf capacitor at a rate of 5 per second delivering about 2 Joules of total electrical energy to the ignitor plug for each shot. A spectroradiometer is used to view the pulses from the ignitor plug and give information about the intensity and wavelength of the radiation. A photodiode located at the top of the vacuum chamber counts the number of pulses from the ignitor plug. After irradiation the sample is then AC conditioned and the pulsed flashover potential measured.

Surface analysis of the insulators after they have been tested for flashover is performed on a PHI model 545 ESCA machine. Also, a JEOL JSM-2 SEM is used to investigate the tracks formed on the surface of the insulator as a result of the flashover events. Other surface analysis techniques used include Fourier Transform Infrared Spectroscopy (FTIR), Ellipsometry, and Surface Resistivity measurements to investigate the insulator surface properties before and after flashover and before and after irradiation.

Results

The pulsed flashover potentials for Delrin (polyacetal), Lucite (polymethyl methacrylate), Lexan (polycarbonate) and Blue Nylon have been measured using the procedures outlined above. The results show that for all materials tested, except Blue Nylon, the pulsed flashover strength is significantly improved after the samples have been irradiated.

The pulsed flashover potentials for these samples are shown in figures 2-5. As a general rule, the flashover potential reaches its maximum value and plateaus after 3 or 4 shots, followed by a sharp decrease in the flashover strength.

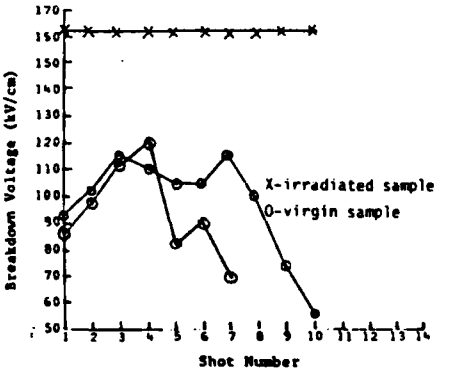

Figure 2. Flashover Potential for a series of consecutive test on Delrin. (X-irradiated sample, O-two different virgin samples)

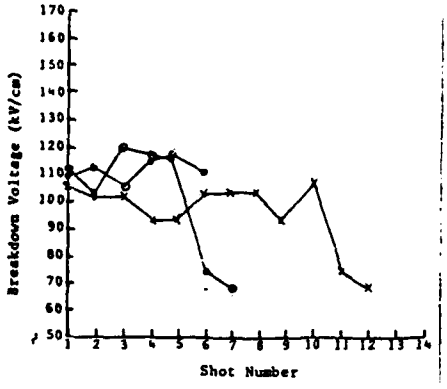

Figure 3. Flashover Potential for a series of consecutive tests of Blue Nylon. (X-irradiated samples O-two different virgin samples)

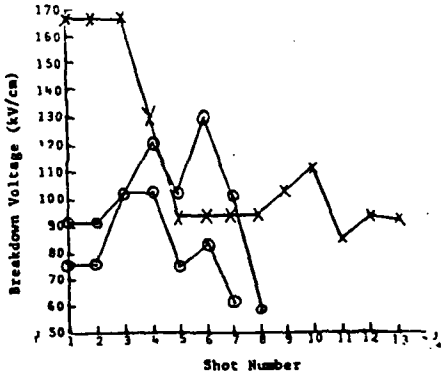

Figure 4. Flashover Potential for a series of consecutive test on Lexan. (X-irradiated sample, O-two different virgin samples)

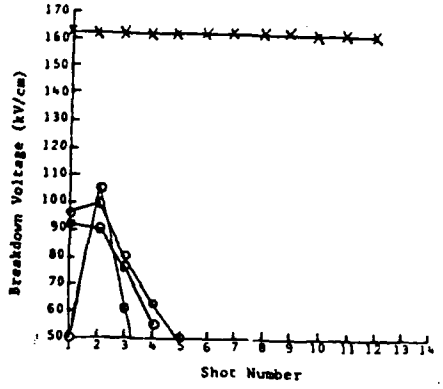

Figure 5. Flashover Potential for a series of consecutive test on Lucite. (X-irradiated sample, O- two different virgin samples).

It is assumed that during the first 3 or 4 shots the sample is being conditioned by the surge flashover pulses, removing any imperfections from the surface. During this conditioning period and the plateau period the surface flashovers are randomly distributed about the circumference of the sample. However, when the flashover strength begins to show a sharp decrease subsequent surface flashovers occur at the same place on the sample. This is probably indicative of the formation of a conductive path (a track) which bridges the gap between the electrodes, causing the lower flashover potential. Blue Nylon and Delrin have the highest average flashover strengths with values of 112 kV/cm and 109 kV/cm respectively. Lexan was third with an average value of 104 kV/cm and Lucite showed inconsistent results. Lucite was the only material which did not form a track along the surface of the insulator because of a flashover and it was also the only material that showed inconsistent results for the flashover potential. When the flashovers on a Lucite sample were viewed through the MgF_2 window they always occurred at the same place.

After a sample was removed from the vacuum chamber it was visually examined for evidence of tracking and the brass electrodes were examined for evidence of pitting or imperfections caused by the flashovers. Every material tested, except Lucite, developed tracks on the surface and the cathode always showed markings near the circumference of the sample which coincided with the appearance of a track on the insulator. Lucite, however, formed no visible tracks on the surface but the cathode developed a pit (approximatley 10 μm long and 2 μm wide containing small pointed protrusions) at the position where flashovers were

observed through the MgF_2 window. It is commonly known that a sharp protrusion located near the surface of an insulator which bridges a vacuum gap causes a lowering of the flashover potential due to field enhancement.[3] This is believed to be the cause of the inconsistent behavior of the flashover voltage for Lucite. However, it is not yet known why this happened for Lucite and no other materials.

After irradiation for 80,000 shots all the samples except Blue Nylon showed a large increase in the flashover potential. The Delrin and Lucite samples could not be flashed over after they were irradiated even though the potential difference between the plates was as high as 161 kV/cm. Lexan did not flash over for the first 3 shots on the rising part of the voltage pulse, however, it did flash over very late during the pulse, and then every time in the succeeding pulses at an average voltage of 92 kV/cm leaving a track wherever it did flashover. Blue Nylon flashed over at a lower voltage after it was irradiated, the average voltage being 99.5 kV/cm as compared to 112 kV/cm for the virgin sample.

After samples were taken from the vacuum chamber they were analyzed using ESCA and an SEM. The SEM was used to investigate the structure of tracks and to aid in the identification of any foreign materials present on the surface. ESCA was used to determine if any chemical structural changes could be found on the surface of the materials after a flashover and/or irradiation.

SEM micrographs of a Lexan insulator, which had been irradiated for 80,000 shots and flashed over, show a track that has bridged the gap and is approximately 375 μm wide. The micrographs show that because of the flashover some of the material on the surface has been eroded away, leaving an area where the sample is different from the surrounding material. The track has a higher secondary electron emission coefficient than the surrounding insulator as seen by its brighter appearance. This is an important consequence of flashover if, as is commonly believed, surface charging is an important mechanism in causing surface flashovers.

The ESCA data has so far not been very useful in determining structural changes on the surface of the polymers due to the low resolution of the machine being used. However, some things do emerge from the present data. For example, Blue Nylon is a polymer composed of the elements carbon, oxygen and nitrogen in the relative ratio of 10.8:2.9:1, respectively. When a Blue Nylon insulator is irradiated for 80,000 shots and flashed over, ESCA shows no nitrogen on the surface, indicating that either the surface of the insulator is coated with something that obscures the nitrogen in the material or that the nitrogen in the sample has been released from the surface by some mechanism. The data show that for this sample the concentration ratio of carbon:oxygen:nitrogen has decreased from 10.8:2.9:1 to 2.0:1.0:0, i.e. that the nitrogen in the material has been liberated through some mecahnism. However, the detailed scans of the carbon and oxygen peaks, which give the most information about the surface structure, do not have the resolution necessary to determine how this has occurred.

For a Lucite sample that was irradiated for 80,000 shots the relative concentrations of carbon to oxygen increased from 2.4:1 for the virgin sample to 3.2:1 for the irradiated sample. The detailed scans of the carbon and oxygen peaks for the virgin sample show a peak on the high binding energy side which is indicative of a carboxyl (C = O) group. However, the detailed scans of the carbon and oxygen peak for an irradiated sample do not show this peak, but instead indicate only hydrocarbon type bonding. These two facts would seem to indicate that the surface of the material has been coated with a thin layer of carbon, due to the irradiation, which is masking the signal from the bulk material.

Conclusions:

It has been shown that the flashover strength of Lexan, Delrin and Lucite increased by a minimum of 65%, 68% and 69% respectively, after they were irradiated for 80,000 shots by the surface discharge iginitor plug. It was also shown that the flashover strength of Blue Nylon decreased by 10% after irradiation.

Others have shown that coatings on insulators can lead to increases in the surface flashover strength.[4] As an example, *H. Miller and E. Furno* coated alumina insulators with a 7:1 Mn:Ti coating and found a 25% improvement in the holdoff voltage of alumina insulators. They attributed this to a lowering of both the surface resistivity and the secondary electron emission coefficient. Consequently, one possible reason for the behavior of the flashover strengths of Lexan, Delrin and Lucite after irradiation is that the irradiation lowers the secondary electron emission coefficient enough to reduce the chances of an electron build-up and subsequent avalanche along the surface.

An SEM was used to investigate the tracks formed on the insulators as a result of flashover events. The results indicate that for a Lexan sample the secondary electron emission coefficient is lowered after irradiation. This could explain why the flashover strength is so much higher after irradiation. With a Blue Nylon sample the secondary electron emission coefficient was no different for an irradiate sample and a virgin sample. Thus, the flashover strength should be the same for both samples. However, the brass electrodes are also irradiated and appear to be coated also. If this coating increases the electron emission from the triple point it would explain why the flashover strength for an irradiated Blue Nylon sample is smaller by 10%.

The ESCA data indicated that for a Lucite sample which has been irradiated the surface has been coated with a carbon film, the thickness of which has not yet been determined. However,

Delrin, Blue Nylon, and Lexan do not appear to have been coated even though some features of the spectrum would tend to indicate that they were. For example, in Blue Nylon the absence of any nitrogen after irradiation could indicate either a coating which obscures the nitrogen peak or that the nitrogen has left the surface through some means. For Lexan the absence of C=O type bonding after irradiation could indicate one or the other of the two mechanisms mentioned above. In order to better understand the damage mechanisms caused by either flashover or irradiation on the surface of these insulators much higher resolution ESCA data will be required.

Acknowledgements

We are indebted to Keith Russell at Texas Instruments Inc. who analyzed the insulators with ESCA and to Mike Foster for his analysis of the insulators with the SEM and James Semrad and Richard Hernandez for their work on the construction of the flashover apparatus.

References

1. D.T. Clark and W.J. Feast, Application of Electron Spectroscopy for Chemical Applications (ESCA) to Studies of Structure and Bonding in Polymeric Systems, J. Macromol Sci.-Revs. Macromol. Chem., vol. C12.

2. O. Johari and A.V. Samudra, Scanning Electron Microscopy, P.F. Kane and G.B. Larrabee (eds), Characterization of Solid Surfaces, New York, Plenum Press, 1978, Chapter 5.

3. J.R. Laghari and A.H. Qureshi, Impulse Breakdown Voltages for a Cylindrical Spacer in the Presence of Electrode Protrusion, Proceedings, Third IEEE International Pulsed Power Conference, Albuquerque, New Mexico, pp. 285-288, June 1981.

4. H.C. Miller and E.J. Furno, The effect of Mn/Ti surface treatment on voltage-holdoff performance of alumina insulators in vacuum, Journal of Applied Physics, vol. 49 no. 11, pp.5416-5420, November 1978.

Project No. 5

Excited State Spectroscopy of Electrically Excited Gases

(S.K. Dhali and P.F. Williams)

A. SUMMARY

Accomplishments during the contract period include 1) Extensive studies of multi-photon ionization in xenon, 2) The construction and initial testing of an experimental apparatus for studying charge motion under space-charge-limited conditions, such as are important in streamer propagation, 3) The further development of a numerical program to calculate charge motion under these conditions, 4) Initial experiments designed to study the feasibility of using inverse bremsstrahlung heating of electrons produced by a multi-photon ionization process to trigger a spark gap with low delay and jitter, and 5) An experimental study of the feasibility of using photodetachment of negative ions as an optical control mechanism for glow discharges. This last work was done in collaboration with Dr. G. Schaefer, and is directly related to the goals of Project No. 8, "Optically Controlled Discharges."

AD-A129 554 COORDINATED RESEARCH PROGRAM IN PULSED POWER PHYSICS (U) TEXAS TECH UNIV LUBBOCK DEPT OF ELECTRICAL ENGINEERING M KRISTIANSEN ET AL. 01 DEC 82 2/3

UNCLASSIFIED AFOSR-TR-83-0503 F49620-79-C-0191 F/G 20/3 NL

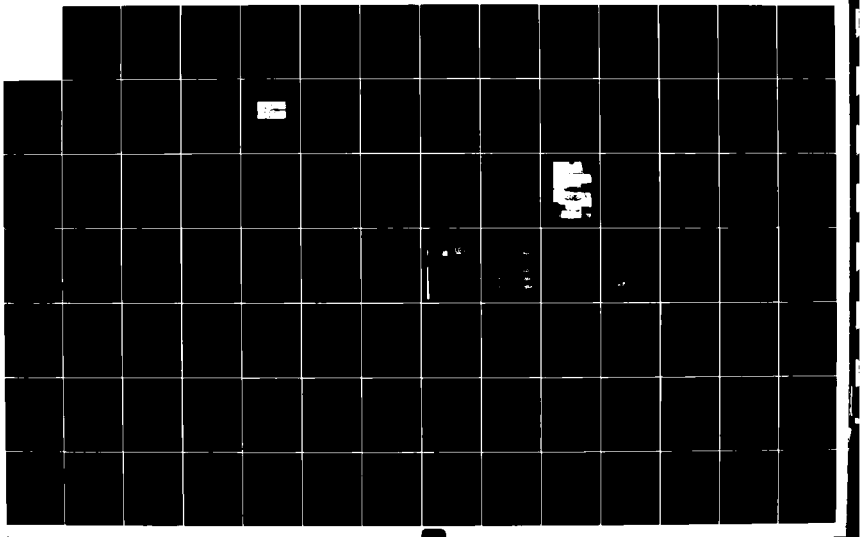

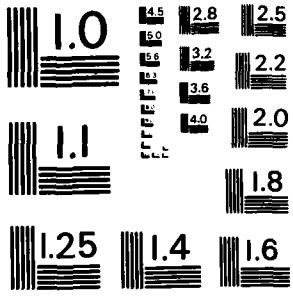

MICROCOPY RESOLUTION TEST CHART
NATIONAL BUREAU OF STANDARDS - 1963 - A

B. ACCOMPLISHMENTS

Work carried out under this project has been aimed at developing diagnostics, and investigating effects and physical processes which might be important for laser-triggered switching. Extensive studies of multi-photon ionization in xenon were carried out as described in Section 1. The purpose of these studies initially was to investigate the feasibility of using multi-photon ionization as a triggering process for laser-triggered switches, and later to characterize the process for use as a source of substantial charge density in experimental studies of charge motion under space-charge dominated conditions. This work is now complete and the results are presented here.

Streamers have been considered responsible for many phenomena occurring during fast breakdown of gases, but there is currently little quantitative understanding of their formation or propagation. In Section 2 an experimental apparatus for studying space-charge motion under these conditions is described, and in Section 3 our recent efforts at developing a numerical procedure for calculating the evolution of an initial charge density under these conditions is described.

Workers at Sandia National Laboratories have carried out a development program to design laser-triggered switches for use on PBFA II. These switches will be laser-triggered using a geometry

in which the laser does not strike either electrode surface. Triggering in this case is provided by the production of charge in the midgap region through processes that are not well understood. It was found that with an SF_6 fill gas, the gap triggered with lower jitter when a U.V. laser trigger was used, and it was suggested that multi-photon ionization might be playing a role in the triggering. We therefore carried out a set of experiments designed to test the validity of this hypothesis. The results to date of this work are described in Section 4.

Finally, in collaboration with Dr. G. Schaefer we have carried out a set of experiments intended to investigate the feasibility of using photodetachment of negative ions to control optically a diffuse discharge. This work was done in direct support of Project No. 8, "Optically Controlled Discharges." A brief description of the work is given in Section 5, and a more complete account is given by G. Schaefer in his report of work carried out under Project No. 8.

1. Multi-Photon Ionization in Xenon

Multi-photon ionization is an attractive technique for producing cleanly tailored volumes of ionization in a gas for the purpose of studying charge motion under space-charge-dominated conditions. For this reason we have carried out extensive experiments in order to charaterize the process in xenon and xenon-nitrogen mixtures for use in this regard. Xenon was chosen for the study because multi-photon

ionization in it is well studied and conveniently carried out with our laser system, and because it is chemically inert and suitable for addition in small quantities to another gas. The multi-phonton ionization process in xenon and our experimental apparatus for studying it are well described in a previous annual report [1].

One addition to the apparatus described previously [1] is the high power Nd:YAG-based laser system described under Project No. 2. With this system we can produce approximately 10 mJ pulses of tunable radiation in the 360-400 nm range. In the work we described previously, we had available only a nitrogen laser based system, and could produce only tens of μJ of energy in this wavelength range. Since the ionization process in xenon is a three-photon process, we would expect to be able to produce up to 10^9 times more ionization with the YAG system. Previously, we had investigated the dependence of the ionization efficiency on laser energy, and found a nearly cubic dependence up to the highest powers available to us. During the most recent contract period we have made use of our new laser system to explore the ionization characteristics for higher powers in order to see if these predicted ionization densities could in fact be realized.

With the new system at low powers we observed behavior very similar to that we had seen with the nitrogen laser system, including an apparent saturation effect for laser energies above about 20 μJ. We previously showed that this saturation was in fact not a real effect, but instead reflected a saturation of the gain of the proportional counter we were using to detect the ionization. Our more recent experiments have verified this conclusion even up to substantially higher powers than we had

previously been able to investigate. By lowering the voltage, and hence the gain, on the proportional counter we were able to observe unsaturated behavior up to higher powers, and hence remove this effect. Since we have absolutely calibrated the gain of our proportional counter, we could use it in a high gain mode for low laser powers when the ionization produced was weak, and then reduce the gain in a well known way for use with higher laser powers. After this correction, we have found two real saturation effects.

We show the results of these measurements for several pressures and for pure xenon and Xe/N_2 mixtures in Figures 1-7. The vertical scale is in units of the absolute number of charges produced and overlapping results for several proportional counter voltages are shown. At low laser energies a cubic dependence of ionization on laser energy is observed. At energies for which approximately 10^8 charges are produced the curve bends over to a roughly quadratic dependence, and at sustantially higher energies still, it bends again reflecting an approximately linear dependence. The obviously discontinuous experimental points shown are a result of operating the counter in the Geiger region due to the large charge densities being produced. Operation in the highest power region, above the second bend, was difficult in the proportional counter cell because of the high charge densities. We therefore carried out a set of experiments in this region using a parallel plate electrode cell, operated with low voltage, for which no gain was expected. The results of these experiments are shown in Figure 8.

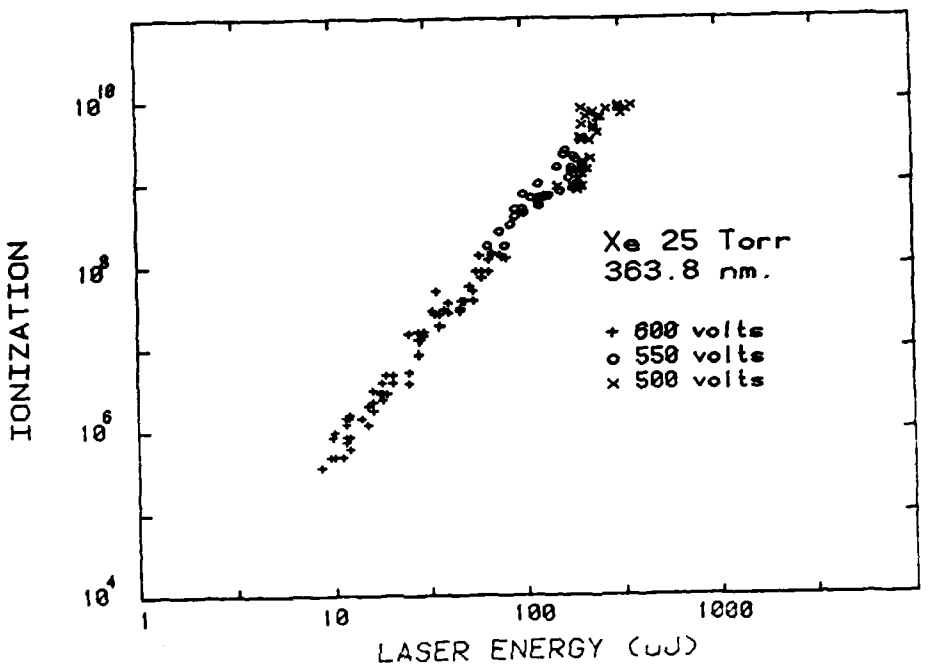

Fig. 1 Multi-photon ionization efficiency vs. laser energy for pure xenon, 25 Torr. Laser wavelength was 363.8 nm and the results for several different proportional counter voltages are shown as indicated. Ionization is in units of absolute number of charges produced.

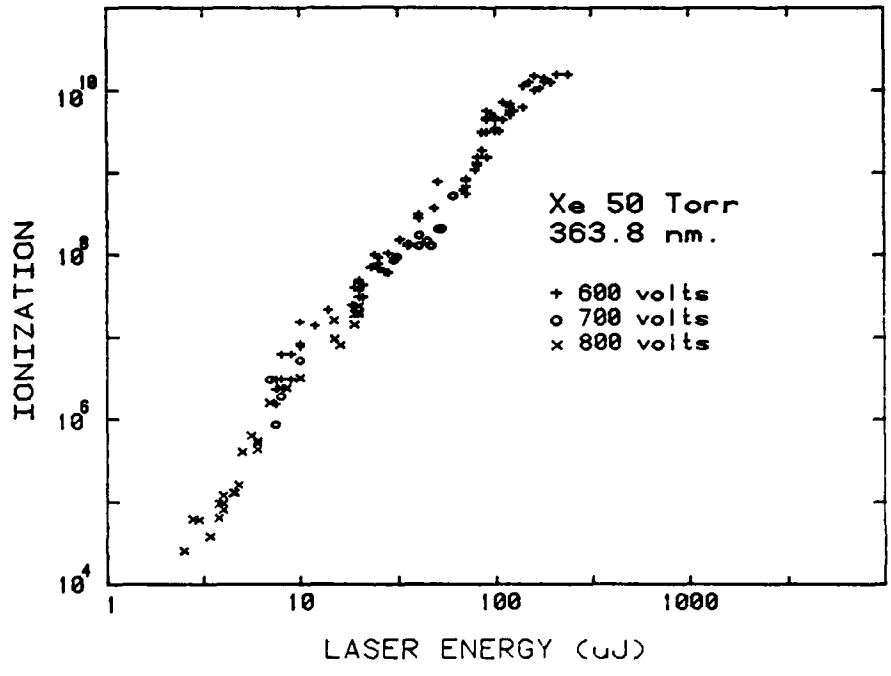

Fig. 2 Multi-photon ionization efficiency vs. laser energy for pure xenon, 50 Torr. Laser wavelength was 363.8 nm and the results for several different proportional counter voltages are shown as indicated. Ionization is in units of absolute number of charges produced.

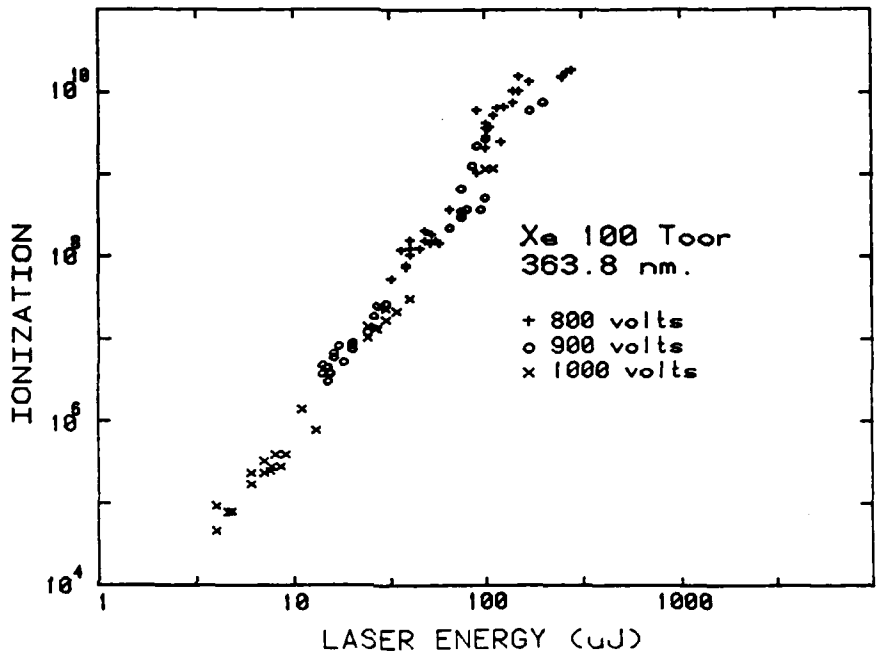

Fig. 3 Multi-photon ionization efficiency vs. laser energy for pure xenon, 100 Torr. Laser wavelength was 363.8 nm and the results are several different proportional counter voltages are shown shown as indicated. Ionization is in units of absolute number of charges produced.

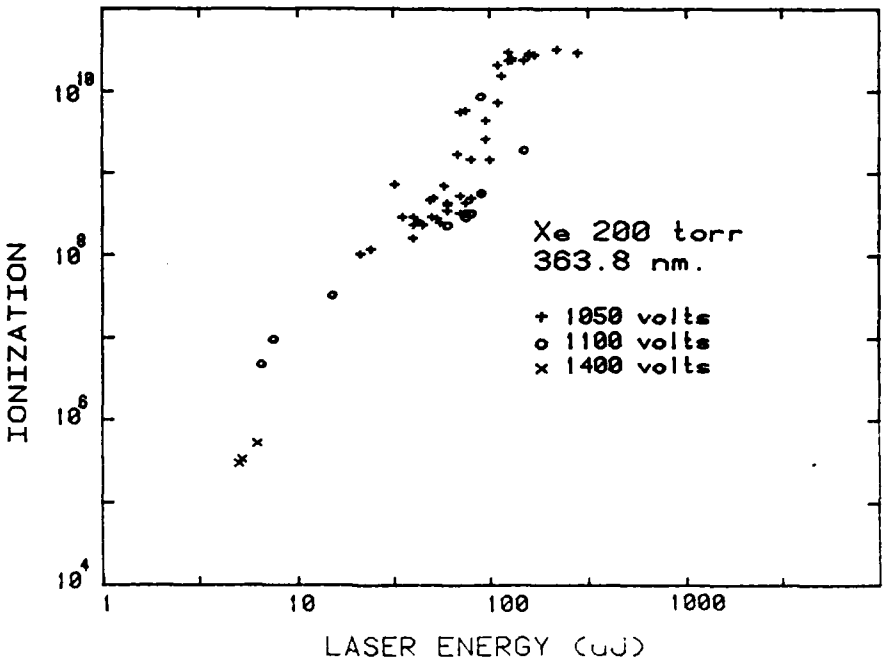

Fig. 4 Multi-photon ionization efficiency vs. laser energy for pure xenon, 200 Torr. Laser wavelength was 363.8 nm and the results for several different proportional counter voltages are shown as indicated. Ionization is in units of absolute number of charges produced.

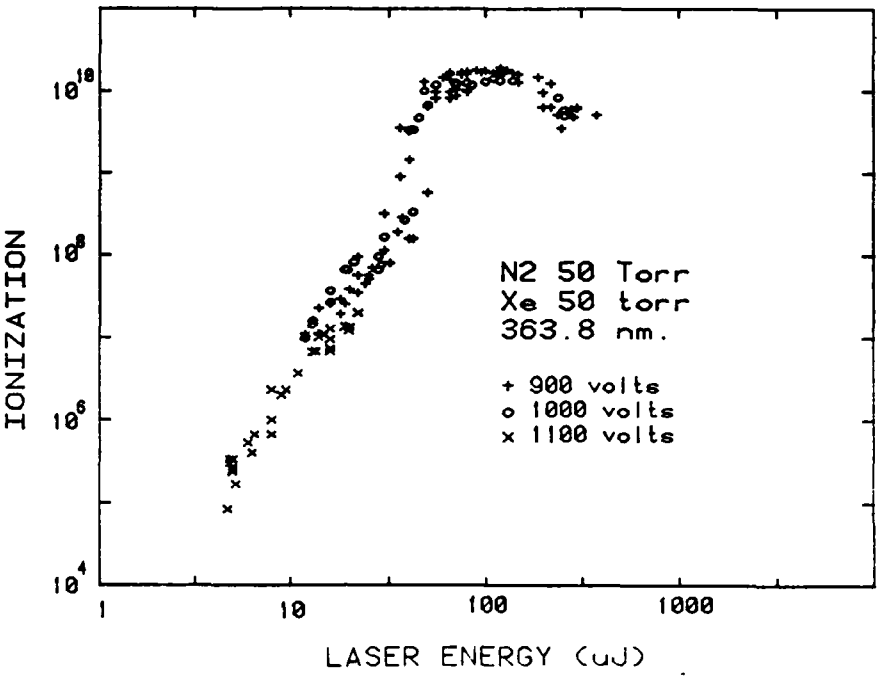

Fig. 5 Multi-photon ionization efficiency vs. laser energy for mixture of 50 Torr N_2, 50 Torr Xe. Laser wavelength was 363.8 nm and the results for several different proportional counter voltages are shown as indicated. Ionization is in units of absolute number of charges produced. Obviously discontinuous points are a result of operating the proportional counter in the Geiger region.

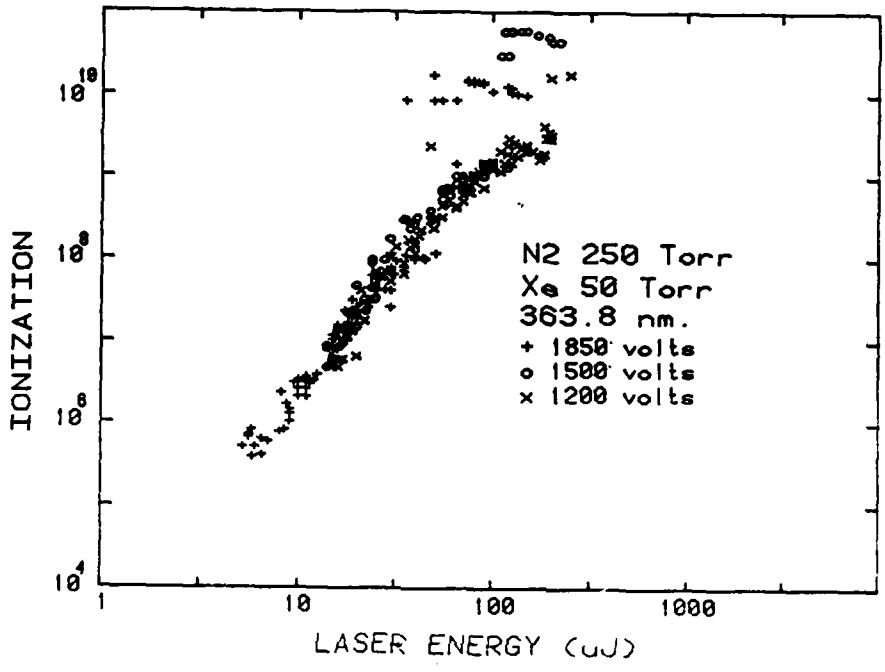

Fig. 6. Multi-photon ionization efficiency vs. laser energy for mixture of 250 Torr N_2, 50 Torr Xe. Laser wavelength was 363.8 nm and the results for several different proportional counter voltages are shown as indicated. Ionization is in units of absolute number of charges produced. Obviously discontinuous points are a result of operating the proportional counter in the Geiger region.

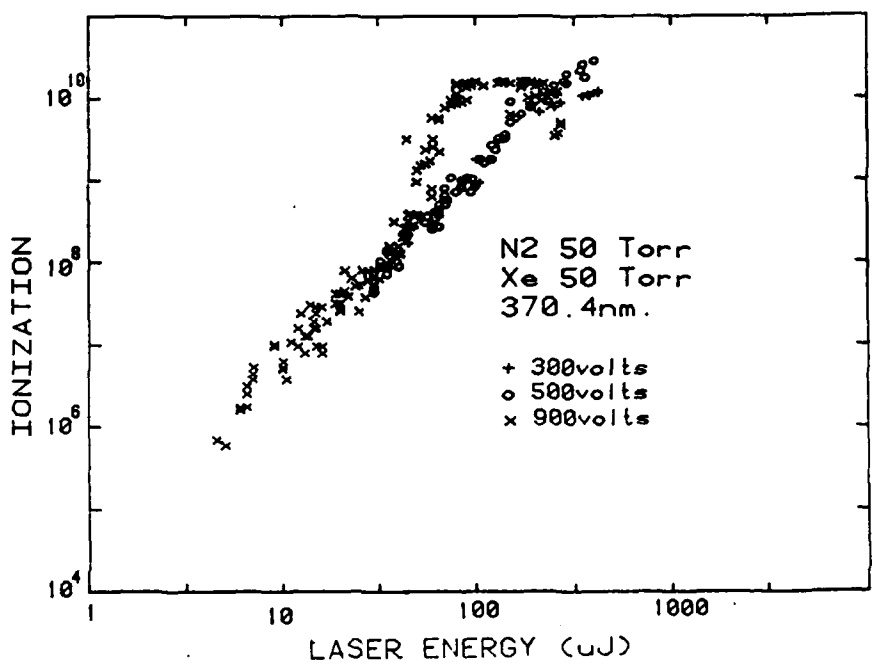

Fig. 7 Multi-photon ionization efficiency vs. laser energy for mixture of 50 Torr N_2, 50 Torr Xe. Laser wavelength was 370.4 nm and the results for several different proportional counter voltages are shown as indicated. Ionization is in units of absolute number of charges produced. Obviously discontinuous points are a result of operating the proportional counter in the Geiger region.

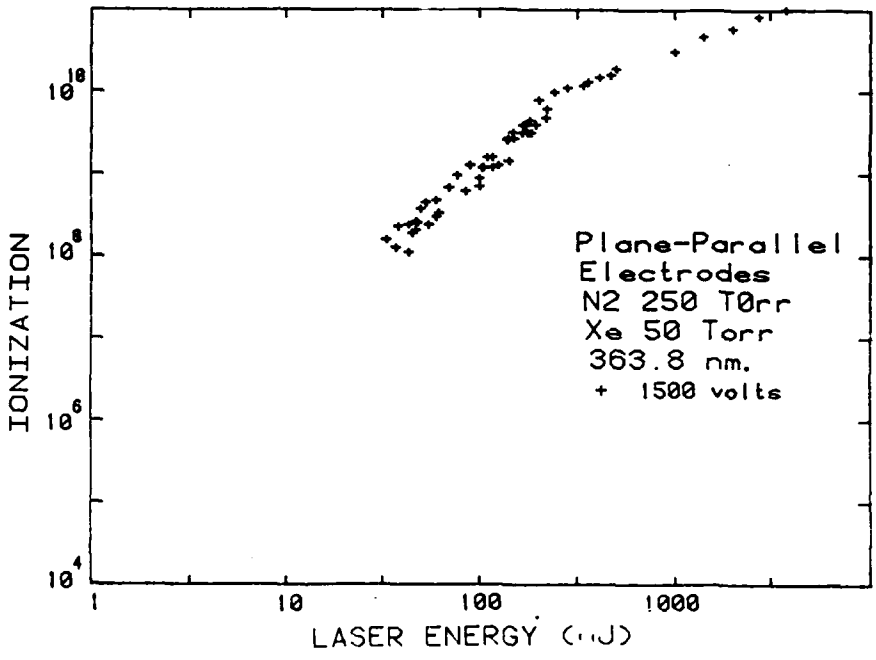

Fig. 8 Multi-photon ionization efficiency vs. laser energy for mixture of 250 Torr N_2, 50 Torr Xe in a plane-parallel electrode cell. Laser wavelength was 363.8 nm. Ionization is in units of absolute number of charges produced.

The first bending of the curve is due to space charge effects. At the charge density where this effect sets in, the charge produced is sufficient so that the plasma produced by the laser can shield itself. In this case, the electrons in the interior will not experience the applied field, and will not drift away from the positive ions. Recombination would then be increased, accounting for the reduced charge collected. We would expect [2-3] that approximately 10^7-10^8 charges would be necessary for this shielding to occur, consistent with the observation that the onset occurs when about 10^8 charges have been produced.

The second bending of the curve is believed to be due to the nearly complete ionization of the volume of the focused laser beam. Assuming a focal volume, 50 μm in diameter and 500 μm long, complete ionization corresponds to the production of about 10^{12} charges. If we extrapolate the low intensity results to the intensity where this bending sets in, we obtain about 10^{11} charges, consistent with our interpretation. It is necessary to extrapolate the low intensity results in order to correct for space-charge-induced recombination.

2. Space-Charge Studies--Experimental

In these studies we were interested primarily in studying the motion and evolution of charges in an externally applied field under conditions for which the internally generated space charge field can dominate the externally applied one. The motivation for this work is

to understand better space-charge controlled phenomena such as streamers, which probably play a crucial role in fast, gaseous switching devices. Although the streamers have been regarded as responsible for breakdown under a wide range of conditions for many years [2-4], to date there is little physical, quantitative understanding of their formation and propagation [5-6]. Since we believe streamers to play a crucial role in fast, laser-triggered switches, as well as other fast triggered switching devices, it is important that these phenomena be understood at the most basic level possible. The experimental work described here is intended to complement the theoretical work which has been under way for some time and which is described in the next section.

A schematic diagram of the apparatus we constructed for these studies is shown in Figure 9. Basically, it consists of a parallel plate electrode assembly enclosed in a clean vacuum chamber which can be evacuated and then backfilled to any desired pressure with any gas. The electrode assembly consists of four plane-parallel electrodes. As shown in the figure, the two inner electrodes are made of a nearly transparent mesh (85%), and the outer electrodes are solid metal plates. The purpose of the mesh electrodes is to detect the displacement current resulting from charge motion in the gap and to shield the solid electrodes from these fields so that they detect primarily the actual arrival of charge. Electrical connection to all four electrodes is made through a high vacuum feedthrough to the outside, where they

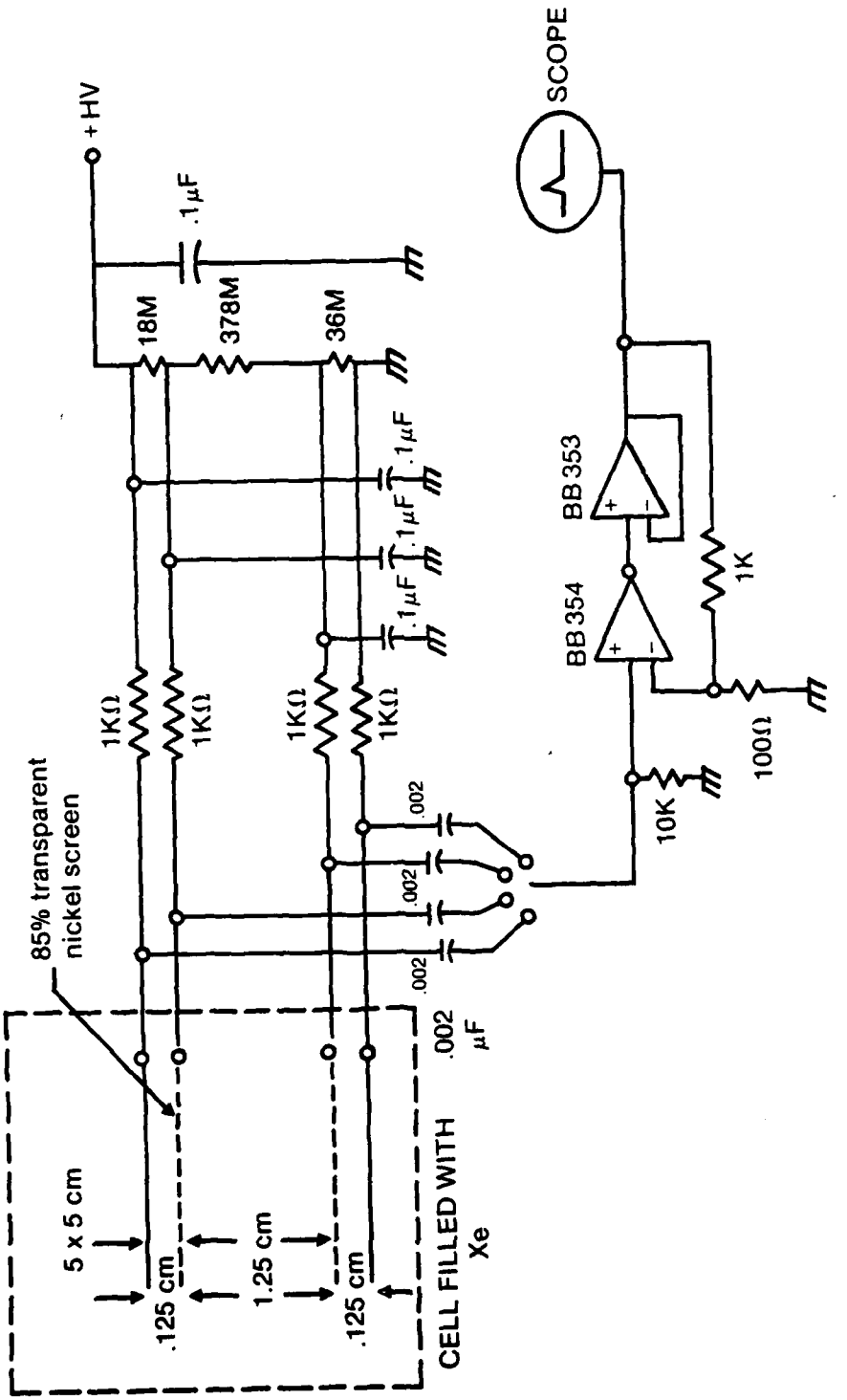

Fig. 9 Schematic diagram of apparatus for monitoring the motion of charges in an external electric field. The screen electrodes monitor the displacement current in the gap and the solid electrodes record the arrival of charge.

are connected to a power supply and, through a coupling capacitor, to a high input impedance preamplifier. In order to provide maximum sensitivity, the preamplifier is placed directly on the cell to minimize stray capacitance and noise pickup.

In operation the cell is filled with either pure xenon or a xenon-containing mixure, and a laser beam, tuned to the 3-photon transition to the 5d(3 1/2) state of xenon (364 nm), is passed transversly through it without striking either electrode surface. The laser is focused to a point roughly centered between the parallel plate electrodes by a 10 cm focal length lens. As discussed in the first section, the laser will, if precisely tuned to resonance with this transition, generate ionization in the focal region. A moderate voltage is applied between the screen electrodes so that the charges produced will be collected and detected. Additionally, a smaller voltage difference is maintained between each screen electrode and the solid electrode it covers in order that the charges will continue to drift through the screen and be collected on the solid electrodes.

Oscillograms showing the voltage waveforms on each of the four electrodes for a typical experiment are shown in Figure 10. In this case, 400 volts was applied between the screen electrodes, the fill gas was pure xenon at 50 Torr, and the laser power was such as to produce about 10^{10} charges. In order to achieve fast time response a 1 kΩ load resistor was used, giving a current sensitivity of 1 mA/V. The laser pulse was about 6 ns long.

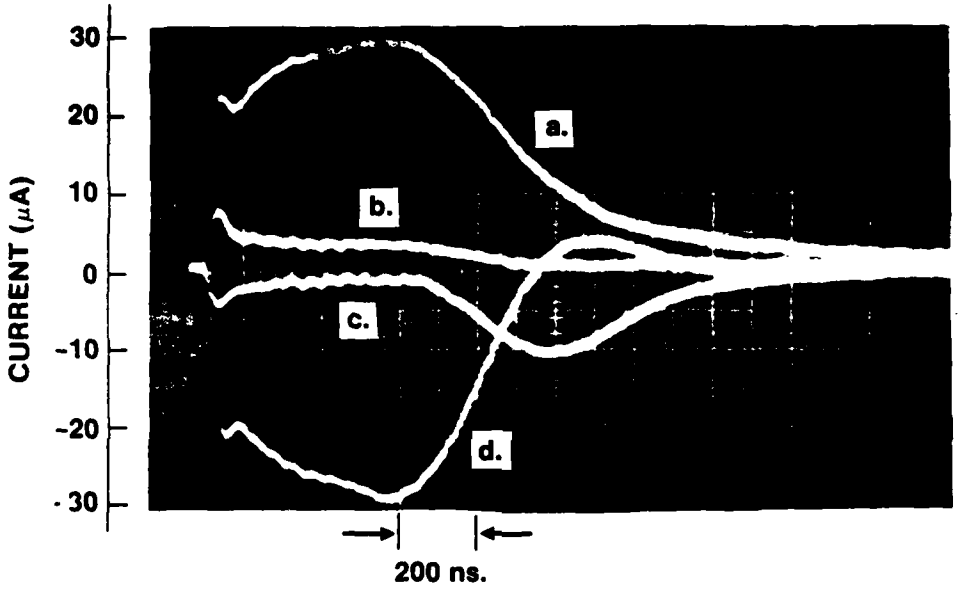

Fig. 10 Current oscillograms obtained with the cell shown in Figure 9. The four traces correspond to currents in the a) solid cathode, b) screen cathode, c) screen anode, and d) solid anode.

These results readily lend themselves to a very clear interpretation. The positive ions drift much more slowly in the field than do the electrons, and for the purpose of this discussion we will consider them to be immobile on the time scales we are considering. From our previous work on multi-photon ionization in xenon, we know that the charge we are producing is sufficient to allow the plasma to shield itself from the external field. In shielding itself, the initially neutral plasma must allow some negative charge to escape in order to set up the charge distribution necessary to cancel out the applied field. This pulse of negative charge drifts across the gap in the applied field and produces the long pulses seen on both screen electrodes.

As long as the electron pulse is entirely between the two screens, the voltage waveforms seen on each should be symmetric. After the front of the pulse crosses the anode screen, its effect on the opposite screen disappears, and the displacement current seen on the anode screen changes sign because at this time the pulse is moving away from the screen. At the same time, the solid plate anode will start to record a displacement current since the pulse is moving towards it and is no longer screened. This situation continues until the pulse intercepts the solid anode and disappears. Similar effects should not be seen on the cathode electrodes.

Exactly these effects are observed experimentally, as seen in Figure 10. Both screen electrodes record roughly rectangular pulses, with the anode electrode recording a pulse which changes sign. The solid anode behind it records a shorter pulse which starts at just the

time that the anode screen current starts to fall. The cathode screen electrode records a current pulse essentially symmetric with that on the anode screen, except that it decays monotonically to zero, starting at the same time that the anode waveform falls. Very little activity is observed on the solid cathode. The small signals we see are believed to be due to the imperfect screening of the solid electrodes by the screen, and, perhaps, capacitive coupling between the two.

After the departure of the electronic charge cloud, there remains a shielded plasma in the gap center. This plasma decays by recombinaion and by the slower drift of positive ions towards the cathode. In this stage electrons leave the cloud at approximately the same rate as do the positive ions. Since the mobility of the ions is relatively low, the displacement current observed during this state is small. In experiments completed by the end of the contract period, we had not clearly seen this current, and an effort was underway to improve the sensitivity of the system without sacrificing time response.

We can estimate the total charge required to shield the plasma from the applied field by integrating the displacement current resulting from the motion of these electrons. Although there will certainly be some dependence on applied field, we can estimate the charge required from the discussion in the preceding section regarding the first saturation in the ionization efficiency vs. laser power curves. We found that space charge effects first appeared when approximately 10^8

charges had been produced, and we therefore expect that roughly this number of charges is necessary for shielding. Integrating the current measured by the cathode screen in Figure 10, we find a charge of about 2×10^{-11} Coulomb ($= 4 \times 10^{8}$ charges), in good agreement with predictions. The total charge collected by the solid anode is considerably less than that detected by the anode screen in this figure. In this experiment the electric field between the screen and solid electrodes was about 40% of that between the two screens, and we believe the discrepancy in charge collected by the two electrodes to be due to the interception of charge by the screen due to the sudden decrease in field strength.

In another experiment, using half the voltage to collect the charges, we find that approximately 70% as much charge is required for shielding. In a simple model we would expect the charge required for shielding to scale roughly linearly with the appled field, implying that only 50% as much charge would be required in the weaker field case. These two figures are in reasonable agreement, considering the crudeness of the model we are using.

Another interesting feature of the current waveforms in Figure 10 is the small, sharp spike on the leading edge of each waveform. The most likely explanation of this feature has to do with the initital motion of the electrons in the plasma to set up the shielding charge distribution. If the plasma was completely formed instantaneously, at the instant of creation all electrons would feel the total applied

field and move accordingly, producing a large displacement current. This motion would rapidly set up a field opposing the applied field inside the plasma, thereby shielding the inerior, and halting the mass motion of electrons. Those electrons on the outer surface, however, still would experience the applied field and drift away. It is these electrons which are detected as the long pulses on both screen electrodes. We believe the short spike feature to be caused by this initial electron mass motion. The spike is probably much larger and narrower than what we observe, but is attenuated and lengthened by the rather slow response time of the amplifier (~ 40 ns). The fact that the spike is about equally strong in either the screen or the shielded, solid electrode waveform is probably due to either incomplete shielding at these high frequencies, or more likely to capacitive coupling between the screen and solid electrodes.

A second possible explanation for the feature involves photoemission from the electrode surfaces. The multi-photon ionization process involves a resonant transition to the 5d (3 1/2) state of Xe, lying about 10 eV above the ground state. Dipole transitions back to the ground state are allowed, and strong U.V. emission with this energy is emitted. These photons are easily able to cause photoemission from the metallic surfaces, and the spike could be the result of these processes. In this case however, we would expect the width of the spike to be significantly longer. Also, we would expect this energetic U.V. emission to be strongly self-trapped in the xenon fill gas.

3. Space Charge Studies--Theoretical

A program aimed at understanding the motion of charges in an externally applied field under space-charge-dominated conditions has been underway for some time. The theoretical side of the program has involved basically the solution of simple conservation equations which include an ionization term. The presence of this term makes the equations non-linear and difficult to solve analytically, and efforts at solution have been primarily numerical ones. These efforts have led to the development of a fairly fast, robust Poisson's equation solving routine for finding the space-charge-induced field, as discussed in our previous annual report [7,8].

We have since turned our attention to the numerical solution of the conservation-based transport equations. Our first efforts in this direction were based on a technique described by Davies et. al [9] which makes use of the method of characteristics to eliminate most of the spatial derivative terms in the equations. The method is rather difficult to implement and time consuming to use because it is necessary to estimate the characteristic path of the system, then calculate its motion based on this estimate, then correct the characteristic estimate, etc. until suitable convergence is attained. Since each cycle of estimation-correction also involves the recalculation of the electric field, this procedure can be quite time consuming [10].

At the close of the contract period, we had decided to abandon this approach in favor of a flux corrected transport algorithm [10,11]. Basically, the type of equations we are trying to solve are of the form

$$\frac{\partial \rho}{\partial t} = - \vec{\nabla} \cdot (\rho \vec{w})$$

This type of equation may be solved numerically using standard finite difference methods, but it is well known that even in the simple case where the velocity, $\vec{w}$, is constant, these methods do not yield a satisfactory solution. For the constant velocity case, the analytic solution consists of the initial charge distribution drifting uniformly without distortion. Depending on the order of the method used, for an initial rectangular charge density, the finite difference solution gives either a diffusing, or a "ringing" charge density. With the flux corrected transport method, the equation is integrated first with a high order method, which tends to produce overshoot. The algorithm works by detecting the onset of this overshoot, and then changing to a low order method for which the solution exhibits numerical diffusion. After this lower order method has corrected the overshoot of the higher order method, the higher order method is again used. The flux corrected transport algorithm has been used with considerable success for one dimensional problems of this type [10], but there has been only a little work reported on the adaptation of it to two dimensional problems [11]. At the close of the contract period we were investigating the feasibility

of using the algorithm in two dimensions. Since that time we have written a computer program to implement it in two dimensions, and the results appear promising, but there are still some problems with numerical diffusion or overshoot. Work is continuing to understand the origin of these problems and to correct them.

4. Multiphoton Ionization/Inverse Bremsstrahlung Heating for Gas Triggering

Hargis [12], Hargis et. al. [13], and Woodworth and Hargis [14] have described the results of several experiments designed to improve the operation of their laser-triggered switches for use on PBFA II. The switching configuration which they propose to use is a longitudinal one in which the laser enters and exits the gap region through holes in the electrodes. Triggering is thought to be the result of free charge left in the gap as a result of the laser, produced through a mechanism that is not well understood. In their early experiments, triggering was accomplished through the use of a high mode-quality, excimer laser system and a spark gap filled with either SF_6 or a mixture containing small quantities of an organic seed gas with a low ionization energy. Although the laser caused the production of a spark in the gas, this initial charge production was thought to be through a photoionization process. Excellent triggering was reported with these switches, with delays of a few ns and easily sub-nanosecond jitter.

More recently, experiments have been reported in which a pulsed, Nd:YAG laser was used for triggering. It was found that excellent triggering could be obtained in SF_6 using the frequency quadrupled 255 nm output of the YAG laser. The use of longer wavelengths (> 355 nm) resulted in longer delays, and more jitter even though more power was available. This observation was explained by postulating that the 255 nm laser produced ionization in the gas through either single or multiple photon ionization. This ionization then acted as a seed for further heating, leading to breakdown of the gas in the laser focus and subsequent rapid switch closure. With a longer wavelength laser, the radiation would not have sufficient quantum energy to drive the photo-ionization process, and the initial charge for the gas breakdown must be supplied from some other source.

This conjecture was partially supported by experiments they carried out using both the fundamental and quadrupled YAG laser frequencies. With only the 1.06 μm YAG fundamental, the gas could easily be induced to break down by the laser, but there was considerable jitter in the time of this breakdown. We have made a similar observation (See Project No.2). The emission from the laser spark with the 1.06 μm fundamental was much more intense than with the 255 nm radiation. When both frequencies were applied it was found that emission from the laser spark appeared immediately, similarly to the 255 nm only case, but the emission was quite intense, similiar to, but even stronger than, the emission with 1.06 μ only. The explanation was that with 1.06 μm

radiation only, the inversie bremmstrahlung heating must build up from a very low initial charge density in the gap. With the addition of the 255 nm radiation, photo-ionization of the gas could take place, providing substantial amounts of charge simultaneously with the 255 nm laser trigger. With this initial seed charge, the inverse bremsstrahlung heating can then act to heat the gas rapidly, to a spark, with much reduced jitter.

We set out to verify this mechanism using our apparatus for producing multiphoton ionization in xenon. The 1.06 μm fundamental and the 365 nm tunable radiation from our YAG-based system were focussed coaxially into a cell containing xenon. The power of the 1.06 μm beam was sufficient to produce easily a spark in the xenon, the emission from which was detected with a fast photo-detector. As expected, we observed a delay of about 5 ns in the formation of the spark when the U.V. was either removed or was detuned from resonance with the multiphoton ionizing transition. At the close of the contract period, we had not, however, observed any significant effect of the U.V. on the spark formation, even when properly tuned. Since the multiphoton ionization process should nearly completely ionize the focal volume of the lens at full laser power, this observation was at first unexpected. We now believe that the null result is the result of a timing problem. For several reasons, the colinear U.V. and the 1.06 μm beams from the WEX-1 frequency mixer were not separated, and were focussed together into the cell with the same lens. Since the ionization process depends on the cube of the laser intensity,

significant ionization is produced only near the peak of the laser pulse. Typically, by the peak of the pulse, the gas had already broken down, so that any ionization produced by the U.V. beam would be superfluous. The obvious next experiment in which the two beams are separated and one is delayed by a few ns with respect to the other had not been carried out at the end of the contract period because of difficulties in separating the beams and then aligning them so that they precisely overlap in the cell. Work in this regard in continuing.

5. Photodetachment for Discharge Control

In collaboration with Dr. G. Schaefer, and in direct support of the work being carried out in Project No. 8, "Optically Controlled Discharges," we have carried out a set of experiments intended to evaluate the feasibility of using photodetachment of negative ion species to provide optical control of diffuse discharges. This work is described in some detail in the report on Project No. 8, and only a very brief summany of the results will be given here.

As a direct result of conversations with Dr. J. Moseley of the University of Oregon and Dr. K. Schoenbach of our Department, we decided to test the possiblity of using a laser to photodetach the dominant negative ion species in a diffuse glow discharge, and, thereby, modify the operation of the discharge. If the photodetachment is sufficiently efficient, the laser will effectively turn off the attach-

ment processes in the discharge and significantly modify the discharge characteristics. The experimental study was divided into two parts, one in which we determined if substantial photodetachment was possible, and the second in which we investigated the range of effects on the glow discharge. The system initially chosen for study consisted of He buffer gas mixed with O_2. The O_2 forms O^- and to a lesser extent O_2^- in the discharge. O^- may be photoionized with visible light, but not with 1.06 μm radiation; whereas O_2^- is photo-ionized with either. Using 10 mJ of 550 nm light, we found that we could photodetach nearly all the O^- in a volume defined by the laser beam dimensions in the discharge, showing that the detachment effect can be substantial. In a separate experiment, we found that we could produce large external effects, in that we could change the discharge voltage by more than 50% with similiar laser energies. Work is continuing to define better the limits of operation of such a device for opening switch applications. Although several serious problems must be solved before a practical device could be made using this technique, the results to date appear promising.

C. REFERENCES

[1] P.F. Williams, et. al, "Excited State Spectroscopy of Electrically Excited Gases," Second Annual Report on Coordinated Research Program in Pulsed Power Physics, pp. 121-132, (December 1981).

[2] H. Raether, Z. Phys. 112, 464 (1939).

[3] H. Raether, Electron Avalanches and Breakdown in Gases, (Butterworths, London, 1964).

[4] L.B. Loeb and J.M. Meek, J. Appl. Phys. 11, 438 (1940).

[5] A.J. Davies, C.S. Davies, and C.J. Evans, Proc. IEE 118, 816 (1971).

[6] U. Timm, "The Development of Single Streamers Started by Laser Light at High Overvoltages in Rare Gases," J. Phys. D: Appl. Phys., 6, 1891 (1973).

[7] P.F. Williams, et. al., "Transient Processes in Laser-Triggered Breakdown" Second Annual Report on Coordinated Research Program in Pulsed Power Physics, pp. 18-26, (December 1981).

[8] E.E. Kunhardt and P.F. Williams, "Direct Solution of Poisson's Equation in Cylindrically-Symmetric Geometry," to be submitted for publication.

[9] A.J. Davies, C.J. Evans, P. Townsend, and P.M. Woodison, "Computation of Axial and Radial Development of Discharges between Plane Parallel Electrodes," Proc. IEE, 124, 179 (1977).

[10] R. Morrow, "A Review of the Methods of the Solution of Hyperbolic Equations for Electron and Plasma Motion in Uniform and Non-Uniorm Field," Conference on Numerical Solutions of Partial Differential Equations, Melbourne, (1981).

[11] S.T. Zalesak, "Fully Multidimensional Flux-Corrected Transport Algorithms for Fluids," J. Comp. Phys. 31, 335 (1979).

[12] P.J. Hargis in the 35th Annual Gaseous Electronics Conference, Dallas (1982).

[13] P.J. Hargis, L.C. Pitchford, T.A. Green, J.R. Woodworth, and R.A. Hamil, "Multifrequency Laser Breakdown in SF_6," in the 35th Annual Gaseous Electronics Conference, Dallas (1982).

[14] J.R. Woodworth and P.J. Hargis, "A Parametric Study of Laser Triggering of a 500 kV Gas-Filled Switch", in the 35th Annual Gaseous Electroncis Conference, Dallas (1982).

Project No. 6

Exploratory Concepts

(R. Curry, B. Maas, D. Johnson, H. Carper, R. Pederson, H. Krompholz, K. Schoenbach, L. Hatfield, M. Hagler, and M. Kristiansen)

A. SUMMARY

In this project several smaller investigations are undertaken. Among them are investigations of surface discharge switches, restrike in gas blown spark gaps, voltage measurements in high current spark gaps, and evaluations of novel opening switch concepts (in cooperation with Project No. 9).

A simple method (blowing air across the switch substrate surface) has been found for maintaining multichanneling over at least 10,000 shots in a surface discharge switch. Substrate damage and changes have been compared for several substrate materials. Some of the results are summarized in the conference paper included as Appendix 1.

The high speed interferometric and schlieren studies of a gas blown spark gap led to a proposal which was separately funded by AFOSR Grant No. 82-0327. The early results are summarized in the conference paper included as Appendix 2.

A new experimental facility has been designed and constructed for making measurements of the resistive voltage drop in a high current arc ($I > 10$ kA). Plans have been formulated for determining all the possible additional, extraneous voltage components which usually make these measurements difficult to interpret.

We have also developed a new opening switch concept which involves using an applied transverse magnetic field to shift the electron distribution into a region of high electron attachment by a neutral gas component. Discussions have been held with industry for a possible cooperative effort to determine the feasibility of this switch concept.

We are planning a cooperation with Dr. G. Gerdin at the University of Illinois on the use of the Dense Plasma Focus as an opening switch. This research is being funded at the University of Illinois under AFOSR Grant No. 79-79-0121. Our initial assistance will be in helping on diagnostics and to design a DPF device which is more reproducible than other, such devices.

B. THE SURFACE DISCHARGE SWITCH
(R. Curry, D. Johnson, L. Hatfield, and M. Kristiansen)

This report covers those points not discussed in the attached conference paper "Multichannel Surface Discharge Switch" (See Appendix 1). Conclusions drawn from surface analysis of the dielectrics used as the switching surface are presented under Project No. 4.

It is worthwhile to point out that all dielectrics gave essentially the same results for the selfbreak field (± 10%) and the number of channels per meter (± 15%), except for the G-10 coated with Boron Nitride. Apparently, the Boron Nitride did not bond very well to the G-10.

Experiments have now also been done with a single channel arrangement. The electrodes were modified by attaching K-33, tungsten-copper composite, hemispheres to the plane electrodes. The arc always occurs in the same place on the dielectrics and all the current passes through

this single arc. The erosion rate per shot is therefore, higher than before and fewer shots are required to evaluate a dielectric. Delrin and Lucite actually show signs of melting after 1000 shots. The thickness of the dielectric samples has been reduced to 0.625 inches to facilitate weight loss measurements. Preliminary results show no weight loss for Delrin after 10,000 shots in the multi-channel mode. If this is borne out by subsequent measurements it would indicate that the Delrin simply melts and moves away from the arc path since visual inspection reveals an indentation at the position of the arc.

The risetime of the pulse applied to the stripline has been decreased by replacing the energy storage capacitor with a 6 ohm transmission line. The faster risetime is required for jitter measurements when the surface switch is trigggered, either electrically or using a laser.

The stripline load resistor has been changed to a stack of ceramic disk resistors replacing the liquid resistor. This improves the reliability of the load voltage and current measurements. Also, the capacitive dividers used in the stripline as voltage probes have been improved and calibrated.

At the present time we are continuing some substrate erosion measurements and trying to understand the associated surface physics. In addition we are investigating electrical and laser trigger methods for producing multi-channeling. (Earlier multi-channeling was produced by overvolting the gap). The ability to produce reliable, low jitter, multi-channel events is of considerable importance to future practical applications of this switch and its unique properties.

C. INTERFEROMETER STUDIES OF GAS BLOWN SPARK GAPS

(H. Carper and R. Pederson)

In the last annual report, preliminary results of some exploratory work on the application of optical techniques to the study of the fluid mechanics aspects of gas blown spark gap switches were presented. At that time, experiments were being planned to attempt to photograph, through the use of a Mach-Zehnder interferometer and high-speed photography, the postulated restrike of the arc through the low density, post arc gas, blown downstream of the minimum gap spacing. These experiments were successful, and the premature restrike was verified for the first time. The resulting interferograms were presented at the Fifteenth Power Modulator Symposium, Baltimore, June 14-16, 1982. (See Appendix 2). This work is continuing under grant number AFOSR 82-0327.

D. SPARK GAP VOLTAGE MEASUREMENTS

(B. Maas, M. Hagler, and M. Kristiansen)

A study has been made of various methods to measure the voltage between the electrodes in a spark gap during the breakdown phase. This is important in order to determine the energy input to the electrodes and hence aid in understanding the erosion mechanism. The measurement is complicated because, prior to breakdown, the voltage across the gap voltage drops rapidly and after a few microseconds is no more than a few hundred volts. The measured voltage drop also has several

components ($V = iR_{arc} + iR_{electrode} + L_{meas\ loop}\, di/dt + L_{arc}\, di/dt + idL_{arc}/dt$) which it is important to distinguish between. Calculations have been made of the expected relative size of these voltage components and methods for determining or eliminating each of them have been tentatively identified.

A method for the elimation of the measuring loop inductive term is given in Ref. [1], and consists basically of introducing a compensation loop in the measuring circuit. Measurements of the arc radius as a function of time are being investigated in order to verify which, if any, of the available expressions [1-5] are correct. Given the arc radius as a function of time, the inductance of the arc can be calculated quite accurately. This calculated value, together with measurements of i and di/dt, take care of the $L_{arc}\, di/dt$ and idL_{arc}/dt terms of the total voltage drop. It should also be possible to calculate accurately the resistive drop in the electrode shafts from skin depth calculations. These calculations can be verified by comparing results from different electrode shaft lengths. Subtracting the above terms from the total measured voltage drop leaves only the resistive drop in the arc.

With the above considerations in mind, the Mark IV spark gap was designed and constructed (Fig. 1). The spark gap is driven with a simple, critically damped, capacitive generator, (1.88 μF, 45 kV, 40 kA, 1.9 kJ). The current risetime is approximately 800 ns. The electrode shafts provide ample room to connect the probe at several different points in order to check the accuracy of the skin depth resistance calculations.

Fig. 1 Mark IV Spark Gap Assembly for V-I Measurements

E. MAGNETICALLY CONTROLLED OPENING SWITCH (in cooperation with Project No. 9)

(K. Schoenbach, G. Schaefer, and M. Kristiansen)

Production and sustainment of diffuse discharges in attaching gases is simpler in low pressure systems ($p<1$ Torr) than at gas pressures of 1 atmosphere and above. However, their application as optically or e-beam controlled opening switches is limited because the mean free path for attachment processes exceeds the geometrical dimensions of the switch.

To overcome this problem, a concept can be used where magnetic fields switch the system from a non-attachment into an attachment-dominated state. Assume that the voltage drop across a low pressure discharge is on the order of 10 to 100 V, occuring mainly in the electrode region. The electrons in the positive column then have a narrow energy distribution around the value of the accelerating energy. If the gas is an attacher with an attachment cross-section peaking below 1 eV, then there is almost no formation of negative ions, which means no attachment loss processes in the discharge.

As soon as a transverse magnetic field is applied to the system, the peak of the electron energy distribution is shifted to lower values, depending on the magnetic field intensity. Simultaneously the distribution is broadened due to the change of the velocity distribution of the gyrating electrons due to the increase in the number of collisions. The result is that electrons are driven into an energy range where attachment is effective. Due to the reduction of the electron density

by attachment the conductivity is reduced and the switch opens.

The opening time is affected by the time necessary to apply a magnetic field and the formation time for negative ions. Time constants on the order of 100 ns should be attainable.

An experimental arrangement for verifying this concept has been designed and "back-of-the-envelope" calculations have been made of the relevant parameters for the switch operation. Discussions have been held with industrial companies regarding a possible joint development effort for this novel idea.

F. DENSE PLASMA FOCUS

(H. Krompholz, K. Schoenbach, and M. Kristiansen)

A cooperative research program has been initiated with the University of Illinois (Dr. G. Gerdin) on the use of the Dense Plasma Focus as an opening switch. Conventional Plasma Focus devices can be considered as opening switches with no load attached. They interrupt approximately 50% of the current flowing through the focus. The interruption causes a strong voltage pulse across the focus plasma. At current levels of up to several MA, voltage spikes of several 100 kV were observed. Typical effective impedances of 0.3 Ω are generated in times of the order of 10^{-8} to 10^{-7} s. Repetitive Operation (repetition frequency: several 100 kHz) was achieved in a burst mode lasting for 50 μs. However, the opening effects were highly nonuniform and couldn't be controlled externally.

In order to use the Dense Plasma Focus as an efficient repetitive opening switch two main problems have to be solved first:

1. diverting the generated power into the load without disturbing the opening effect in the focus plasma
2. external control of repetitive switch events.

An experimental and theoretical research program in the Plasma Focus Group at the University of Illinois, is planned to determine whether the potential of a plasma focus repetitive opening switch can be realized.

The contribution of Texas Tech University consists mainly of consulting (Drs. Schoenbach and Krompholz). Dr. Krompholz will spend one month at the University of Illinois to consult on electrical and microwave measurement techniques and on methods to increase the homogeneity and reproducibility of the focus discharge. Besides consulting, high speed dignostic techniques which have been developed at TTU will be provided for application in the University of Illinois plasma focus work.

G. MISCELLANEOUS STUDIES

(M. Kristiansen)

The effect of various quenching materials on the interruption time and hold-off voltage and time for electrical fuses was investigated briefly. An interesting observation was that sugar apparently gave better results than the commonly used NaCl and silicon beads. Due to a lack of manpower availability a resource management decision was made to delay

indefinitely any further work along these lines.

Some modest efforts were also made to study the limitations on magnetic opening switching. Most of the locally available magnetic cores were found to have too wide and gradually changing hysteresis loops but current interruption was achieved at t ~ 150 ns with a switch efficiency of about 50%. Some continuing modest efforts along these lines are planned using Metglass cores.

A planned study of shock reduction in liquid filled spark gaps was deferred indefinitely due to lack of available manpower. A field effect electrolyte switch was studied theoretically. The switch held the promise of handling high average powers and to be "self repairing". The studies indicated, however, that its operation would be too slow to be of practical interest.

H. REFERENCES

[1] A.B. Hillan, Proc. of the 4th International Conference on Ionization Phenomena in Gases, p. IID 472, (1959).

[2] S.I. Braginskii, Soviet Physics - JETP, 34, 1068, (1958).

[3] G. Herziger, L. Bakowsky, W. Peschko, and F.W. Linder, Physical Letters, 69A, 273, (1978).

[4] A.I. Pavlovskii, G.V. Karpov, G.G. Katraev, N.I. Leonova, and E.N. Smirnov, Sov. Phys. Tech. Phys. 20, 182, (1975).

[5] S.I. Andeev, M.P. Vanykov, and A.B. Kotolov, Sov. Phys. Tech. Phys., 7, 37 (1962).

APPENDIX I

MULTICHANNEL SURFACE DISCHARGE SWITCH*

D. Johnson and M. Kristiansen
Department of Electrical Engineering
and
L. Hatfield
Department of Physics

Texas Tech University
Lubbock, Texas 79409

ABSTRACT

The performance of a multichannel surface discharge switch has been investigated as a function of the dielectric material. The switch operates at 45 kV and transfers 180 joules per shot at a rate of 1.2 pps in ambient air. Dielectrics presently under investigation include Delrin, Blue Nylon, Kapton, Lucite, G-10, Macor ceramic, and two forms of boron nitride. The dielectrics are compared by observing their erosion, changes in breakdown voltage, and the number of channels per meter during discharges. The surfaces of three of the dielectrics exposed to 10,000 shots have been studied using ESCA.

INTRODUCTION

A surface discharge switch conducting the same current as many switches in parallel has a lower impedance and avoids the complications of simultaneous triggering of parallel switches. The surface switch owes its unusually low impedance to the geometry of the arc paths.

---

* Supported by the U.S. Air Force
Office of Scientific Research

Designed as a section of a parallel planar transmission line, the switch offers minimum impedance change in the current path. This technique can also be applied to a coaxial line if the switch dielectric is available in the form of a cylinder.

Measurements have been made on the delay and operating times of a surface discharge switch [1] and on the development and characteristics of the arc channels [2]. Little research has been done in the crucial area of dielectric damage and erosion rates for various combinations of dielectrics, electrode materials, and filler gases. Because of the large number of possible combinations of these three parameters, we have chosen as a starting point to study only the dielectrics. The best dielectric candidates from this study can then be combined with several gas-electrode pairs to determine the combination of the three parameters which produces the "best" surface discharge switch. This paper describes the test arrangement and results of the first of a set of experiments developed to determine which dielectric materials are best suited for use in triggered surface switches.

EXPERIMENTAL ARRANGEMENT

The experimental apparatus diagramed in Figure 1 includes a 0.18 microfarad capacitor in series with a railgap which is connected to the end of a 6 ohm stripline. The surface switch shown in Figure 2 is designed so that electrodes and dielectric samples can be easily replaced. The switch electrodes are 20.3 cm wide and the gap separation can be varied from 0.0 to 4.0 cm. The dielectric sample is placed in a slot that has been cut into the line insulator so that the discharge path is along the original dielectric/strip-conductor interface. In this arrangement the switch geometry introduces very little additional inductance. The line is terminated in a matched, 6 ohm, copper sulfate water load.

A surface switch gap of 2.3 cm results in a selfbreak voltage of 20-25 kV with the railgap shorted. Setting the railgap to selfbreak at 45 kV causes the surface switch to be overvolted by approximately 200% before each discharge. This promotes intense multichanneling (100 to 150 channels per meter) across the dielectric. The multichanneling

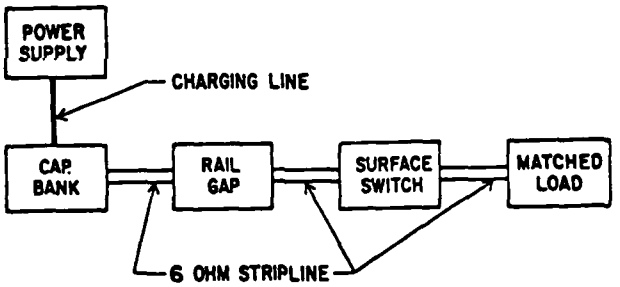

Fig. 1 Surface Discharge Switch Block Diagram

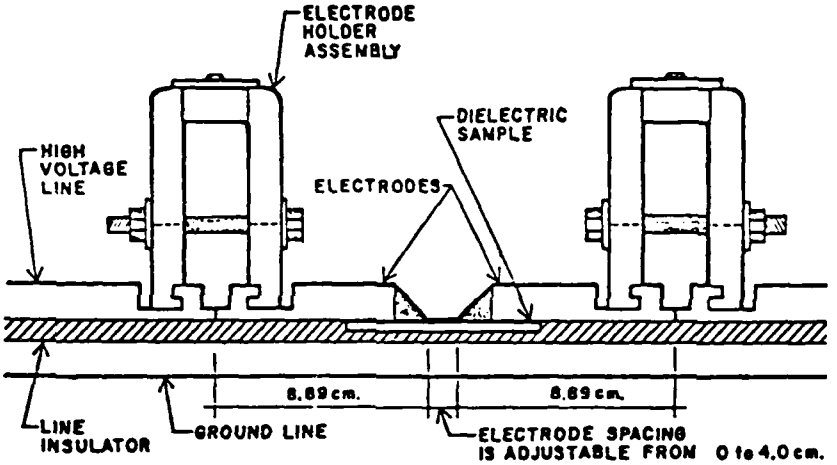

Fig. 2 Side View of Switch Assembly

characteristics for different dielectrics can then be compared without actually triggering the surface switch.

Capacitive probes in the stripline allow monitoring of the load voltage with an oscilloscope while a video camara records the multichanneling events at the switch. By using the pause feature of a video recorder when viewing the video tapes, the number of discharge channels can be counted and compared on a shot-to-shot basis.

EVALUATION PROCEDURE

To compare dielectrics, samples of each material are subjected to an identical evaluation procedure. Each sample is cut and machined to fit the stripline slot dimensions, 25.4 cm by 7.62 cm by 0.48 cm. Care is taken during machining to minimize contamination of the samples. The sample is cleaned with methanol and then transformer oil is wiped onto the underside of the sample to reduce microscopic voids between the line insulator and the dielectric sample. The brass electrodes are wiped with methanol and paper towels before they are clamped into position.

Each dielectric sample is subjected to 10,000 shots at 45 kV. The energy per shot at this voltage is 180 Joules. The peak current is 8 kA and the charge transferred per shot is approximately 8 mC. The shot rate is 1-1.2 pulses per second.

During the first several hundred shots of a run, three measurements are recorded. First, the selfbreak voltage is recorded for 10 shots and averaged. Next, the test voltage is recorded to insure uniformity between runs. Then, 20-30 consecutive shots are recorded with the video cassette recorder for later counting of arc channels per meter. The above procedure is repeated near the end of the run, i.e. after 9500-9800 shots, establishing a "before" and "after" data base from which to compare degradation of dielectrics.

RESULTS AND CONCLUSIONS

Only one of the samples compared in Table I, Boron Nitride sprayed on a G-10 substrate, was damaged enough to noticeably alter the performance of the switch. Several samples showed grooves or eroded arc tracks up to 0.5 mm deep caused by the repeated occurance of arcs at the damage site. The samples were inspected with the aid of an 80 power optical microscope. Two of the samples, G-10 and Macor, showed no visible evidence of erosion.

Electron Spectroscopy for Chemical Analysis (ESCA) has been completed on three of the dielectrics: G-10, Lucite, and Delrin. The analysis of the virgin sample of G-10 showed the composition to be approximately 74% carbon and 26% oxygen. After 10,000 shots the surface material

DIELECTRIC MATERIAL	SELFBREAK FIELD(kV/cm) BEFORE	AFTER	CHANNELS/METER BEFORE	AFTER
Blue Nylon	9.7	9.3	150	140
Boron Nitride (BN)	9.3	9.3	120	120
BN Coating Sprayed on G-10 Base	10.6	5.3	160	150
Delrin	10.3	10.1	140	120
G-10	9.0	8.7	140	160
Kapton	8.8	8.0	150	150
Lucite	10.2	10.2	150	130
Macor	7.5	7.9	120	120

Table I Comparison of Dielectric Samples "Before" and "After" 10,000 Shots in the Surface Switch.

was found to be composed of 60% carbon and 40% oxygen. Delrin behaved similarly with a decrease in carbon from 75% to 33% and an increase in oxygen content from 25% to 67%. By contrast, the analysis of Lucite showed an increase in carbon from 71% to 77% and a decrease in oxygen from 29% to 23%.

These changes indicate an oxidization of the G-10 and Delrin surfaces although the analysis was not detailed enough to determine the particular oxygen bonding or the compounds involved. The surface of the Lucite appears to have carbonized slightly which should have lowered the surface resistivity of the material. Although this would eventually lower the selfbreak voltage, it might be beneficial in that surface charging would be reduced promoting enhanced multichanneling. The surface changes of the three materials, while significant, are difficult to evaluate in terms of performance of the dielectric in a switch. The preceding data taken together with the visual inspection of all the samples and results from other investigations indicate that a higher peak current is necessary to damage the dielectrics sufficiently to make a valid performance comparison.

Some of the samples showed a strong tendency to build up surface charges during the test procedure. After several hundred shots, the number of channels per shot would decrease until only 2-5 channels would occur on any shot. It was found that an air flow across the dielectric surface between the electrodes would remove these charges, allowing the switch to multichannel with 20 to 30 channels

per shot throughout the entire 10,000 shot run. To make the comparison between dielectrics consistent, the air flow was used during each run, even if a particular sample did not tend to collect charges.

The conclusions drawn from the data are that: a) A higher peak current per channel is needed to damage most of the dielectrics significantly so that they can be compared accurately. b) For several dielectric materials, air flow for removal of surface charging (or some other charge removal technique) is essential to achieve dense multichanneling and, hence, low impedance and low erosion rates of the dielectric and electrode materials. c) Several of the samples tested, such as Delrin, Kapton, and Lucite, showed a tendency to arc repetitively in a few tracks and cause significant erosion only in those tracks. It is likely that these materials would erode too quickly to make a reliable switch, capable of conducting higher current than the test switch.

In order to compare dielectrics that showed no significant erosion, a higher current per channel or higher repetition rate is required. One method to be used to increase the current per channel will be to alter the electrode geometry so that only one channel occurs for each discharge. The modification will increase the peak channel current to 7-8 kA, a regime that has shown a marked increase in damage rates in other investigations [3].

REFERENCES

[1] G.O.Belyaev, P.N.Dashuk, and M.A.Chernov, "Time characteristics of a multichannel grazing-discharge high-voltage switch," Soviet Physics-Technical Physics, vol. 24, pp. 578-581, May 1979.

[2] M.P.Vanyukov and E.V.Daniel', "Spark discharge over the surface of films of different composition," Soviet Physics-Technical Physics, vol. 12, pp. 1416-8, April 1968.

[3] P.M.Dashuk, A.K.Zinchenko, and M.D.Yarysheva, Erosion of dielectrics in the switching of high-pulsed currents by a grazing discharge," Soviet Physics-Technical Physics, vol. 26, p.198, Feb. 1981.

-138-

Flow Visualization in a Gas Blown Spark Gap

R. J. Pederson
H. J. Carper

Mechanical Engineering Department
Texas Tech University
Lubbock, Texas 79409

Summary

This paper presents results obtained during the initial phase of a study of effects of fluid mechanics and heat transfer on the performance of gas blown spark gaps. Air was blown between hemispherical electrodes with arc pulse rates of up to 300 pps. A Mach-Zehnder interferometer system was used to visualize the gas density variations during the flushing process. High-speed photographs show the flow patterns as the heated gas resulting from arc discharges convects out of the gap. These interferograms also show the effects of boundary layers near the electrodes, as well as the path of a typical prefire arc passing through the heated gas from the previous arc discharge. From this initial investigation, it is apparent that the interferometer represents a useful tool to obtain qualitative information about flow patterns in gas blown spark gaps. Work is continuing to develop this tool to obtain quantitative data for the post-arc gas density distribution as a function of time.

Introduction

It is well known that there is an important influence of the interelectrode fluid mechanics and related heat transfer processes on the performance of gas blown spark gap switches. In fact, for heavy-duty, rep-rated operation of these types of switches, the fluid mechanics often becomes the controlling factor in governing maximum rep rate. In general, the qualitative nature of switch behavior is such that if it is desired to increase rep rate, the gas blowing rate must also be increased in order to flush the postarc hot gas from the gap more rapidly. However, the physics of the flushing process is complex and poorly understood, and quantitative relationships between gap recovery time and the fluid mechanics and heat transfer are needed.

One problem involves relating gap breakdown voltage to the nonuniform gas density distribution which exists in the gap after an arc discharge and which changes with time as the hot gas is purged from the gap. The related problem is to determine, for a given arc discharge, this postarc gas density distribution history as a function of fluid mechanics, heat transfer, and electrical variables. Important variables influencing the gas density distribution history are the characteristics of the arc, properties of the electrode materials, electrode geometry, type of gas, and the mass flowrate through the interelectrode region.

In an effort to address the problem of experimentally determining the gas density distribution history following an arc discharge, the work reported here was undertaken. The short time scale on which the energy released by the arc and the subsequent flushing process occurs, the physically small space involved, and the high voltage potential between the electrodes render the use of probes to measure local density difficult if not impossible. Thus, the approach taken in this study was to use an optical method and high-speed photographic techniques in an initial attempt to visualize the flow in a gap, and to determine if effects on the gas density distribution history of several of the aforementioned variables could be seen. The electrode geometry chosen for this study is somewhat simplified, and the gas velocities and rep rates are admittedly low compared to those contemplated in practical gas blown spark gap designs. However, it was felt that many of the questions associated with the experimental methods could be answered using these simplified conditions.

Experimental Setup

A photograph of the experimental setup is presented in Figure 1. An electrode configuration consisting of two 1-inch diameter brass electrodes with spherical ends was used for all experiments. The electrodes were mounted between parallel insulating plates with no side enclosures. Thus, the electrodes were open to the laboratory air environment. Flushing of the interelectrode gap was accomplished by a jet of air issuing from a 2-inch diameter PVC pipe connected to a variable flowrate blower. The exit of the pipe was placed about two inches from the electrodes with the axis of the jet perpendicular to the axis of the electrodes. The gap was thus exposed to an essentially uniform free-stream blowing velocity with a direction normal to the path of the arc discharge. Arcs were generated by a relaxation oscillator arrangement with a 0-20 kV, 10 kW power supply. The values of the charging and load resistors were 100 KΩ and 25 Ω, respectively.

The electrode assembly was placed in the test section of a Mach-Zehnder interferometer with 6-inch diameter optical elements and a 15 mW helium-neon laser light source. The orientation of the blowing jet was such that a side view of the flushing process could be observed. Two different high-speed, 16-mm motion picture cameras were used to obtain the sample interferograms presented. With a 110-volt power supply, one camera provides full-frame pictures at up to about 4,800 pictures per second, and the other provides half-frame pictures at about twice the rate of the full-frame camera. A telephoto lens was employed with each camera.

Discussion of Results

The results of the present study are presented in Figures 2-5. Each figure presents a series of interferograms printed from 16-mm, high-speed, black and white reversal film (Kodak TRI-X Reversal film No. 7278). Since the prints were made from positives, they appear as negatives; that is, what would normally appear white to the eye appears black on the prints. This is particularly evident for the arcs shown in the figures.

All figures show a sequence of six photographs obtained at a camera speed of approximately 4700

CH1785-5/82/0000-0105$00.75 - 1982 IEEE

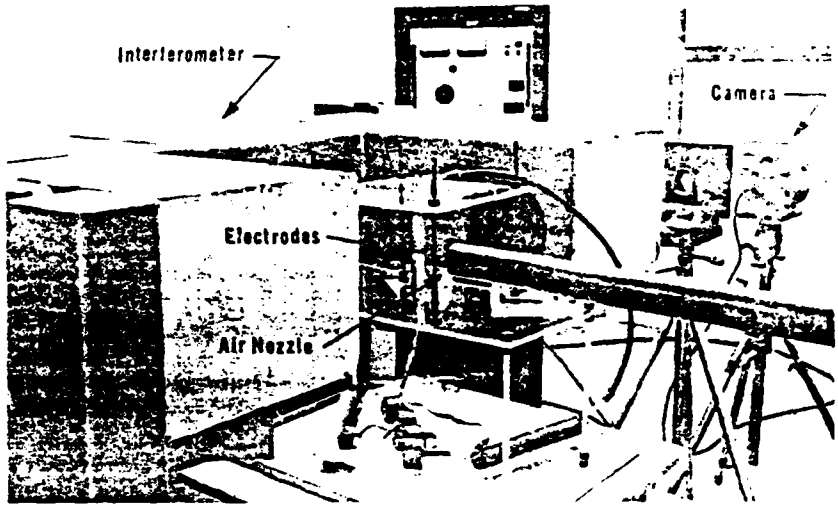

Figure 1. Experimental Setup

frames per second. The exposure time for each picture is about 80 μs. In all pictures, the tips of the hemispherical electrodes appear to the upper and lower left. For reference purposes, the black line drawn on each picture indicates the vertical axis of the electrodes. Lighting conditions, the position of the electrodes within the frame, and the field of view vary somewhat between figures due to the exploratory nature of the investigation.

The flow of air is from left to right in all photographs. As discusssed earlier, the flow approaches the electrodes as a uniform stream discharging from a 2-inch diameter pipe about two inches from the electrodes. The electrodes and air stream are located in a large room, and because of this, the pressure is essentially constant throughout the interelectrode region.

The infinite fringe method of utilizing the interferometer is illustrated in all figures. With this method, the undisturbed flow field appears as a region of uniform intensity on the photographs. The presence of a density variation within the test section results in a variation of the index of refraction in that region and a local change of velocity for the light passing through. This light is recombined with the light passing through the reference section at the second splitter plate, and a series of interference fringes are formed. Photographs of these fringe patterns convey information about the integral of the density variation along the optical axis of the test section. For this particular application, the density disturbance is three-dimensional in nature, and these single-view photographs cannot be directly interpreted to yield local density within the disturbed regions. They can, however, be used to infer the general extent of the affected region and its motion. It is these general characteristics that are being described at this time. Work is presently underway to improve the quantitative capabilities of the interferometer as applied to this situation.

Figure 2 presents photos of the density variation of the gas in the interelectrode region following an arc discharge. The blowing velocity was 5 ft/s, and the capacitance of the discharge capacitor was 0.01 μF. The gap spacing was 0.15 in. and the breakdown voltage was approximately 12.5 kV. The resulting arc current waveform was underdamped, had a maximum current of approximately 200 A, and decreased to zero in about 10 μs. An arc discharging at the minimum electrode separation point is seen in Figure 2(a) along with fringes generated during the time of exposure. Also shown in the far right of the picture is a region of lower gas density due to a previous arc. This region appears somewhat faded due to a decrease in the background lighting toward the right of the photos. The sequence of photos 2(b) through 2(f) shows a general flattening of the affected region as it moves out of the gap. Also evident is a general elongation of the affected region, with the upstream edge moving to the right much slower than the downstream edge. It should be mentioned here that the apparent velocity of the affected region is due to a combination of heat transfer and fluid motion. The general tendency is for the fringe pattern to maintain its shape as it progresses out of the gap, at least for a distance of one to two gap spacings. This would seem to indicate a laminar flow pattern in this region. Beyond this distance the flow separates from the electrodes, and the upper and lower portions of the heated region are caught in a relatively low velocity recirculation region behind both the upper and lower electrodes. This gives rise to the long "tails" evident in the heated gas from the previous arc.

Figure 3 presents results for the same conditions as those for Figure 2, except that the capacitance of the discharge capacitor was increased to 0.32 μF. The breakdown voltage was also essentially the same (~ 12.5 kV). This resulted in an overdampe arc current waveform peaking at approximately 450 A and decreasing to zero in about 20 μs. A different

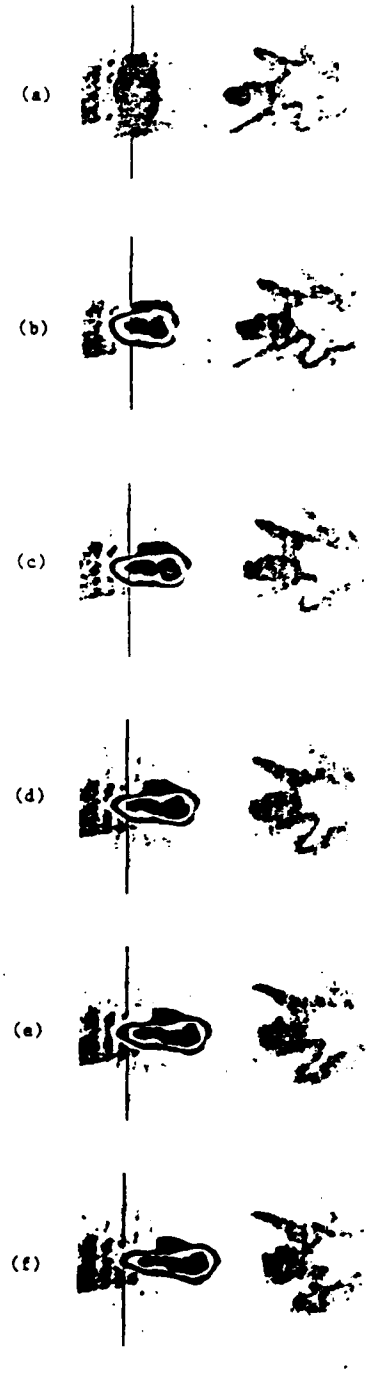

Figure 2. Interferograms for Low Jet Velocity (~ 5 ft/s) and Small Capacitor (~ 0.01 μF).

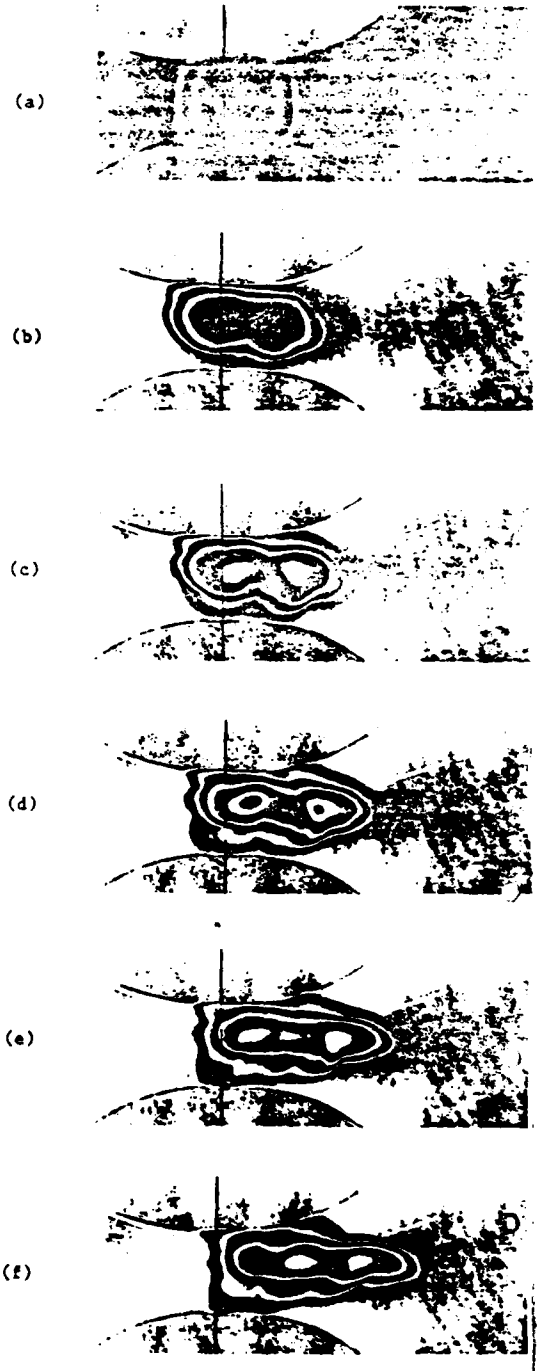

Figure 3. Interferograms for Low Jet Velocity (~ 5 ft/s) and Large Capacitor (~ 0.32 μF).

camera setup was used for these photos resulting in a slightly larger magnification and a somewhat different region of the flow field covered in the photos. The photos in Figure 3 are somewhat out of focus and this results in a slight optical distortion of the electrode shape. A much slower arc repetition rate was used in Figure 3. Because of this, heated gas from the previous arc does not appear in this sequence.

A comparison of Figures 2 and 3 shows the effect of the energy of the arc discharge on the density distribution within the electrode region during single-shot operation. Apparent in the figures is the difference in the size of the region affected by the discharge. For the smaller discharge, the heated region is primarily confined to the central region between the electrodes with only a small portion in contact with the upper electrode. As expected, the higher energy discharge results in a much larger affected area with a much larger contact area between the affected region and the electrodes. This larger contact area emphasizes the importance of the electrodes in the overall problem of cooling the interelectrode region.

Figure 4 presents a sequence of photos illustrating the phenomena to be avoided in rep-rated operation of a spark gap, that is, restrike. The overall conditions for these photos are the same as in Figure 2. In fact, these photos came from the same roll of film. Again, an arc discharging at the minimum electrode spacing is seen in the left portion of Figure 4(a) along with a region of lower density from a previous arc in the right portion. Figures 3(b) and 3(c) show the heated region moving downstream, and in Figure 3(d) a restrike is seen to occur through the heated region as opposed to occurring at the minimum electrode separation distance. Figures 3(c) and 3(f) show the heated region from the initial arc and the restrike continuing to be moved from the interelectrode space.

Comparing Figures 2 and 4, one can see that the general shape of the region heated by the initial arc is essentially the same in both cases. However, comparing photos (c) and (d) of each sequence, it appears that an additional half-fringe is present in Figure 4. This would seem to indicate that the heated region in Figure 4 is slightly hotter, and this may account for the restrike observed in this sequence.

Figure 5 shows the result of increasing the approach velocity to approximately 22 ft/s. The small capacitor was again used, but the gap spacing was reduced to 0.1 in., resulting in a lower breakdown voltage (~ 10 kV) and consequently lower energy release in the arc. Figure 5(a) shows the affected area immediately after the arc discharge and Figures 5(b) through 5(f) show the movement of the heated gas out of the interelectrode region. The rate at which the heated region moves out of the gap is noticeably higher for this case. For the situations shown in Figures 2, 3 and 4, the upstream edge of the heated region moves to the right at approximately 6 ft/s, while the downstream edge moves at about 16 ft/s. With the higher jet velocity, Figure 5, the upstream edge exits the gap region at about 19 ft/s while the downstream edge moves at about 28 ft/s. These velocities give indications of the movement of the central portion of the heated region. However, as is evident in Figure 5, the region near the electrodes stays relatively hot even after the core region is cooled. This is a result of the much

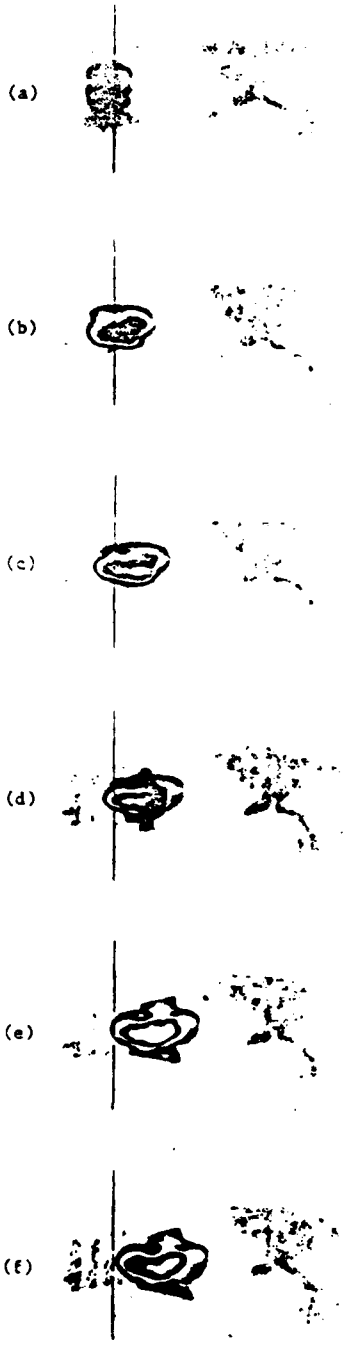

Figure 4. Interferograms Showing Restrike for Low Jet Velocity (~ 5 ft/s) and Small Capacitor (~ 0.01 μF).

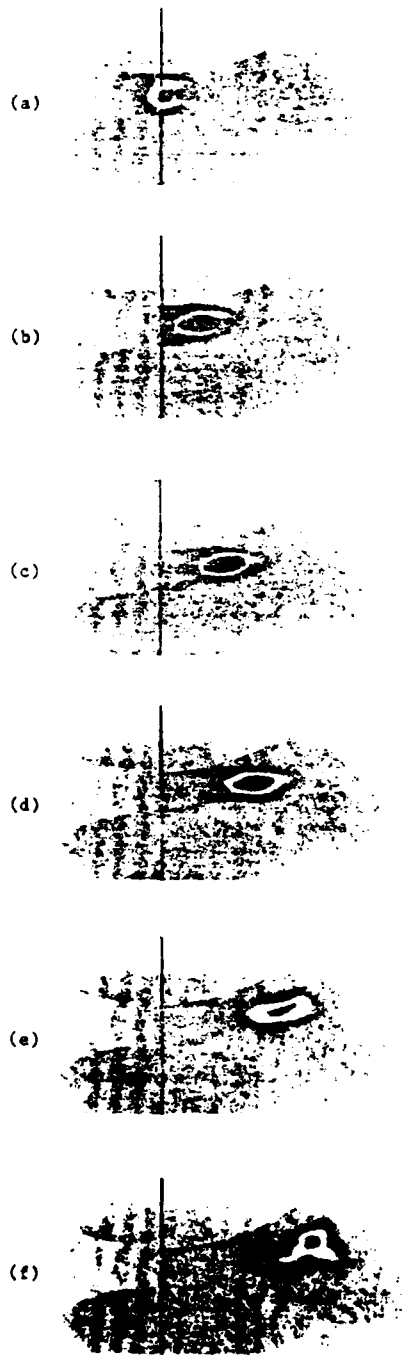

Figure 5. Interferograms for High Jet Velocity (~ 22 ft/s) and Small Capacitor (~ 0.01 μF).

lower velocities in the boundary layer near the electrode. Work is currently being done to investigate the possibility of visualizing [illegible] these higher velocities.

Conclusions

The interferometer was used to visualize the density distribution in a gas blown spark gap of simple geometry. The interferograms obtained clearly show the effects of the heating of the gas by the arc and the flushing of this heated region by the purging gas. The effects of the magnitude of the blowing velocity, of the characteristics of the arc, and of the hydrodynamic boundary layers on the electrodes can be seen. Similar qualitative results could be readily obtained for more practical gap designs provided that light can be passed through the gap region. Work is continuing on this technique to provide quantitative as well as additional qualitative information for the study of the fluid mechanics and heat transfer aspects of gas blown spark gaps.

Acknowledgment

The authors wish to acknowledge the partial support of this work by the Air Force Office of Scientific Research.

Project No. 7

Electromechanical Pulse Device (Final Report)*

(B. H. Dunlap and J. P. Craig)

A. INTRODUCTION

1. Conventional Pulsers

To deliver an energy, E_o, to an electrical resistance load in a period, τ_o, requires a power, p(t), such that

$$\int_o^{\tau_o} p(t)dt = \int_o^{\tau_o} \frac{v^2(t)}{R_L(t)}\, dt = E_o. \qquad (1.1)$$

As E_o becomes large, and/or τ_o becomes small, the power p(t), may be larger than the available prime power source. The energy can then be stored at a lower power for a longer period of time until the energy stored is $E_s \geq E_o$, and subsequently dumped into the load in τ_o seconds. If the prime power source is electrical, the energy can be stored in capacitors or inductors. Then η percent of E_s can be switched into R_L, where η percent is the efficiency. If the prime power source is mechanical, it can be converted into electrical form to charge the capacitive or inductive energy stores at a lower power and longer duration than the output pulse values.

If capacitive energy storage is used, the switch needed to switch the energy into the load is a closing switch. If inductive energy

*This Project is not being continued in the current, 1982-83, funding period. This section thus constitutes a final report on this project.

storage is used, the needed switch is an opening switch. The volume and cost of capacitive storage are large compared to those for inductive energy storage. Hence, for large E_o, inductive energy storage would be preferable. However, the associated opening switch problem is much more difficult than the closing switch problem. Both the opening and closing switch problems are enhanced at higher power and energy levels, particularly for repetitive pulses.

If the load resistance, R_L, is constant and an ideal closing switch is used with a single storage capacitor, C, then the energy is dumped into the load at a rate $(V_o^2/R_L)e^{-(2t/R_L C)}$. If $\tau_o = 3/2\ R_L\ C$, then 95% of the energy is dumped into the load during τ_o, but the power varies greatly during the period τ_o. However, at least some load resistances of interest decrease with time during τ_o. Hence, the power would then be more nearly uniform during τ_o.

If the load resistance, R_L, is constant and an ideal opening switch is used with a single storage inductance, L, the energy is dumped into the load at a rate $(I_o^2\ R_L)e^{-2R_L\tau/L}$. If $\tau_o = 3/2\ L/R_L$ then 95% of the energy is dumped into R_L during τ_o. Here, an increasing R_L would be required during τ_o to make the power more uniform.

Also, pulse forming networks (PFN's) with a few lumped L's and C's can be used to make the power more uniform during τ_o. Either the inductors or the capacitors can be charged. If R_L is constant, the power, voltage, and current can be made nearly constant during τ_o. If R_L varies during τ_o, then different charging of the multiple L's and/or C's could be used

to shape either the power, voltage or current to desired values during τ_o, but multiple, synchronized switches would be required.

To date, most high power pulsers have utilized the more expensive capacitive energy storage (either single C's or PFN's), because of the difficulty in building suitable opening switches (for τ_o's less than a microsecond some distributed PFN's have been used).

Mechanical, or kinetic, energy storage is also compact and inexpensive compared to capacitive energy storage. Therefore, mechanical energy storage has been considered for high power pulsers. The "compulsator" has produced pulses on the order of 500 μs between half power points with a rise time of about 200 μs [1]. Homopolar generators have been used for longer duration pulses [2]. Both these machines utilize closing switches.

2. Electromechanical Pulse Amplifier

The electromechanical pulse amplifier, EPA, described in this report was conceived to try to overcome the fundamental limitations in producing shorter pulses than with other electromechanical energy converters, and to reduce or eliminate the switching requirements.

Without switching, rise and fall times for electromechanical generators, and therefore pulse periods, are limited by

1. flux fringing
2. relative speeds of mechanical parts
3. leakage reactance
4. time to build up flux (L/R time constants).

These limitations can be overcome by the EPA described in this report. The EPA is not expected to be a complete solution to the pulse power problem, but it does offer an alternative which may be beneficial for some applications. Application characteristics and associated problems are discussed in Section C and D.

The theory on which the EPA is based is derived in Section B. A brief description of the device and some of its operating characteristics are given in the present Section.

Basically, the device is a transmission line, with mechanically time-varied parameters, which delays, amplifies, and compresses an input pulse and delivers it to a load without switching. Because the device has gain and pulse compression, the input pulse is at a lower power and energy and is of longer duration than the output pulse. If the gain and pulse compression are sufficiently high, the input pulse may be generated with an electromechanical generator without switching [3]. If wave shaping were required, inefficiencies would not be too serious because the input energy level is much lower than the output level. Alternatively, a conventional switched pulser could be used for the input, with the switching problem reduced because of the lower power level.

The transmission line's inductance and/or capacitance per unit length may be mechanically varied. The transmission line may be approximated by a number of sections of lumped L's and C's. This approximation is not a restriction on the device. It could conceivably be built in a true distributed form. The latter form may be preferable or necessary if the

device was to be applied for pulses shorter than a few microseconds. However, only the lumped parameter line has been studied to date. Of course, as the number of lumped sections increases, the lumped line more closely approaches the true distributed line. Note that the explosively driven flux compression pulsers could be considered as one section of such a line. Here, the energy is stored in the explosive and then converted to mechanical energy to decrease the inductance of the section to convert the energy to electrical form.

The EPA is represented by the block diagram in Fig. 1

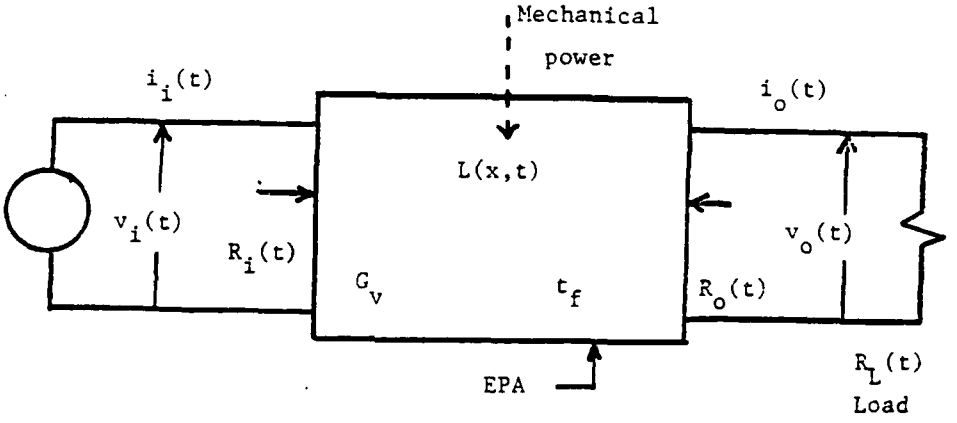

Fig. 1. Block diagram of electromechanical pulse amplifier.

A square wave voltage input and output pulse for an ideal pulser are shown in Fig. 2.

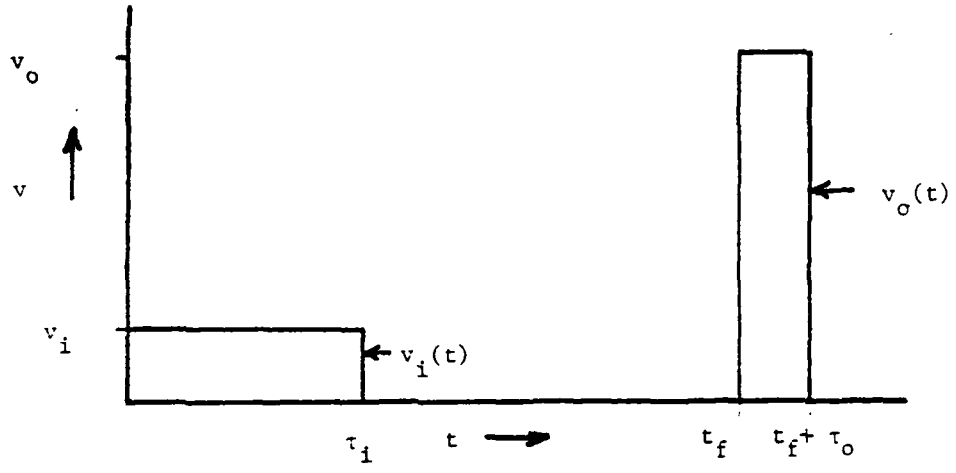

Fig. 2. Square wave voltage at the input with resulting output.

For the EPA discussed in this report, only the inductance parameters are mechanically varied with time. It is shown in Section B that both the L and C parameters must vary with their position along the line. For this configuration of the EPA, R_i, R_o and $R(x,t)$ decrease linearly with time. Therefore, the currents increase with time as shown in Fig. 3. This is an important consideration in the application of this version of the EPA.

A previous study of an EPA showed that if the capacitors are also mechanically varied with time, then the R_i, R_o and $R(x,t)$ are constant (see Appendix A). However, time varying capacitors are even more bulky

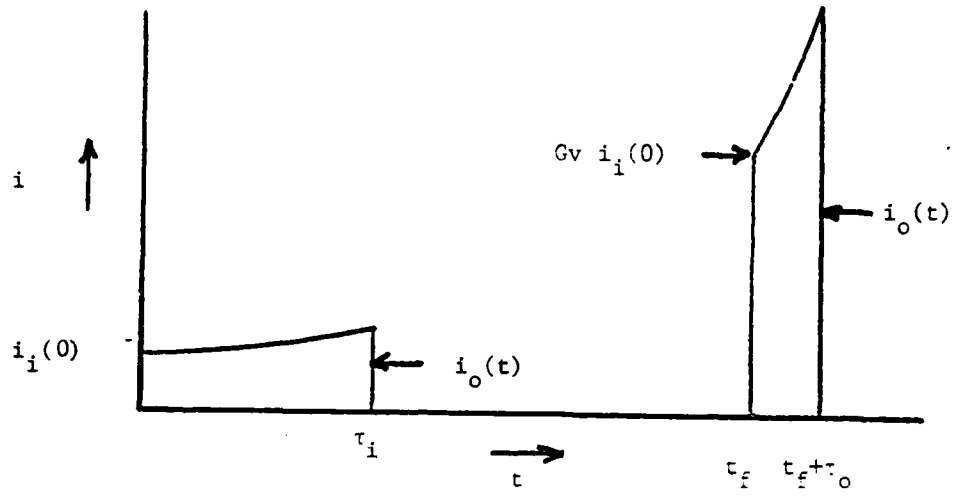

Fig. 3. Input and output currents for ideal EPA with static capacitors.

and expensive than static capacitors. Therefore, ways to operate with the static capacitor EPA are studied.

The fact that the EPA requires some capacitors is a disadvantage, since one of its purposes is to utilize mechanical energy storage rather than capacitive energy storage. Therefore, the EPA can only have an advantage in this respect if the capacitive energy storage requirement E_c, which must be provided in the EPA, is less than the output pulse energy, E_o. That is, it is desirable to have $E_o/E_c \gg 1$.

A second desirable property for the EPA is that its output impedance, $R_o(t)$ should match the load $R_L(t)$.

It will be shown that these two desirable attributes, $E_o/E_c \gg 1$ and $R_o(t) \tilde{=} R_L(t)$ require some compromise, unless $R_L(t)$ decreases appreciably with time during τ_o.

For a given application, the output energy, E_o, the pulse period, τ_o, the voltage $v_o(t)$, and $R_L(t)$ are determined by the load. The application may be for a single pulse, a burst of pulses with a duty cycle of τ_o/T_p, or continuous pulses with duty cycle τ_o/T_p, where $T_p - \tau_o$ is the time between pulses. The designer can then choose the voltage gain, G_v, and delay time, t_f, in an optimum manner to accomplish the purposes of the EPA.

B. THEORETICAL ANALYSIS

A distributed transmission line with time-varying inductors and/or time-varying capacitors per unit length can amplify an arbitrary function applied to the input of the line. This chapter is devoted to the theoretical analysis of a distributed transmission line that uses a time-varying inductance and time-invariant capacitance per unit length. Appendix A includes the case of a distributed transmission line that uses both time-varying inductors and capacitors.

The voltage and current relations for a distributed lossless transmission line are

$$v_x = -(Li)_t \tag{2.1}$$

$$i_x = -(Cv)_t \tag{2.2}$$

where the subscripts x and t indicate the derivative of a particular variable with respect to x or t.

It is desired to find the functions L(x,t) and C(x) such that the voltage across the line is of the form

$$v(x,t) = e^{\alpha x} f(x-st) \ , \tag{2.3}$$

where α is a positive real gain constant, f(x-st) is an arbitrary function, and s may be a function of time and will be shown to be related to the velocity of propagation. Therefore, the task is to solve for L(x,t) and C(x) such that Eq. (2.3) satisfies Eq. (2.1) and (2.2) simultaneously.

By taking derivatives and making substitutions, Eqs. (2.1) and (2.2) yield

$$v_{xx} = LCv_{tt} + L_tCv_t + \frac{L_x}{L} v_x + (\frac{L_xL_t}{L} - L_{tx})i. \tag{2.4}$$

The above equation can be simplified if

$$L = X(x)T(t) , \tag{2.5}$$

where X is a function of x only and T is a function of t only. From Eq. (2.5),

$$L_x = X_xT,\ L_t = XT_t \text{ and } L_{tx} = X_xT_t. \tag{2.6}$$

Equation (2.6) implies that the coefficient for i in Eq. (2.4) is zero. Also, if

$$X = K_1e^{\beta x}, \tag{2.7}$$

where K_1 and β are constants, then the coefficient for v_x in Eq. (2.5) is

$$\frac{L_x}{L} = \frac{X_xT}{XT} = \frac{X_x}{X} = \frac{\beta K_1e^{\beta x}}{K_1e^{\beta x}} = \beta . \tag{2.8}$$

With the above restrictions, Eq. (2.4) may be simplified to yield

$$v_{xx} - \beta v_x = LCv_{tt} + L_tCv_t . \tag{2.9}$$

Equation (2.3) and its derivatives,

$$v_t = -e^{\alpha x}(s_tt + s)f' , \tag{2.10}$$

$$v_{tt} = e^{\alpha x}(-(ts_{tt} + 2s_t)f' + (s_t^2t^2 + 2ss_t t + s^2)f''), \quad (2.11)$$

$$v_x = e^{\alpha x}(\alpha t + f'), \quad (2.12)$$

and

$$v_{xx} = e^{\alpha x}(\alpha^2 f + 2\alpha f' + f'') \quad (2.13)$$

where primes on f indicate derivatives with respect to its argument, may be substituted into Eq. (2.9). The result is

$$e^{\alpha x}((\alpha^2 f + 2\alpha f' + f'') - \beta(\alpha t + f')) =$$

$$e^{\alpha x}(-LC(ts_{tt} + 2s_t)f' + LC(s_t^2t^2 + 2ss_t t + s^2)f'' - L_tC(s_t t + s)f'), \quad (2.14)$$

an equation involving f, L, C, and s and their first and second derivatives.

In order for f to be an arbitrary function, the coefficients of f, f', and f'' must be zero; therefore

$$\alpha(\alpha - \beta) = 0, \quad (2.15)$$

and

$$-(2\alpha-\beta) = LCts_{tt} + 2LCs_t + L_tCts_t + L_tCs \quad (2.16)$$

and

$$1 = LC(s_t^2 t + 2ss_t t + s^2) \tag{2.17}$$

follow.

Equation (2.15) shows that

$$\alpha = \beta \text{ or } \alpha = 0 \tag{2.18}$$

The zero solution is not of interest. Functions L(x,t), C(x), and s(t) are sought which will simultaneously satisfy Eqs. (2.16) and (2.17). Two additional restrictions which simplify finding of a set of functions are

$$C = Y(x) \tag{2..19}$$

and

$$XY = K_2 \tag{2.20}$$

where Y is a function of x only and K_2 is a constant. Combining Eqs. (2.7) and (2.20) yields

$$Y = \frac{K_2}{K_1} e^{-\beta x} . \tag{2.21}$$

Substituting Eqs. (2.5), (2.7), (2.18), (2.19), (2.20) and (2.21) into Eqs. (2.16) and (2.17) yields

$$s_{tt} + (\frac{2}{t} + \frac{T_t}{T})s_t + \frac{T_t}{T}\frac{s}{t} = \frac{-\alpha}{tTK_2}, \tag{2.22}$$

and

$$s_t + \frac{s}{t} = \pm \frac{1}{t\sqrt{TK_2}} . \tag{2.23}$$

By manipulating Eqs. (2.22) and (2.23), one finds Eq. (2.24):

$$T = \frac{(T_t)^2 K_2}{4\alpha^2} \tag{2.24}$$

A functional form for T which satisfies Eq. (2.24) is

$$T = at^2 - bt + c, \tag{2.25}$$

where a, b and c are positive real constants and

$$a = \frac{\alpha^2}{K_2}$$

$$c = \frac{b^2 K_2}{4\alpha^2} \quad .$$

Substituting Eq. (2.25) into Eq. (2.24) results in

$$T = \frac{b^2 K_2}{4\alpha^2} \left(1 - \frac{2\alpha^2 t}{bK_2}\right)^2 \quad . \tag{2.26}$$

Using Eqs. (2.5), (2.7), (2.16), (2.20) and (2.26) one may obtain the desired L(x,t) and C(x) functions as

$$L(x,t) = L_o e^{\alpha x}\left(1 - \frac{\alpha t}{\sqrt{L_o C_o}}\right)^2 \tag{2.27}$$

and

$$C(x) = C_o e^{-\alpha x} \quad , \tag{2.28}$$

where L_o and C_o are the inductance and capacitance per unit length at $x = 0$ and $t = 0$. The values of L_o and C_o are

$$L_o = \frac{K_1 K_2 b^2}{4\alpha^2} \tag{2.29}$$

and

$$C_o = \frac{K_2}{K_1} \quad . \tag{2.30}$$

With L and C given in Eqs. (2.27) and (2.28), the voltage and current solutions for Eq. (2.1) and (2.2) are given by Eq. (2.3) and

$$i(x,t) = \frac{\sqrt{\frac{C_o}{L_o}}\, f(x-st)}{1 - \frac{\alpha t}{\sqrt{L_o C_o}}} \quad . \tag{2.31}$$

The function s(t) which will satisfy Eqs. (2.22) and (2.23) when T is expressed by Eq. (2.26) can be found by using an integrating factor and is

$$s(t) = \frac{1}{t\alpha} \ln \frac{1}{1 - \frac{\alpha t}{\sqrt{L_o C_o}}} \quad . \tag{2.32}$$

The velocity at which the function f(x-st) propagates along the line is obtained by differentiating the equation

$$x - st = \text{constant} \ , \tag{2.33}$$

or

$$\text{velocity} = x_t = (st)_t = s_t t + s \quad . \tag{2.34}$$

An equation expressing x can be obtained by integrating Eq. (2.34); thus, a voltage applied to the line input at t = 0 will be at position

$$x_o = st_o = \frac{1}{\alpha} \ln \frac{1}{1 - \frac{\alpha t_o}{\sqrt{L_o C_o}}} \tag{2.35}$$

at some later time t_o. Equation (2.35) solved for t_o is

$$t_o = \frac{\sqrt{L_o C_o}}{\alpha} (1 - e^{-\alpha x_o}) . \tag{2.36}$$

Figures 4 and 5 show a rectangular input voltage and the corresponding output voltage as a function of time, respectively. The voltage $v(x-st)$ as a function of x at times τ_1, t_K (arbitrary time) and t_f are shown in Figs. 6, 7, and 8, respectively.

Equation (2.34) shows that the velocity of propagation is related to s(t) and t. The velocity increases with t, but is independent of x, so that the portion of the line that is charged at any time between τ_i and t_f is x_1. Therefore, in Figures 6, 7, and 8

$$x_f - x_4 = x_3 - x_2 = x_1 . \tag{2.37}$$

The output pulse will continue until the trailing edge at time t_f is at x_f at time $t_f + \tau_o$. Since the velocity of the pulse is greater for times between t_f and $t_f + \tau_o$ than for times between 0 and τ_i, pulse compression is obtained.

The load is matched to the line, if the load impedance is

$$R_L = \frac{v(x_f,t)}{i(x_f,t)} = R_o e^{\alpha x_f} (1 - \frac{\alpha_t}{\sqrt{L_o C_o}}) \tag{2.38}$$

where $R_o = \sqrt{\frac{L_o}{C_o}}$. (2.39)

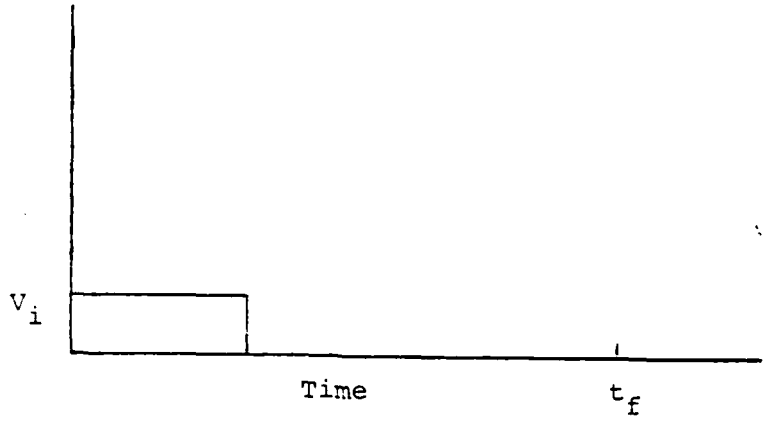

Figure 4. Input Voltage at x = 0.

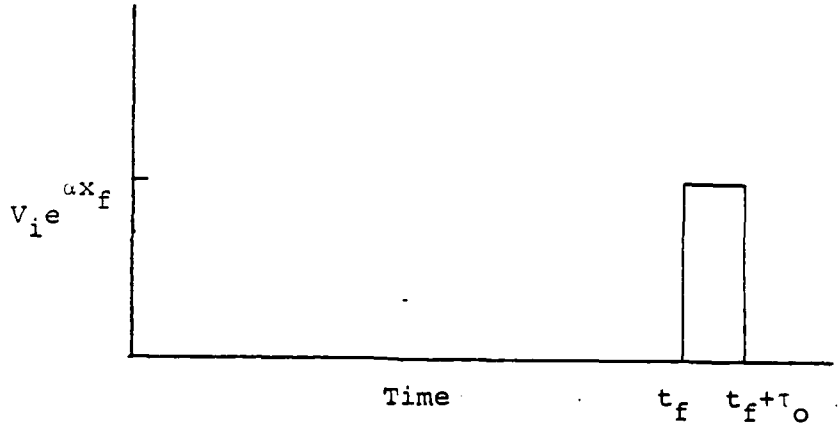

Figure 5. Output Voltage at $x = x_f$.

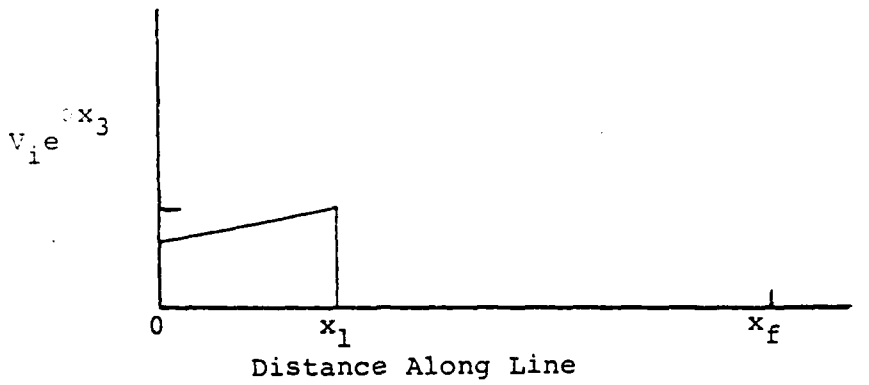

Figure 6. Voltage at $t = \tau_i$.

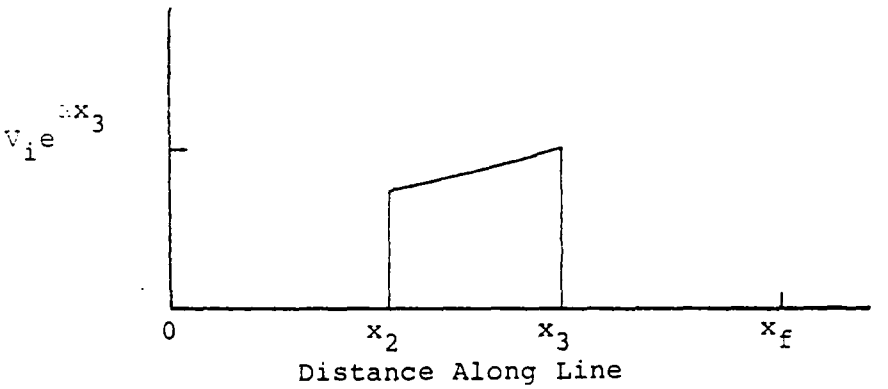

Figure 7. Voltage at $t = t_K$.

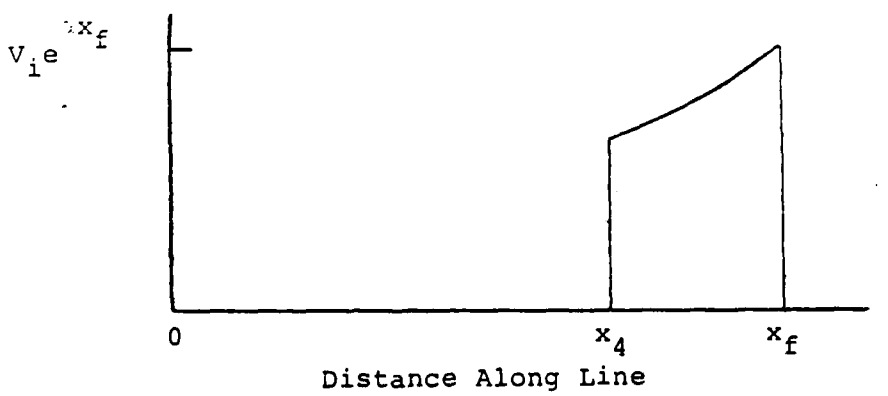

Figure 8. Voltage at $t = t_f$.

The output pulse ends at the time $t_f + \tau_o$, which is the time required for the leading edge of the input pulse to travel a distance

$$x_f(t_f) + x_1(\tau_i) = x_f(t_f + \tau_o), \tag{2.40}$$

where $x_f(t_f + \tau_o)$ is the distance traveled by the leading edge of the input pulse. Equation (2.35) can be used in Eq. (2.40) to yield

$$\frac{\alpha}{\sqrt{L_o C_o}} = \frac{\tau_i - \tau_o}{\tau_i t_f} . \tag{2.41}$$

As the voltage pulse propagates toward the load, it increases exponentially. From Eqs. (2.3), (2.35), and (2.41) the voltage gain is

$$G_v = e^{\alpha x_f} = \frac{\tau_i}{\tau_o} . \tag{2.42}$$

The current gain (G_I), power gain (G_p), and energy gain (G_E) are also fixed by τ_i and τ_o as

$$G_I = \tau_i/\tau_o , \tag{2.43}$$

$$G_p = (\tau_i/\tau_o)^2 , \tag{2.44}$$

and

$$G_E = \tau_i/\tau_o . \tag{2.45}$$

For the inductance variation to be physically realizable, the inductance cannot be less than or equal to zero. This restriction sets a maximum delay time, t_f, (for fixed values of L_o, C_o, and α) as

$$t_f \text{ maximum} = \frac{\sqrt{L_o C_o}}{\alpha} \quad . \tag{2.46}$$

The minimum delay time is

$$t_f \text{ minimum} = \tau_i - \tau_o \quad . \tag{2.47}$$

When $t_f = t_f$ minimum, the matching load impedance is zero at $t_f + \tau_o$.

C. OPERATING CHARACTERISTICS

Several parameters and equations that are useful in describing the operating characteristics of an EPA are discussed. In the early sections of this chapter the discussion is based on a distributed transmission line, whereas, the latter sections are based on a lumped parameter transmission line. In all cases, the discussion is limited to a rectangularly shaped pulse.

1. Distributed Transmission Line

Five fundamental variables are used to describe the behavior of an EPA. These variables are:

Input voltage	V_i,
Characteristic impedance	R_o,
Input pulse period	τ_i,
Output pulse period	τ_o,
and Time delay	t_f.

These fundamental variables, in turn are used to derive other parameters. By analyzing these derived parameters, for a particular application, the fundamental variables can be chosen. The derived parameters are:

Capacitive energy storage	E_c,
Energy of input pulse	E_i,
Energy of output pulse	E_o,
Inductance variation ratio	LVAR,
and Load impedance percent change	ΔR_L.

The main advantages of using inertial stored energy in machines such as the homopolar generator are the high energy densities obtainable and the elimination of capacitor banks. Unlike a homopolar device, the EPA uses capacitors in its operation. When designing an EPA for a particular application, one should consider the ratio of the energy output to the energy stored by the capacitors. This ratio may be considered an essential parameter, or figure of merit, of an EPA.

2. Capacitive Energy Storage

The capacitive energy storage capability of the transmission line is

$$E_c = \frac{1}{2}\int_o^{x_f} C(x)V^2(x)dx. \tag{3.1}$$

Substituting for C(x) and V(x) from Eqs. (2.28) and (2.3) for a rectangular input pulse V_i one may write Eq. (3.1) as

$$E_c = \frac{1}{2} C_o V_i^2 \frac{1}{\alpha}\left(\frac{\tau_i}{\tau_o} - 1\right) . \tag{3.2}$$

Using Eq. (2.41) and substituting for $\frac{1}{\alpha}$ in Eq. (3.2), one sees that

$$E_c = \frac{1}{2}\frac{V_i^2}{R_o}\frac{\tau_i t_f}{\tau_o} . \tag{3.3}$$

The energy input to this transmission line can be calculated from

$$E_i = \int_o^{\tau_i} v(t)i(t)dt, \tag{3.4}$$

or

$$E_i = \frac{V_i^2}{R_o}\int_o^{\tau_i} \frac{dt}{\left(1 - \frac{\alpha t}{\sqrt{L_o C_o}}\right)} . \tag{3.5}$$

Using Eq. (2.41), one may simplify Eq. (3.5)

$$E_i = \frac{V_i^2}{R_o} \frac{\tau_i t_f}{\tau_i - \tau_o} \ln\left(\frac{t_f}{t_f - \tau_i + \tau_o}\right). \tag{3.6}$$

As a result, the energy at the output is

$$E_o = E_i \frac{\tau_i}{\tau_o} = \frac{V_i^2}{R_o} \frac{\tau_i}{\tau_o} \frac{\tau_i t_f}{\tau_i - \tau_o} \ln\left(\frac{t_f}{t_f - \tau_i + \tau_o}\right). \tag{3.7}$$

Thus, from Eqs. (3.3) and (3.7) the ratio of output energy to capacitive energy is

$$\frac{E_o}{E_c} = 2 \frac{\tau_i}{\tau_i - \tau_o} \ln\left(\frac{t_f}{t_f - \tau_i + \tau_o}\right) . \tag{3.8}$$

For the EPA to operate efficiently on a one-shot basis, it is desirable to choose values for τ_i, τ_o, and t_f such that the above ratio is greater than one. This may be accomplished by letting t_f approach $\tau_i - \tau_o$. As will be shown later,, when t_f approaches $\tau_i - \tau_o$ the inductance variation ratio and the change in the matching load resistance increases.

3. Inductance Variation Ratio

LVAR is the ratio of the maximum to minimum inductance at a particular position on the line during the inductance charging time interval. This parameter is helpful in determining what type of device is used to vary the inductors. This parameter is not a function of distance along the line. The time t_1 when the leading edge of the pulse reaches a particular distance x is expressed by Eq. (2.36) as

$$t_1 = \frac{\sqrt{L_o C_o}}{\alpha} (1 - e^{-\alpha x}) \ . \qquad (3.9)$$

From Eq. (2.27) and the above equation, the maximum inductance is the inductance when the leading edge of the pulse reaches x, and this inductance is

$$L_{LE}(x,t_1) = L_o e^{-\alpha x} \ . \qquad (3.10)$$

The time, t_2 when the trailing edge of the pulse reaches x, is expressed as

$$t_2 = \frac{\sqrt{L_o C_o}}{\alpha} (1 - e^{-\alpha(x+x_1)}) \ , \qquad (3.11)$$

where x_1 is the length of line which is charged at $t = \tau_i$. From Eqs. (2.27) and (3.11) the minimum inductance occurs when the trailing edge of the pulse is at x and is

$$L_{TE}(x,t_2) = L_o e^{-\alpha x} e^{-2\alpha x_1} . \qquad (3.12)$$

Equation (3.12) can be simplified by first substituting the following for αx_1 in Eq. (3.12)

$$\alpha x_1 = \ln \frac{1}{1-\frac{\alpha \tau_i}{\sqrt{L_o C_o}}} \qquad (3.13)$$

and then by using Eq. (2.41) to obtain Eq. (3.14):

$$L_{TE}(x,t_2) = L_o e^{-\alpha x}\left(\frac{t_f - \tau_i + \tau_o}{t_f}\right)^2 \ . \qquad (3.14)$$

From Eqs. (3.10) and (3.14) LVAR is written as

$$\text{LVAR} = \frac{L_{LE}(x,t_1)}{L_{TE}(x,t_2)} = \left(\frac{t_f}{t_f-\tau_i+\tau_o}\right)^2 . \tag{3.15}$$

4. Load Percentage Change

An EPA that uses time-varying inductors and time-invariant capacitors has a time-varying characteristic impedance. To eliminate reflections, the load should be matched to the characteristic impedance. However, for a constant load it is helpful to estimate the mismatch by calculating the percent change of the characteristic impedance of the EPA. The impedance at the output is, from Eq. (2.38)

$$R_L(x_f,t) = R_o e^{\alpha x_f}\left(1-\frac{\alpha t}{\sqrt{L_o C_o}}\right) . \tag{3.16}$$

At time t_f when the leading edge reaches the output terminals, the matching resistance is

$$R_L(x_f,t_f) = R_o e^{\alpha x_f}\left(1-\frac{\alpha t_f}{\sqrt{L_o C_o}}\right) . \tag{3.17}$$

Using Eq. (2.36), Eq. (3.17) simplifies to

$$R_L(x_f,t_f) = R_o . \tag{3.18}$$

At time $t_f + \tau_o$, when the pulse leaves the line, the load impedance is

$$R_L(x_f,t_f+\tau_o) = R_o\left(1-\frac{\tau_i}{t_f}+\frac{\tau_o}{t_f}\right) . \tag{3.19}$$

The percentage change in matching impedance from t_f to $t_f + \tau_o$ is

$$\Delta R_L = \frac{\tau_o - \tau_i}{t_f} \times 100\ \% \ . \tag{3.20}$$

For convenience, the previously derived parameters are listed below:

$$E_c = \frac{1}{2} \frac{V_i^2}{R_o} \frac{\tau_i t_f}{\tau_o} \ , \tag{3.21}$$

$$E_i = \frac{V_i^2}{R_o} \frac{\tau_i t_f}{\tau_i - \tau_o} \ln\left(\frac{t_f}{t_f - \tau_i + \tau_o}\right) \ , \tag{3.22}$$

$$E_o = \frac{V_i^2}{R_o} \frac{\tau_i}{\tau_o} \frac{\tau_i t_f}{\tau_i - \tau_o} \ln\left(\frac{t_f}{t_f - \tau_i + \tau_o}\right) \ , \tag{3.23}$$

$$\frac{E_o}{E_c} = \frac{2\tau_i}{\tau_i - \tau_o} \ln\left(\frac{t_f}{t_f - \tau_i + \tau_o}\right) \ , \tag{3.24}$$

$$LVAR = \left(\frac{t_f}{t_f - \tau_i + \tau_o}\right)^2 \tag{3.25}$$

$$\Delta R_L = \frac{\tau_o - \tau_i}{t_f} \times 100\ \% \ . \tag{3.26}$$

5. Lumped Transmission Line

The waveform of an electrical pulse being amplified on a lumped transmission line will more closely approximate the waveform on a distributed transmission line as the number of lumped sections increases.

One way to approximate the L's and C's of a lumped transmission line is shown in Figure 9. For example, a 10 section line (M = 10) has 11 time-varying inductors and 10 capacitive elements. This configuration is classified as an L-section. If the dependent value of the inductance is determined at a point half-way between the ends of the unit section, the inductance for each element is

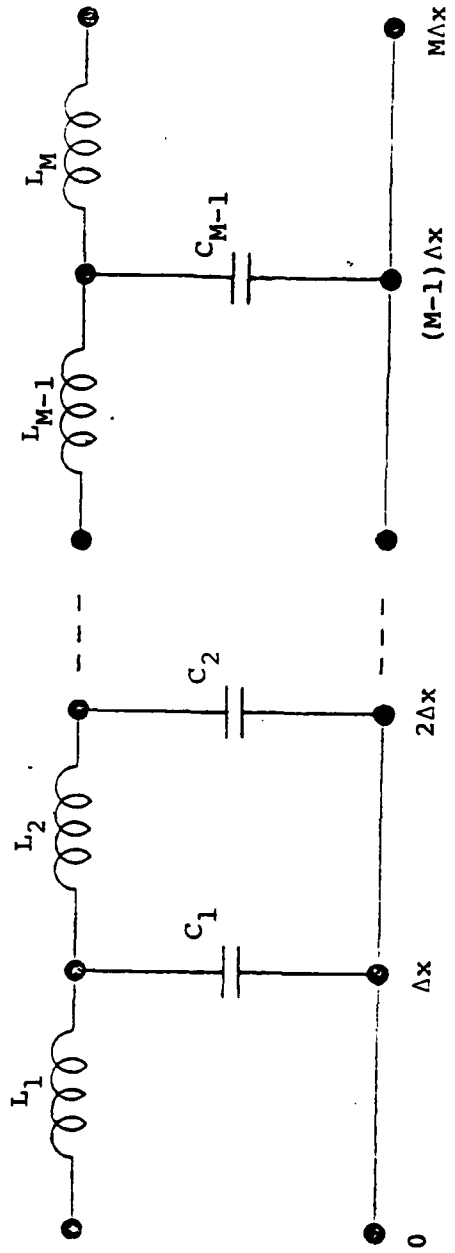

Fig. 9. L - Section Lumped Transmission Line.

$$L(j,t) = \frac{L_o X_f}{M} e^{\left[\frac{\alpha X_f}{M}\left(\frac{1}{2} + (j-1)\right)\right]} \left(1 - \frac{\alpha t}{\sqrt{L_o C_o}}\right)^2 \qquad (3.27)$$

where $j = 1, 2, 3, \ldots M$.

From Eqs. (2.41) and (2.35), one may rewrite Eq. (3.27) as

$$L(j,t) = \frac{R_o}{M} \frac{\tau_i t_f}{(\tau_i - \tau_o)} \ln\left(\frac{\tau_i}{T_o}\right) \left(\frac{\tau_i}{\tau_o}\right)^{\left(\frac{1}{2M} + \frac{(j-1)}{M}\right)} \left(1 - \frac{(\tau_i - \tau_o)}{\tau_i t_f} t\right)^2 . \qquad (3.28)$$

Correspondingly, if the capacitance is determined at the end of the unit section, the value for the capacitors are

$$C(j) = \frac{C_o X_f}{M} e^{\frac{-\alpha X_f}{M} j} \qquad (3.29)$$

where $j = 1, 2, 3, \ldots M$.

If one uses Eqs. (2.41) and (2.35), Eq. (3.29) may be rewritten as

$$C(j) = \frac{1}{R_o M} \frac{\tau_i t_f}{(\tau_i - \tau_o)} \ln\left(\frac{\tau_i}{\tau_o}\right) \left(\frac{\tau_o}{T_i}\right)^{j/M} . \qquad (3.30)$$

Computer Program

A specialized computer program was developed to solve the approximate transmission line. The program uses numerical integration to obtain solutions of an L-section line.

The numerical integration routine was written with a variable step size to minimize error and maintain solution stability. (A realizable amplifier will, of course, have inductive and capacitive losses.) The program was written to take into account the effect of inductive series

resistance, but not capacitive parallel conductance.

Input variables are: input pulse width (TAUI), output pulse width (TAUO), time delay (TF), inductance per unit length (LO), capacitance per unit length (CO), and the number of sections (M).

With the above input data, the program solves for the currents in each loop at time t = 0 and then, subsequently, t is incremented to solve for the currents again at t + t'. This iterative process continues until the user-provided time TMAX is reached. The output is a table of the inductance and current for each section from t = 0 to t = TMAX. These data may also be plotted on a digital, incremental plotter.

D. APPLICATION CHARACTERISTIC OF THE EPA

1. Example

An example will illustrate how the equations developed in the preceeding section may be employed to design an electromechanical pulse amplifier. The example is chosen somewhat arbitrarly, but is selected to have a shorter output pulse period with a considerably faster rise time than has previously been produced with an electromechanical pulser. The output energy per pulse, the pulse repetition rate, the rotor tip speeds, and magnetic saturation flux densities are all chosen to be well within practically achievable values. With this example as a bench mark, a discussion of the techniques and associated problems to extend the design to higher energy levels and shorter duration pulses with higher repetition rates may be clearly discussed. The example application specifications are:

Rectangular output voltage pulse,

Pulse period: 200 μs

Rise time: 20 μs

Energy per pulse: 2 kJ

Load resistance: 10 ohms at leading edge of pulse, decreasing to 4 ohms at end of pulse

For the load to match the EPA,

$$R_o = 10\ \Omega \tag{4.1}$$

and, from Eq. (3.20)

$$\Delta R = \frac{R_{TE}-R_{LE}}{R_o} = -0.6\ \text{p.u.} = \frac{\tau_o-\tau_i}{t_f} \tag{4.2}$$

and, from Eqs. (3.15) and (4.2)

$$\text{LVAR} = \left(\frac{1}{1+(\tau_o-\tau_i)/t_f}\right)^2 = \frac{1}{(1+\Delta R)^2} = 6.25 \qquad (4.3)$$

The gain selection is a compromise between a low value to reduce capacitive energy storage requirements and a high value to reduce the input power level and increase the input pulse period. Using Eqs. (2.42), (3.8) and (3.15),

$$\frac{E_o}{E_c} = -\frac{2G}{G-1}\ln[1+\Delta R] = -\frac{2G}{G-1}\ln(0.4). \qquad (4.4)$$

Gain and E_o/E_c may be tabulated as:

G	2	4	6	8
E_o/E_i	3.66	2.44	2.12	2.09

Thus, for a gain of 4, the capacitive energy storage required for the EPA is 1/2.44 times the output pulse energy. The input pulse duration is then

$$\tau_i = G_v\,\tau_o = 800 \ \mu s, \qquad (4.5)$$

and the input power is reduced by a factor of G_v^2, or 16.

Using Eq. (2.42), the inductance of section j given in Eq. (3.28) can be written as

$$L(j,t) = \frac{R_o}{M}\,\frac{G}{G-1}\,t_f\,(\ln G)(G)^{(j-1/2)/M}\left(1-\frac{G-1}{G}\,\frac{t}{t_f}\right)^2 \qquad (4.6)$$

The maximum value of L(j,t) during the pulse period of the jth section, is when the leading edge arrives, which from Eqs. (2.41) and (3.9) is

$$t_{1j} = \frac{G}{G-1} t_f (1-G^{-(j-1/2)/m}) \tag{4.7}$$

Using (4.7) in (4.6) yields

$$L_{LE}(j) = \frac{R_o}{m} \frac{G}{G-1} t_f (\ln G)(G)^{-(j-1/2)/m} \tag{4.8}$$

The inductance that must be designed for the jth section decreases from the value given in Eq. (4.8) down to $L_{LE}(j)/LVAR$ at time

$$t_{2j} = \frac{G}{G-1} t_f (1-G^{-(j-1/2)/m} G^{-\frac{x_1}{x_f}}) , \tag{4.9}$$

where

$$\frac{x_1}{x_f} = \frac{\ln(1-\frac{G-1}{G}\frac{\tau_i}{t_f})}{\ln(1/G)} . \tag{4.10}$$

The flux path shown in Fig. 10 traverses one pole pair and two air gaps of length g. Maxwell's equation requires

$$\oint \vec{H}\cdot\vec{d\ell} = 2Ni \tag{4.11}$$

where the integral is taken along the flux path and N is the number of turns per pole. If the permeability of the pole pieces is much larger than that of the air gap, μ_o, then the integral in Eq. (4.10) may be approximated by

$$2gH = 2Ni , \tag{4.12}$$

where H is the magnetic field intensity in the air gap. If the magnetic flux density in the air gap, $\mu_o H$, is not to exceed a value B_{max}, then Eq. (4.12) requires

$$i \leq \frac{g\, H_{max}}{N} = \frac{g\, B_{max}}{\mu_o N} \qquad (4.13)$$

If g is small compared to w and l in Fig. 10, the flux fringing will be small and the inductance may be approximated by

$$L = \frac{\mu_o N^2}{g} A, \qquad (4.14)$$

where A is the shaded area in Fig. 10 and is

$$A = 1/2\ w l\ (1 - \frac{v_{st}\ t'}{w})^2 , \qquad (4.15)$$

where t' is the time measured from the time the poles are in the position shown in Fig. 10.

If the geometry shown in Fig. 10 is used to construct the coil for the jth section of the EPA, and the timing is synchronized such that

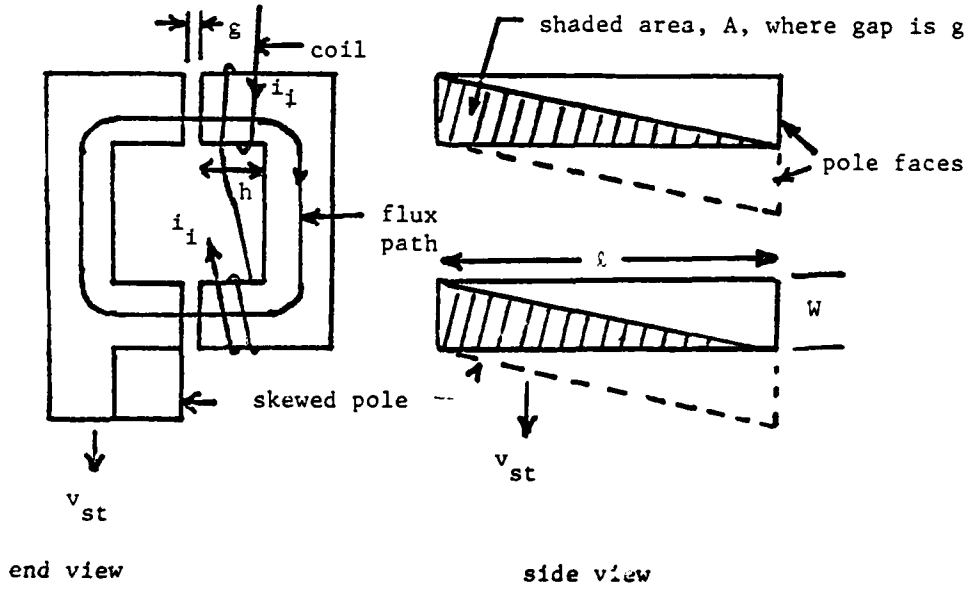

Fig. 10. A time variable inductance geometry.

t' = 0 when the leading edge of the pulse reaches section j, then

$$L_j(t_{1j}) = \frac{\mu_o N_j^2 w_j \ell_j}{g_j} \quad , \tag{4.16}$$

and

$$L_j(t_{2j}) = \frac{\mu_o N_j^2 w_j \ell_j}{g_j} \left(1 - \frac{v_{stj}(t_{2j}-t_{1j})}{w_j}\right)^2 \quad . \tag{4.17}$$

From Eq. (4.3)

$$LVAR_j = \frac{L_j(t_{1j})}{L_j(t_{2j})} = \frac{1}{\left(1 - \frac{v_{stj}(t_{2j}-t_{1j})}{w_j}\right)^2} = \frac{1}{(1+R)^2} \tag{4.18}$$

from which

$$w_j = -\frac{v_{stj}(t_{2j}-t_{1j})}{\Delta R} \tag{4.19}$$

Numerical solutions of the lumped-parameter form of the EPA indicate the rise time is on the order of 0.1 τ_o if M = 20 sections are used. For j = 20, Eq. (4.8) determines the last section inductance to be 239 μH when the leading edge of the pulse arrives, which is reduced to 38.3 μH at the end of the pulse period. Using Eqs. (4.2), (4.7), (4.9) in (4.19) yields

$$w_{20} = 0.069 \text{ meters} \tag{4.20}$$

if v_{st} is taken as 200 m/s for this example. To use a rotating geometry, a number of pole pairs of the skewed shape shown by the dotted lines in Fig. 10 can be placed on the rotor. With a rotor speed of 3600 RPM, the radius to the pole tips is

$$r_r = \frac{v_{ts}}{\omega} - \frac{200}{2\pi(3600)(1/60)} = 0.53 \text{ m} \tag{4.21}$$

Since each pole pair requires approximately 6w meters,

$$P/2 \leq \frac{2\pi r_r}{6w} = 8 \text{ pole pairs,} \tag{4.22}$$

If all eight poles pairs are connected in series for L_{20}, then the area in Eq. (4.15) is multiplied by P/2. Equation (4.14) then yields, for section j,

$$L_j = \frac{\mu_o N_j^2}{2\, g_j} w_j \ell_j (P_j/2)\left(1 - \frac{v_{st}\, t'}{w}\right)^2 \tag{4.23}$$

which can be set equal to Eq. (4.6), and solved for

$$\ell_j = \frac{4\, g_j}{\mu_o P_j N_j^2 w_j} L(j, t_{1j}) \tag{4.24}$$

For the present example each term in Eq. (4.21) has been selected for j = 20 except ℓ_j, g_s and N_j. Equation (4.13) can be solved for g_j and substituted into Eq. (4.24) to yield

$$\ell_j = \frac{4\, i_{maxj}}{P_j N_j B_{max_j}} L(j, t_{1j}) \tag{4.25}$$

The maximum current for each section is that at the trailing edge of the pulse:

$$i_{max20} = \frac{G\, V_i}{R_o(1+\Delta R)} = 2{,}023 \text{ amps} \tag{4.26}$$

and V_i is determined to be 2,023 volts from Eq. (3.23). B_{maxj} is selected from the saturation flux densities available from electrical steels and is

used as two Tesla for this example. Four different considerations are involved in sections N_j:

1) ℓ_j in Eq. (4.22) is smaller for larger N_j.
2) g_j is smaller for larger N_j, and must be small compared to ℓ_j and w_j.
3) smaller winding resistances are possible for smaller N_j
4) smaller leakage inductances are possible with smaller N_j.

A compromise value of $N_{20} = 5$ is selected for trial. This yields $\ell_{20} = 1.2$ cm and $g_{20} = 0.63$ cm. Thus g is not much less than ℓ_{20}, so a smaller $N_j = 1$ is selected. This gives $\ell_{20} = 6$ cm and $g_{20} = 0.13$ cm. Since w_{20} was found to be 6.3 cm, the length of the one turn would be 16 times the length required to encircle a 6 x 6.3 cm pole face. The cross-sectional area for the turn and insulation would be w x h in Fig. 10. Thus, the winding resistance, R_w, could be made very low. However, its shape should be optimized for skin effect.

A small R_w is desirable, but such a low value as would be obtained above with, say, w = h would not be necessary. A better compromise, that would utilize less copper and steel would be to use this multipole rotor for more than one of the L_j's. For example, if only eight of the poles were used for L_{20}, with $N_{20} = 2$, $g_{20} = 0.26$ cm then L_{20} and ℓ_{20} would be unchanged. R_w would be approximately doubled and the skin effect problem would be considerably reduced. The other eight poles could then be used for L_{19}. The pulse period for L_{19} is slightly longer than for

L_{20}, so w_{19} is larger than w_{20}. This may require a slight increase in the radius. But, the point is that only about half the copper and steel would be needed for the latter design per inductive section. Even the latter design is not necessarily the optimum, but it will suffice for an approximation of the size of the EPA.

Some additional consideration in optimizing the design for small size and weight will be considered. Just how large the winding resistance can be is determined by two separate considerations:

1) winding heating (I^2R_w)

2) the effect of the IR_w voltage drops on the gain of the amplifier.

For the winding heating problem, there are three different considerations. For the single pulse case, R_w is limited by the heat capacity of the winding, the safe insulation temperature, and the integral of I^2R_w for one period. For a burst of pulses, both the winding heat capacity and winding cooling are important. For a steady state chain of pulses the cooling and the RMS value of the current would determine the maximum R_w that could be used.

The voltage drop due to R_w causes the gain of each stage of the amplifier to drop compared to the ideal T-line theory. The voltage drop across the jth inductor is

$$e_j = \frac{d(L_j i_j)}{dt} + R_w i_j = (R_w + \frac{dL}{dt})\, i_j + L_j \frac{di_j}{dt} \qquad (4.27)$$

The term R_w in Eq. (4.27) is the difference between the actual and the ideal T-line case (R_w may be increased to account for core losses as

well as winding resistance.) Since dL/dt is negative, its magnitude could be made larger by the amount necessary to cancel R_w in the i_j coefficient in Eq. (4.27). However, then the coefficient, L_j, of the di_j/dt term would decrease too rapidly. Therefore, the performance of the line including losses would be somewhat less than that for the ideal line. It is apparent that considerably more work is involved in optimizing a particular design than is within the scope of this report. Two computer programs are available to aid in such an optimization study.

The inductors near the output end of the EPA convert larger power from mechanical to electrical form than do those near the input end. Therefore, the other L_j's will become progressively smaller until, for L_1, the radius of the disc need only be one quarter of the 0.53 m used for L_{20} to yield the same pole width w_1. And, since the current in L_1 is only one quarter of that in L_{20}, more turns and/or a smaller air gap can be used in the optimized design for L_1. Also the voltages across L_1 and from L_1 to ground are only one fourth those for L_{20}, so less space for insulation is needed in L_1.

It should be pointed out that the voltage across L_{20} may be appreciably less than the output voltage; hence, excessive insulation is not required within the time-variable inductor machine. Rather, the frame of each L_j may be floated (stand-off insulators) and the capacitance to ground included in the section capacitance required by the line.

The capacitance for the 20th section is obtained from Eq. (3.30) and (2.40) and is

$$C(20) = \frac{1}{20R_o} \frac{G_v t_f}{G_v - 1} (\ell n\ G_v)\ G_v^{-20/20} = 2.3\ \mu F \qquad (4.28)$$

and must have a minimum voltage rating in excess of 8100 volts.

Similarly, the capacitance for the first section is

$$C(1) = \frac{1}{20R_o} \frac{G_v t_f}{G_v - 1} (\ell n\ G_v) G_v^{-1/20} = 6.8\ \mu F \qquad (4.29)$$

and must have a voltage rating greater than 2,023 volts. The other sections will have values of capacitance and voltage between the values for C(1) and C(20) and 2,023 and 8,100 volts.

The minimum repetition period is approximately the time required for the rotor of the first section to travel a distance of 3 W_1 or

$$T_p = 3 \frac{\tau_o}{\Delta R} = 4 \times 10^{-3} \text{ seconds}, \qquad (4.30)$$

or

$$f_p = 250 \text{ Hz}. \qquad (4.31)$$

Since the EPA only produces an output pulse when an input pulse is supplied, any pulse repetition rate

$$f = \frac{250}{q} \text{ Hz} \qquad (4.32)$$

can be used, where q is an integer.

2. Extension to other energy levels, pulse periods, gains, and repetition rates

If a gain of eight, rather than four had been selected for the EPA in section one, the capacitive energy storage which must be supplied for the EPA would have been 1/2.09 times the output pulse energy. The input pulse period would be

$$\tau_i = 1{,}600\ \mu s\ , \qquad (4.33)$$

and the input power level would be only 1/64 of the output power level. This would simplify producing the input pulse directly from an electro-mechanical generator.

To obtain shorter duration pulses, for example τ_o = 100 μs, a 400 μs pulse could be applied to the input of the EPA described in Section 1. However, the output energy would be reduced by more than a factor of two. Such a design might be utilized for an application that required 200 μs pulses at times, but 100 μs pulses at other times.

If pulses of only a hundred microseconds duration were desired, a more compact machine could be designed following the same procedures described in Section 1. The same tip speed, v_{st}, could be used, but the output energy would be reduced to one half that described in Section 1. Of course, one could obtain the same energy by using two EPA's in parallel, with each designed for twice the R_o of the previous example.

For pulses appreciably shorter than 100 μs, it would be difficult to design the required L(j)'s for the 200 m/s tip speed. Higher values of tip speed, v_{ts}, would allow designs for pulse duration on the order of

$$\tau_o = \left(\frac{200\text{m/s}}{v_{ts}}\right) 100\ \mu s \qquad (4.34)$$

For rotating machine designs, the maximum tip speeds that can be used are limited by the strength and mass density of the rotor material. Values in excess of 200 m/s are achievable for practical materials, but not by a large factor. However, where space is not a problem, a linear machine

with appreciably higher velocities could be designed. Unless an appreciable fraction of the energy used to accelerate the linearly moving part were reclaimed, the energy efficiency would be low. With the linear machine, output pulses on the order of 10 μs could be produced.

The higher velocities available from the linear machines could also be used for higher power and energy levels for pulses of up to a few hundred microseconds. For the high velocities, the pole widths, w_j, would increase proportionally. To obtain a proper or economic balance between conductor, insulator and steel in the inductance construction, the length, l_j, and the gaps, g_j, should increase in proportion to w_j. For a single pole-pair, this might produce a larger L(j) than is desired for a single section. A lower L(j) and a higher current rating could then be obtained by paralleling the L's from two or more pole-pairs.

E. CONCLUSION

An electromechanical machine, an EPA, has been described in sections A-D, which is capable of producing high power, repetitive or single shot pulses, of shorter duration and faster rise times than have previously been produced by electromechanical means. The EPA itself requires no switches; however, various types of switched pulsers may be used to provide input pulses at reduced power levels to control output pulses of appreciably higher power and energy levels. Since pulse compression is achieved in the EPA, the input pulses required for some applications may be sufficiently long that they may be produced directly from electromechanical pulse generators without switching.

The EPA does require some energy storage capacitors. However, it is possible to reduce the amount of capacitive energy storage required by a factor of one third to one half over a purely capacitive store pulser, and since the capacitors that are required are distributed along the time-varying inductors and require no switching, the wiring and protection of the capacitors is considerably simplified.

The design equations for both the distributed and the lumped-parameter approximation EPA have been presented. Two computer programs have been developed to aid in optimizing designs for specific applications.

An example of the procedure to design a lumped-parameter EPA for a specific pulse requirement was presented. From this example and discussion it can be concluded that more compact time-varying inductors can be obtained for higher magnetic flux densities and higher relative speeds between the mechanical parts of the EPA.

The EPA is designed for a given output pulse width, energy and load resistance. A compromise voltage gain is selected for the EPA. The current and energy gain are equal to the voltage gain. The power gain is the square of the voltage gain. The input pulse period is the voltage gain times the period of the output pulse period. The period of the maximum repetition rate is

$$T_p = 3\tau_i/\Delta R = 3Gv\tau_o/\Delta R \qquad (4.35)$$

Since the EPA produces an output pulse only after an input pulse is applied, repetition rates with pulse periods that are integer multiples of the value given by Eq. (4.35) are also possible. It is also possible to obtain shorter duration pulses from this EPA by simply applying input pulses of shorter duration than $G_v\tau_o$. However, the output energy per pulse is also reduced so that the EPA is relatively massive per unit output energy if τ_o is much below its design value.

The example of section D illustrates that an output pulse of 2 kJ with 200 μs duration is quite feasible using rotating geometry for the time varying inductors. It can readily be deduced that output energies from one to several tens of kilojoules per pulse with pulse periods from one hundred to a few hundred microseconds duration can be similarly produced.

Using linear machines with higher velocities makes feasible higher energy levels per pulse and/or shorter duration pulses. Pulse periods as short as 10 μs are probably feasible.

Large capacitor banks are assembled by paralleling large numbers of capacitors. Similarly, separate EPA's can be connected in series/parallel combination for larger power and energy levels. Alternatively, the individual L sections of a single EPA may be made up of series/parallel combinations of inductors similar to these described in section D.

A small model of an EPA was designed, built and tested [4]. It demonstrated voltage gain, time delay and pulse compression. However, energy gain was not obtained and the pulse wave shape was not as good as expected. There were two reasons for the performance deficiency: (1) the winding resistance was too high and (2) the load, R_L, was constant, rather than matching the output characteristic impedance. The inductances were constructed with standard "C" cores rather than the construction described in section D. The window area for these cores were not sufficiently big to make the winding resistance low enough.

F. REFERENCES

1. W. F. Weldon, H. G. Rylander, H. H. Woodson, "Detailed Design, Fabrication and Testing of an Engineering Prototype Compensated Pulsed Alternator," Final Report to LLL, March 1980.

2. W. F. Weldon, M. D. Driga, H. H. Woodson, and H. G. Rylander, "The Design Fabrication and Testing of a Five-Megajoule Homopolar Motor-Generator." International Conference on Energy Storage, Compression and Switching, Torino, Italy, 5-7 November 1974.

3. F. F. Chiang, "The Theory and Design of a New Electromechanical Pulser," MSEE Thesis, Texas Tech University, August 1976.

4. B. H. Dunlap IV, "Electromechanical Pulse Amplifier," MSEE Thesis, Texas Tech University, May 1982.

APPENDIX A

THEORETICAL ANALYSIS FOR AN L(t) AND C(t) EPA

The theoretical analysis of a distributed transmission line that uses both time-varying inductors and capacitors follows the same procedure as discussed in Section B. The main difference is in the solutions for L(t), C(t), i(x,t), and R_L. The L(t) and C(t) functions can be written as

$$L(t) = L_o\left(1 - \frac{\alpha}{\sqrt{L_o C_o}}\, t\right) \qquad (A.1)$$

and

$$C(t) = C_o\left(1 - \frac{\alpha}{\sqrt{L_o C_o}}\, t\right) \quad . \qquad (A.2)$$

As one can see from equations (A.1) and (A.2), neither function is dependent on the distance along the line x. Also, both functions decrease linearly with respect to an increasing time t.

With the voltage across the transmission line varying as

$$v(x,t) = e^{\alpha x} f(x-st) \qquad (A.3)$$

and from Eqs. (A.1) and (A.2) the current solution is

$$i(x,t) = \frac{e^{\alpha x}}{R_o}\, f(x-st) \quad . \qquad (A.4)$$

Since both the inductance and capacitance per unit length are varying, the matching load impedance is constant and, from Eqs. (A.3) and (A.4), R_L is

AD-A129 554 COORDINATED RESEARCH PROGRAM IN PULSED POWER PHYSICS (U) TEXAS TECH UNIV LUBBOCK DEPT OF ELECTRICAL ENGINEERING M KRISTIANSEN ET AL. 01 DEC 82 3/5

UNCLASSIFIED AFOSR-TR-83-0503 F49620-79-C-0191 F/G 20/3 NL

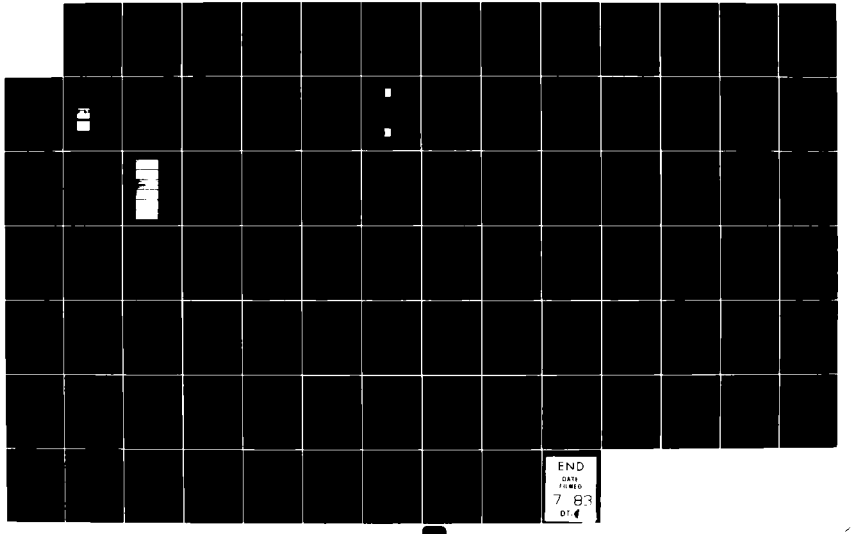

END
DATE FILMED
7 83
DTIC

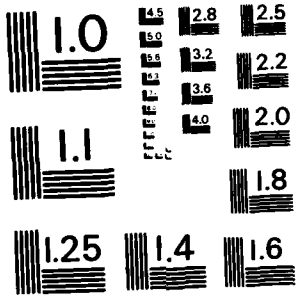

$$R_L = \frac{v(x_f,t)}{i(x_f,t)} = R_o \quad , \tag{A.5}$$

a constant.

Project No. 8

Optically Controlled Discharges

Project No. 9

Opening Switches*

(C. Harjes, G. Hutchinson, G. Leiker, L. Thurmond, J. Gahl, R. Cooper K. Pinegar, K. Schoenbach, G. Schaefer, H. Krompholz, L. Hatfield, and M. Kristiansen)

A. SUMMARY

These two Projects (8 & 9) are so closely related in objective, theory, and diagnostic techniques that they are described together as one project in order to save duplication of description. The primary objective of this work is to study the controlled processes in externally sustained or controlled diffuse discharges, with respect to their application as opening switches. Concepts for diffuse discharge opening switches have been developed and experimental facilities have been designed to investigate the applicability of these concepts.

*This project is funded by the Army Research Office. Project No. 1 which was earlier funded by AFOSR has been incorporated in this Project.

Two generally different groups of concepts are:

- the electron-beam sustained diffuse discharge (Section B)
- the optically controlled diffuse discharge where optical control either means sustainment of the discharge by means of laser radiation or optical stimulation of loss processes in self-sustained discharges (Section C).

Although these two concepts may also be combined in one system they are discussed in separate chapters.

For the investigation of the electron-beam sustained discharge an apparatus was designed which allows the investigations of repetitive opening in the time range of 100 ns at current levels of up to 10 kA.

The work done in the last year includes:

1) construction and testing of an electron beam gun with thermionic cathode.
2) design and construction of an e-beam control system, which allows for the generation of two sucessive e-beam pulses.
3) developed and testing of ns electrical and e-beam diagnostics.
4) design and construction (in progress) of a high pressure discharge chamber with a transmission-line current source
5) search for suitable gases for separate diffuse discharge opening switches (in cooperation with L. Christophorou at Oak Ridge National Laboratory) and

6) modification (in progress) of a computer program (developed for the optically controlled opening switch) which allows modelling of an e-beam controlled diffuse discharge.

For investigations of optically controlled discharges the following steps were taken to approach a feasible switch system:

1) Several switching concepts have been considered based on available data on basic photon-molecule and molecule interactions.
2) Small scale experiments have been performed to investigate the general feasibility of one of these concepts.
3) A high power discharge cell was constructed and tested.
4) Calculations on one specific system have been performed to calculate the time-dependent behavior of the discharge.

Several other exploratory opening switch concepts have also been examined for potential use as opening switches. Among these are the dense plasma focus, and a magnetically controlled switch.

B. E-BEAM CONTROLLED OPENING SWITCH SYSTEM

1. Introduction

An electron-beam controlled discharge circuit has been designed and is presently under construction to study the behavior of an e-beam sustained, attachment dominated discharge

a) at high discharge current densities,

b) in gases which are suitable for low loss, fast opening operation,

c) for rep-rated operation.

The objective of the investigation is to determine a set of criteria concerning electrical and gas parameters of an e-beam sustained discharge, which will guide the design of the rep-rated electron-beam controlled opening switch.

Figure 1 shows a block diagram of the e-beam opening switch system. It consists of four sections. The e-beam gun, a trigger system which allows production of two successive e-beam pulses, the e-beam controlled switch, and the associated electrical and optical diagnostics.

The e-beam gun is completed and tests have been performed. The grid pulser has been built and tested, but is not yet attached to the e-beam gun. A switch chamber with pulse-forming network has been designed and is presently under construction. Several diagnostic techniques with high time resolution have been developed and are used for e-beam diagnostics.

2. E-Beam Gun

For the investigation of electron-beam sustained discharges an e-beam gun was designed and constructed which generates electron currents of up to 100 A over an approximately 100 cm^2 area at electron energies of $E_e \leq 250$ kV. The arrangement is shown in Fig 2. An FRP-250 pulse

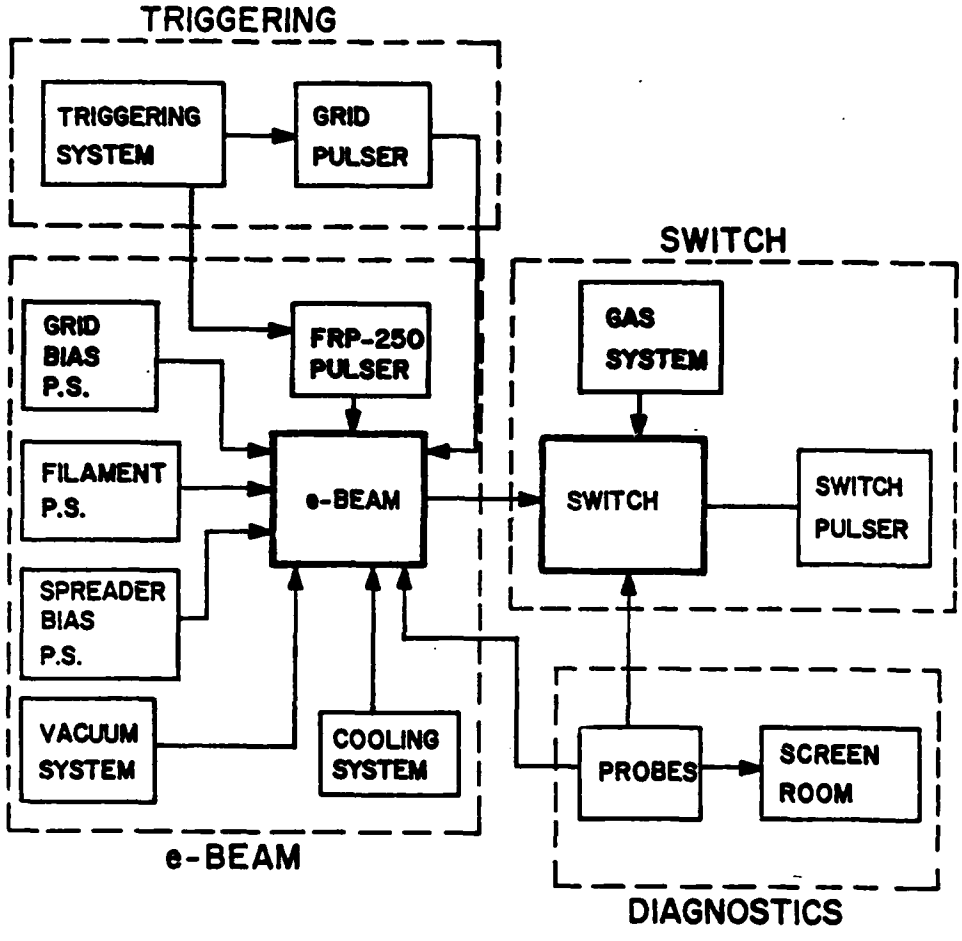

Fig. 1 Block Diagram of the E-Beam Controlled Opening Switch System

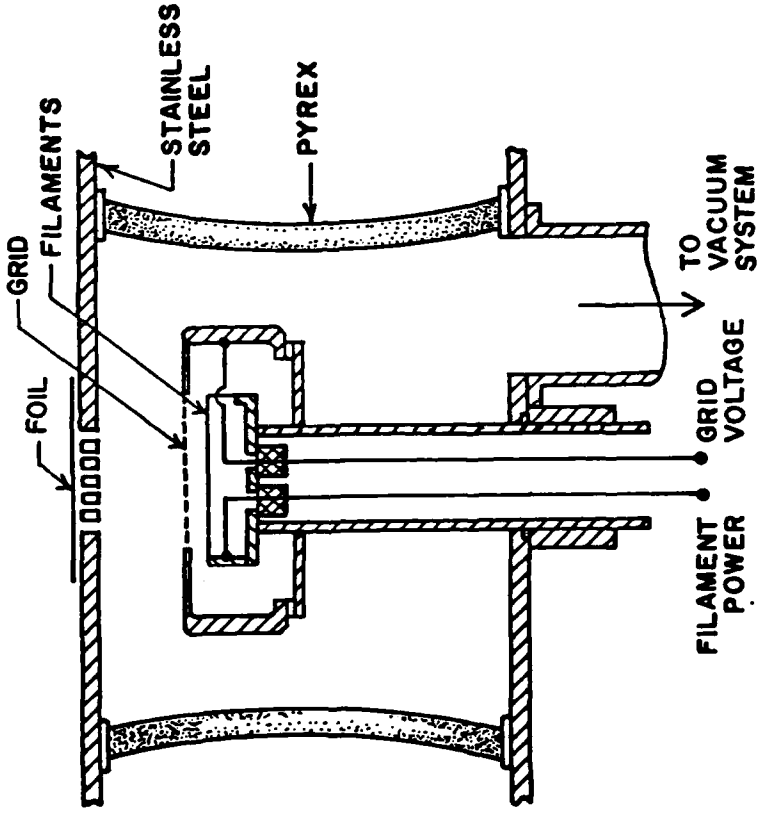

Fig. 2 Cross Section of the e-Beam Triode

generator, which generates voltage pulses of up to 250 kV, with a rise-time of 10 ns and an 1/e-fall time of 1 μs is used to supply the electron accelerating plate voltage. The e-beam generator is located in an evacuated pyrex glass chamber between the plates of the pulse stripline, which is terminated by a resistance of R = 100 Ω. The terminating resistor also serves as a 1 : 1500 voltage divider for monitoring the e-beam voltage. The e-beam current is monitored by means of a Rogowski coil around the grounded cathode. The e-beam chamber is evacuated by a 280 ℓ/s diffusion pump. It provides an ultimate pressure of $6 \cdot 10^{-7}$ Torr in the chamber.

The thermionic cathode is shown more detailed in Fig. 3. An array of electrically heated Th-W filaments are stretched between supports which are anchored to a water cooled aluminum heat sink, The filaments have to be activated in order to realize improved electron emission over that of pure tungsten. The activation procedure requires heating the filaments to temperatures in excess of 2700 K for some seconds. The operational filament temperature is in the range from 1500 K to 2000 K. A 200 V, 200 A, DC power supply is used to heat the filaments.

A spreader plate is located just below the filaments and is electrically insulated from the rest of the cathode. It serves several purposes: it shades the lower part of the cathode from the intense filament radiation and it helps to control the e-beam by the application of negative voltage to this plate [1]. It also protects the filament array during the time when no voltage is applied to the e-beam gun. It

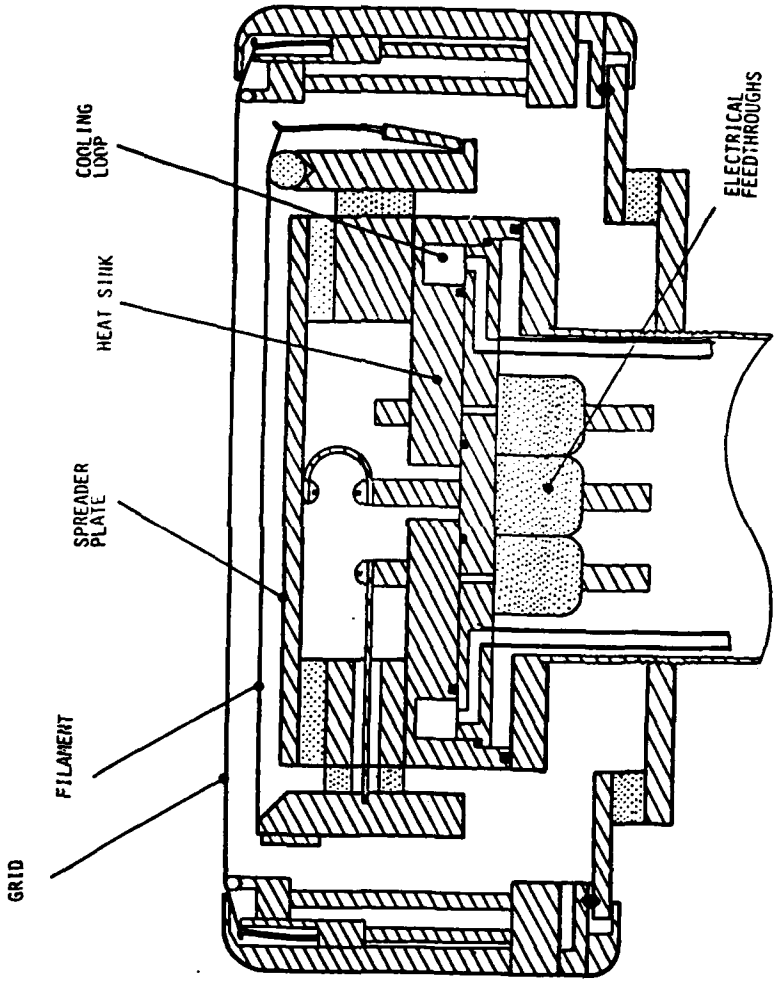

Fig. 3 Cross Section of the Thermionic Cathode

prevents excessive heating of the positive (w.r.t its neg.or low pot. side) pole of the filament array by repelling electrons from the filament, which would otherwise be accelerated to the positive pole.

The entire cathode is enclosed in a shroud which is electrically insulated from the rest of the cathode. Molybdenum wires (10 mil ϕ) are stretched across the opening in the top of the shroud just above the filaments. These wires form a grid which is used to control the e-beam

The entire cathode-system and the anode - a Ti foil - is cooled The cooling system provides cooling water for the e-beam gun and the diffusion pump. The system is closed and cooling is accomplished by circulating the water through a fan-cooled radiator. .

Tests have been performed to confirm the calculated emission characteristics of the thermionic cathode. The total cathode emission current has been measured at low filament temperatures (<1750 K) by applying a modest voltage of 3 kV to the e-beam diode. Figure 4 shows the experimental results together with the theoretical curves for Th-W and pure W.

The e-beam gun itself has been tested at voltages of 200 kV. To reduce the possibility of a spark breakdown during the high voltage pulse the e-beam electrodes were conditioned for several hours by an Argon glow discharge. The filament temperature was T = 1900 K and the spreader voltage V_s = -1000 V. The spatial, time integrated, e-beam distribution was measured by using a NE 102 plastic scintillator

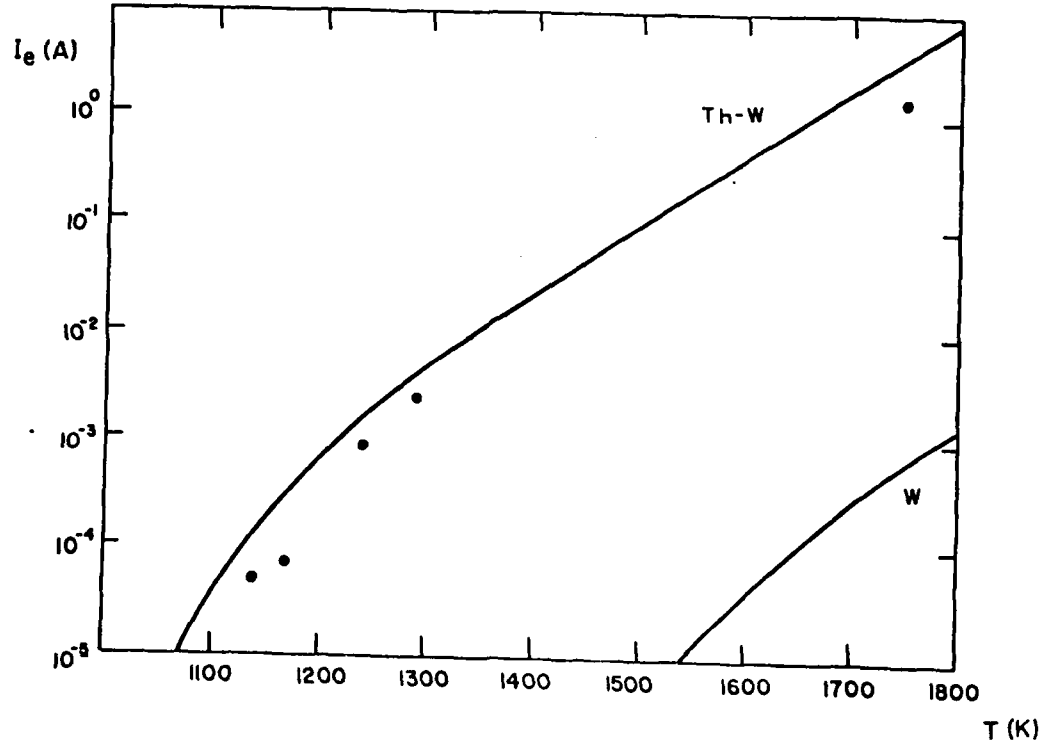

Fig. 4 Calculated Electron Emission from Pure Tungsten and Thoriated Tungsten (dots: experimental results)

plate located 1 cm above the e-beam anode. The e-beam voltage was monitored by means of the resistive voltage divider. Figure 5a shows an oscilloscope trace of the e-beam voltage with $V_{max} \sim 200$ kV. The current was measured by means of a Rogowski coil wrapped around the cathode. Besides the e-beam current, an oscillatory displacment current is flowing through the diode. Its amplitude is on the same order of magnitude as the e-beam current. To discriminate between these currents, two measurements were performed: one with cold cathode (no e-beam) and a second one with heated cathode. The traces are shown in Fig. 5b. The e-beam current was obtained by subtracting the two currents. The result is an approximately rectangular pulse with a duration which reflects the characteristic transit time of the Rogowski coil (see Section 4). From these measurements it can be concluded that the initial e-beam current is $I_e = 60A \pm 10A$. The accuracy of the current measurements can be improved by reducing the oscillatory displacement current component. This will be achieved by a more compact terminating resistor arrangement which reduces the stray inductances.

3. E-Beam Control System

To investigate the repetitive opening of the e-beam controllled discharge, two successive e-beam pulses of variable duration and distance between pulses will be generated by pulsing a grid between cathode and anode. Figure 6a shows the schematic of the pulser circuit. Cable 1 with length d_1 is charged to a high voltage V_0 and then discharged

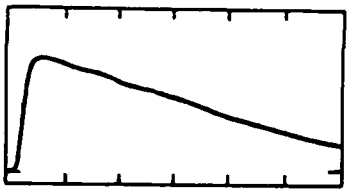

Fig. 5a E-Beam Voltage, 200 ns/div

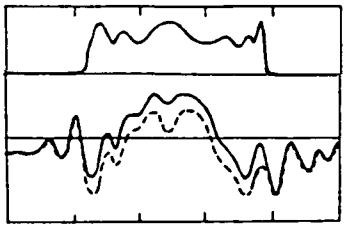

Fig. 5b Rogowski-Coil Signal of E-Beam Current, 20 ns/div

E-Beam current, 20 ns/div (upper trace) evaluated by subtracting the Rogowski-coil signals of the currents with and without e-beam (lower traces). Solid line; current with heated cathode; dashed line, current with cold cathode

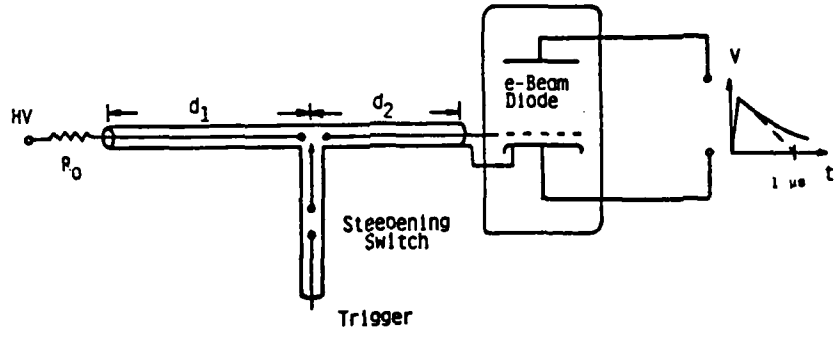

Fig. 6a Schematics of Grid Pulser Circuit

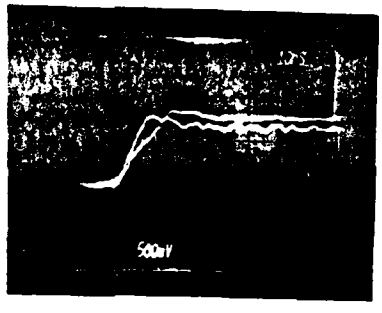

Rise of Voltage at Open Ended Cable 2

a) Self-Triggered (slower rise)

b) Externally Triggered (faster rise)

Successive Pulse Amplitude : 12 kV

Pulse Duration : 100 ns

Time Between Pulses: 100 ns

Fig. 6b Pulse Shapes Recorded at Open Ended Cable

through a triggered switch into cable 2 with length d_2. This cable is terminated in the e-beam triode. This termination acts like an open end so that the pulse is reflected, maintaining its polarity. After reflection at a large resistor at the charging side it is travelling back with the same polarity and almost same amplitude as the first pulse. The pulse length t_1 of the successive rectangular pulses is determined by the length $d_1 (t_1 = 2d_1/v)$. The distance between pulses is given by the length $d_2 + d_1$ $(t_2 = (d_1 + d_2)/v)$. The timing of subsequent e-beam pulses can be controlled by varying the cable length.

Figure 6b shows the rise of the first voltage pulse in self breakdown mode (slower rise) and triggered (faster rise) with a 7.5 kV trigger pulse which was steepened to a risetime of 10 ns by means of a gap in the trigger line. Figure 6c shows the first two pulses generated in this way. The amplitude is $V_o = 12$ kV. The pulse duration and the time between pulses is t = 100 ns. The risetime and amplitude of the second pulse is reduced due to losses in the cable. However this should not influence the efficiency of the triode control because the anode voltage of the e-beam gun is decreasing even faster.

4. Electrical and E-Beam Diagnostics

a) Electrical Diagnostics

The voltage across the e-beam diode is measured by means of a resistive voltage divider, which is part of the $R = 100\ \Omega$ resistive termination of the e-beam pulser. The risetime, T_r, of this divider can be calculated from the equation [2]

$$T_r = 0.24\ RC_g$$

where C_g is the stray capacitance of the divider. Due to the low value of R, risetimes of less than 5 ns might be expected. Voltage measurements at the e-beam pulser demonstrated a risetime better than 10 ns.

The current through the diode is monitored by means of a Rogowski coil. The coil which is surrounded by a metallic housing (Fig. 7a), can be considered as a coaxial waveguide. The impedance of this waveguide is $Z = \sqrt{\frac{L'}{C'}}$, the transit time $2\tau = 4\pi r \sqrt{L'C'}$, where L' and C' are the distributed inductance and capacitance, respectively, and $2\pi r$ is the mean circumference of the coil. Due to the large value of L', the transit time [$2\tau \sim 50$ ns] and impdance [$Z \sim 500\ \Omega$] are much higher than that of common coaxial lines.

Usually Rogowski coils are terminated with a resistor, which is small compared to the coil impedance, to provide for self integration of the coil signal [2]. For our measurement we terminated the coil with

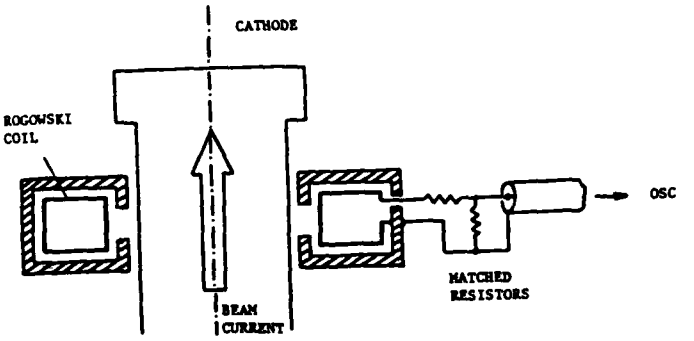

Fig. 7a Schematics of Current Recording System

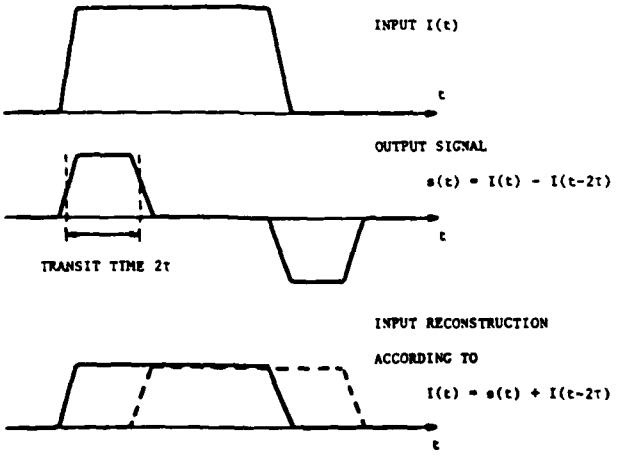

Fig. 7b Reconstruction of Current Pulse

a resistor, which is matching the impedance of the system. This method requires a numerical evaluation of the signal, as shown in Fig. 7 b. However it has the advantage that the gain of the detector system can be increased -- noise problems can be avoided without changing the risetime of the system.

b. E-Beam Diagnostics

The spatial distribution of the e-beam intensity is recorded by means of a plastic scintillator (NE 102A) located 1 cm above the foil-anode. The thickness of the scintillator is 3 mm. Besides open shutter photography, time resolved measurements of the scintillator light are performed by means of a filter-photo multiplier system. The recorded pulses yield information on the time dependence of the e-beam current.

Another way to measure the e-beam current, as a function of time is by using a Faraday-cup. Figure 8 shows the experimental set up. The Faraday cup consists of an aluminum plate connected to ground through a coaxial system of resistors with a total resistance of 1 Ω. If placed directly on top of the e-beam anode, the entire Faraday cup is raised to the anode potential of the e-beam diode during the e-beam operation. To isolate the Faraday cup electrically from the recording system inside the screen room, an optical coupling system is used. The current from the cup drives a photodiode. The emitted light is guided through an optical fiber and recorded by a photocell. The optical link was tested by applying a fast rising pulse at the photodiode (pulse, shown at the left in Fig. 8). The response is shown on the right side. The risetime of the link is, according to these measurements, less than 5 ns.

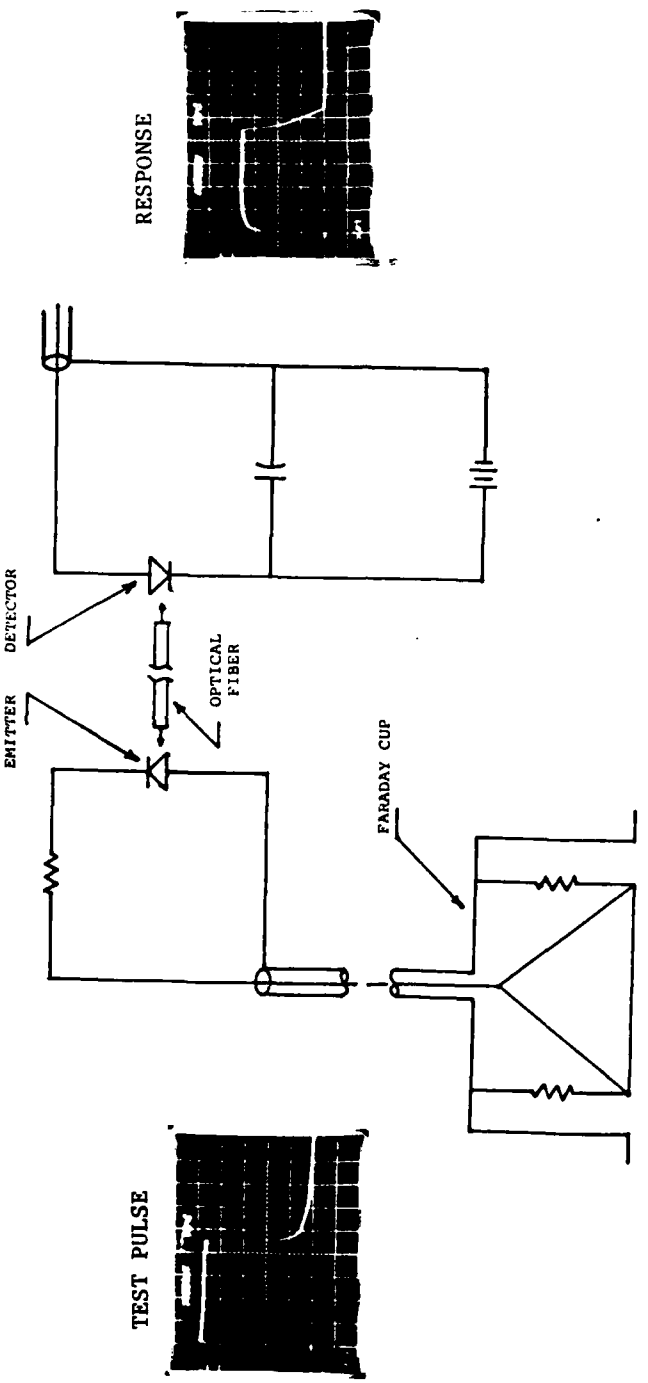

Fig. 8 Detector System for E-Beam Current (Faraday Cup and Optical Link)

Because of the nonlinear characteristics of the photo diode and the receiver, the output pulse shape has to be evaluated numerically. For this purpose a fast digitizer-computer system will be used.

5. High Pressure Discharge Chamber

A high pressure stainless steel chamber was designed and is presently under construction. It can be pressurized to p = 10 atm. The discharge current will be provided by a pulse forming network consisting of a 10-stage L-C PFN. The numerically calculated pulse shape is shown in Fig. 9. For C = 20 nF and L = 125 nH the pulse duration is approximately τ = 1 µs and the impedance is $\sqrt{\frac{L}{C}} \approx 1.25$. If the PFN is charged to the maximum voltage of V = 50 kV (determined by the available capacitors) the maximum current flowing through the matching resistor and the electron beam controlled switch in series is I = 20 kA, for a switch resistance small compared to the matching resistor $R_m = \sqrt{\frac{L}{C}}$.

6. Gases for the E-Beam Controlled Switch

Gas mixtures used in diffuse discharge opening switches should satisfy the following conditions:

- high mobility at low E/N
- low attachement rate at low E/N
- high attachment rate at high E/N
- high dielectric strength.

It is planned to use as a first gas mixture $N_2 + N_2O$. One reason for this choice is that for this mixture the conditions con-

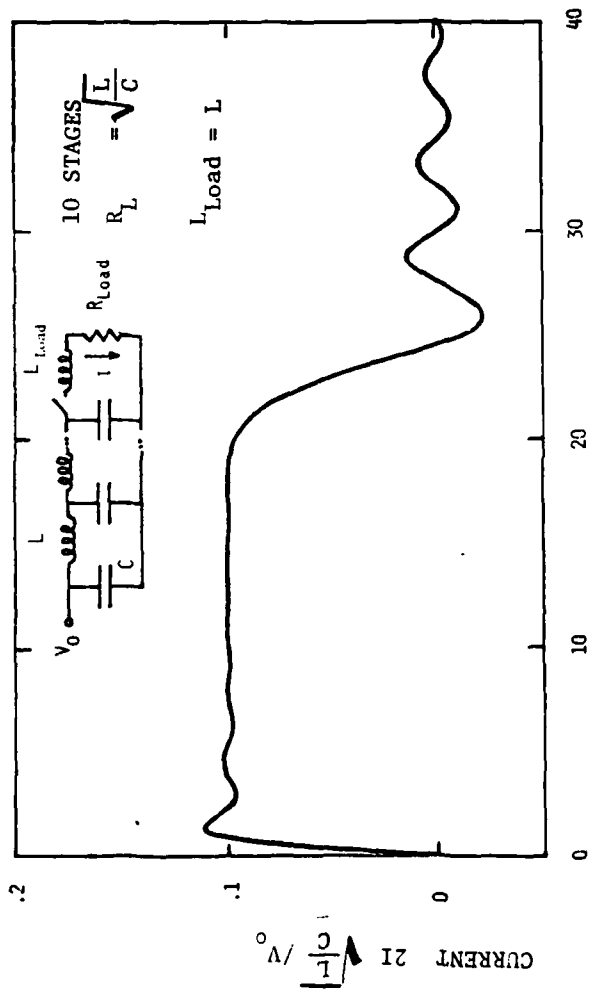

Fig. 9 Pulse Shape of Discharge Current ($R_{Discharge} << R_{Load}$)

cerning attachment and dielectric strength are satisfied. A second reason is that a computer program which was developed for the optically controlled switch (see Section C) can be easily modified to model the e-beam switch in these gases.

To find gases which satisfy all conditions mentioned above, a joint program with the Atomic Molecular and High Voltage Physic Group at Oak Ridge National Laboratory is planned. In a proposal to the National Science Foundation it is proposed to measure mobility, attachment coefficient and breakdown voltage of suitable gases. The measurement will be performed at Oak Ridge National Laboratory, the switch experiments will be performed at Texas Tech University.

C. OPTICALLY CONTROLLED DISCHARGES

1. Introduction

To operate an optically controlled discharge means to make use of an optogalvanic effect. Optogalvanic effects have been investigated for several years but the main emphasis in all these investigations was to use the optogalvanic signal for spectroscopy; to investigate the state structure of atoms and molecules or as a tool for sensing impurities. In this case a detectable signal is required but the magnitude of the effect is of minor importance. For switching applications, however, only processes that show a strong influence on the charge carrier balance of the discharge are of interest. The following four research areas are felt necessary for the solution of this problem:

a. Concepts for optical control of diffuse discharge opening switches must be developed, based on known effects from optogalvanic experiments.

b. Small scale optogalvanic experiments must be performed on those systems where data are not yet available.

c. High power discharge system experiments must be carried out to check the scaling laws for the optogalvanic processes and to investigate promising control systems.

d. Detailed calculations on promising systems must be performed to predict optimum experimental conditions with respect to the suggested transient behavior of the discharges.

Although these four research areas and the ongoing research on the e-beam controlled discharge (Project No. 9) interact strongly with each other, they will be discussed in separate sections.

2. Concepts for Optical Control of Diffuse Discharge Opening Switches

The aim of this work is to investigate several types of opto-galvanic processes and to estimate the magnitude of the change of the discharge resistivity that might be achieved using these effects. An overview of several possible processes is presented in our paper in IEEE Trans. Plasma Sci., which will be published in December 1982 (See Appendix 1).

In ongoing studies some additional processes have been studied in more detail. One important process seems to be photo-detachment (See Section 3).

3. Small Scale Experiments (in collaboration with Project No. 5 and J. Mosely, Univ. Oregon)

Although the basic data available for several processes allow us to estimate the magnitude of certain optogalvanic effects, small scale experiments are necessary to prove the feasibility of these concepts. The reasons are that in a discharge the optogalvanic effect competes with a large number of processes and that a full set of rate constants is not available in most cases. Even if fairly complete sets of cross sections are available the necessary calculations are difficult and time consuming. Good examples of such experiments are the investigations on He and Ne discharges by Smyth, Tam, and Lawler

(see [24-26] in Appendix 1). In these experiments the conductivity of glow discharges could be changed significantly and we think that these systems are also interesting candidates to be investigated in our high power discharge cell.

In a project carried out in close cooperation with Frazer Williams (Project No. 5) we performed experiments to investigate the feasibility of photodetachment as an optical control mechanism. Since photodetachment is not a resonant process it has never before been investigated in opto-galvanic discharge experiments. On the other hand the broad cross section may allow the combination of photodetachment with another resonant process for increased efficiency.

In the first study we looked at photodetachment of O^- in the flowing afterflow of a discharge containing O_2 to show that the produced negative ions can be efficiently detached using a pulsed dye laser operating in the visible range. A paper describing the results of this experiment will be submitted to IEEE Trans. Plasma Sci. (See Appendix No. 2).

The investigations of photodetachment of O^- are now continued as optogalvanic experiments in the discharge itself. DC discharges in O_2 show a very interesting behavior. There are two different discharge forms at similar currents and pressures, with a sharp transition, the T and the H form as shown in Fig. 10 and 11. The H form shows a much higher voltage gradient than the T form. A transition from H to T can be induced either by increasing the pressure or by decreasing the current of the discharge. In preliminary experiments with the H form, close to the transition region, the photodetachment of O^- could cause

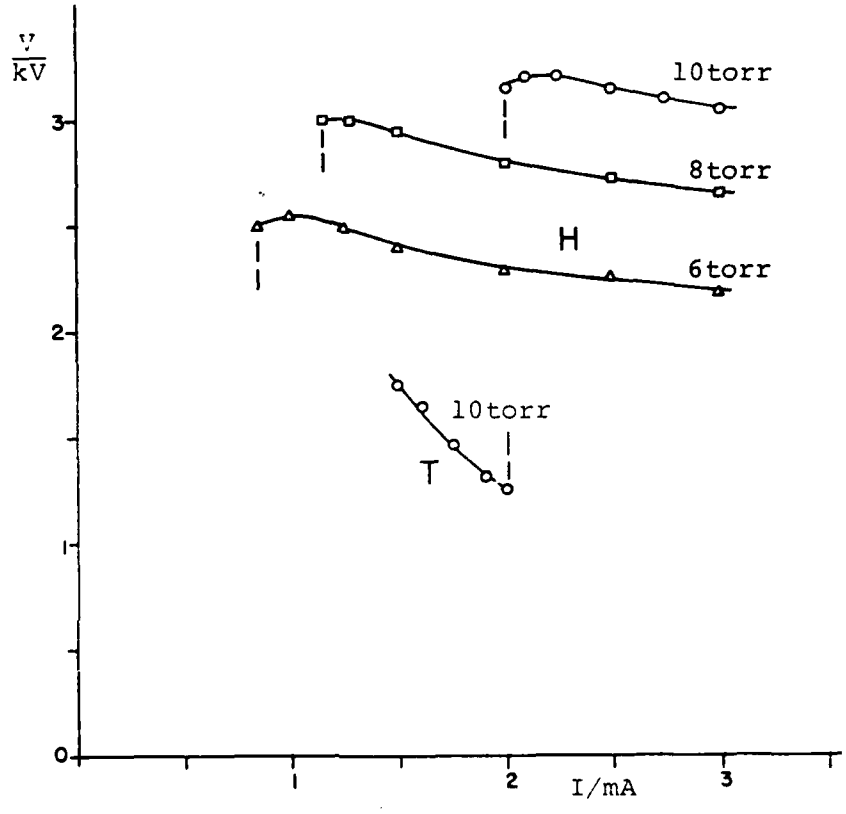

Fig. 10 Voltage vs current for different pressures in a O_2 glow discharge (tube length L = 15 cm, diameter d = 3mm). (-- unstable region)

Note: H-form and T-form are derived from the German words:

H: "hohes Feld" (high field strength)

T: "tiefes Feld" (low field strength)

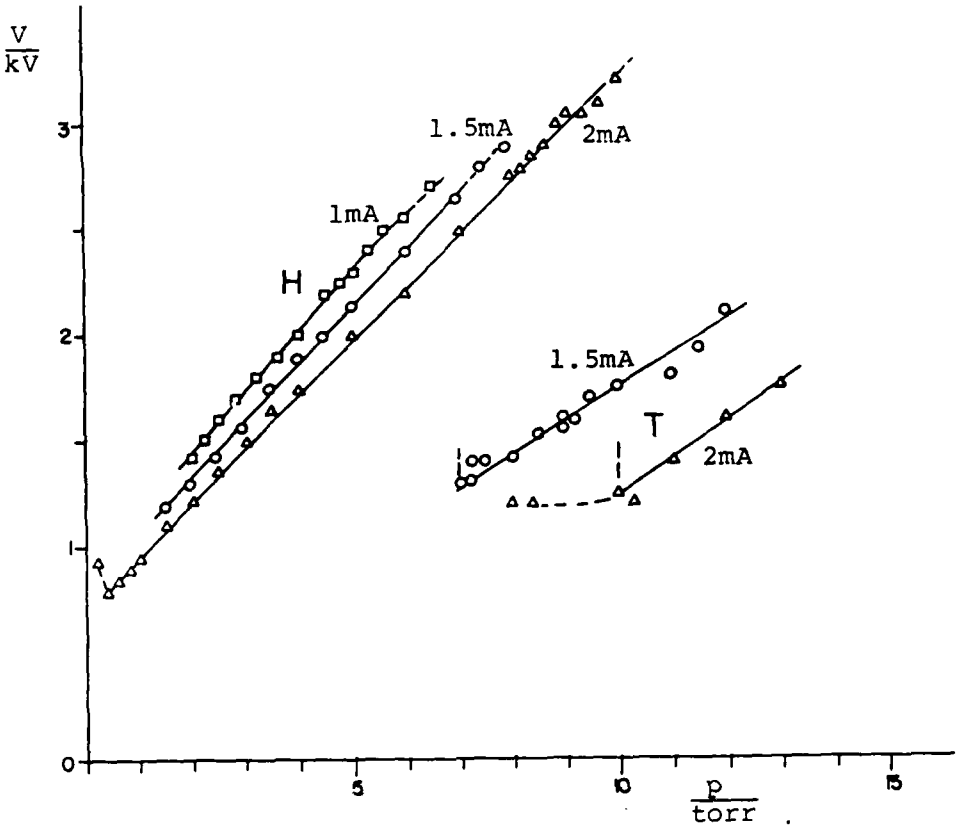

Fig. 11 Voltage vs pressure for different currents in a O_2 glow discharge (tube length L - 15 cm, diameter d = 3 mm) (-- unstable region)

gradient changes of more than 50%. Figure 12 shows the optogalvanic signal for decreasing current at constant pressure. The separation between the two oscilloscope traces equals 1/1000 of the voltage drop across the discharge. Although the time dependence of the gradient is not understood, these preliminary results indicate that significant changes of the resistivity of the discharge can be achieve using photo-detachment. This work is being continued to obtain better information about the processes in discharges producing O^-.

4. High Power Discharge System

The design of an optically controlled high power discharge system was described in the last Annual Report. The main requirements that must be fullfilled by this system are outlined below:

A. Requirements for the production of a high pressure diffuse discharge:

1. voltage across the main gap large compared to the breakdown voltage of the gas mixture (large overvoltage)
2. fast voltage rise (dV/dt > 10 kV/ns)
3. uniform preionization
4. uniform initial electric field
5. possibility to vary discharge current

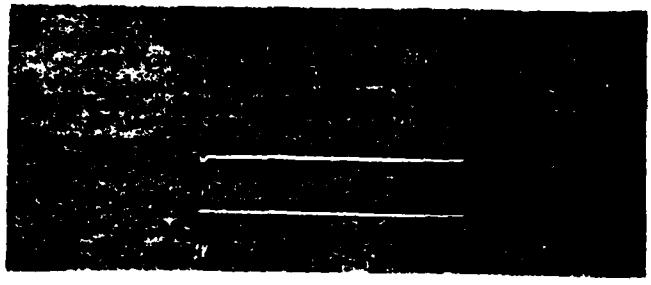

I = 1.5 mA

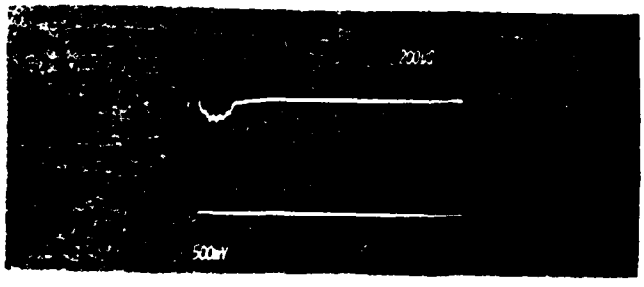

I = 1.2 mA

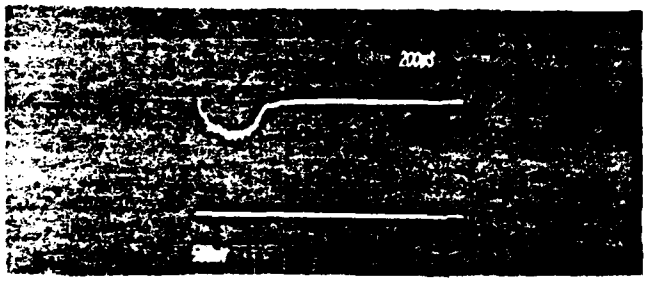

I = 1.1 mA

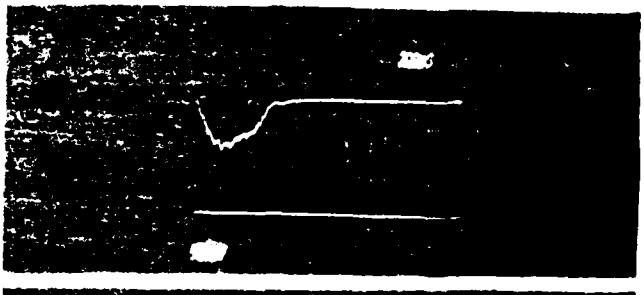

I = 1.05 mA

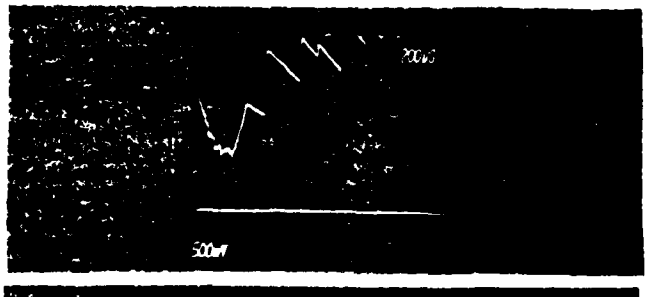

I = 1.0 mA

I = 0.95 mA

Fig. 12 Optogalvanic signal vs time (scale: 200 μs/div) for different currents (p= 6 torr)

B. Requirements for optical control of the diffuse discharge:

1. optical access to the diffuse discharge
2. tunability of laser
3. possibility to shape the laser pulse with rise and fall times shorter than the desired opening time of the diffuse discharge switch

C. Diagnostics Requirements:

1. ns-time resolution of voltage and current measurements
2. side-on and end-on optical access

The system shown in Fig. 13 has been constructed. The main parts of this system are (Fig. 13 from left to right):

a) the 50 Ω oil-filled transmission line
b) the laser triggered spark gap used as a closing switch to ensure a fast risetime of the voltage across the main discharge. The laser is coupled into the spark gap through a large diameter (Ø = 600 - 1000 μm) quartz fiber
c) the main discharge chamber with the cathode the inner conductor, a grid anode, and a quartz window behind the anode for optical access to the discharge.
d) matching resistors, voltage and current probes.

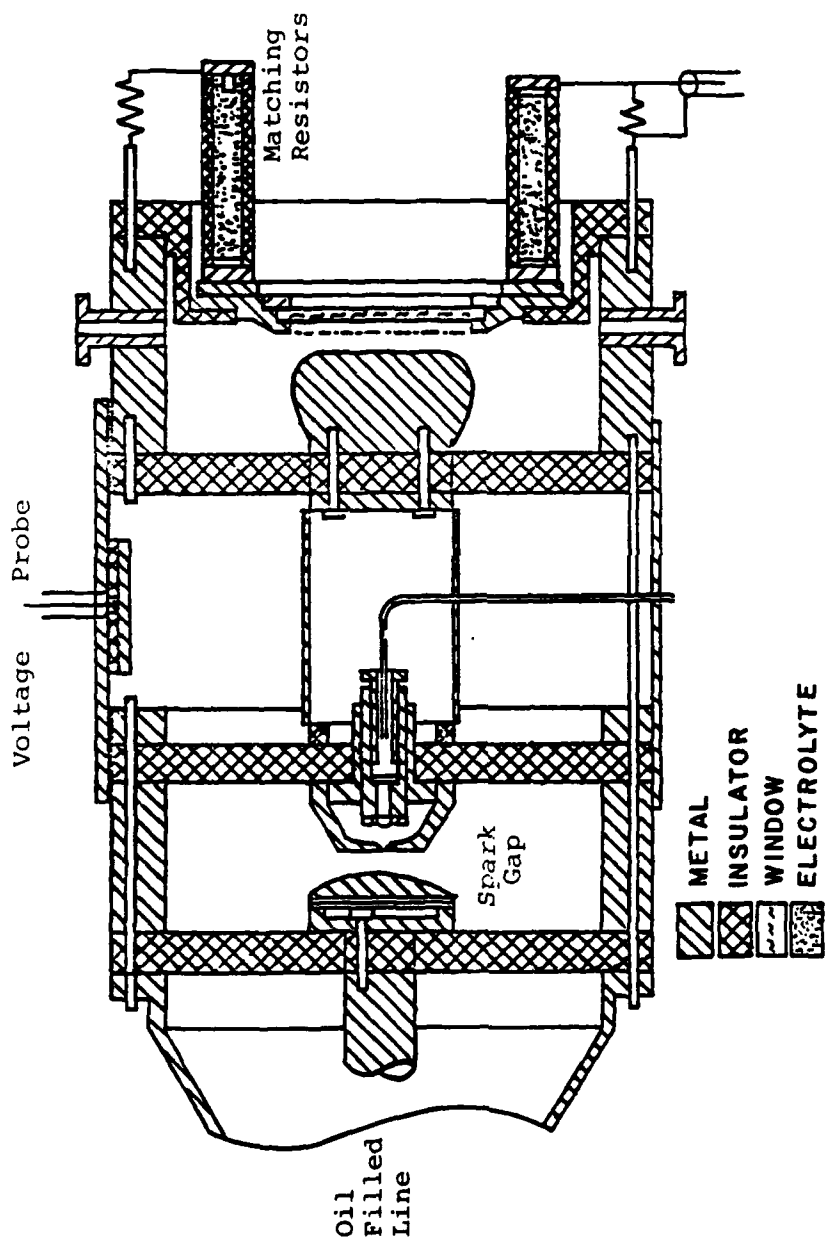

Fig. 13 Experimental Arrangement

This system has been tested with discharges in He and N_2 - He mixtures up to 700 torr and with discharges in Freon - 113 at low pressures (5×10^{-2} Torr to 1 Torr). The following changes were found necessary as a result of early measurements:

a) Matching resistors and voltage probes

The first experiments used electrolytic matching resistors and voltage probes which turned out to be less reproducible than necessary. In addition, the location of the matching resistor in the circuit behind the main discharge unables operation of discharges at very low pressure. In this case the discharge tends to burn from the center cathode to the chamber walls, bypassing the matching resistors. Therefore the matching resistor has been moved to the center conductor, between the closing switch and the opening switch. Capacitive voltage probes before and after the matching resistor are used to make voltage measurements of the incoming pulse and across the diffuse discharge. As current probes may be used either a small resistor in series with the matching resistor or Rogowski probes.

b) Preionization

A more powerful preionization system has been developed to allow operation of the diffuse discharge at higher pressures and with admixtures of attachers. The system consists of

eight individual transmission lines that are triggered by one master spark gap (see Fig. 14). Each of these transmission lines is terminated by a series of multispark UV sources. The master gap is laser triggered like the closing switch in the main system. The emitted light pulses of these eight sources are synchronized within less than one ns and have a half width of less than 10 ns. The use of a trigger laser with a beam splitter and individual optical delay lines for both gaps allow precise timing of the voltage rise across the discharge cell and the preionization light pulse. This system has been tested up to 40 kV. Work is continuing to optimize the laser triggering and the timing of preionization and main system.

5. Calculations of the time dependent behavior of an optically controlled discharges

To evaluate the time-dependent behavior of an externally controlled discharge in a given circuit a computer code has been developed and calculations were performed for the N_2-NO system with N_2O as an attacher. In order to allow fast calculations for different discharge and circuit parameters we used a code with two independent steps. In a first step, all rate constants necessary for the calculation of all rates of the significant processes are calculated, depending on E/N, for a representative gas mixture. These calculations require knowledge of the E/N dependent electron energy distribution function or the calculation of this distribution function. In a second step a system of time-

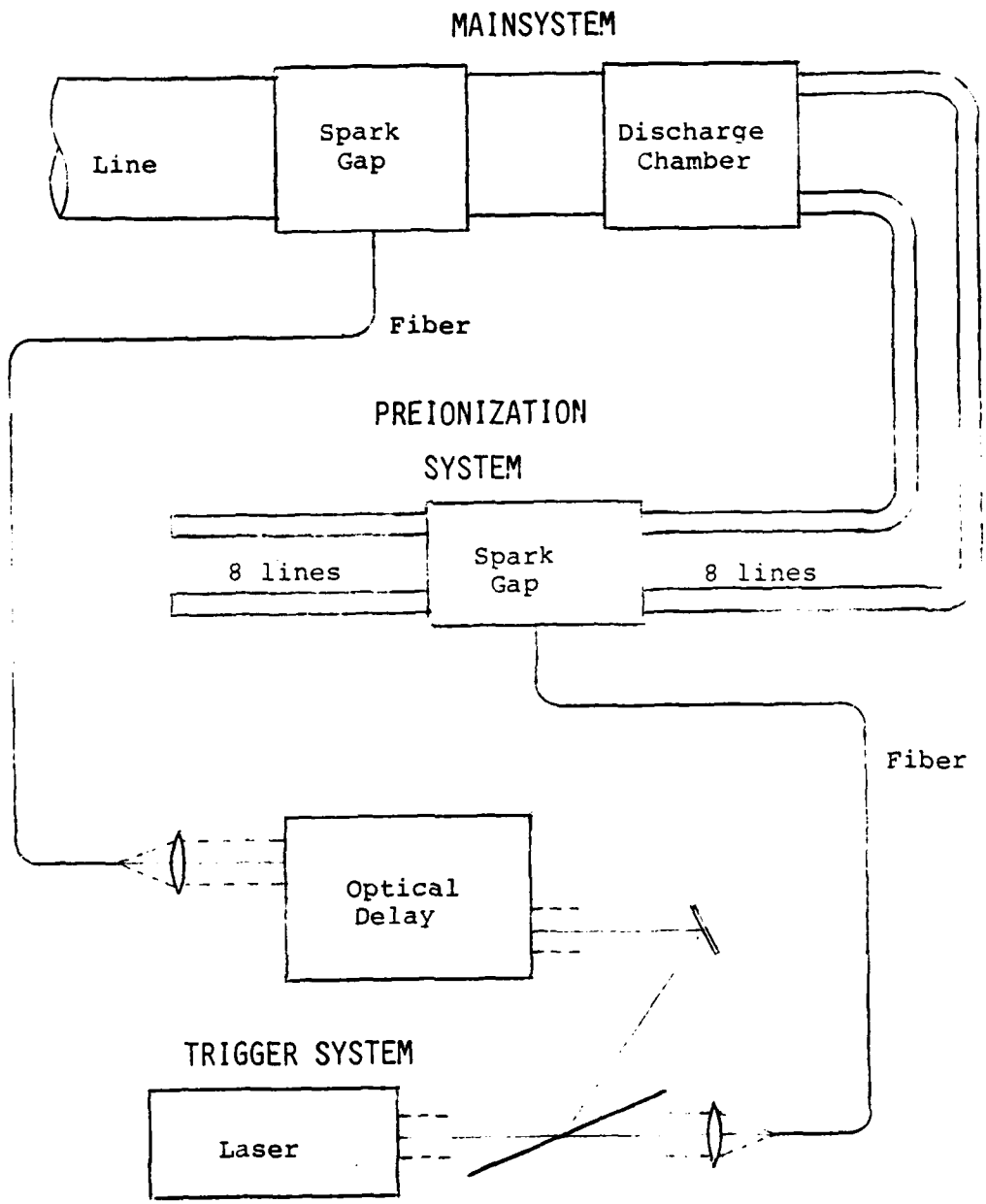

Fig. 14 Preionization Arrangement

dependent rate equations is solved using the E/N dependent rate constants and the circuit equation to incorporate the feedback of the circuit. It is assumed in this code that the electron energy distribution function and subsequently the E/N dependent rate constants do not change significantly if the gas mixture is chaged in a certain range around the value for which the rate constants have been determined in step one. For the rate equation system all rates have been taken into account, as shown in Fig. 2 of Appendix 1, and as an attacher we used N_2O with the attachment coefficient shown in Fig. 6 of Appendix 1. Since only small additives of NO and N_2O will be used (less than 1%) the rate constants have been evaluated using the electron energy distribution in pure N_2. In a first approach the Maxwell distribution has been used with the experimentally given values for the mean energy.

Since the intended optical control is resonant two step ionization of NO starting from the A $^2\Sigma^+$ state, the density of this state is of major importance. Therefore, the first set of calculations was performed to calculate the steady state density of this state without optical control, depending on the admixture of NO (in %), as shown in Fig. 15. As a result, in all the following calculations an NO admixture of 0.6% was used.

A second set of calculations was performed to show the influence of admixtures of the attacher N_2O on the time-dependent behavior of the discharge. As a starting condition we assumed that a preionization system provided an electron density of $n_e = 10^{10}$ cm^{-3} at time $t = 0$. For these calculations it was assumed that a high power laser tuned to to the transition in question was on from the beginning of the discharge.

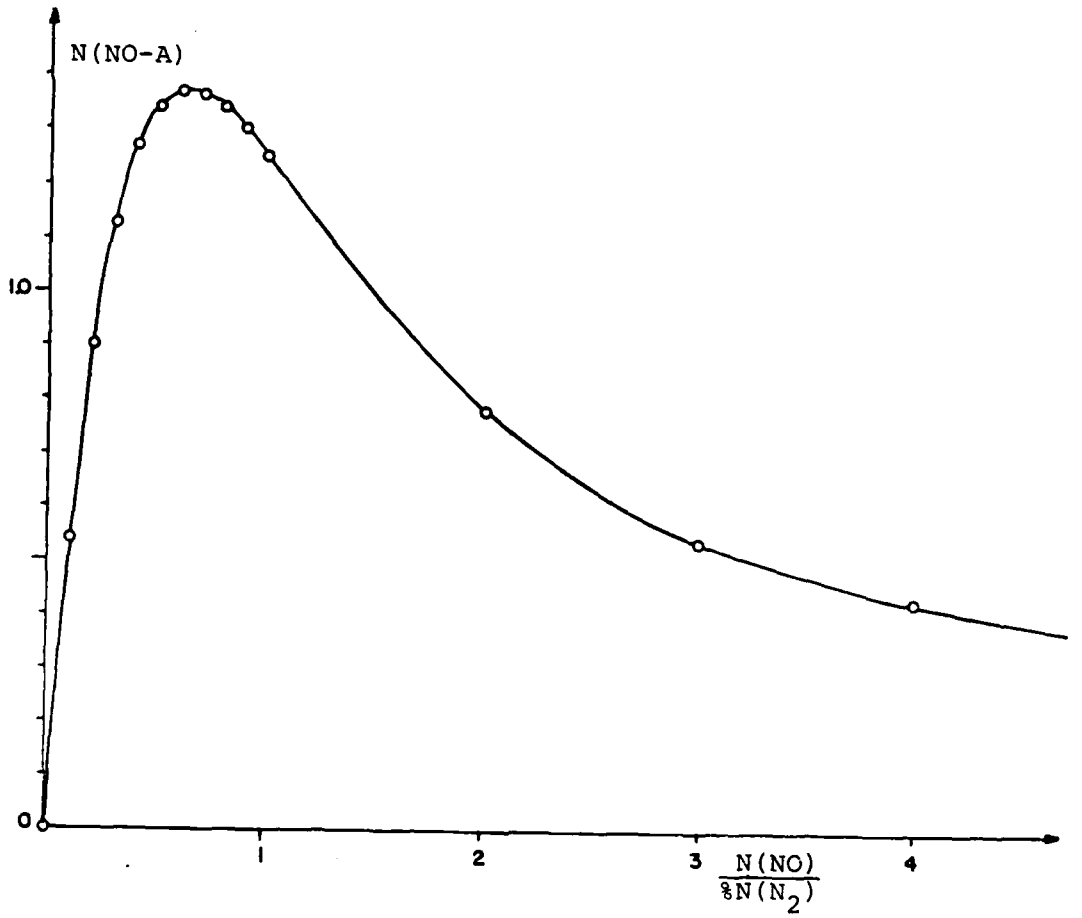

Fig. 15 Density of the NO molecules in the A-state vs the NO partial pressure in % (1 atm N_2).

The important result (Fig. 16) is that for an increasing, partial pressure of N_2O the time required to reach the minimum E/N value increases. Since a reservoir of metastable N_2 molecules is produced during the time of high E/N, an overshoot occures and E/N slowly increases again until the E/N values are reached, where attachment of N_2O becomes important. Therefore, after approximately 250 ns, a strong increase of E/N starts. Since our calculations are not space dependent we have to assume that at this time the discharge may become unstable.

In a third set of calculations the time dependent behavior of the discharge was calculated for the case where the laser was on for 100 ns, off for 100 ns, and so on (Fig. 17). The calculations were performed for two laser power densities. The higher value of $\Phi = 10^6$ W/cm^2 can experimentally only be achieved using a transverse, multipass optical system. For comparison, the initial phase without laser irradiation is shown. These results show that a strong influence on the discharge conductivity should be possible using an optical control mechanism.

It should be pointed out again that these calculations are based on several approximations. The most important approximation is using the Maxwellian electron energy distribution function to evaluate the E/N dependence of the rate constants. In present, continuing, calculations the electron energy distribution function is calculated using a Monte Carlo code and a set of cross sections of N_2 to improve the accuracy of the rate equation system. In addition, plasma chemistry has been neglected in our code (that is all the collisions that produce new products in the discharge).

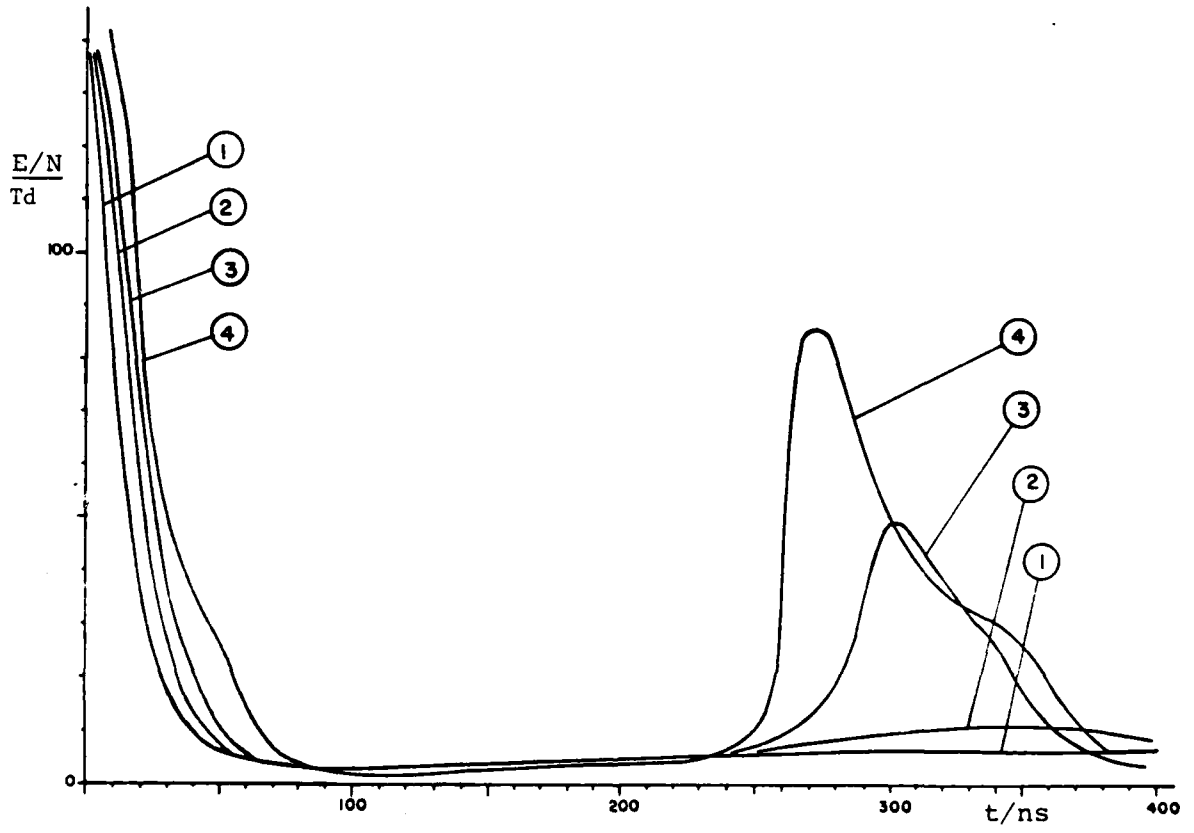

Fig. 16 Reduced electric field E/N vs time for different partial pressures of of the attacher N_2O (1 atm N_2 + 0.6% NO + (1): no N_2O, (2): 0.25% N_2O, (3): 0.5% N_2O, (4): 1.0% N_2O). The laser power is 10^6 W/cm^2.

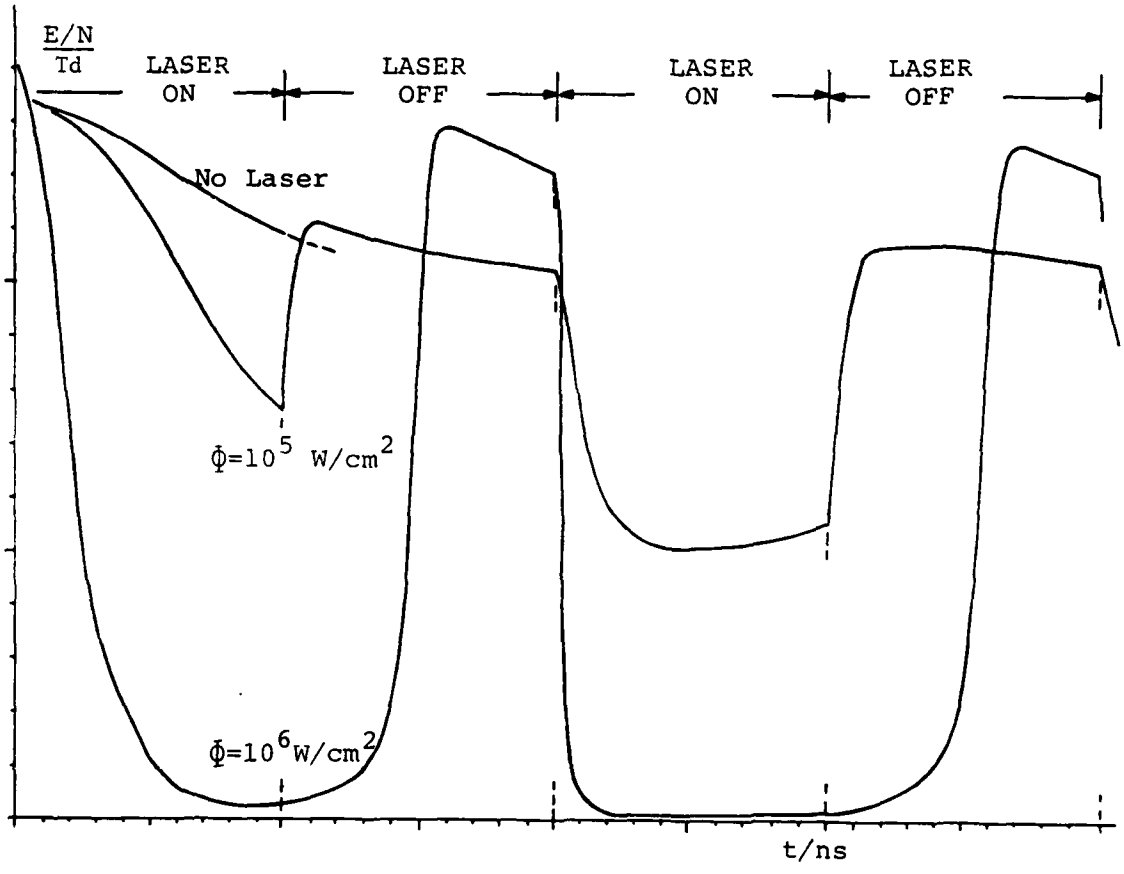

Fig. 17 Reduced electric field E/N vs time for different laser irradiations (1 atm N_2 + 0.6% NO + 0.5% N_2O).

The code is, in general, not restricted to the optical control mechanisms. Calculations for the e-beam controlled switch are presently also being performed.

D. REFERENCES

[1] G.A. Thioahanis, J.H. Jacob and S.J. Sackett, Avco-Everett Report F29601-73-C-0116.

[2] A.J. Schwab, High Voltage Measurement Techniques, MIT-Press (1972) p. 62.

[3] J. Cooper, Plasma Phys. 5, 285 (1963).

APPENDIX NO. 1

CONCEPTS FOR OPTICAL CONTROL OF DIFFUSE DISCHARGE OPENING SWITCHES

K. H. Schoenbach, G. Schaefer, M. Kristiansen
Department of Electrical Engineering
Texas Tech University
Lubbock, Texas 79409 USA

and

L. L. Hatfield
Department of Physics
Texas Tech University
Lubbock, Texas 79409 USA

and

A. H. Guenther
Air Force Weapons Laboratory
Kirtland Air Force Base, New Mexico 87117 USA

ABSTRACT

Optical control of diffuse discharges is discussed as opening mechanism for rep-rated switches. Diffuse discharges can be sustained or terminated by making use of optogalvanic effects, that means resonant interaction of laser radiation with diffuse plasma. Independent of control mechanisms, the performance of diffuse discharge opening switches is strongly affected by such fill gas properties as attachment and electron mobility.

*This work was supported by the Air Force Office of Scientific Research

To appear in IEEE Trans. Plasma Sci., December 1982.

1. Introduction

Energy storage using inductive elements is attractive in pulsed power applications because of its intrinsic high energy density, some 10^2 to 10^3 times higher than for capacitive storage [1]. However, the effective use of inductive stores requires a rapidly opening switch with high reliability under rep-rated operating condition. The use of various combinations of mechanical switches and fuses has been successful for single shot operation [2]. For rep-rated operation [3] at high voltages, power levels, and repetition rates these approaches do not extrapolate to the conditions of interest (P>1 MW, rep-rate > 1 kpps, and V > 10kV).

On the other hand, external discharge control techniques, e.g. e-beam and laser control of diffuse discharges, seem to offer access into fast rep-rated opening switching. Diffuse discharges are advantageous for switching because of their low inductance, small electrode erosion rates, and moderate energy density which allows control (perturbation) by means of e-beams and/or lasers with reasonable power. "Control" means either increasing or decreasing the conductivity of the diffuse plasma. However, whereas e-beam ionization, as one possible control mechanism, only provides for an enhanced conductivity, laser control, using optogalvanic effects, allows the change of conductivity in either direction [4]. The optogalvanic effect is a change in the electrical properties of a discharge with radiation at a wavelength range corresponding to an atomic or molecular transition in the discharge, i.e., in most cases an interaction at a resonance. The resonant nature of

the interaction not only means a selectivity, but a high efficiency in the use of the incident optical energy, resulting in less demand for control energy. It is this resonant interaction which allows one to modify the distribution of species, change reaction kinetics, radiation rates etc. in diffuse discharges.

The opening of a switch means reduction of the conductivity of the conducting medium, in this case the diffuse plasma. There are two methods to use optogalvanic effects in opening a diffuse discharge switch [5-11]. In the first concept the laser is used to sustain the diffuse plasma, that means to keep its conductivity at a certain level by means of photoionization, allowing a reasonable current flow through the switch. After turn-off of the laser the conductivity is reduced due to recombination and attachment processes in the plasma and the switch "opens". To obtain a fast reduction of conductivity (rapid opening) the plasma should be attachment dominated during the opening phase. This is a requirement which determines the type of gases usable in diffuse discharge opening switches. For a second concept, laser induced loss processes (e.g. attachment) are used to reduce the plasma conductivity. For this concept the way the discharge is sustained is independent of the control mechanism during the opening phase.

The first concept - optical generation of electrons in the conduction phase of the switch - is discussed in the fol-

lowing section. Concepts based on laser controlled reduction of electrons in the opening phase are outlined in Sec. 3, followed by considerations and calculations of the influence of fillergases on the performance of diffuse discharge opening switches. Experimental arrangements designed to prove these control concepts are described in the last section.

2. Optically Enhanced Electron Density

Concepts for using lasers for electron production (i.e. for sustainment of diffuse discharges) are shown in Fig. 1. The opening process after turn-off of the laser in each case is determined by attaching processes of an added attacher that satisfies the conditions discussed in Sec. 4.

The simplest conceptual way to generate electrons optically in a gas is by single step photo-ionization from the ground state. However, considering that available lasers only produce photons up to energies of 7 eV efficiently, only certain gases like alkali vapors are suitable for direct ionization [12]. Alkali vapors on the other hand react very agressively with most attachers. A better way to generate electron-ion pairs seems to be resonant two-step photo-ionization by means of UV-laser radiation. In organic gases, like Dimethyaniline, Fluorobenzene, or Tripropylamine, resonant two-step processes can produce [13,14] electrons with densities of up to some 10^{15} cm^{-3}. With Cs_2 a maximum yield was achieved for frequencies in the blue-green spectral range [15]. Two-step ionization in atoms is resonant for the first step while for the second step a flashlamp might also be used [12].

Tunable, visible lasers offer a wide variety of ionization mechanisms, which, however, have to be collisionally assisted. A self sustained discharge has to be ignited to provide either collisional ionization from an optically excited state [16] or collisional excitation and successive one- or two-step photo ionization [4, 17-19]. The laser radiation changes the conductivity of the diffuse discharge from a low level to a higher level and thereby closes the switch for a certain time, the switch conduction time. After laser turn-off the initial state of low conductivity is approached on time scales determined by the loss processes in the gas.

Two-step photoionization from a collisionally excited state was considered in some detail for a gas system consisting of N_2 of buffer gas, NO as gas which is photoionized and an attacher with the desired attachment properties [20]. Pertinent transitions in such a system are shown in Fig. 2. Resonant two-step photoionization from the NO A-state through the NO E-state provides the conduction electrons. The NO A-state is collisionally excited via the metastable N_2 state which is highly populated and serves as a reservoir for the two-step photoionization in NO. Once the laser is turned off, the ionization process is interrupted and the electrons are removed by the attaching gas. Although a molecular system has the disadvantage that, according to vibrational and rotational excitation, the absorption cross-section is low, the $\Sigma^2\Sigma^+ \rightarrow A^2Z^+$ system in NO has the advantage of having nearly the same molecular constants for both electronic states, and

therefore overlapping cross sections for different vibrational states [21].

Instead of molecular gases like NO, atomic gases can be used for two-step photoionization from a collisionally excited state. Advantages of atomic systems like Hg [22,23] (Fig. 3) are the higher absorption cross-section and a reduction in complexity, which makes it easier to predict the behavior in diffuse discharge systems. Two possible ways for two-step ionization are sketched in the energy diagram of Hg; one from the resonant 6^3P_1 state and a second one from the metastable 6^3P_0 state. The density of these states very much depends on the discharge conditions. For the metastable 6^3P_0 state the density can be higher than 50% of the gas density.

A similar concept is based on optical detachment by means of laser radiation. In this case an attacher with a significant attachment rate for the conduction phase also (low E/N) is used. In the conduction phase the attachment is then compensated by photodetachment.

3. Optically Decreased Electron Density

A second way to use lasers to control diffuse discharges is optical stimulation of electron loss processes. In contrast to the considerations discussed so far, the laser is now used to induce and control processes which lead to a reduction of conductivity, an effect which is used in the opening phase of the diffuse discharge.

In systems where the electron production is determined by collisional ionization via a metastable state the ioniza-

tion rate can be reduced by optically depopulating the metastable level. A laser is used to populate a higher state which is optically connected to the ground state [23-27]. The density of atoms in the metastable state, which serves as reservoir for collisional ionization, is then reduced and so is the total ionization rate.

Another method to reduce the electron density and hence the conductivity by means of a laser is given by optical decomposition of molecules. The objective is to produce fragments, radicals or ions, where, at least one of them, has a higher attachment cross-section than the original molecule.

A third method to stimulate loss processes optically is based on photoenhanced attachment by excitation of molecules. Certain attachers such as, for instance, HCℓ have an increased attachment cross-section in their rotational and/or vibrational excited states. The mechanism can be understood by considering the potential energy curves of an attacher and its ion. In Fig. 4 a general type of dissociative electron attachment process is illustrated. The potential energy curve of a neutral diatomic molecule AB is crossed at an energy E_ν^* above the ground state by a repulsive branch of the negative ion AB^-. The probability of electron attachment and succeeding dissociation depends on the energetic state of the vibrationally excited molecule relative to the curve crossing. For the example shown the attachment cross-section increases with vibrational excitation up to v = 4. On the other hand the electron energy necessary to form the negative ion AB^- shifts

to smaller values if the molecule AB is excited into a vibrational state closer to the curve crossing.

Figure 5 shows attachment cross-sections for the ground state and the first two vibrationally excited states of HCℓ [27], demonstrating both the strong increase in attachment cross-section and the related shift of the attachment peak towards lower electron energies. The results shown in this figure are based on attachment cross-section measurements for different temperatures in HCℓ [28]. More detailed calculations, yielding cross-sections for different vibrationally and rotationally excited states of HCℓ, have recently been performed [29]. By means of an IR-laser it should be possible to excite vibrational states selectively, thus increasing the attachment cross-section in a controlled way. Photoexcitation in competition with collisional excitation may be effective if the curve crossing is several kT_e above the ground state at an internuclear distance $R > R_o$. For a curve crossing at $R \tilde{>} R_o$ vibrational excitation will only cause a small increase of the attachment cross-section, as has been shown [30] for I_2.

HCℓ seems to be the molecule where most data are available, but due to its attachment cross-section peaking at low energies ($E_e < 1$ eV), it is not the best choice for a suitable gas for opening switch operation. A way to select gases for the special purpose of using them as triggerable attachers in diffuse opening switches is to look at first for gases with molecular structures which promise strong absorption in spectral regions where efficient IR-lasers (for example CO_2 lasers)

are available. Figure 6 shows groups of gases with bondings which show strong absortion in the spectral region between 9 and 11 μm (of course there are several others). A second step is to consider the attachment properties of these gases. A criterion for suitable gases where the curve crossing is a few kT above the potential minimum is the temperature behavior; in particular, the rate of increase of attachment rate with increasing temperature. A strong increase was, for example, found for some halo-generated hydro carbons [31,32]. More detailed information is obtained by measurements of the temperature dependence of the attachment cross-section, which are available [33-35] for gases like N_2O, O_2 and SF_6. It can be assumed that gases with increasing attachment rate with increasing E/N show the same temperature dependence [36-38]. The temperature dependent change of the cross-section in SF_6 occured at too low electron energies for switching applications in these experiments [35]. In this case, however, an increase of the attachment rate after laser excitation was observed for the first time. The number of gases suitable for opening switches is limited by the further consideration that the attachers should have an attachment cross-section with a maximum at moderate electron energies (a few eV) to get a low attachment rate at $E/N \approx 3$ Td and a strong increase of the attachment rate at $E/N \geq 5$ Td. Finally, chemical properties, like materials compatibility and toxicity have to be considered.

The disadvantage of this type of attachers, the shift of attachment peak cross-sections to lower energies with increasing vibrational energy, can be compensated by adding another attacher with E/N characteristics which satisfy the previously mentioned desirable properties for opening switch gases.

According to the limited number of small molecules that satisfy all the mentioned requirements, larger molecules should also be considered. In recent experiments with C_2F_5Cl it has been shown that there can be a strong spectral structure in the quasicontinuum [39], which indicates that there are highly excited states with appropriate lifetimes to allow attachment before internal thermalization.

4. Gas Requirements

The switch operation is determined by the control mechanism, but equally important is the gas mixture used. The consideration of atomic and molecular collisional processes, dependent on the reduced electric field strength E/N in the switch, is important in order to optimize switch performance. Generally, admixtures of attachers have to be used to achieve fast opening of the switch by formation of negative ions with low mobility. On the other hand, additives of attachers increase the power losses during conduction. Both low forward voltage drop and fast opening can only be obtained by choosing gases or gas mixtures which satisfy the following properties:

a) For low E/N values (conduction phase) the gas mixture should have a high drift velocity and low attachment rate coefficients.

b) For high E/N values (opening phase) the gas mixture should have lower drift velocities and high attachment rate coefficients.

Gas mixtures with the desired behavior can be found among mixtures of Ar and CF_4 [36]. Gas mixtures, which at least satisfy the attachment conditions, contain attachers with a maximum of the attachment cross-section of electron energies of 1 to 2 eV. One example for such an attacher is N_2O. Figure 7 shows the electron decay rate constant for N_2O in 350 Torr of N_2 as buffergas [40]. The decay rate has a low value at E/N below 5 Td and increases by at least one order of magnitude between 5 and 30 Td.

To demonstrate the effect of the attachment rate characteristic on the performance of a opening switch, its opening phase was simulated by means of a computer code (SCEPTRE). The switch was considered as part of a divertor in an inductive circuit (Fig. 8). The operation of the circuit is as follows: the energy stored in the capacitor C is transferred to the inductor L upon closure of switch α. Subsequently, switch α is opened and switch β is closed and the energy stored in the inductor is transferred to the load R_L.

The component values shown in Fig. 8 are reasonable for laboratory experiment. Switch α is the opening switch and switch β is assumed to be a switch which closes in a short time with small jitter. The buffer gas, the major constituent of the gas mixture in the opening switch, was assumed to be N_2

for which the field dependent electron mobility μ_e is known. The operating point of switch α was set by taking the electric field to gas density ratio (E/N) to be 2 Td when the switch was on. For a gap d of 1 cm and a gas pressure of 1 atmosphere, this corresponds to about 0.6 kV between the electrodes in the on state. Neglecting the ion current contribution the resistance R of the diffuse discharge is given by

$$R = \frac{d}{A\, n_e\, e\, \mu_e}$$

where n_e is the electron concentration and A the discharge cross-section. The current flow through the discharge in the on-state is $I \simeq 1$ kA for $n_e\, A/d = 10^{16}\ cm^{-2}$.

With the assumption that the electron density is reduced by attachment processes only, the resistance increases according to

$$R = \frac{d}{A\, n_{eo}\, e\, \mu_e}\ \exp\left[k\, n_A (t-\tau)\right]$$

Where n_{eo} is the electron density at the time of turn-off ($t=\tau$), n_A is the density of the attaching gas and k the attachment rate coefficient. Both μ_e and k are depending on the reduced field strength E/N and thus provide for coupling of the diffuse discharge resistance and the current in the circuit. To demonstrate the importance of this coupling effect for the opening switch operation, calculations were performed for three attachers [41, 42] (Fig. 9) with different attachment rate coefficient characteristics.

As an example of gases with decreasing attachment rate coefficient k as a function of E/N we used F_2 (SF_6 belongs to this type of attachers), NF_3 was chosen as an example of constant k in the range of possible values of E/N, and I_2 as an example of an attacher with strongly increasing k. Experimental results for I_2 exist up to E/N = 50 Td [42]. A constant value of k was assumed for reduced field strengths above 50 Td. In each case the product of the electron attachment rate coefficient and the attaching gas density, $k\,n_A$, was assumed to be $5 \times 10^7\ s^{-1}$. This requires a pressure of only a few Torr of the attaching gas. The results for the current development after turn-off of the external electron source at $t = \tau = 100$ ns are shown in Fig 8. The use of I_2 results in a rapid current decrease in the switch compared with the other attaching gases.

This result can be considered as due to a feedback effect or attachment instability [43]: Once the electron production is stopped, the electron concentration will be reduced by attachment. This causes an increase in resistance and, due to the dynamics of the circuit, E/N in the switch increases. This in turn gives rise to enhanced attachment, if the attachment rate increases with E/n and causes higher resistivity, etc. A feedback effect is thus initiated which causes a rapid growth of switch resistance, which means rapid opening. This effect does not depend on the way the discharge is sustained. The considerations concerning attachment characteristics hold for optically as well as e-beam sustained diffuse discharges.

Two experiments have been designed where diffuse plasmas can be produced either by means of a selfsustained discharge or by an e-beam sustained discharge. Both experimental arrangements will be used to test the applications of the optical control concepts for diffuse discharge opening switches.

Summary

Controllability of pulse parameters and wavelength tunability makes lasers very attractive for control of diffuse discharges. Using resonant optogalvanic effects the laser can be coupled very efficiently to the discharge. Optical electron production, as well as electron reduction mechanisms, are discussed. Two concepts are considered as most promising for optically controlled, rep-rated switch operation:
a) Discharge sustainment by two-step photoionization from an excited state in NO using an N_2-NO-attacher gas mixture.
b) Discharge termination through controlled increase of attachment rate by selective vibrational excitation of gases like HCℓ.

The properties of the gas mixtures were shown [by means of a computer simulation] to be very important for efficient operation of diffuse discharge opening switches in an inductive storage system. For a low loss, rapidly opening switch, the attachment rate of the gas mixture should generally be small at low values of reduced field strength E/N and increase with E/N. The electron mobility should behave in just the opposite way. Optically controlled diffuse discharge open-

ing switches are a potential solution for rep-rated inductive storage systems. However, exact predictions are not possible at this time because of the lack of basic data on various atomic and molecular processes in diffuse discharges.

References

[1] J. K. Burton, D. Conte, R. D. Ford, W. H. Lupton, V. E. Scherrer, and I. M. Vitkovitsky, "Inductive Storage - Prospects for High Power Generation," Proc. of 2nd IEEE Intern. Pulsed Power Conf., Lubbock, Texas, pg. 284 (1979).

[2] R. J. Harvey and A. J. Palmer, "Opening Switch Technology," Proceedings of the ARO Workshop on Repetitive Opening Switches, Tamarron, Co., pg. 20 (1981).

[3] M. Kristiansen and K. H. Schoenbach, "Workshop Summary," Proceedings of the ARO Workshop on Repetitive Opening Switches, Tamarron, Co., pg. 6 (1981).

[4] William B. Bridges, "Characteristics of an opto-galvanic effect in cesium and other gas discharge plasmas," J. Opt. Soc. Am., Vol. 68, pg. 352 (1978).

[5] K. H. Schoenbach, L. Hatfield, and E. E. Kunhardt, "An Opening Switch Using a Divertor," First Annual Report on Coordinated Research Program in Pulsed Power Physics, Texas Tech University, Lubbock, Tx., pg. 158 (1980).

[6] K. H. Schoenbach, M. Kristiansen, E. E. Kunhardt, L. L. Hatfield, and A. H. Guenther, "Exploratory Concepts of Opening Switches," Proceedings of the ARO Workshop on Repetitive Opening Switches, Tamarron, Co, pg. 66 (1981).

[7] K. H. Schoenbach, G. Schaefer, E. E. Kunhardt, M. Kristiansen, L. L. Hatfield, and A. H. Guenther, "An Optically Controlled Diffuse Discharge Switch," Proceedings of the 3rd IEEE International Pulsed Power Conference, Albuquerque, N.M., pg. 142 (1981).

[8] K. H. Schoenbach, G. Schaefer, M. Kristiansen, L. L. Latfield, and A. H. Guenther, "Diffuse Discharge Opening Switches," Proceedings of the NATO Conference on Electrical Breakdown and Discharges in Gases", Les Arcs, France, Pergamon Press (in press).

[9] K. H. Schoenbach, G. Schaefer, L. L. Hatfield, M. Kristiansen, H. C. Harjes, G. Hutcheson, and G. Leiker, "Opening Switches," Second Annual Report on Coordinated Research Program in Pulsed Power Physics, Texas Tech University, Lubbock, Tx., pg. 209 (1981).

[10] K. H. Schoenbach, A. Schaefer, M. Kristiansen, L. L. Hatfield, and A. H. Guenther, "Optical Control of Diffuse Discharge Opening Switches," Proceedings of the Workshop on Diffuse Discharge Opening Switches, Tamarron, Co. (1982).

[36] L. G. Christophorou, S. R. Hunter, J. G. Carter and S. M. Spyrou, "Gases for Possible Use in Diffuse-Discharge Switches, (to be published*).

[37] T. G. Lee, "Electron attachment coefficients of some Hydrocarbon Flame Inhibitors", J. Phys, Chem, Vol. 67, pg. 360 (1963).

[38] L. M. Chanin, A. V. Phelps and M. A. Biondi, "Measurements of the Attachment of Low-Energy Electrons to Oxygen Molecules," Physical Review, Vol. 128, pg. 219, (1962).

[39] E. Borsella, R. Fantoni, A. Giardini-Guidoni and C. D. Cantrell, "Observation of Structure in the Quasicontinuum of Multiple-Photon-Excited $C_2F_5C\ell$, (to be published in Chemical Physics Letters).

[40] L. C. Lee, C. C. Chiang, K. Y. Tang, D. L. Huestis and D. C. Lorents, "Gaseous Electronic Kinetics for e-beam Excitation of $C\ell$, NO and N_2O in N_2",(to be published).

[41] K. J. Nygaard, H. L. Brooks and J. R. Hunter, "Negative Ion Production Rates in Rare Gas-Halide Lasers," IEEE QE-15, pg. 1216 (1979).

[42] H. L. Brooks, S. R. Hunter and K. J. Nygaard, "Temperature Dependence of the Electron Attachment Coefficient in Iodine," J. Chem. Phys. Vol. 71, pg. 1870 (1979).

[43] T. H. Douglas-Hamilton, S. E. Mani, "Attachment Instability in an Externally Sustained Discharge," J. Appl. Phys. Vol. 45, pg. 4406 (1976).

[11] J. E. Lawler and A. H. Guenther, "Applications of Opto-galvanic Effects in Opening Switches," Proceedings of the 3rd IEEE International Pulsed Power Conference, Albuquerque, N.M., pg. 147 (1981).

[12] Ali Javan and Jeffrey S. Levine, "The Feasibility of Producing Laser Plasma via Photoionization," IEEE Journal of Quantum Electronics, Vol. QE-8, pg. 827 (1972).

[13] J. R. Woodworth, C. A. Frost and T. A. Green, "UV Laser Triggering of High-Voltage Gas Switches," (to be published in J. Appl. Phys.).

[14] L. C. Lee and W. K. Bischel, "Two-Photon-Ionization Coefficients of Propana, 1-Butane, and Methylarnines," (to be published).

[15] E. H. A. Granneman, M. Klewer, K. J. Nygaard and M. J. Van der Wiel, "Two-photon ionization of Cs_2, Rb_2 and RbCs using an Ar-ion laser," J. Phys. B: Atom. Molec. Phys., Vol. 9, pg. 865 (1976).

[16] R. B. Green, G. J. Havrilla and T. O. Trask, "Laser-Enhanced Ionization Spectrometry: Characterization of Electrical Interferences," Applied Spectroscopy, Vol. 34, pg. 561 (1980).

[17] P. Camus, M. Dieulin and C. Morillon, "Optogalvanic detection of barium high-lying levels with a two-step pulsed laser excitation," Le Journal de Physique, Vol. 40, Pg. L-513 (1979).

[18] D. Feldmann, "Opto-Galvanic Spectroscopy of some Molecules in Discharges: NH_2, NO_2, H_2 and N_2," Optics Communications, Vol. 29, pg. 67 (1979).

[19] E. P. Glotov, V. A. Danilychev, A. I. Milanich and A. M. Soroka, "Self-sustained electric photoionization discharge in three component mixtures containing rare gases and hologen bearing molecules," Sov. J. Quantum Electron, Vol. 9, pg. 1176 (1979).

[20] In collaboration with D. Lorents and L. C. Lee. SRI.

[21] M. W. Feast, "Two New $^2\Sigma$-$^2\Sigma$ Systems Due to the Molecule NO," Canadian Journal of Research, Vol. 28, pg. 492 (1950).

[22] W. J. van den Hoek and J. A. Visser, "Optogalvanic spectroscopy and thermal relaxation in high-pressure mercury and sodium arc discharges," J. Appl. Phys., Vol. 51, pg. 5292 (1980).

[23] Carl Kenty, "Role of Metastable ($^3P_2$) Hg Atoms in Low Current Discharges in Hg Rare Gas Mixtures," Phys. Rev. Vol. 80, pg. 95 (1950).

[24] Kermit C. Smyth, "Photon-Induced Ionization Changes in a Neon Discharge," Chemical Physics Letters, Vol. 55, pg. 473 (1978).

[25] A. C. Tam, "Quenching Effect of Helium 2-μ Light On a Weak Helium Discharge," (to be published in IEEE Transactions on Plasma Science).

[26] J. E. Lawler, "Experimental and Theoretical Investigation of the Optogalvanic Effect in the Helium Positive Column," Physical Review A, Vol. 22, pg. 1025 (1980).

[27] W. L. Morgan, M. J. Pound, "Kinetics of E-Beam Excited XeCℓ," Proceedings of the 33rd Gaseous Electronics Cont. Oklahoma, Abstract FB-3, Oct., 1980.

[28] M. Allan and S. F. Wong, "Dissociative attachment from vibrationally and rotationally excited HCl and HF[a)]," J. Chem Phys. Vol. 74, pg 1687 (1981).

[29] J. Norman Bardsley, private communication.

[30] R. J. Hall, "Dissociative attachment and vibrational excitation of F_2 by slow electrons[a)]," J. Chem. Phys. Vol. 68, pg. 1803 (1978).

[31] W. E. Wentworth, R. George and H. Keith, "Dissociative Thermal Electron Attachment to Some Aliphatic Chloro, Bromo, Iodo Compounds," Journal Chemical Physics, Vol. 51, pg. 1791 (1969).

[32] D. Spence and G. J. Schulz, "Temperature dependence of electron attachment at low energies for polyatomic molecules," Journal Chemical Physics, Vol. 58, pg. 1800 (1973).

[33] P. J. Chantry, "Temperature Dependence of Dissociative Attachment in N_2O," Journal of Chemical Physics, Vol. 51, pg. 3369 (1969).

[34] W. R. Henderson, W. L. Fite and R. T. Brackmann, "Dissociative Attachment of Electrons to Hot Oxygen," Physical Review, Vol. 183, pg. 157 (1969).

[35] C. L. Chen and P. J. Chantry, "Photon-enhanced dissociative electron attachment in SF_6 and its isotopic selectivity," Vol. 71, pg. 3897 (1979).

Figure Captions

Fig. 1 Optically Controlled Electron Generation.

Fig. 2 Energy Level Diagram for the N_2-NO System.

Fig. 3 Energy Level Diagram of Hg with Proposed Two Step Photoionization from Excited States.

Fig. 4 Resonance Dissociative Electron Attachment.

Fig. 5 Dissociative Attachment Cross Sections for Vibrationally Excited HCℓ Molecules.

Fig. 6 Chemical Compounds which Absorb Radiation within the Emission Range of the CO_2 - Laser. The Spectral Range of Strong Absorption Bands and the Absorbing Bands or Groups are Indicated.

Fig. 7 The Decay Rate Constant of the Electron Conduction Current in NO in an Atmosphere of 350 Torr of N_2 at Varous E/N.

Fig. 8 Time Dependence of the Current Through the Opening Switch in a Divertor Circuit.

Fig. 9 Reduced Field Dependence of Attachment Rate Coefficient for I_2, F_2 and NF_3.

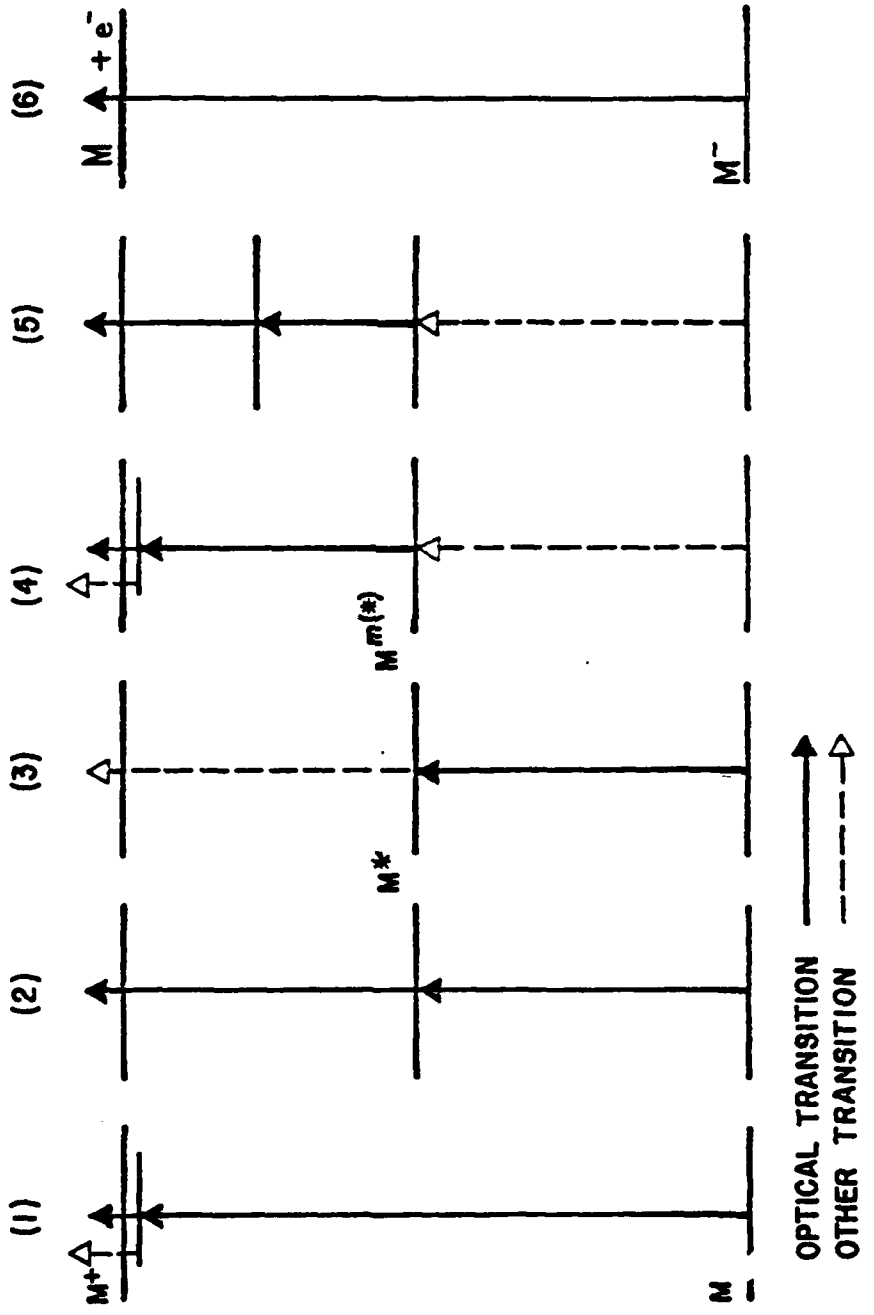
(1)
(2)
(3)
(4)
(5)
(6)
M
M+
M*
Mm(*)
M−
M + e−
OPTICAL TRANSITION
OTHER TRANSITION

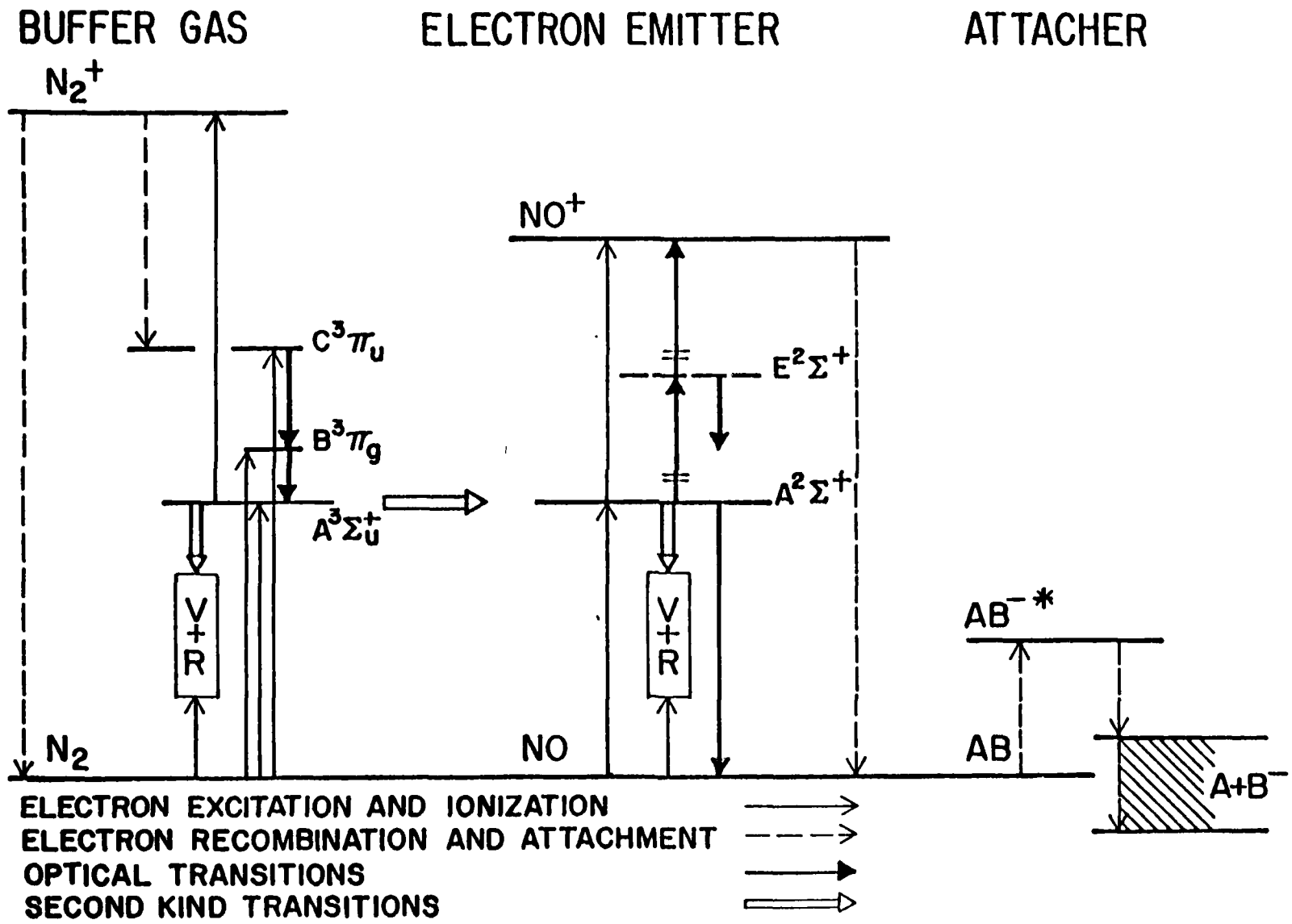
BUFFER GAS
ELECTRON EMITTER
ATTACHER
N_2^+
$C^3\pi_u$
$B^3\pi_g$
$A^3\Sigma_u^+$
V+R
N_2
NO^+
$E^2\Sigma^+$
$A^2\Sigma^+$
V+R
NO
AB^{-*}
AB
$A+B^-$
ELECTRON EXCITATION AND IONIZATION
ELECTRON RECOMBINATION AND ATTACHMENT
OPTICAL TRANSITIONS
SECOND KIND TRANSITIONS

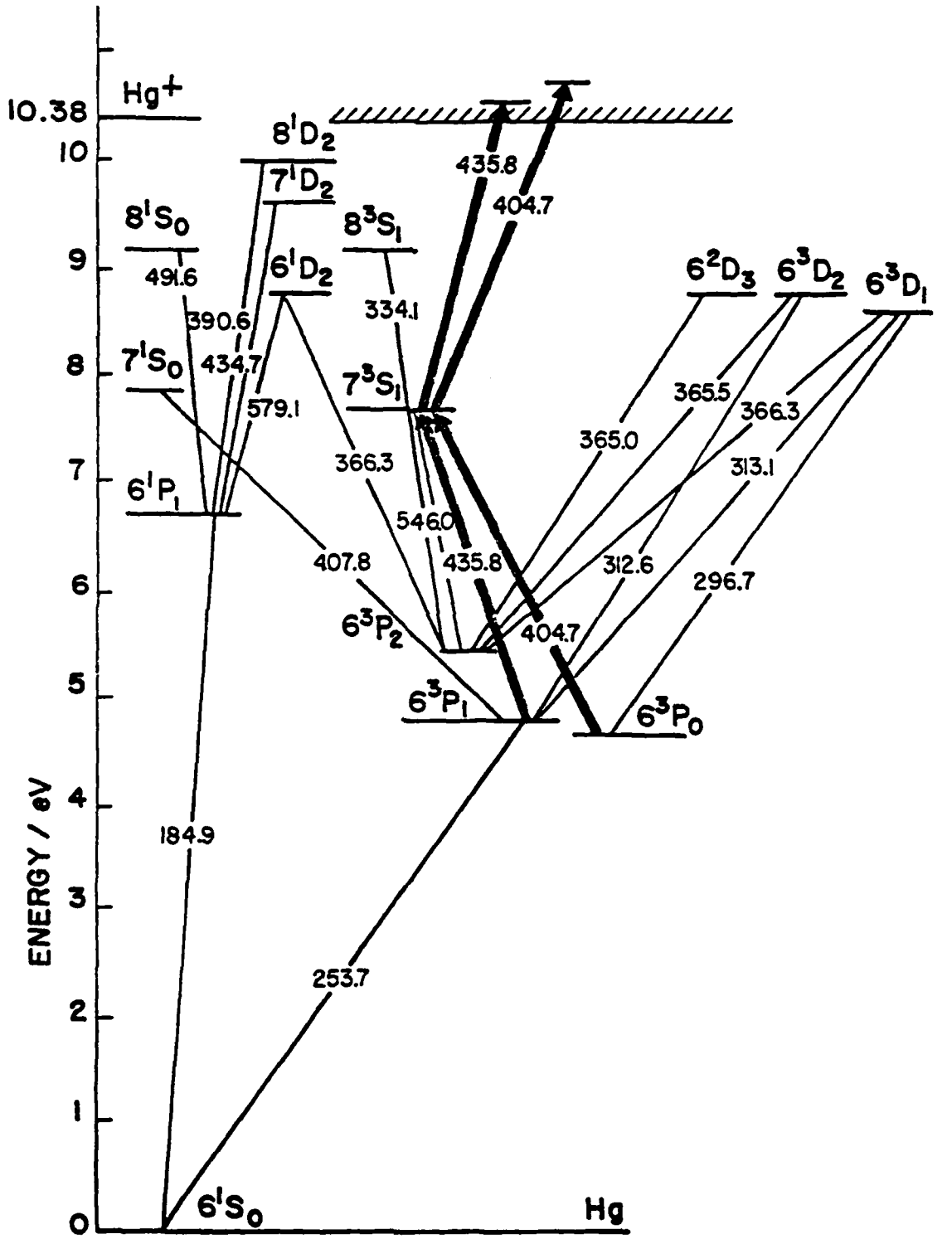
Hg+
10.38
10
9
8
7
6
5
4
3
2
1
0
ENERGY / eV
8¹D₂
7¹D₂
8¹S₀
8³S₁
6¹D₂
491.6
390.6
434.7
579.1
334.1
7¹S₀
7³S₁
6¹P₁
366.3
546.0
435.8
404.7
407.8
6³P₂
6³P₁
6³P₀
184.9
253.7
6¹S₀
Hg
6²D₃
6³D₂
6³D₁
365.0
365.5
366.3
313.1
312.6
296.7

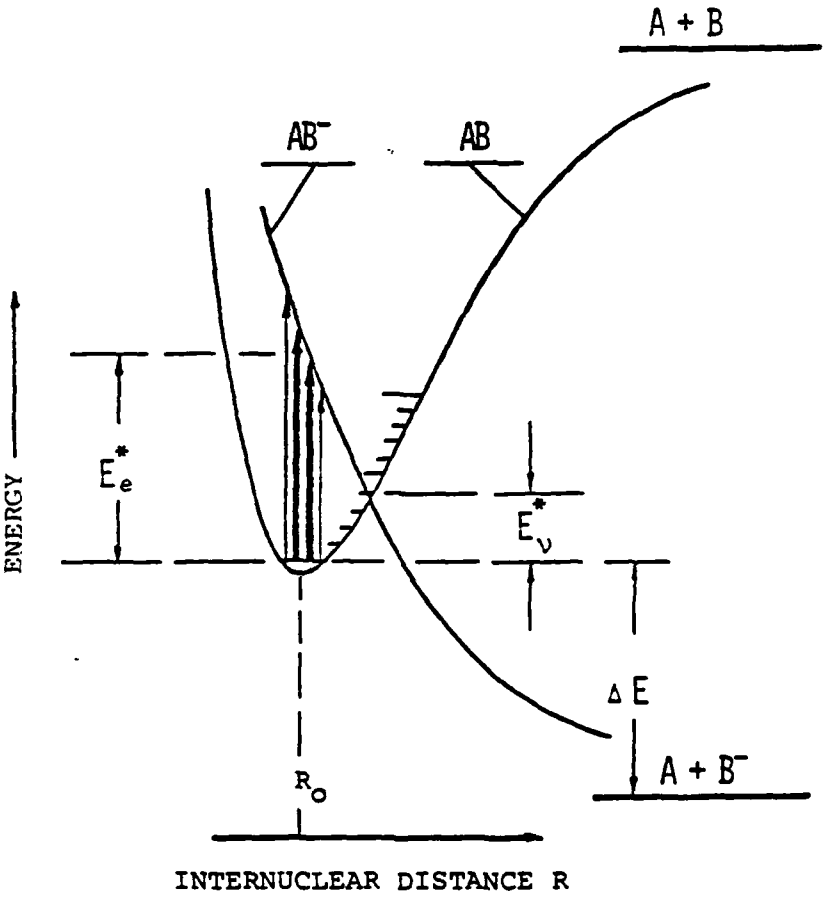
A + B
AB⁻
AB
ENERGY
E*e
E*ν
ΔE
A + B⁻
R₀
INTERNUCLEAR DISTANCE R

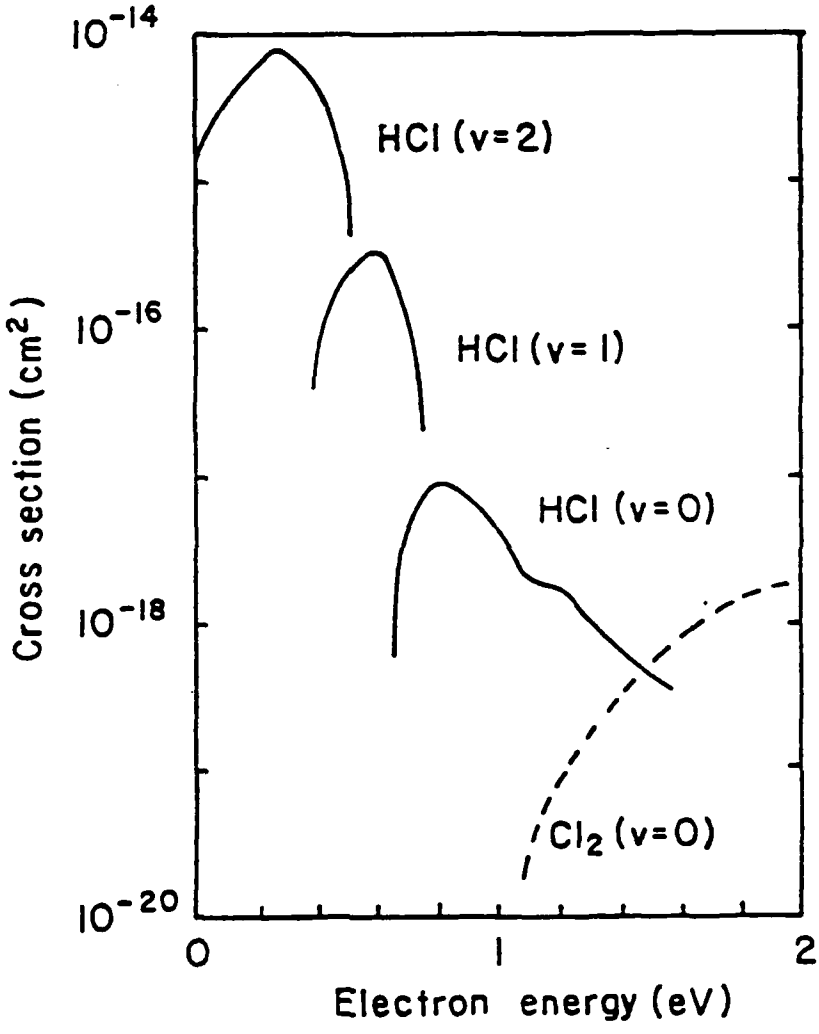
10^{-14}
10^{-16}
10^{-18}
10^{-20}
Cross section (cm^2)
HCl (v=2)
HCl (v=1)
HCl (v=0)
Cl_2 (v=0)
0
1
2
Electron energy (eV)

Compounds	Strong Absorption Bands (μm)	Absorbing Bond or Group
NON-AROMATIC ALCOHOLS	8 - 10	C-O Stretch
NON-AROMATIC ESTERS, ACETATS AND EPOXIDES	8 - 11	C-O Stretch
NON-AROMATIC AMINES	8.1 - 9.4	C-N Stretch
NON-AROMATIC ALDEHYDES	8.5 - 9.5	C-O Stretch
NON-AROMATIC ESTERS AND LACTONES	9 - 10	O C-O-C Stretch
NON-AROMATIC ANHYDRIDES	8 - 11	O O C-O-C Stretch
NON-AROMATIC ACID HALIDES	10 - 11	O C-Cl
NON-AROMATIC AMIDES	8.4 - 9.5	C-N Stretch
NON-AROMATIC PHOSPHORUS COMPOUND	9 - 11.5	P-O-C Stretch
AROMATIC HALOGENATED HYDROCARBONS	9 - 10	Ø-Cl, Ø-Br, Ø-I
AROMATIC ETHERS	9.5 - 10	C-O - Ø Stretch
AROMATIC NITRO AND NITROSO COMPOUNDS	9.5 - 10.5	N-O Stretch
AROMATIC ESTERS AND LACTONES	7.8 - 10	C-O Stretch
AROMATIC ACID HALIDES	10 - 11.7	O C-Cl

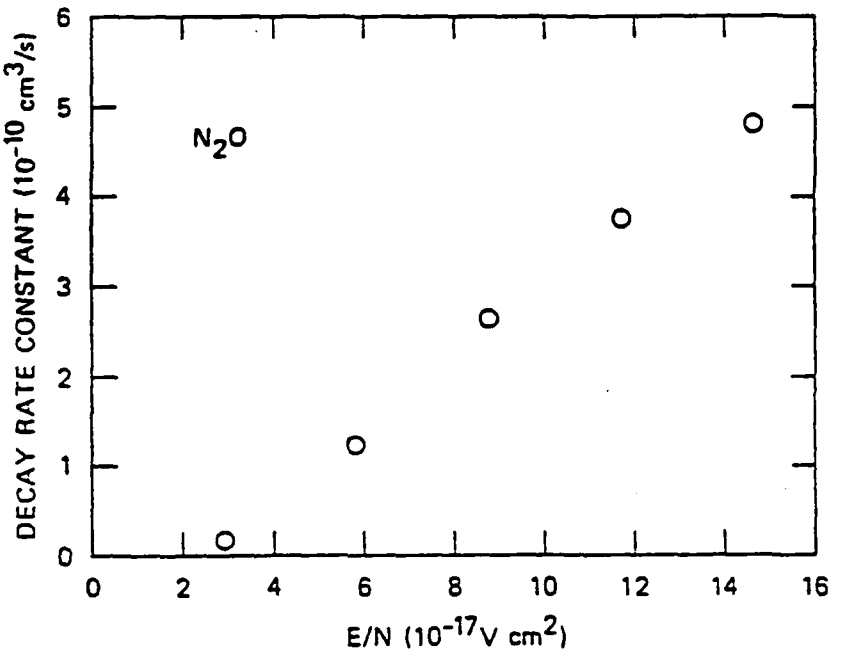
DECAY RATE CONSTANT (10^{-10} cm^3/s)
N_2O
0
1
2
3
4
5
6
0
2
4
6
8
10
12
14
16
E/N (10^{-17}V cm^2)

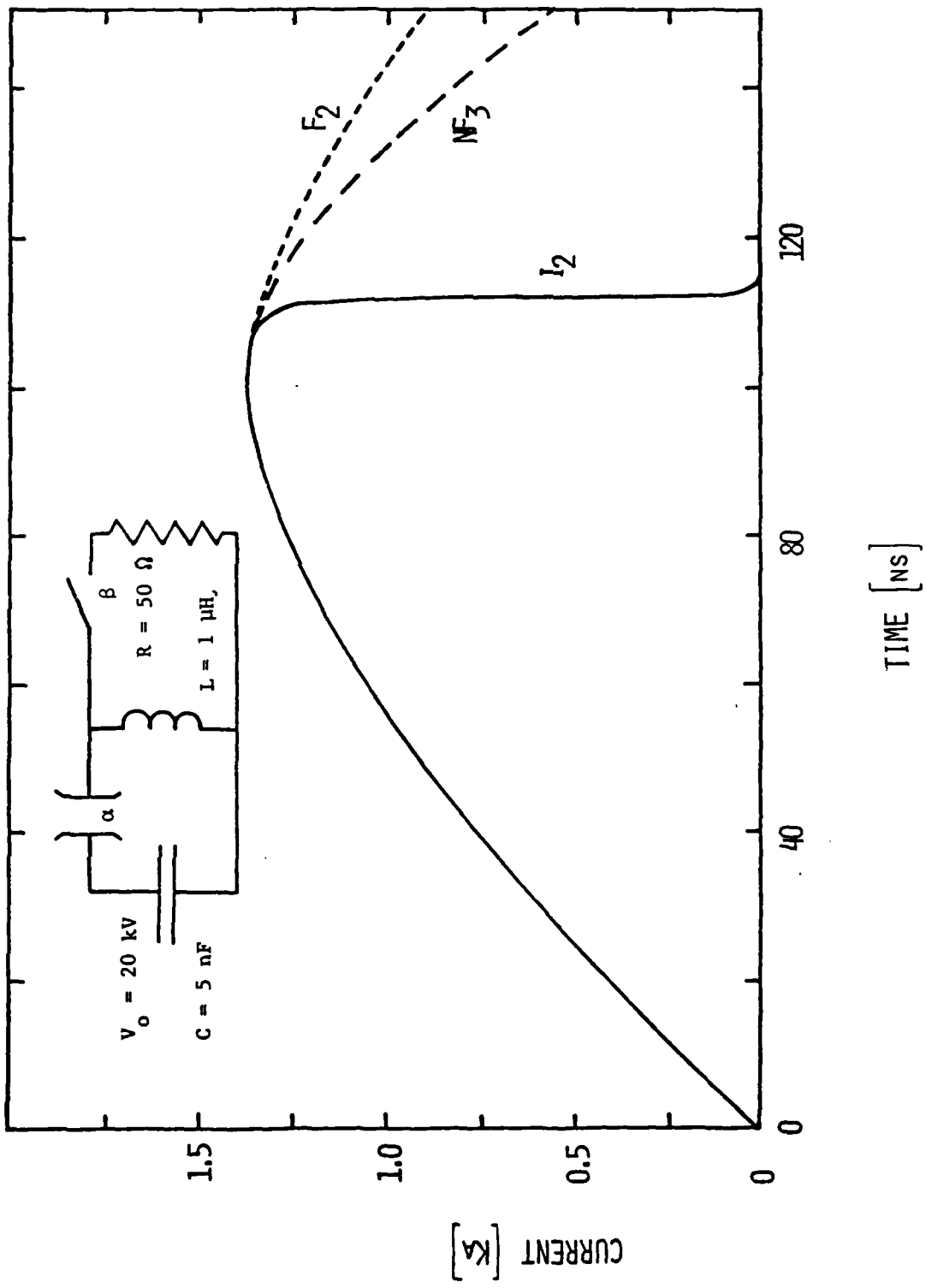
CURRENT [kA]
1.5
1.0
0.5
0
0
40
80
120
TIME [ns]
F_2
NF_3
I_2
V_o = 20 kV
C = 5 nF
α
β
R = 50 Ω
L = 1 μH,

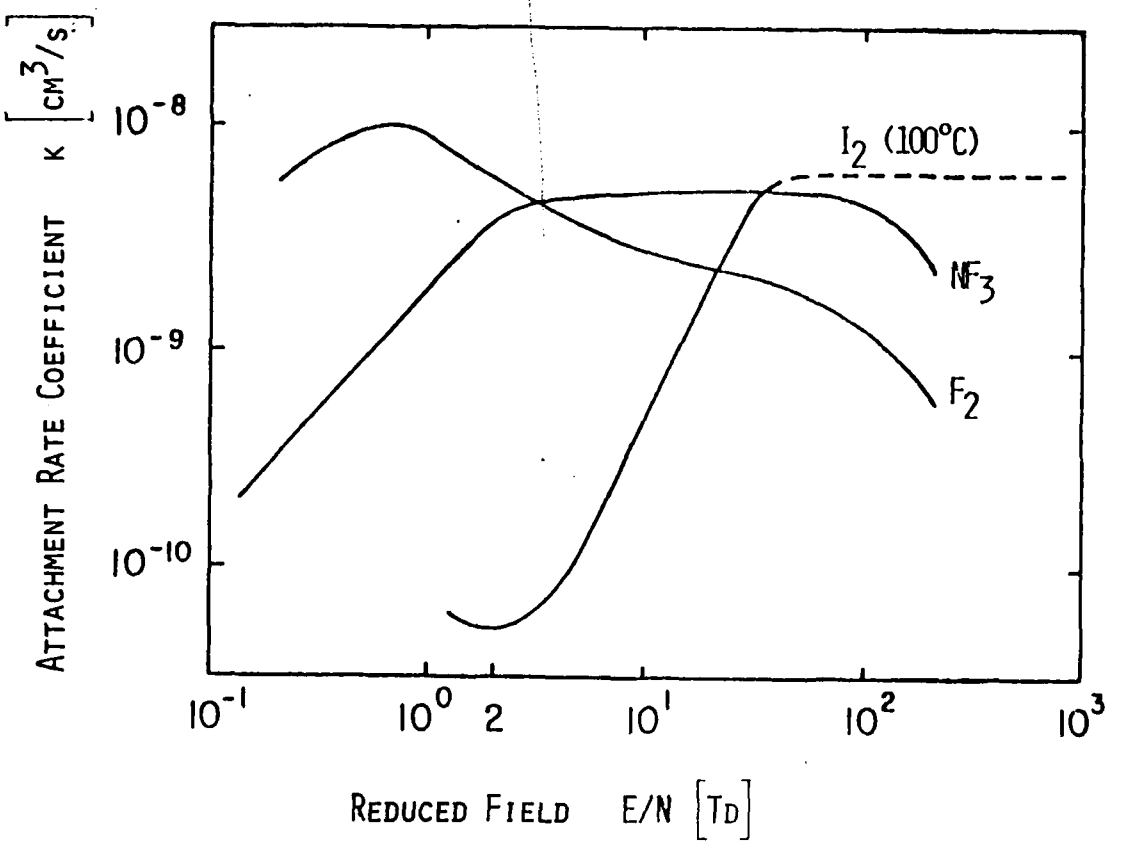
ATTACHMENT RATE COEFFICIENT K [CM³/S]
10⁻⁸
10⁻⁹
10⁻¹⁰
I₂ (100°C)
NF₃
F₂
10⁻¹
10⁰
2
10¹
10²
10³
REDUCED FIELD E/N [TD]

APPENDIX NO. 2

PHOTODETACHMENT AS A CONTROL MECHANISM FOR DIFFUSE DISCHARGE SWITCHES*

Gerhard Schaefer, P. F. Williams, Karl H. Schoenbach

Dept. of Electrical Engineering
Texas Tech University
Lubbock, Texas 79409

and

John Mosely

Chemical Physics Institute
University of Oregon
Eugene, Oregon 97403

ABSTRACT

Photodetachment is considered as a control mechanism for diffuse discharge switches. Experiments have been performed on photodetachment of ions in the flowing afterglow of a dc glow discharge in oxygen. Experiments with different laser wavelengths and the dependence of the optogalvanic signal on the laser energy flux indicate that O^- is the dominant negative ion. For an energy flux of 35 mJ/cm^2, 50% of the O^- ions can be photodetached.

*Work supported by the A.F.O.S.R.

This paper has been submitted to IEEE Trans. Plasma Sci.

I. Introduction

Recently externally controlled diffuse discharge opening switches have been considered for applications in inductive energy storage systems [1]. The discharges have to fulfill the requirement of low resistance during the conduction phase and high resistance during the opening phase. For fast opening times, which, in general, require rapid depletion of the electron density, the discharge has to be attachment-dominated in the opening phase. In optically controlled diffuse discharges the influence of the light can either be to enhance or to decrease the conductivity. For processes that increase the conductivity the opening effect is achieved when the laser is turned off. Photodetachment has been considered as a conductivity-enhancing process [2]. Using photodetachment a strong change of the conductivity of the discharge should be possible, if without photodetachment the negative ion density is much larger than the electron density and if the electrons of the existing negative ions can be mostly detached by means of photodetachment.

To investigate the feasibility of photodetachment for optically controlled diffuse discharge switches we chose the negative ion O^- for several reasons:

1. The photodetachment cross section $\sigma_{p.d.}$ has a threshold at a photon energy of $h\nu = 1.47$ eV and reaches a first plateau with $\sigma_{p.d.} \approx 6 \times 10^{-18} cm^2$ at a photon energy of $h\nu = 2$ eV [3].
2. O^- can easily be produced in discharges containing

O_2^-, SO_2^-, N_2O^-, or other oxides.

3. From O_2 glow discharges it is well known that the negative ion density N_- can be much larger than the electron density N_e [4].

II. Experimental Setup

The experimental setup for our experiment is shown in Fig. 1. The flow tube has a rectangular cross section with dimensions 3x14 mm^2. Five grids, separated from each other by 2 mm, are placed perpendicular to the flow axis. Each grid is made of 10 individual Pt wires with 0.127 mm dia. For photo detachment experiments in the flowing afterflow, a discharge was operated between grid 1 (cathode) and grid 2 (anode), with each wire of the cathode grid separately ballasted for discharge homogeneity. The region between grid 2 and grid 3 was generally kept nearly field-free, although for discharges with small admixtures of O_2 a small negative voltage was applied to grid 3 to achieve zero current through grid 3 in dc operation. Between 3 and 4 a voltage of 5 to 100 V was applied to collect the photodetached electrons. The optogalvanic signal was detected by measuring the voltage across a resistor of between 1 kΩ and 1 MΩ in series with grid 3. The light source was a Quanta-Ray PDL, dye laser pumped by the Q-switched, frequency-doubled output of a Quanta Ray DCR-1, Nd:YAG laser. The dye laser delivered pulses of about 50 mJ energy in 7 ns.

III. Experimental Results

In a discharge containing O_2, several different attachment processes and subsequent ion-molecule reactions are possible. For these, the important ions are O^-, O_2^-, and O_3^-, and the processes with large reaction rates are shown in Table 1. The dominant attachment process in the range ($E/p \leq 2$ V cm$^-$ Torr^{-1}) is the three-body attachment (reaction 2), while for higher values ($E/p \geq 2$ V cm^{-1} Torr^{-1}) the dissociative attachment dominates [5]. Among the ion molecule reactions, reaction (3), which produces O_2^-, is important at higher values of E/p, while reaction (4), which produces O_3^-, dominates at lower E/p values [6]. The important photo-induced processes for these ions are also given in Table 1. Of these, the Nd:YAG fundamental output with a photon energy of 1.17 eV can induce only reaction (6).

In our experiment the ions can either be produced in the discharge itself, where the value of E/p varies in the range of $5 \leq E/p \leq 27$ V cm^{-1} Torr^{-1} or in the nearly field-free drift region between grid 2 and 3. To learn which ions are the dominant species under various discharge conditions, we performed optogalvanic experiments using either visible light ($h\nu \approx 2.2$ eV) from the dye laser or the Nd:YAG fundamental at 1.17 eV.

Some experimental results are shown in Table II. They indicate that for the range of discharge conditions we investigated, O_2^- is produced best in pure O_2 discharges at pressures above 3 Torr. We found that the O_2^- production was not

a strong function of the voltage across the drift region (between grid 2 and 3), indicating that the attachment processes occur mainly in the discharge. Since the E/p values for all discharge conditions are such that reaction (1) strongly dominates, we conclude that the production of O_2^- at O_2 pressures above 3 Torr results from reaction (3) in the discharge. This reaction should preferably occur at E/p values above 10 V cm^{-1} $Torr^{-1}$ [6] and at the highest O_2 pressures.

To distinguish between optogalvanic signals caused by O^- and O_3^- we note that the dominant photoprocess in O_3^- for $h\nu > 2$ eV is photodissociation (reactions (8) and (9)), and that of these, only reaction (8) is possible with the photon energies produced by our dye laser source ($h\nu \approx 2.2$ eV). The cross section for reaction (8) has a spectral structure [9] which we did not observe in our experiments when the laser was tuned through the range 2.18 - 2.28 eV. We therefore conclude that the dominant optical electron generation mechanism in our experiment is direct photodetachment of O^-.

To investigate whether the existing negative ions can be completely detached we performed saturation experiments in which the dependence of the optogalvanic signal strength on laser energy flux was determined. These results are shown in Fig. 2. The solid line shows the calculated result, assuming a photodetachment cross section of $\sigma = 6.5 \times 10^{-18} cm^2$, and the circles indicate the result of our measurement. Since the optogalvanic signal is only measured in arbitrary units the scale of the experimental curve was adjusted so that the slopes of the two curves agreed in the linear region

(< 10 mJ/cm^2). These results indicate that only 35 mJ/cm^2 of light energy flux is needed to photodetach 50% of the O^- ions.

IV. Conclusion

Our experiments demonstrate that photodetachment may be an attractive control mechanism for optically controlled diffuse discharge switches in systems where the negative ion density is much larger than the electron density. Assuming a time constant for attachment $t_a \approx 10^{-8}$ sec., for a gas mixture in a discharge producing O^-, a power of 3.5 MW/cm^2 is necessary to reduce the steady state negative ion density by a factor of 0.5. Work is continuing to determine the optogalvanic response of the discharge to photodetachment.

Table I

IMPORTANT PROCESSES IN O_2 DISCHARGES

	Reaction		Charged Product	
Attachment	(1) $e + O_2 \rightarrow O^- + O$		O^-	
	(2) $e + 2\,O_2 \rightarrow O_2^- + O_2$		O_2^-	
Ion Molecule Reactions	(3) $O^- + O_2 \rightarrow O_2^- + O$		O_2^-	
	(4) $O^- + 2\,O_2 \rightarrow O_3^- + O_2$		O_3^-	
Photo-detachment	(5) $O^- + h\nu \rightarrow O + e$	($h\nu > 1.47$ eV)	e^-	[3]
	(6) $O_2^- + h\nu \rightarrow O_2 + e$	($h\nu > 0.434$ eV)	e^-	[7]
	(7) $O_3^- + h\nu \rightarrow O_3 + e$	($h\nu > 2.103$ eV)	e^-	[8]
Photo-dissociation	(8) $O_3^- + h\nu \rightarrow O^- + O_2$	($h\nu > 1.7$ eV)	O^-	[9]
	(9) $O_3^- + h\nu \rightarrow O_2^- + O$	($h\nu > 2.7$ eV)	O_2^-	[10]

Table II

Optogalvanic signal for different discharge conditions and pump frequencies.

Discharge I=15 mA / Laser	p = 10 torr He : O_2 = 20:1	p = 0.3-0.8 torr O_2 only	p = 3-10 torr O_2 only
Dye Laser **560 nm 10mJ**	strong OGS	medium OGS	medium OGS
Nd-YAG Laser **1060 nm 100mJ**	weak OGS	weak OGS	medium OGS

REFERENCES

1. Proc. ARO Workshop on Diffuse Discharge Opening Switches, Tamarron, CO, Jan. 1982, Texas Tech Univ. (K. Schoenbach and M. Kristiansen, Eds.).

2. K. H. Schoenbach, G. Schaefer, M. Kristiansen, L. L. Hatfield and A. H. Guenther, "Concepts for optical control of diffuse discharge opening switches," IEEE Trans. Plasma Sci., vol. PS-10, Dec. 1982.

3. L. M. Branscomb, S. J. Smith and G. Tisone, "Oxygen metastable atom production through photodetachment," J. Chem. Phys., vol. 43, p. 2906, 1965.

4. H. Sabadil, "Experimentelle Untersuchungen an wandernden Niederfelddomaenen (T-Schichten) in der positiven Säule von Gleichstrom und HF-Entladungen in Sauerstoff und Sauerstoff-Stickstoff-Gemischen," Beitr. Plasma Phys., vol. 11, p. 327, 1971, and vol. 11, p. 53, 1971.

5. L. M. Chanin, A. V. Phelps and M. A. Biondi, Phys. Rev., "Measurements of the attachment of low-energy electrons to oxygen molecules," vol. 128, p. 219, 1962.

6. J. L. Moruzzi and A. V. Phelps, "Survey of negative-ion-molecule reactions in O_2, CO_2, H_2O, and mixtures of these gases at high pressures," J. Chem. Phys., vol. 45, p. 4617, 1966.

7. D. S. Burch, S. J. Smith and L. M. Branscomb, "Photodetachment of O_2^-," J. Chem. Phys., vol. 69, p. 2771, 1978.

8. P. C. Cosby, J. T. Moseley, J. R. Peterson and J. H. Ling, "Photodissociation spectroscopy of O_3^-," J. Chem. Phys.,

vol. 69, p. 2771, 1978.

9. P. C. Cosby, R. A. Bennett, J. R. Peterson and J. T. Moseley, "Photodissociation and photodetachment of molecular negative ions. II. Ions formed in oxygen," J. Chem. Phys., vol. 63, p. 1612, 1975.

10. L. C. Lee and G. P. Smith, "Photodissociation and photodetachment of molecular negative ions. VI. Ions in $O_2/CH_4/H_2O$ mixtures from 3500 to 8600 A," J. Chem. Phys., vol. 70, p. 1727, 1979.

11. G. Schaefer, P. F. Williams, K. H. Schoenbach and J. T. Moseley, "Photodetachment as a control mechanism for diffuse discharge switches," 35th G.E.C., p. EA-5, 1982.

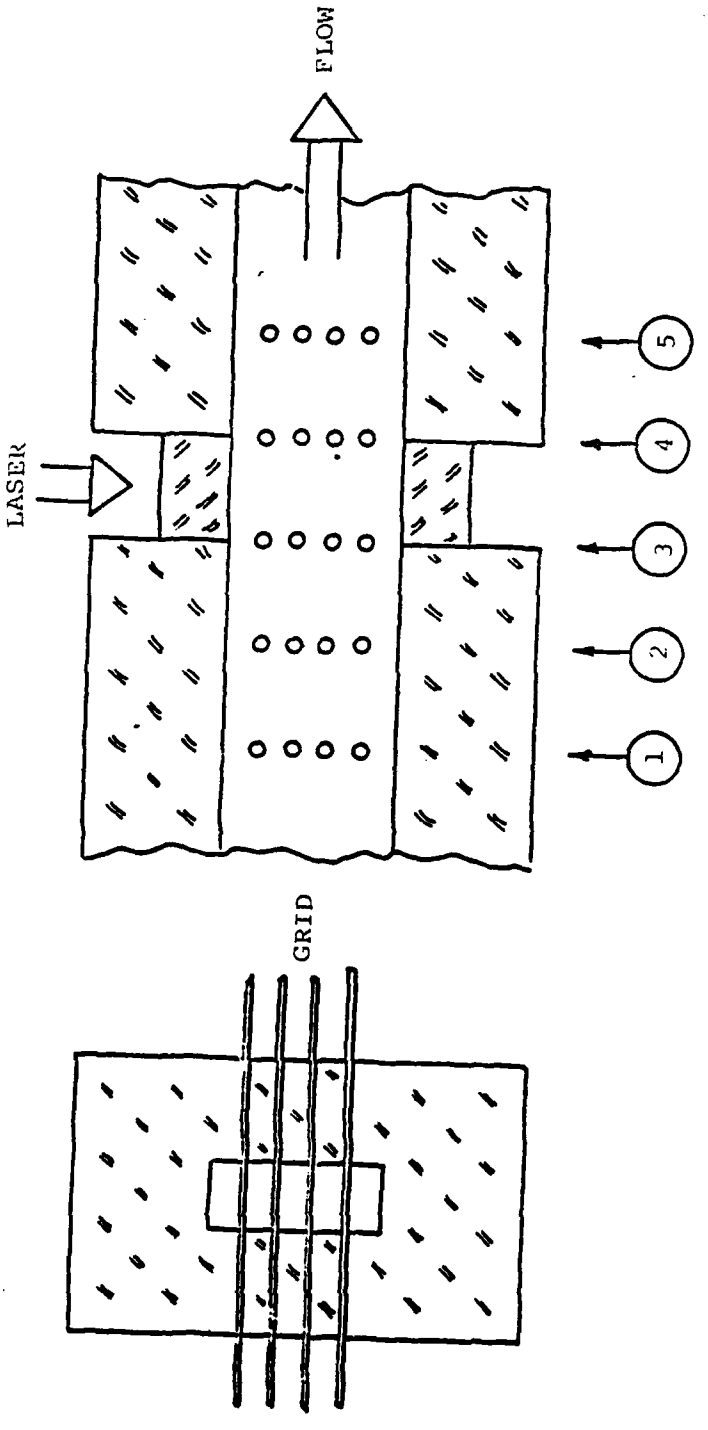

Fig. 1 Experimental setup

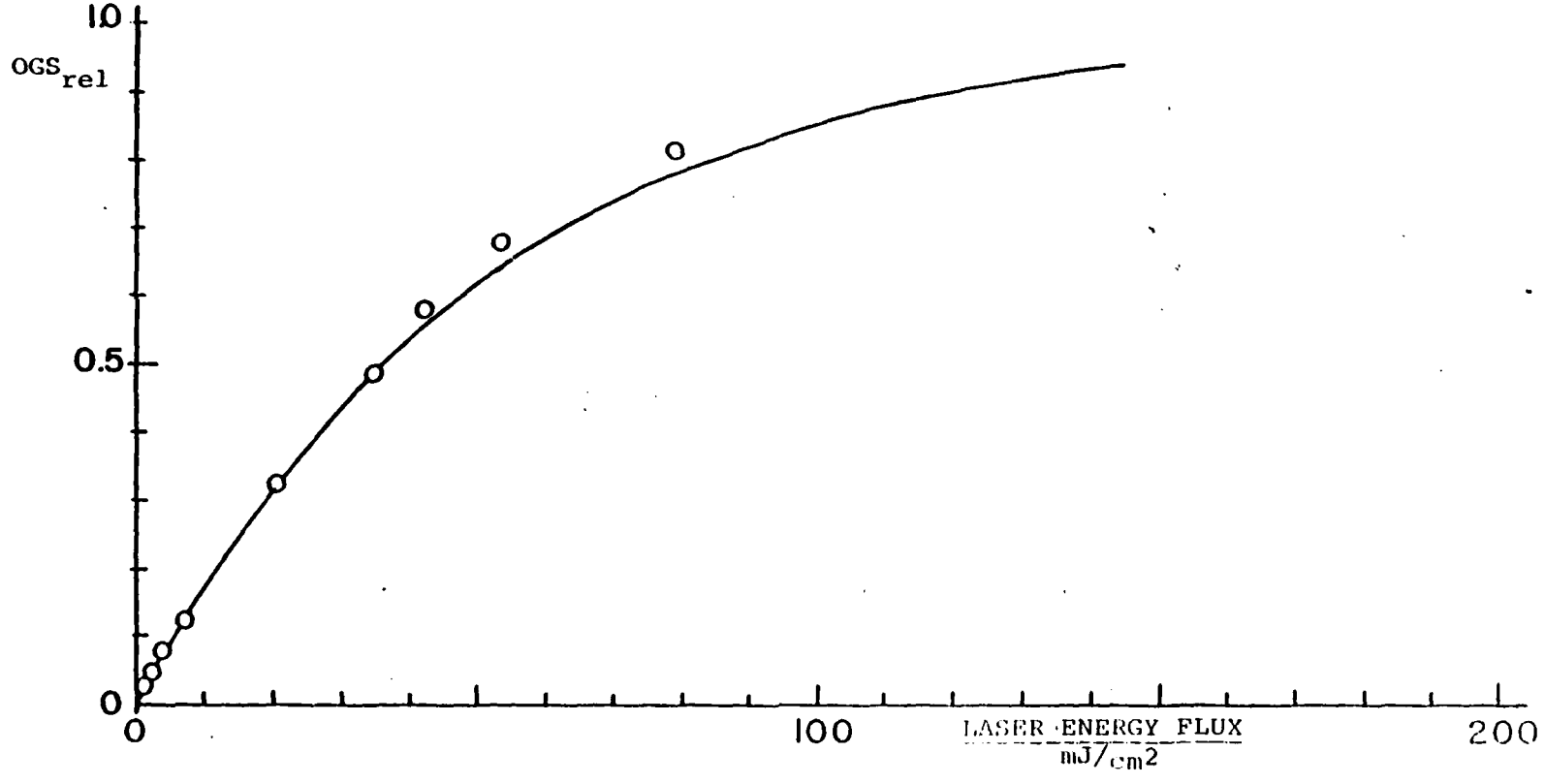

Fig. 2 Relative optogalvanic signal depending on laser energy flux
(I = 1.5 mA, p = 10 Torr, He: O_2 10:3)

JOURNAL PAPERS AND CONFERENCE PROCEEDINGS PAPERS, 1979-82

(Published with AFOSR/ARO Support)

1. E. Chu, R. Druce, M. Kristiansen, M. Hagler, and R. Bengston, "Beat Heating in Plasmas Using CO_2 Lasers", Journal de Physique, Colloque C7, supplement No. 7, 40, C7-747, (1979).

2. K. McDonald, M. Newton, E. Kunhardt, M. Kristiansen, and A.H. Guenther "An Electron beam Triggered Spark Gap", IEEE Transactions on Plasma Science, PS-8, 181 (1980).

3. S. Levinson, E. Kunhardt, M. Kristiansen, and A.H. Guenther, "Simulation of Inductive and Electromagnetic Effects Associated with Single and Multichannel Triggered Spark Gaps", Proc. 2nd IEEE International Pulsed Power Conference, Lubbock, Texas, 433, (1979).

4. K. McDonald, M. Newton, E.Kunhardt, M. Kristiansen, and A.H. Guenther, "An Electron-Beam-Triggered Spark Gap", Proc. 2nd IEEE International Pulsed Power Conference, Lubbock, Texas, 437 (1980).

5. M. Newton, K. McDonald, E. Kunhardt, M. Kristiansen, and A.H. Guenther, "Applications of Electron Beams for Precise Switching of High Voltages", Proc. 3rd International Topical Conference on High Power Electron and Ion Beam Research and Technology, Novosibirsk, USSR, 1979.

6. M. Kristiansen and A.H. Guenther, "Digest of Technical Papers", 2nd IEEE International Pulsed Power Conference, Lubbock, Texas.

7. M. Kristiansen and B. Miedzinski, "Investigations of Reed Switch Dynamics When Switching Heavy Loads", Proc. 10th International Conf. Contact Phenomena, Bucharest, Hungary, Aug. 25-29, 1980.

8. R.J. Crumley, P.F. Williams, M. Gundersen and A. Watson, "Electron Densities in Laser-Triggered Spark Gap Discharges", Proc. 2nd IEEE International Pulsed Power Conference, 119 (1979).

9. R.J. Crumley, P.F. Williams, and M. Gundersen, "Studies of the Basic Processes Responsible for Laser-Triggered Breakdown in Gases", Journal de Physique, Colloque C7, Supplement No. 7, 40, 27-305 (1979).

10. R.J. Crumley, P.F. Williams, and M. Gundersen, "Temporal Behavior of Electron Densities in Laser-Triggered Gaps", IEEE Trans. Plasma Sci., PS-8, 164 (1980).

11. *E. Kunhardt and W.W. Byszewski, "Development of Overvoltage Breakdown in High Pressure Gases", Physical Review, A, 21, 2069 (1980).

12. J.P. Craig, "Multi-Megajoule Energy Storage and Conversion Device", Proc. Conf. on Electromagnetic Guns and Launchers, San Diego, CA, Nov. 1980.

---

*Also partially supported by NSWC.

13. IEEE Trans. Plasma Science, Special Issue on Plasma Switches, Sept., 1980, A.H. Guenther and M. Kristiansen, Guest Editors.

14. R.L. Druce, M. Kristiansen, and M.O. Hagler, "An Experimental and Numerical Investigation of Laser-Plasma Interactions", submitted to Journal of Applied Physics.

15. K.H. Schoenbach, G. Schaefer, E.E. Kunhardt, M. Kristiansen, L.L. Hatfield, and A.H. Guenther, "An Optically Controlled Diffuse Discharge Switch", Proc. 3rd IEEE International Pulsed Power Conference, Albuquerque, N.M., June 1981. (Invited Paper)

16. Y.H. Tzeng, E.E. Kunhardt, M. Kristiansen and A.H. Guenther, "The Effect of Electron Beam Induced Space Charge on Spark Gap Breakdown", Proc. 3rd IEEE International Pulsed Power Conference, Albuquerque, N.M., June 1981. (Invited Paper)

17. M. Kristiansen, A.H. Guenther, J. Ungvarsky, F.C. Brockhurst, R.D. Franklin, A.K. Hyder and R.L. Gullickson, "Modular Instructional Material in Pulsed Power Technology", Proc. 3rd IEEE International Pulsed Power Conference, Albuquerque, N.M., June 1981.

18. H.C. Harjes, E.E. Kunhardt, M. Kristiansen, L.L. Hatfield and A.H. Guenther, "Space Charge Effects in a Laser-Fiber Optics Triggered Multichannel Spark Gap", Proc. 3rd IEEE International Pulsed Power Conference, Albuquerque, N.M., June 1981.

19. B.H. Dunlap and J.P. Craig, "Time Varying Inductors for Electromechanical Pulsers", Proc. 3rd IEEE International Pulsed Power Conference, Albuquerque, N.M., June 1981.

20. L.B. Gordon, M.O. Hagler, M. Kristiansen and H.C. Kirbie, "Investigations of a 60 KV, 5 CM Spark Gap for Several Electrode, Insulator, and Gas Types", Proc. 3rd IEEE International Pulsed Power Conference, Albuquerque, N.M., June 1981.

21. G.L. Jackson, Kai-Chi Yuan, L.L. Hatfield and M. Kristiansen, "Surface Damage of Dielectrics in a Spark Gap", Proc. 3rd IEEE International Pulsed Power Conference, Albuquerque, N.M., June 1981.

22. K.H. Schoenbach, G. Schaefer, H.C. Harjes, G. Leiker, and M. Kristiansen, "Opening Switches", Proc. 3rd IEEE International Pulsed Power Conference, Albuquerque, N.M., June 1981.

21. S. Dhali and P.F. Williams, "Multiphoton Ionization - A Potential Trigger and/or Control for Electrical Breakdown", Proc. 3rd IEEE International Pulsed Power Conference, Albuquerque, N.M., June 1981.

22. M. Kristiansen, et. al., "Report of Workshop on Repetitive Opening Switches", Proc. 3rd IEEE International Pulsed Power Conference, Albuquerque, N.M., June 1981. (Invited Paper)

23. K. Schoenbach, G. Schaefer, M. Kristiansen, L.L. Hatfield, and A.H. Guenther, "Diffuse Discharge Opening Switches", Proc. NATO Advanced Study Institute: Electrical Breakdown and Discharges in Gases, Les Arcs, France, July 1981.

24. M. Kristiansen and A.H. Guenther, "Plasma Applications" Proc. NATO Advanced Study Institute: Electrical Breakdown and Discharges in Gases, Les Arcs, France, July 1981.

25. B. Miedzinski and M. Kristiansen, "Investigations of Reed Switch Dynamics and Discharge Phenomena when Switching Intermediate and Heavy Loads", IEEE Trans.on Components, Hybrids, and Manfacturing Technology, CHMT-5, 231 (1982).

26. Proceedings of ARO Workshop on "Repetitive Opening Switches", Tamarron, Colorado, January 1981 (M. Kristiansen and K.H. Schoenbach, Editors).

27. K.H. Schoenbach, M. Kristiansen, E.E. Kunhardt, L.L. Hatfield, and A.H. Guenther, "Exploratory Concepts of Opening Switches", Proc. ARO Workshop on Repetitive Opening Switches, Tamarron, Colorado, January 1981, p 65.

28. L.B. Gordon, M. Kristiansen, M.O. Hagler, H.C. Kirby, R.M. Ness, and L.L. Hatfield, "Material Studies in a High Energy Spark Gap", to appear in IEEE Trans. on Plasma Science, Dec. 1982.

29. Y.H. Tzeng, E.E. Kunhardt, M. Kristiansen, and A.H. Guenther, "The Effect of Space Charge Induced by an Electron Beam on Spark Gap Operation", to appear in IEEE Trans. on Plasma Science, Dec. 1982.

30. H.C. Harjes, E.E. Kunhardt, M. Kristiansen, L.L. Hatfield, and A.H. Guenther, "Space Charge Effects in a Laser-Fiber Optics Triggered Mutichannel Spark Gap", to appear in IEEE Trans. on Plasma Science, Dec. 1982.

31. K.H. Schoenbach, G. Schaefer, M. Kristiansen, L.L. Hatfield, and A.H. Guenther, "Concepts for Optical Control of Diffuse Discharge Opening Switches", to appear in IEEE Trans. on Plasma Science, Dec. 1982.

32. D. Johnson, M. Kristiansen, and L.L. Hatfield, "Multichannel Surface Discharge Switch", Proc. Electrical Insulation and Dielectric Phenomena Conf., Amherst, Ma., Oct. 1982.

33. A.L. Donaldson, R. Ness, M.O. Hagler, and M. Kristiansen, "Electrode Erosion in High Power Spark Gaps", Proc. Fifteenth Power Modulator Symposium, Baltimore, Md., June, 1982.

34. G.L. Jackson, L L. Hatfield, M. Kristiansen, J. Marx, and A. Bowling, "Pulse Flashover of Solid Dielectrics in Vacuum", Proc. Xth International Symposium on Discharge and Electrical Insulation in Vacuum, Columbia, S.C. Oct. 1982.

35. Proceedings of ARO Workshop on "Diffuse Discharge Opening Switches", Tamarron, Colorado, January 1982 (K.H. Schoenbach and M. Kristiansen, Editors).

36. R.J. Pederson and H.J. Carper, "Flow Visualization in a Gas Blown Spark Gap, IEEE Conf. Record of 1982 Fifteenth Power Modulator Symp., Baltimore, Md. June. 1982.

37. R.A. Dougal, P.F. Williams, D.C. Pease, "Time Resolved Two-Dimensional Imaging of Ground State Species using Laser-Induced Fluorescence", Submitted to Rev. Sci. Inst.

38. G. Schaefer, P.F. Williams, K.H. Schoenbach, and J. Moseley,"Photo-detachment as a Control Mechanism for Diffuse Discharge Switches", submitted to IEEE Trans. Plasma Science.

Interactions

(Oct. 1, 1981 - Sept. 30, 1982)

a) Papers Presented

1) D. Johnson, M. Kristiansen, and L.L. Hatfield, "Multichannel Surface Discharge Switch", Electrical Insulation and Dielectric Phenomena Conf., Amherst, Ma., Oct. 1982.

2) G.L. Jackson, L.L. Hatfield, M. Kristiansen, J. Marx, and A. Bowling, "Pulse Flashover of Solid Dielectrics in Vacuum", Xth International Symposium on Discharges and Electrical Insulation in Vacuum, Columbia, S.C., Oct. 1982.

3) A.L. Donaldson, R. Ness, M.O. Hagler, and M. Kristiansen, "Electrode Erosion in High Power Spark Gaps", Fifteenth Power Modulator Symposium, Baltimore, Md., June 1982.

4) R.J. Pederson and J.J. Carper, "Flow Visualization in a Gas Blown Spark Gap", Fifteenth Power Modulator Sympsoium, Baltimore, Md., June 1982.

5) K.H. Schoenbach, G. Schaefer, M. Kristiansen, L.L. Hatfield, and A.H. Guenther, "Optical Control of Diffuse Discharge Opening Switching", ARO Workshop on Diffuse Discharge Opening Switches, Tamarron, Colorado, January, 1982.

6) M. Kristiansen, "Pulsed Power Research at Texas Tech University", Univ. of Trondheim, Norway,, June, 1982.

7) G. Schaefer, "A Tunable CO_2 Waveguide Laser and Injection Locking of a CO_2 TEA Laser", Center of Laser Studies, University of Southern California, Los Angeles, March 1982.

8) S.K. Dhali and P.F. Williams, "Multiphoton Ionization of Xe as a Charge Source for Electrical Breakdown", 34th Annual Gaseous Electronics Conference, Boston, Ma., Oct. 1981.

b) Consultative and Advisory Functions

1) Prof. M. Kristiansen coordinates the AFOSR sponsored Pulsed Power Lecture Series together with Dr. A. Guenther of the AFWL.

2) Prof. Kristiansen serves on the Basic Science Panel of the Air Force Scientific Advisory Board and attended the Fall meeting at Eglin AFB, Fl. on Nov. 3-5, 1981 and the Spring meeting at Peterson AFB, Co. on April 28-29, 1982.

3) Professors M. Kristiansen and K. Schoenbach organized a Workshop on Diffuse Discharge Opening Switches for the USARO at Tamarron, Co. on January 13-15, 1982.

4) Prof. M. Kristiansen serves on the advisory committee for the 1983 NATO Advanced Study Institute on "Fast Optical and Electrical Diagnostic Principles and Techniques", to be held in Italy, July, 1983.

5) Prof. M. Kristiansen serves as a Visiting Staff Member at Los Alamos National Laboratory and supervises a Ph.D. Thesis project on repetitive opening switches, conducted by one of their staff members.

c) Other Interactions

1) Professors Williams, Schoenbach, and Schaefer cooperated with Prof. J. Moseley of the University of Oregon on a joint research project related to diffuse discharge opening switches.

2) Prof. Schaefer visited Martin Gundersen at the University of Southern California, Los Angeles in March 1982 to discuss concept of optical control of diffuse discharges.

3) Prof. Schaefer visited Santosh Srivastava and Ara Chutjian at Jet Propulsion Laboratory in Pasadena, California in March 1982 to discuss their possibilities to measure attachment rates and cross sections.

4) Professors Schoenbach and Schaefer visited M.A. Biondi and Norman Bardsley at the University of Pittsburgh, Pa. in Oct. 1981 to discuss basic processes in diffuse discharges.

5) Professors Schoenbach and Schaefer visited Peter Chantry and C. Kimblin at Westinghouse Research Laboratory, Pittsburgh, Pa. in Oct. 1981. They discussed optical control of diffuse discharge switches and opening switches.

6) Prof. Schaefer visited C.B. Collins and C.D. Cantrell at the University of Texas at Dallas in Feb. 1982 to discuss possibilities of photoexcitation of large molecules.

7) Professors Williams, Schaefer and Schoenbach discussed with J. Mosely of the University of Oregon and S. Srivastave of JPL the effects of negative ions on diffuse discharges in May, 1982. (TTU)

8) Prof. Williams discussed with Dr. Martin Gundersen of the University of Southern California applying Boltzman code to diffuse discharges in hydrogen and other gases. This discussion was held at TTU.

9) Prof. Williams discussed with L. Pitchford of Sandia National Laboratories the influence of multiphoton ionization on the breakdown of gases, at Texas Tech University in June 1982.

10) Prof. Hatfield and G. Jackson have collaborated with A. Bowling at Texas Instruments, Dallas, Texas on surface analysis of conductors and insulators using ESCA, AES, and AEM facilities at Texas Instruments in 1982.

11) Prof. Hatfield invited Prof. J.E. Thompson, University of South Carolina as a consultant for two days in Sept. 1982. Topics discussed in detail included surface flashover measurements and models, surface charging of dielectrics, and surface discharges in the presence of various gases.

12) Prof. Hatfield made arrangement with G.J. Lapeyne at CRISS (Center for Research in Surface Science and Submicron Analysis), an NSF Regional Instrumentation User Facility at Bozeman, Mt., for use of ESCA, AES, and SEM on samples generated in our laboratories. A possible collaboration with a surface scientist at CRISS was also discussed.

13) Professors Kristiansen and Hatfield visited GTE, Waltham, Ma. in Aug. 1982 to discuss joint research efforts with J. Proud and W. Byszerski. Surface analysis, opening switch concepts, and closing switches were discussed.

14) Professors Hatfield and Hagler visited Sandia National Laboratories, Albuquerque, NM in Feb, 1982 to discuss closing switches with M. Buttram and triggering of surface switches with J. Rohwine.

15) Mr's. M. Bushell and George Crowson from Harry Diamond Laboratory visited our Laboratory on March 25-26 to discuss various possible options for EMP testing.

16) Prof. Kristiansen visited LLNL in Jan 1982 and discussed with Dr's Longerbeam, Hofer and, various other scientists research problems in pulsed power.

17) Prof's. Schaefer and Schoenbach cooperated with Dr. L. Christophorou of ORNL on a joint proposal to NSF for carrying out basic measurements of interest to our opening switch research.

18) Dr. A. Guenther from AFWL, Dr. M. Buttram from SNL, and Dr. A. Engelhardt from LANL serve on graduate student theses committees in our department.

19) A special meeting of leading spark gap specialists was held at TTU on Sept. 20-21 to plan the forthcoming DoD sponsored workshop on "Repetitive Spark Gap Operation" to be held in Tamarron, Co. in Jan. 1983.

20) A special meeting of leading solid state experts was held at TTU on Sept. 30 - Oct. 1 to plan the forthcoming ARO sponsored workshop on "Solid State, Pulsed Power Switching" to be held at Tamarron, Co. in Jan. 1982.

21) General R. Mathis, AF Vice Chief of Staff gave a lecture at TTU on February 2, 1982. The talk was part of the Halliburton Distinguished Lecture Series and the topic was "Technology and Defense: An Air Force Perspective. Arrangements were made by Prof. Kristiansen.

22) Prof. Kristiansen visited with Mr. K. Herron of the WAL at WPAFB and with representatives of the FTD on Aug. 9 and discussed various common research interests and problems. He also briefly visited with Prof. Fontana of AFIT to discuss the pulsed power lecture series.

23) Dr. R. Voshall of Westinghouse R&D Center spent one month of his sabbatical leave in our laboratory and cooperated on various research problems and lectured on vacuum switches.

24) Prof. Kristiansen visited the Laboratory of Dr. L. Lee at California State University at San Diego, Ca. in August, 1982 and discussed their experiments related to our opening switch research.

25) Prof. Kristianson visited various industrial companies in the pulsed power technology area in August, 1982 to assess their technology level in high power switching.

26) Prof. Schoenbach visited Dr. Christophorou, Oak Ridge National Lab on March 7-9 and discussed a joint program on the investigation of gases for Diffuse Discharge Opening Switches.

27) Prof. Schoenbach visited Dr. S. Srivastava and Dr. A. Chutjian to discuss cooperative work on diffuse discharges. (Search for suitable gases for diffuse discharge opening switches and measurement of attachment cross-sections) on Dec. 20-21, 1981.

28) Prof. Kristiansen visited Mr. T. Martin and M. Buttram, Sandia National Laboratories and discussed research programs and possible cooperative work on March 9, 1982.

29) Prof. W. Pfeiffer of Technische Hochschule, Darmstadt, FRG spent one week in our laboratory and consulted in high-speed diagnostics for pulsed power experiments.

30) Dr. Shekhar Guha from Martin Gundersen's Laboratory at the University of Southern California, Los Angeles spent the period of February 15-19, 1982 in Dr. Williams laboratory using our fast streak camera for investigations related to thyratron operation.

ADVANCED DEGREES AWARDED (1981-82)

1.	A. Donaldson	"Electrode Erosion Measurements in a High Energy Spark Gap" MSEE Thesis
2.	D. Johnson	"Multichannel Surface Discharge Switch" MSEE Thesis
3.	L. Gordon	"Material Studies in a High Energy Spark Gap" Ph.D. Thesis
4.	H. Dunlap	"Electromechanical Pulse Amplifier" MSEE Thesis


ATE
LME